NOVA SCHOOL OF SCIENCE & TECHNOLOGY

DEPARTAMENT OF CHEMISTRY

DEVELOPMENT OF NEW BIOACTIVE MATERIALS BASED ON EXOPOLYSACCHARIDES OF MARINE ORIGIN

PATRÍCIA CONCÓRDIO DOS REIS

Master in Biotechnology

DOCTORATE IN CHEMICAL AND BIOCHEMICAL ENGINEERING

NOVA University Lisbon

September, 2022

DEPARTAMENT OF
CHEMISTRY

DEVELOPMENT OF NEW BIOACTIVE MATERIALS BASED ON EXOPOLYSACCHARIDES OF MARINE ORIGIN

PATRÍCIA CONCÓRDIO DOS REIS

Master in Biotechnology

Adviser: Maria Filomena Andrade de Freitas
Assistant Professor, NOVA University Lisbon

Co-advisers: Maria Ascensão C. F. Miranda Reis
Full Professor, NOVA University Lisbon

Ana de Jesus B. M. de Amorim Ferreira
Assistant Professor, Universidade de Lisboa

Examination Committee:

Chair: Ana Isabel N. M. Aguiar de Oliveira Ricardo
Full Professor, *NOVA University Lisbon*

Rapporteurs: Carmen Sofia da Rocha Freire Barros
Principal Researcher, University of Aveiro

Miguel Ângelo Parente Ribeiro Cerqueira
Researcher, International Iberian Nanotechnology Laboratory

Adviser: Maria Filomena Andrade de Freitas
Assistant Professor, NOVA University Lisbon

Members: Alberto José Delgado dos Reis
Assistant Researcher, National Laboratory of Energy and Geology

Susana Maria Pereira Gaudêncio de Matos
Assistant Researcher, NOVA University Lisbon

DOCTORATE IN CHEMICAL AND BIOCHEMICAL ENGINEERING

NOVA University Lisbon
September, 2022

Development of new bioactive materials based on microbial exopolysaccharides of marine origin

Acknowledgements

This work marks the end of a journey, one of the most challenging of my life, that I could never gone through without the support of so many. To them, I'm extremely thankful.

First, I would like to express my sincere gratitude to my thesis adviser, Prof. Filomena Freitas, and co-advisers, Prof. Maria Ascensão Reis and Prof. Ana Amorim, for sharing their knowledge and for the support, motivation, guidance and wise advises, without which I would never be able to accomplish this achievement. In particular, I would like to thank Filomena for her kindness and friendship during these years, she was an amazing mentor.

I would like to thank Pacific Biotech S.A.S., that kindly supplied the bacterial polymers and the strain used in this thesis. Also, I would like to recognize the support of Dr. Jean Guézennec from Institut Français de Recherche pour l'Exploitation de la Mer, Dr. Xavier Mopper from Pacific Biotech, Prof. Vítor Alves from Instituto Superior de Agronomia, Prof. Christian Grandfils from University of Liège, Dr. Ana Teresa Serra, from Instituto de Biologia Experimental e Tecnológica, and Prof. Manuel Coimbra, from University of Aveiro. Thank you for your help and availability. Also, I gratefully acknowledge my colleagues João Pereira, Bruno Serafim, Diana Araújo and Kleyde Ramos, for their help.

I also acknowledge Fundação para a Ciência e a Tecnologia for the financial support for this thesis (SFRH/BD/131947/2017).

I would like to thank all BIOENG members for the assistance, the stimulating discussions, the helpful advises and the great work environment. João, Diana, Sílvia, Ana Teresa, Rita, Patrícia and Cátia, I am truly grateful for our friendship and the fun moments we shared. My gratefulness also goes to Helena David and Bernardo Vicente, from Universidade de Lisboa, for the friendly welcoming and the helpful assistance.

Finally, I would like to acknowledge my friends, for listening and offering me advice, for the joyful moments and for the emotional support. You make my life brighter, and I truly appreciate your friendship. To my family, especially my parents and my fiancé, I express my profound gratitude for all the continuous encouragement and unconditional love throughout these years.

Abstract

The arising of novel bio-based products and processes is vital for the sustainable development of society. The exploitation of marine resources towards the development of new ecological products with commercial interest is a promising solution. In this thesis, marine biodiversity was explored for the development of new and improved biomaterials and/or bioactive compounds based on marine exopolysaccharides (EPS). Marine microorganisms, including both microalgae and bacteria, were prospected for their EPS production capacity.

The results obtained in this study showed that marine microalgae have an enormous potential as producers of EPS with unique chemical compositions, including high contents in sulphate and unusual sugars. These characteristics are often associated with biological activities, which supports the potential of microalgal EPS to be employed as bioactive compounds. Indeed, in this work, the EPS produced by microalga *Heterocapsa* AC210 demonstrated antioxidant and anti-inflammatory properties.

Additionally, the EPS produced by bacteria isolated from unusual marine environments showed interesting compositions, including high uronic acids contents, and relevant functional properties. These biopolymers presented thickening, gel and film forming capacities, suggesting that they might be successfully used as structuring biomaterials.

This work showed that it was possible to use low-cost feedstocks for the cultivation of the bacterium *Alteromonas macleodii* Mo169, resulting in higher productivities and distinctive EPS compositions. The EPS produced by this strain also revealed potential in the nanotechnology field, as it might be used for the ecological synthesis of gold, silver, and selenium nanoparticles with wound healing and antioxidant properties.

Overall, this work supports that natural EPS bioprospected from marine microorganisms can be used for the development of bio-based products with application in high-value markets, thus, contributing to a sustainable future powered by marine biotechnology.

Keywords:

Marine bacteria, Marine microalgae, Exopolysaccharide (EPS), Bioactive materials, Structuring biomaterials, bio-nanocomposites, blue biotechnology.

Resumo

O aparecimento de novos produtos e processos de origem biológica é vital para o desenvolvimento sustentável da sociedade. Uma solução promissora é a exploração dos recursos marinhos para o desenvolvimento de novos produtos ecológicos com interesse comercial. Esta tese explora a biodiversidade marinha com o objetivo de desenvolver novos biomateriais e/ou compostos bioactivos a partir de exopolissacáridos (EPS) marinhos. A capacidade de produzir EPS foi avaliada para vários microrganismos marinhos, incluindo microalgas e bactérias.

Os resultados obtidos neste trabalho demonstraram que as microalgas marinhas têm um enorme potencial na produção de EPS com composições químicas únicas, que incluem um elevado conteúdo em sulfato e monossacáridos invulgares. Estas características estão frequentemente associadas a atividades biológicas, reforçando a ideia de que os EPS das microalgas têm potencial para serem utilizados como compostos bioactivos. De facto, neste trabalho, o EPS produzido pela microalga *Heterocapsa* AC210 demonstrou ter propriedades antioxidantes e anti-inflamatórias.

Além disso, os EPS produzidos por bactérias isoladas de ambientes marinhos incomuns apresentaram composições interessantes, incluindo altos teores de ácidos urónicos, e propriedades funcionais relevantes. Estes biopolímeros mostraram ter capacidade espessante, bem como a capacidade de formar géis e filmes, o que sugere que possam ser utilizados como biomateriais estruturais.

Este trabalho demonstrou ser possível utilizar substratos de baixo custo no cultivo da bactéria *Alteromonas macleodii* Mo169, o que resultou em produtividades superiores e EPS com composições distintas. O EPS produzido por esta cultura também revelou ter potencial na área da nanotecnologia, dado que pode ser utilizado na síntese ecológica de nanopartículas de ouro, prata e selénio com propriedades regenerantes e antioxidantes.

No geral, este trabalho apoia a convicção de que os EPS naturais obtidos de microrganismos marinhos podem ser utilizados para o desenvolvimento de bioprodutos com aplicações em mercados de elevado valor comercial, contribuindo assim para um futuro sustentável baseado na biotecnologia marinha.

Palavras-chave:

Bactérias marinhas, Microalgas marinhas, Exopolissacáridos (EPS), Materiais bioactivos, Biomateriais estruturais, Bio-nanocompósitos, biotecnologia azul.

List of Contents

List of figures

List of tables

Acronyms

AAPH	2,2'-Azobis(2-amidinopropane) dihydrochloride
Abs	Absorbance
Ac	Acetate
AgNP	Silver nanoparticles
ANOVA	Analysis of variance
AP	Apple pulp waste
Ara	Arabinose
ATCC	American Type Culture Collection
AuNP	Gold nanoparticles
CCRD	Central composite rotatable design
CDW	Cell Dry Weight
CMC	Carboxymethyl cellulose
CNCM	Collection Nationale de Cultures de Microorganismes
CPS	Capsular polysaccharide
DCFH-DA	2′,7′-dichlorofluorescein diacetate
DD	Dextran derivates
DFKZ	Deutsches Krebsforschungszentrum
DLS	Dynamic light scattering
DMEM	Dulbecco's Modified Eagle medium
DO	Dissolved oxygen
ELISA	Enzyme-linked immunosorbent assay
EPS	Exopolysaccharide

FBS	Fetal bovine serum
FTIR	Fourier Transform Infra-Red
Fuc	Fucose
GAG	Glycosaminoglycans
Gal	Galactose
GalA	Galacturonic acid
GalN	Galactosamine
GalNAc	N-acetyl galactosamine
GC-FID	Gas chromatography with flame ionization detector
GCqMS	Gas chromatography quadrupole mass spectrometry
Glc	Glucose
GlcA	Glucuronic acid
GlcN	Glucosamine
GlcNAc	N-acetyl glucosamine
Gly	Glycerol
HA	Hyaluronic acid
^{1}H NMR	Proton nuclear magnetic resonance
HPAEC-PAD	High-performance anion exchange chromatography with pulsed amperometric detection
HPLC	High performance liquid chromatography
ICP-AES	Inductively Coupled Plasma – Atomic Emission Spectroscopy
IL	Interleukin
IR	Infrared
LDPE	Low-density polyethylene
LPS	Lipopolysaccharides

LVE	Linear viscoelastic region
Man	Mannose
ManA	Mannuronic acid
NBP	NutriBloom Plus
NEAA	Non-essential amino acids
NMWCO	Nominal molecular weight cut-off
NP	Nanoparticles
OD	Optical density
PBS	Phosphate-buffered saline
PCV2	Porcine circovirus type 2
PDI	Polydispersity index
PES	PolyEtherSulfone
PET	Polyethylene terephthalate
PHA	Polyhydroxyalkanoates
PHB	Polyhydroxybutyrate
PS	Penincilin-strepmycin
PUFAs	Polyunsaturated fatty acids
PVC	Polyvinyl chloride
Pyr	Pyruvate
RH	Relative humidity
Rha	Rhamnose
Rib	Ribose
ROS	Reactive oxygen species
RSM	Response surface methodology

SCM	Semi-complex medium
SE-HPLC	Size Exclusion-High Performance Liquid Chromatography
SEM	Scanning electron microscopy
SeNP	Selenium nanoparticles
SLPM	Standard liters per minute
Std	Standard cultivation conditions
Suc	Succinate
T_{deg}	Maximal degradation temperature
TEM	Transmission electron microscopy
TFA	Trifluoroacetic acid
TG	Thermogravimetric
UA	Uronic acids
XRD	X-ray diffraction
Xyl	Xylose

Symbols

A	Pre-exponential factor (Pa s)
a^*	Red/green value of the colour space
b^*	Yellow/blue value of the colour space
C_{ab}	Chroma
CDW	Cell dry weight (g L^{-1})
dP	Variation of concentration of product (g L^{-1})
dt	Variation of time (d or h)
E_a	Activation energy (J mol^{-1})
G'	Storage modulus
G''	Loss modulus
h_{ab}	hue
*L**	Lightness
M_n	Number average molecular weight
M_w	Average molecular weight
n	Viscosity exponent
N_w	Water vapour molar flux (mol m^{-2} s^{-1})
P	Gas permeability (mol m m^{-2} s^{-1} Pa^{-1})
q_P	Specific Exopolysaccharide productivity (g g^{-1} d^{-1} or g g^{-1} h^{-1})
R	Gas constant (J mol^{-1} K^{-1})
R^2	Determination coefficient
r_P	Exopolysaccharide volumetric productivity (g L^{-1} d^{-1} or g L^{-1} h^{-1})
r_x	Biomass volumetric productivity (g L^{-1} d^{-1} or g L^{-1} h^{-1})
t	Time (s)

T	Absolute temperature (K)
WVP	Water vapour permeability (mol m s^{-1} Pa^{-1})
x_0	Initial biomass concentration (g L^{-1})
X_i	experimental variables in RSM
Y	observed response in RSM
Y_p	Predicted response in RSM
$Y_{p/s}$	Product yield on substrate (g g^{-1})
$Y_{x/s}$	Biomass yield on substrate (g g^{-1})
ΔE_{ab}	Colour differences
Δp	Product produced (mg L^{-1} or g L^{-1})
ΔP	Pressure difference between the feed and permeate compartment (mbar)
$\Delta P_{w.eff}$	Effective driving force (Pa)
ΔS	Substrate consumed (g L^{-1})
Δt	Cultivation time (d or h)
Δx	Biomass produced (g L^{-1})
β	Geometric parameter of the gas permeation cell
β_i	Model coefficients
β_o	Model coefficient for interception
β_1, β_2	Model coefficients for linear correlation
β_{12}	Model coefficient for interaction
β_{11}, β_{22}	Model coefficients for quadratic correlation
$\dot{\gamma}$	Shear rate (s^{-1})
ω	Angular Frequency (rad s^{-1})

η_0	Zero-shear rate viscosity (Pa s)
η	Apparent viscosity (Pa s)
η^*	Complex viscosity (Pa s)
η_∞	Viscosity of the second Newtonian plateau (Pa s)
η_{sp}	zero-shear rate specific viscosity (Pa s)
μ	Specific growth rate (h^{-1})
μ_{max}	maximum specific cell growth rate (d^{-1} or h^{-1})
λ	Time constant (s)
ε	Elongation at break (%)
εm	Young's modulus (MPa)
Ƈ	Tensile strength at break (MPa)
δ	Film thickness (m)

1

Background and Motivation

Part of this chapter was published in the following book chapter:

Freitas, F., Torres, C. A. V., Araújo, D., Farinha, I., Pereira, J. R., Concórdio-Reis, P., & Reis, M. A. M. (2021). Advanced Microbial Polysaccharides. In B. Rehm & M. F. Moradali (Eds.), *Biopolymers for Biomedical and Biotechnological Applications* (1st ed., pp. 19–62). Wiley. DOI: 10.1002/9783527818310.ch2

Bioeconomy, the emerging new economic solution for the sustainable development of society, comprises the development of new biotechnological innovations based on the use of renewable biological resources and processes as alternatives to the traditional fossil-based systems (Vieira et al., 2020). The European Commission estimates that the shift for bio-based products could save up to 2.5 billion tons of CO_2 equivalent per year by 2030, being an important sector of the bioeconomy (https://ec.europa.eu/). The European Bioeconomy program also acknowledges the major role of marine biotechnology in the development of new bio-based products, suggesting that innovative biotechnological solutions can be found by bioprospecting natural marine resources. In line with this, the development of novel and enhanced biomaterials based on biopolymers, including natural polysaccharides, is an essential area of research for the successful achievement of sustainable and competitive bio-based industries. Marine microorganisms are an excellent source of natural compounds with applications on human health and well-being, thus, worth exploring for the development of bioactive materials based on polysaccharides.

1.1. Polysaccharides

Polysaccharides are high molecular weight polymers composed of saccharide monomers, linked to each other through glycosidic linkages. Based on their chemical composition, polysaccharides can be classified as homopolysaccharides (e.g., cellulose, dextran), when composed of only one type of monosaccharide, or heteropolysaccharides (e.g., xanthan, hyaluronic acid) with several different monosaccharides, usually up to ten, in their composition (Casillo et al., 2018; Rana & Upadhyay, 2020). In addition to the most common sugar monomers, glucose and galactose, other neutral sugars such as rhamnose, arabinose or fucose, uronic acids and aminosugars are also frequently found. In addition, non-sugar constituents, namely organic acyl groups (e.g., acetate, pyruvate) and inorganic compounds (e.g., phosphate, sulphate) are often reported in their composition (Freitas et al., 2021; Rana & Upadhyay, 2020). The presence of ionizable groups that grant a polyelectrolyte character to these macromolecules, greatly affects their properties (Freitas et al., 2021). Considering their structure, diverse combinations of monosaccharide units can be found, with regular repeating units or random monomeric units. Most common linkages between monomers are β-1,4 or β-1,3, resulting in a more rigid backbone, and α-1,2 and α-1,6 with more flexible zones (Dave et al., 2020; Delbarre-Ladrat et al., 2014). The multiple linkage possibilities results in linear or branched structures (Casillo et al., 2018; Freitas et al., 2021).

Polysaccharides are the most abundant organic material in the world, being essential molecules found in all life forms (Casillo et al., 2018; Rana & Upadhyay, 2020). Additionally, polysaccharides are widely employed in industry, including the pharmaceutical, cosmetic, food and paper industries, due to their functional properties (e.g., emulsifying, stabilizing, thickening or gelling capacity) (Cruz et al., 2011). Polysaccharides obtained from natural sources have the advantages of being biodegradable, renewable, biocompatible, and usually non-toxic (Ferreira et al., 2014; Moscovici, 2015). Natural polysaccharides can be extracted from plants (e.g., starch), seaweeds (e.g., alginate), or animal resources (e.g., chitin). Moreover, several microorganisms such as microalgae, fungi, bacteria and yeasts can produce these complex molecules (Rana & Upadhyay, 2020), which are arising as competitive alternatives to other natural and synthetic polymers due to their improved properties and easier production (Freitas et al., 2021). Microorganisms usually have higher growth rates and the bioreactor production conditions can be easily manipulated, improving productivity and the polymer's desirable characteristics (Freitas et al., 2021). Also, the production process is not influenced by uncontrollable conditions, such as climate and season, and can rely on the use of low-cost by-products or wastes as feedstocks (Donot et al., 2012; Freitas et al., 2021; Rana & Upadhyay, 2020). The bioreactor production of these microbial polysaccharides in a controlled environment without the risk of viral or pathogen contamination is in agreement with the Good Manufacturing Practices (Delbarre-Ladrat et al., 2014).

1.2. Microbial exopolysaccharides

Microbial polysaccharides can be produced by bacteria, fungi, yeasts and microalgae and, depending on their biological function, can be found in different cellular components and also in the extracellular boundary. Intracellular polysaccharides, present in the cell cytoplasm, are associated with the storage of carbon and energy (e.g., glycogen), cell-wall polysaccharides contribute to maintaining the shape and rigidity of the cell structure (e.g., chitin), and extracellular polysaccharides, secreted by the cells, can be found covalently bound to the cell membrane (capsular polysaccharides, CPS) or as a slime which is loosely bound to the cell surface (exopolysaccharides, EPS) (Freitas et al., 2021; Gaignard et al., 2019; Kumar et al., 2007; Nwodo et al., 2012; Poli et al., 2010). CPS are frequently associated with pathogenicity and virulence promoting factors, whereas EPS are secreted as a protective barrier against environmental harmful conditions and possible predators, to adhere and colonize surfaces, for biochemical interactions, and to serve as carbon

reserve (Delattre et al., 2016; Freitas et al., 2021; Hamidi et al., 2019; Laroche, 2022; Poli et al., 2010). Harvesting the EPS from the extracellular environment is rather easy and does not involve any environmental toxic compounds (Delbarre-Ladrat et al., 2014; Schmid et al., 2015). In addition, microbial EPS have interesting composition and properties, thus, have emerged as a valuable alternative in the biopolymers' market. Their main applications are: 1) as biomaterials due to their capacity to form polymeric structures and matrices (e.g., films, gels, emulsions, micro- and nanoparticles), and 2) as bioactive compounds in novel pharmaceutical drugs, due to their biological properties (immunomodulator, antitumor, antiviral, antioxidant, antimicrobial) (Costa et al., 2021; Freitas et al., 2021; Hamidi et al., 2019; Moscovici, 2015).

1.3. Marine biosphere as source of microbial biodiversity

The potential of microbial polysaccharides is limitless as newly isolated EPS-producing microorganisms can be considered sources of polysaccharides with novel or improved properties. This is particularly true for microorganisms of marine origin. Covering more than 70% of the Earth's surface and comprising more than 95% of the entire biosphere's biological diversity (Dufourcq et al., 2014), marine ecosystems undoubtedly have a great biodiscovery potential, which is still underexplored and underexploited (Concórdio-Reis et al., 2021). Including extreme environments such as, deep-sea hydrothermal vents, sea ice, or hypersaline locations, the marine realm is highly heterogenous (Delbarre-Ladrat et al., 2014). It comprises very complex environments characterized by diverse conditions of temperature, salinity, pressure, light, nutrient availability and pH (Casillo et al., 2018; Delbarre-Ladrat et al., 2014; Poli et al., 2010; Roca et al., 2016). Marine life is found in all these contrasting systems and shows an incredible ecological and metabolic diversity, a consequence of evolution and adaptation in these extreme environments (Overmann & Lepleux, 2016; Singh & Saxena, 2015). This high diversity is also translated into the distinct structures and composition found in EPS of marine origin namely bacteria and microalgae, and often display great functional and bioactive properties. (Poli et al., 2010). Examples of EPS synthesized by marine algae and bacteria displaying functional and bioactive properties are depicted in Table 1.1. Although these microorganisms have been studied for decades, the potential of their EPS in Biotechnology is being investigated only recently (Delbarre-Ladrat et al., 2014).

Table 1.1. Examples of EPS produced by marine microorganisms displaying functional and bioactive properties (Ara, arabinose; Fuc, fucose; Gal, galactose; GalA, galacturonic acid; GalN, galactosamine; GalNAc, N-acetyl galactosamine; Glc, glucose; GlcA, glucuronic acid; GlcN, glucosamine; GlcNAc, N-acetyl glucosamine; Man, mannose; ManA, mannuronic acid, Rha, rhamnose; Rib, ribose; Xyl, xylose).

Microbial source	Composition	Mw (Da)	Properties and applications	References
Bacteria				
Alteromonas sp. PRIM-28	ManA, Glc, GlcNAc	7.80×10^5	Biocompatible, immune modulation, assisting in cell proliferation and migration. Wound care.	Sahana & Rekha (2019)
Alteromonas HYD-1545	Glc, Gal, GlcA, GalA, pyruvated Gal	1.8×10^6	Anticoagulant, bone regeneration.	Vincent et al. (1994); Zarandona et al. (2020)
Alteromonas macleodii sub. f*ijiensis* biovar deepsane HYD 657	Fuc, Rha, Glc, Gal, Man, GlcA, GalA Sulphate, lactate and pyruvate groups	1.6×10^6	Keratinocytes protection, cosmetic.	Cambon-Bonavita et al. (2002); Le Costaouëc et al. (2012)
Alteromonas macleodii sub. *fijiensis* strain ST716	Glc, Man, Gal, GalA, GlcA Pyruvated Man	3.3×10^5	Gel forming, thickener.	Raguénès et al. (1996); Rougeaux et al. (1998)
Alteromonas infernus GY785	Glc, Gal, GalA, GlcA	1×10^6	Gel forming, metal binding.	Raguénès et al. (1997)
Colwellia psychrerythraea 34H	N-acetyl quinovosamine, GalA, alanine	n.a.	Anti-freeze.	Casillo et al. (2017)
Hahella chejuensis strain 96CJ1035	Glc, Gal	2.2×10^6	Emulsifier.	Yim, Kim, Aan, et al. (2004)
Halomonas eurihalina F2-7	Glc, Man, Rha Uronic acids, aminosugars, acetyl and sulphate groups	n.a.	Emulsifier.	Bejar et al. (1996); Martínez-Checa et al., (2007)
Pantoea sp. YU16-S3	Glc, Gal, GalN, GlcN	1.75×10^5	Biocompatible, cell adhesion and cell proliferation properties, facilitated fibroblast migration. Wound care.	Sahana & Rekha (2020)

Table 1.1. Examples of EPS produced by marine microorganisms displaying functional and bioactive properties (Ara, arabinose; Fuc, fucose; Gal, galactose; GalA, galacturonic acid; GalN, galactosamine; GalNAc, N-acetyl galactosamine; Glc, glucose; GlcA, glucuronic acid; GlcN, glucosamine; GlcNAc, N-acetyl glucosamine; Man, mannose; ManA, mannuronic acid, Rha, rhamnose; Rib, ribose; Xyl, xylose) (cont.).

Microbial source	Composition	Mw (Da)	Properties and applications	References
Pseudoalteromonas sp. strain MD12-642	GalA, GlcA, Rha, GlcNAc	> 1×10^3	Thickener.	Roca et al. (2016)
Pseudoalteromonas strain SM20310	Rha, Xyl, Man, Gal, Glc, GalNAc, GlcNAc	> 2×10^6	Cryoprotectant.	Liu et al. (2013)
Pseudoalteromonas arctica KOPRI 21653	Glc, Gal	n.a.	Cryoprotectant.	Kim & Yim (2007)
Pseudoalteromonas elyakovii Arcpo 15	Man, GalA	1.7×10^7	Cryoprotectant.	Kim et al. (2016)
Pseudoalteromonas sp. SM9913	Glc, Gal, Xyl, Ara	4×10^4	Metal binding, flocculant.	Qin et al. (2007)
Pseudomonas sp. WAK1	Gal, Glc, sulphate groups	n.a.	Anti-cancer.	Matsuda et al. (2003)
Pseudomonas stutzeri 273	GlcN, Rha, Glc, Man	1.9×10^5	Antibiofilm, antibiofouling, antioxidant, anti-infection.	Wu et al. (2016)
Pseudomonas sp. ID1	Glc, Gal, Fuc	> 2×10^6	Emulsifier, cryoprotectant.	Carrión et al. (2015)
Polaribacter sp. SM1127	Rha, Fuc, GlcA, Man, Glc, GlcN	2.2×10^5	Cryoprotectant, antioxidant.	Sun et al. (2016)
Vibrio MO245	GlcA, GalNAc, GlcNAc, Glc	5.1×10^5	Gel forming.	Martin-Pastor et al. (2019)
Vibrio diabolicus	GlcA, GlcNAc, GalNAc.	8×10^5	Bone and skin regeneration.	Zanchetta et al. (2003);Senni et al. (2013)
Vibrio harveji VB23	Gal, Glc, Rha, Fuc, Man, Rib, Ara, Xyl, sulphate groups	n.a.	Emulsifier.	Bramhachari & Dubey (2006)
Vibrio furnissii VB0S3	Gal, Glc, Man, Rha, Fuc, Rib, Ara, Xyl	n.a.	Emulsifier.	Bramhachari et al. (2007)

Table 1.1. Examples of EPS produced by marine microorganisms displaying functional and bioactive properties (Ara, arabinose; Fuc, fucose; Gal, galactose; GalA, galacturonic acid; GalN, galactosamine; GalNAc, N-acetyl galactosamine; Glc, glucose; GlcA, glucuronic acid; GlcN, glucosamine; GlcNAc, N-acetyl glucosamine; Man, mannose; ManA, mannuronic acid, Rha, rhamnose; Rib, ribose; Xyl, xylose) (cont.).

Microbial source	Composition	Mw (Da)	Properties and applications	References
Microalgae				
Chlorella stigmatophora	Glc, GlcA, Xyl, Rib, Fuc, sulphate groups	22×10^3	Anti-inflammatory, Immunomodulatory (immunosuppressant).	Guzmán et al. (2003)
Cochlodinium polykrikoides	Man, Gal, Glc, uronic acids and sulphate groups	n.a.	Antiviral.	Hasui, Matsuda, Okutani, et al. (1995)
Gyrodinium impudicum	Gal and sulphate groups	1.9×10^7	Immunomodulatory and antitumor activity.	Yim et al. (2004); Bae et al., (2006); Yim et al. (2007)
Navicula directa	Fuc, Xyl, Gal, Man, Rha, Glc, GlcA, sulphate groups	2.2×10^5	Antiviral.	Lee et al. (2006)
Phaeodactylum tricornutum	Glc, GlcA, Man, uronic acids and sulphate groups	$27–449 \times 10^3$	Anti-inflammatory, immunomodulatory (immunostimulatory).	Guzmán et al. (2003)
Porphyridium sp.	Xyl, Gal, Glc, GlcA and sulphate groups	$0.24–1.8\times10^6$	Anti-inflammatory, Antioxidant, Hypocholesterolemic, biolubricant (for bone joints)	Matsui et al. (2003); Soanen et al. (2016); Sun et al. (2009); Dvir et al. (2009); Arad et al. (2006)
Porphyridium cruentum	Gal, Glc, Ara, Man, Fuc, Xyl, Rha, uronic acids and sulphate groups	n.a.	Antibacterial, Antiviral, antihyperglycemic.	Raposo et al. (2014); Setyaningsih et al. (2020)

1.4. Marine exopolysaccharide-producing microalgae

Microalgae can use carbon dioxide (CO_2) as carbon source and incorporate it into complex organic molecules. These microorganisms comprise a large group of photosynthetic unicellular and multicellular organisms, including both prokaryotic (e.g., cyanobacteria/blue-green algae) and eukaryotic organisms (e.g., green algae). Besides the use of biomass as feed in aquaculture and livestock production (Roy & Pal, 2015; Spolaore et al., 2006), microalgae are also the source of high-value products, such as natural pigments (e.g., β-carotene and astaxanthin), polyunsaturated fatty acids, proteins and antioxidants, that are commercialized mainly for the nutraceutical (Nicoletti, 2016) and skin-care (Stolz and Obermayer, 2005) industries. Moreover, microalgae are increasingly investigated as a new sustainable and environment friendly alternative to fossil fuel resources, since they accumulate high amounts of lipids and carbohydrates that can be used as feedstocks for biofuel production (Chen et al., 2013; Laroche, 2022; Markou & Nerantzis, 2013). However, almost all commercial microalgae products are obtained from the biomass, and only recently their relevance as producers of valuable EPS has started to be considered (Delattre et al., 2016; Gaignard et al., 2019).

Microalgae EPS producers are found in several microalgae phyla and their EPS are characterized by complex chemical structures generally with a high diversity of sugar monomers in the same macromolecule, often up to 9–12, including rare sugars (e.g., fucose, rhamnose and ribose) and sulphate groups (Table 1.1), which are known to confer biological activity to the biopolymers (Delattre et al., 2016; Freitas et al., 2017). Reported bioactive properties are presented in Table 1.1 and include anti-inflammatory, immunomodulatory, antiviral, antibacterial, antitumor and antihyperlipidemic activity. The exploitation of marine microalgae EPS holds great potential of development, representing a sustainable and environmentally friendly strategy to capture CO_2 while producing high-value products with interesting application in therapeutics, cosmetics, and regenerative medicine. In fact, there are already a few successful examples of commercially available marine microalgae EPS mainly associated with the cosmetic area, such as the sulphated EPS from the red algae *Porphyridium* sp., marketed by FRUTAROM under the trade name Alguard™ (Freitas et al., 2017). Alguard™ has been used in cosmetics as an antiaging, anti-irritant, UVB damage protection, anti-inflammatory, lip balm, healing and smoothing creams (Jesus Raposo et al., 2014). Also, a mixture of microalgae EPS named Alguronic Acid™ is

used in cosmetic products from Algenist™ capable of improving health and skin appearance (Ariede et al., 2017).

1.4.1. Exopolysaccharide production by microalgae

The detection of EPS producers among microalgae is not always easy since these molecules are often synthesized under specific cultivation conditions or during specific growth phases (Delattre et al., 2016). Different strategies, such as nutrient depletion (e.g., nitrogen), high salinity or high light fluxes can be employed to trigger EPS production in microalgae depending on the strain (Laroche, 2022). Nitrogen limitation seems to be the most described environmental constrain leading to EPS synthesis (Gaignard et al., 2019; Laroche, 2022). Although the mechanism in which nitrogen concentration promotes EPS synthesis remains unclear, it seems that a higher carbon to nitrogen ratio might promote the redirection of the carbon metabolism towards EPS production (Gaignard et al., 2019; Laroche, 2022). Other strategies for optimizing EPS production include determining optimal irradiance (light intensity and time of exposure), supplementation of CO_2 in the air stream, pH, medium salinity and temperature (Delattre et al., 2016; Laroche, 2022). Nonetheless, the optimal strategy for EPS production seems to be strain dependent (Delattre et al., 2016; Laroche, 2022). For example, EPS production by cyanobacteria *Cyanothece* sp. CCY 0110 was dependent on the number of cells rather than the amount of EPS produced by each cell, thus, being maximized with higher light intensities and the presence of nitrogen (Mota et al., 2013). By contrast, nitrogen starvation increased EPS production by red microalga *Porphyridium marinum* (Soanen et al., 2016). For the diatom *Achnanthes brevipes*, EPS synthesis increased when phosphorous was the limiting nutrient, whereas nitrogen starvation had no significant effect. Interestingly, the combined effect of nitrogen and phosphorous depletion induced the accumulation of intracellular carbohydrates (Guerrini et al., 2000).

In addition to the changes in EPS productivity, the cultivation conditions might also affect the EPS chemical composition (Laroche, 2022). For the diatom *Thalassiosira pseudonana*, the fucose content of the EPS was significantly reduced from 30 to 5 mol% when the microalgae was cultivated in phosphorous depleted conditions (Urbani et al., 2005). Additionally, nitrogen starvation in marine diatom *Cylindrotheca fusiformis* led to a decrease of the EPS content in galactose, mannose and xylose, and an increase in rhamnose and galactose concentration (Magaletti et al., 2004).

1.5. Marine exopolysaccharide-producing bacteria

Bacteria were one of the first forms of life that appeared on earth and can be found almost everywhere, including in extreme environments (Hamidi et al., 2019). It is estimated that 10^6 out of the 10^9 taxa of bacteria in earth are found on the ocean (Hamidi et al., 2019). Numerous genera of marine bacteria have been reported as EPS producers (Table 1.1), including extremophilic microorganisms such as psychrophilic, thermophilic and halophilic bacteria (Delbarre-Ladrat et al., 2014; Poli et al., 2010). Most of the reported marine bacterial EPS contained glucose, galactose and/or mannose as neutral sugars, but some atypical sugar monomers (e.g., fucose, ribose, rhamnose) were also found (Table 1.1). Uronic acids (glucuronic and galacturonic acid) and amino sugars have also been found in high contents. Glycosaminoglycans (GAG), polysaccharides composed of uronic acid and neutral or hexosamine moieties, are essential for animal's life, being involved in cell physiology (Delbarre-Ladrat et al., 2014). Additionally, these molecules have an important role in the treatment of some pathologies (Delbarre-Ladrat et al., 2014). GAG-mimetic polysaccharides, such as hyaluronic acid and heparin-like polysaccharides, such as hyaluronic acid and heparin-like polysaccharides, are particularly interesting for biomedical and cosmetic applications such as in tissue engineering, regenerative medicine, osteoarthritis treatment, ophthalmology, and skin care. Also, these glycosaminoglycans can as used as active components in anti-coagulant, anti-thrombotic and anti-inflammatory drugs (Delbarre-Ladrat et al., 2017; Roca et al., 2016). In fact, due to their complex and diverse structure and compositions, these EPS have shown various biological, including antioxidant, anticancer, anti-infectious, antifreeze, immune modulation, and tissue regeneration (Table 1.1). Despite their potential and proven bioactivities, only few examples of marine bacterial EPS made it to the market. One example is EPS produced by the deep sea bacterium *Vibrio diabolicus* which was commercialized as Hyalurift® by Seadev-Fermen Sys and Infremer (Freitas et al., 2017). This EPS efficiently promoted bone and skin regeneration, and accelerated collagen fibrillation (Senni et al., 2013; Zanchetta et al., 2003). Another example is the EPS from *Alteromonas macleodii* subsp. *fijiensis* which is currently commercialized for cosmetic purposes under the name Abyssine®, due to its capacity to reduce skin irritation against mechanical, chemical, and UVB exposure (Zarandona et al., 2020). Also available in the cosmetic's market is Hyanify™, an EPS obtained from a marine γ-proteobacteria, described as stimulating hyaluronic acid synthesis in human dermal fibroblasts and reducing the nasolabial wrinkles (Rana & Upadhyay, 2020). Another example is SeaCode®, developed by LIPOTEC, which consists in a mixture of

extracellular glycoproteins and EPS produced by fermentation of a *Pseudomonas* sp. isolated from Antarctic waters. SeaCode® is described to improve collagen I synthesis and is used in anti-aging skincare (Núñez-Pons et al., 2018). The same company has also developed another anti-aging product from extracellular glycoproteins of marine *Pseudoalteromonas antarctica* NF3, named Antarcticine® (Núñez-Pons et al., 2018).

1.5.1. Exopolysaccharide production by bacteria

EPS biosynthesis starts with the assimilation of carbon, followed by the intracellular synthesis of the polysaccharide and, finally, its secretion to the extracellular environment (Finore et al., 2014). Although the microorganism's survival and cell growth might be dependent on their presence, EPS production requires a substantial amount of energy and, consequently, a high carbon input (Finore et al., 2014; Poli et al., 2010). Thus, supplying a suitable carbon source in generous concentration is usually the first step to induce EPS production (Poli et al., 2010). However, there is no single solution that guarantees high EPS yields since marine bacteria differ in their optimal cultivation conditions for maximum EPS production. Factors such as nitrogen source and concentration, media composition, temperature, salinity or pH should be investigated (Poli et al., 2010). Since in Nature EPS production seems to be a response to biotic (e.g., competition) and abiotic (e.g., high salinity, pH, or temperature, nutrients) stress conditions (Finore et al., 2014), a production strategy might be to challenge cell growth and bacterial survival. Higher EPS production is, in some cases, obtained when growth is restricted by a suboptimal temperature of growth, a limitation on nutrient availability (e.g., nitrogen, phosphorous), or by inducing osmotic stress (Delbarre-Ladrat et al., 2014; Poli et al., 2010). Nonetheless, in general, the presence of an organic nitrogen source promotes both growth and EPS production (Poli et al., 2010). For example, EPS production by *Alteromonas* strain 1644 was improved after cell growth was controlled by substituting the complex medium by a mineral defined medium that contained ammonium chloride as sole nitrogen source (Samain et al., 1997). After exponential growth, a feeding solution containing a low concentration of nitrogen was supplied to the bioreactor to maintain the synthesis of essential proteins. Nitrogen did not accumulate in the medium, suggesting that cell growth ceased due to nitrogen limitation, and an increase of 50% of the EPS yield was observed compared to the complex medium (Samain et al., 1997). However, for other marine bacteria (e.g., *Halomonas caseinilytica* K1), EPS production was maximized during exponential cell growth and, hence, growth limiting conditions might not be

adequate for maximal EPS synthesis (Joulak et al., 2022; Poli et al., 2010). Additionally, the cultivation conditions might also affect the polymer's composition, molecular mass distribution or degree of branching, thus affecting its properties (Delbarre-Ladrat et al., 2014; Finore et al., 2014).

1.6. Motivation

EPS are interesting macromolecules that can significantly contribute to the arising of more sustainable bio-based products in multiple commercial markets. Marine habitats, due to their unique conditions, are considered excellent sources of high-value biomolecules with improved properties. Despite their biodiscovery potential, marine environments are still overlooked and underexploited as sources of novel EPS-producing microorganisms. In line with the EU bio-based economy issue, with research areas that include novel sources of bioproducts, added-value bioproducts and bioprocesses, this PhD thesis aimed at exploring marine microorganisms (bacteria and microalgae) as sources of advanced EPS with potential application as biomaterials and/or bioactive compounds. The applicability of the EPS on specific areas, namely cosmetics, biomedical and/or pharmaceuticals, was defined according to their functional and bioactive properties.

Bioactive EPS with potential use in such high-value areas might considerably increase the bioprocess' economic viability since it represents a biotechnological route for the generation of novel products with high market value. To reduce the production costs and improve their competitiveness, the EPS production process was investigated using agro-industrial wastes as carbon sources.

1.7. Thesis outline

The work developed in this PhD thesis is organized in eight chapters. Each chapter includes a short description of the context, presents the materials and methods used and discusses the results and main conclusions obtained. The methodology used in each individual chapter is detailed in the context of the respective subject and, when applicable, is related to that used in previous chapters. In this thesis, both microalgae and bacteria were investigated as EPS producers in sections 2 and 3, respectively. After an initial screening, one microalga species and one bacterial strain were selected for bioreactor cultivation and investigation of the EPS' properties. A brief description of the contents of each chapter is explained:

Section 1 – Background and motivation – introduces an overview of the state of the art and provides some insight on the motivation of this PhD thesis.

Section 2 – Microalgae exopolysaccharides:

Chapter 2.1. – Bioprospecting for new EPS-producing microalgae – is dedicated to the investigation of different marine microalgae as EPS producers. Both the production yields and EPS composition were investigated.

Chapter 2.2. – Novel bioactive EPS produced by the microalgae *Heterocapsa* AC210: production and characterization – describes the standard cultivation for EPS production of *Heterocapsa* AC210, the microalgae chosen based on the results from Chapter 2.1. Additionally, the produced EPS was characterized for its chemical and linkage composition, molecular mass distribution, cytotoxicity, thermal and biological properties, specifically its antioxidant and anti-inflammatory capacity.

Section 3 – Bacterial exopolysaccharides:

Chapter 3.1. – Bioprospecting for new EPS-producing bacteria from unusual marine environments – reports the screening for EPS production of six *Alteromonas* strains isolated from *French Polynesia* marine environments. The EPS compositions, molecular mass distribution and thermal properties were investigated. Additionally, the EPS potential as structuring agents was evaluated by determining the preliminary thickening and gel forming capacities.

Chapter 3.2. – Films based on bacterial EPS from unusual marine environments – describes the film forming capacity of the EPS produced by the six *Alteromonas* strains. The morphology, appearance, mechanical and barrier properties of the different films were characterized in this chapter.

Chapter 3.3. – *Alteromonas macleodii* Mo169 EPS production using agro-industrial wastes – investigates the use of the industrial by-product glycerol and apple pulp waste from the juice industry as feedstocks for the production of EPS by *A. macleodii* Mo169, the strain that stood out in Chapter 3.1. The chemical composition and molecular mass distribution of the produced EPS are also described.

Chapter 3.4. – *Alteromonas macleodii* Mo169 EPS potential as structuring biomaterial: thickening and gelling capacity – presents a detailed rheological

study of the EPS produced by *A. macleodii* Mo169. Additionally, its gelling capacity was investigated through a modelling approach.

Chapter 3.5. – *Alteromonas macleodii* Mo169 EPS potential in nanotechnology: bioactive nanoparticle/EPS bio-nanocomposites – deals with the potential of *A. macleodii* Mo169 EPS to be used as reducing and/or stabilizing agent for the synthesis of gold, silver and selenium nanoparticles. The characterization and biological activity, namely antioxidant and wound healing capacity, of the EPS bio-nanocomposites is presented in this chapter.

Section 4 – Conclusions and future work – reviews the main outputs of this work and proposes suggestions for future research.

The work performed during this PhD resulted in one book chapter and three research papers, which have been published in a peer-reviewed international scientific journal. In addition, two manuscripts have already been submitted to international scientific journals and five more are in preparation. The information regarding the publications and the manuscripts is disclosed at the beginning of each chapter.

2

Microalgae Exopolysaccharides

Chapter | 2.1

Bioprospecting for new exopolysaccharide-producing microalgae

The results presented in this chapter resulted in the following manuscript:

Concórdio-Reis, P., David, H., Amorim, A., Reis, M.A.M. & Freitas, F. Bioprospecting for new exopolysaccharide-producing microalgae of marine origin. In preparation.

2.1.1. Summary

Microalgae are photosynthetic organisms that can produce biomolecules with industrial interest, including EPS. Due to their structural and compositional diversity, microalgae EPS present interesting properties that can be considered in cosmetic and/or therapeutic areas. Seven microalgae strains from three different lineages, namely Dinophyceae (phylum Miozoa), Haptophyta and Chlorophyta, were investigated as EPS producers. All strains were found to be EPS producers, though the highest EPS yield was obtained for *Tisochrysis lutea*, followed by *Heterocapsa* sp. AC210 (126.8 and 75.8 mg L^{-1}, respectively). Upon assessment of the polymers' chemical composition, significant contents of unusual sugars, including fucose, rhamnose and ribose, were found. *Heterocapsa* sp. AC210 EPS stood out due to its high content in fucose (40.9 mol%), a sugar known to confer biological properties to the polysaccharides. The presence of sulphate groups (10.6–33.5 wt. %) was also noticed in the EPS produced by all microalgae strains, thus contributing to the possibility that these EPS might have biological activities worth exploring.

2.1.2. Introduction

Microalgae are photosynthetic microorganisms found among diverse water bodies, such as freshwater, seawater, hypersaline waters (Hamidi et al., 2019; Wu et al., 2021). Microalgae represent a huge taxonomic diverse group including theoretically between 200 000 and 800 000 different species, of which only 50 000 have been identified (Gaignard et al., 2019; Hamidi et al., 2019; Wu et al., 2021). This photosynthetic group can be divided in prokaryotes, namely blue-green algae (Cyanobacteria), and eukaryotes, which include green microalgae (Chlorophyta and Charophyta), red microalgae (Rhodophyta) and brown-golden microalgae (Ochrophyta, Haptophyta and Dinophyceae) (Gaignard et al., 2019; Hamidi et al., 2019). As photosynthetic microorganisms, microalgae use light and inorganic nutrients, including CO_2, to synthesize complex organic molecules (Hamidi et al., 2019), being the source of the food chain for more than 70% of the world's biomass (Singh & Saxena, 2015). Additionally, these microorganisms are a rich source of natural functional materials with industrial interest, including polyunsaturated fatty acids (PUFAs), pigments, essential vitamins and minerals, antioxidants, enzymes, peptides, and polysaccharides (Laroche, 2022; Wijesekara et al., 2011).

Among the high value compounds, EPS are very promising due to their biological activities, such as immunomodulatory, anti-inflammatory, anti-cancer,

antioxidant, anti-coagulant, antibacterial and anti-viral properties (Freitas et al., 2021; Gaignard et al., 2019; Raposo et al., 2013). EPS from eukaryotic microalgae are usually very complex heteropolysaccharides, with rare sugars (e.g., fucose or rhamnose), uronic acids and non-sugar groups, such as sulphate and methyl groups in their composition (Freitas et al., 2021; Laroche, 2022). Cyanobacterial EPS' compositions are apparently more conserved, usually with fewer sugar monomers and glucose as the main or second monosaccharide (Laroche, 2022). Despite their potential and the large taxonomic diversity, the majority of microalgae explored as EPS producers belong to the eukaryotic families Desmidiaceae, Chlamydomonadaceae and Chlorellaceae, Porphyridiaceae and Glaucosphaeraceae (Gaignard et al., 2019).

Nonetheless, different screening studies have been performed to increase the knowledge of microalgae as EPS-producers (De Philippis et al., 1998; Di Pippo et al., 2013; Gaignard et al., 2019). For example, Gaignard et al. (2019) evaluated the EPS production capacity of 150 microalgae strains from diverse phylogenetic groups and compared those results with the literature to find a possible relationship between EPS production and phylogenic group. Out of those, 49 were classified as EPS producers and the composition analysis reported the monosaccharide composition of 16 new EPS produced by microalgae from 7 genera, including species belonging to the Isochrysidacae and Pavlovaceae families (Haptophyta), and Chlorodendraceae and Prasinococcaceae families (Chlorophyta) (Gaignard et al., 2019).

In line with this, the present study aimed at investigating the EPS production ability of seven microalgae strains belonging to microalgae groups for which little information is available, namely belonging to the Dinophyceae families Ostreopsidaceae, Gymnodiniaceae and Heterocapsaceae, the Haptophyta families Noelaerhabdaceae and Isochrysidaceae, and the Chlorophyta families Dunaliellaceae, and Coccomyxaceae. In addition, the synthesized EPS were characterized in terms of their chemical composition.

2.1.3. Materials and methods

2.1.3.1. Microorganisms and media

The screening was performed on seven marine microalgae species from ALISU, the Algae collection from University of Lisbon (Table 2.1.1). The microalgae were cultivated in f/2 medium (Guillard & Ryther, 1962) which was prepared using

natural seawater (Naturitas, Spain), after salinity adjustment (30 g L^{-1}) and sterilization (121 ºC, 20 min, 2 bar).

Table 2.1.1. Microalgae strain and origin.

Microalgae strain	Geographical Origin
Coolia monotis	Portuguese coast (Cascais)
Amphidinium carterae	Portuguese coast (estuary of the Mira River)
Heterocapsa sp. AC210	Spanish coast (Balearic Sea)
Emiliania huxleyi	Portuguese coast (Sesimbra)
Tisochrysis lutea	unknown
Dunaliella sp.	unknown
Coccomyxa sp.	Portuguese coast (west coast)

2.1.3.2. Screening procedure

The microalgae were cultivated photoautotrophically in 500 mL flasks containing 250 mL of medium inoculated with 125 mL of microalgae culture in the exponential phase of growth. The cultures were maintained at 20 ºC, with 16/8 hour light/dark cycles, with a light intensity of 56 µmol s^{-1} m^{-2}, provided by three external fluorescent lamps (4000 K). The incident light intensity was measured with a LI-COR light meter (LI-250 A), equipped with a pyranometer sensor LI-200 SA (LI-COR, USA).

The strains were cultivated for 30 days. At the end of the cultivation, the cultivation broth was centrifuged (11000 × *g*, 45 min, 10 ºC), the pellet and the supernatant were used for biomass and EPS quantification, respectively.

2.1.3.3. Analytical techniques

For cell dry weight (CDW) determination, the cells were washed twice with ammonium formate (0.5 M) by re-suspension of the cell pellet and centrifugation (11000 × *g*, 45 min, 10 ºC). The obtained pellets were freeze dried and weighted for determination of the final CDW. For EPS quantification, three volumes of cold ethanol (-20 ºC, 24 h) were added to the cell free supernatants for EPS precipitation. After centrifugation (11000 × *g*, 45 min, 10 ºC), the EPS were resuspended in deionized water and dialyzed using a 3.5 kDa NMWCO (nominal molecular weight cut-off) membrane (ZelluTrans/Roth) against deionized water, at room temperature, under constant stirring. The efficiency of the process (i.e., removal of low molecular weight

compounds) was monitored by measuring the conductivity of the dialysis water until it reached a value bellow 10 μS cm^{-1}. Sodium azide (10 mg L^{-1}) was added to prevent any biological contamination and possible EPS degradation. Finally, the EPS solutions were freeze dried for 48 h and the EPS concentration was determined gravimetrically.

2.1.3.4. EPS composition

The polymers' monosaccharide composition and acyl groups content were determined after controlled hydrolysis as previously reported by Concórdio-Reis, Reis, et al. (2020). Briefly, the lyophilized EPS samples were dissolved in deionized water (1 g L^{-1}) and hydrolyzed with 2% (v/v) trifluoroacetic acid (TFA, 99%), at 120 ºC, for 2 h. The hydrolysates were used for the identification and quantification of the constituent monosaccharides by liquid chromatography (HPLC) using a Carbopac PA10 column (Thermo Scientific™ Dionex™, Sunnyvale, CA, USA) equipped with an amperometric detector. Fucose (Fuc), rhamnose (Rha), arabinose (Ara), glucosamine (GlcN), galactosamine (GalN), galactose (Gal), glucose (Glc), ribose (Rib), glucuronic acid (GlcA), galacturonic acid (GalA), and fructose (Fru) (Sigma-Aldrich) were used as standards (1 to 100 ppm). The same compounds were added to the samples (20 ppm) to confirm the monomers' identification. For mannose identification and quantification, the analysis was performed using a Carbopac SA10 4 × 250 mm column (Thermo Scientific™ Dionex™, Sunnyvale, CA, USA) and the same amperometric detector, at 40 °C, using NaOH (1 mM, 1.2 mL min^{-1}) as eluent (Joulak et al., 2022).

The acid hydrolysates were also used for the quantification of acyl groups by HPLC with an Aminex HPX-87H 300×7.8 mm column (Biorad, Hercules, CA, USA) coupled with UV detector (210 nm), as described by Concórdio-Reis, Reis, et al. (2020). Acetate, pyruvate, and succinate (Sigma-Aldrich) were used as standards at concentrations between 0.015 and 1.0 g L^{-1}.

Sulphate concentration in the hydrolysates was determined by HPLC using a Thermo Ionpac AS9-HC 250x4 mm column and a Thermo Ionpac AG11HC column (Thermo Scientific™ Dionex™, Sunnyvale, CA, USA), equipped with a conductivity detector. The analysis was performed at 25 ºC, using sodium acetate (8 mM) at a flow rate of 1 mL min^{-1}.

2.1.4. Results and discussion

2.1.4.1. Biomass and exopolysaccharide production

The seven strains were selected from diverse phylogenetic groups, including classes and families not previously described for EPS production (Table 2.1.2). The different microalgae strains were grown on f/2 medium for 30 days. Cell growth was observed for all the microalgae strains, with CDW values in the range of 0.11–0.30 g L^{-1} (Table 2.1.2). The EPS yield was dependent on the microalgae strain, but *Tisochrysis lutea* stood out as the best EPS producer among the tested strains, with a concentration of 0.127±0.035 g L^{-1}, followed by *Heterocapsa* sp. AC210 that produced 0.076±0.003 g L^{-1}. In fact, *Heterocapsa* sp. AC210 had a higher EPS concentration (0.08 g L^{-1}) than what was previously reported for this specie and other microalgae belonging to the Miozoa phylum (0.01–0.05 g L^{-1}) (Gaignard et al., 2019). These differences might be due to variations in the cultivation conditions, namely irradiance, agitation and/or the cultivation time. Within the Dinophyceae, only *Gymnodinium impudicum* strain KG03 presented a higher EPS production (0.135 g L^{-1}) after the optimization of the cultivation conditions (Yim et al., 2003). Regarding the other studied microalgae strains, the values obtained were within the range reported in screening assays of microalgae from the same phyla: Miozoa (0.01–0.05 g L^{-1}), including *A. carterae* (0.05 g L^{-1}); Haptophyta (0.02–0.77 g L^{-1}), including *E. huxleyi* (0.07 g L^{-1}) and *Isochrysis braardii* (0.06 g L^{-1}); and Chlorophyta (0.01–0.21 g L^{-1}), that included two *Dunaliella* strains (0.02–0.06 g L^{-1}) (Gaignard et al., 2019).

In addition to the differences in EPS extraction and quantification methods, as EPS are often produced as a response to stress conditions, the EPS yield also depends on the cultivation conditions, such as the availability of nutrients, salinity, temperature or irradiance (Laroche, 2022). Since the metabolic pathways are not resolved yet, it is not possible to predict which parameter will improve EPS synthesis, thus, the optimal operational conditions have to be investigated for each strain (Laroche, 2022). For example, *Dunaliella salina* EPS production was enhanced from 56 to 944 mg L^{-1} when the medium's salinity was increased from 0.5 to 5 M (Mishra & Jha, 2009). That strain has the typical cellular organelles of green algae but lacks a rigid polysaccharide cell wall. Therefore, its survival in high salinity environments is due to the protection effect of the EPS produced, which reduces the penetration of ions through the cell surface (Mishra & Jha, 2009).

Table 2.1.2. Biomass and EPS obtained for the seven microalgae strains cultivated in this study.

Phyla	Classes	Families	Microalgae strain	CDW (g L^{-1})	EPS (mg L^{-1})
Miozoa	Dinophyceae	Ostreopsidaceae	*Coolia monotis*	0.13±0.04	10.4±0.6
		Gymnodiniaceae	*Amphidinium carterae*	0.30±0.02	33.4±0.1
		Heterocapsaceae	*Heterocapsa* sp. AC210	0.11±0.03	75.8±3.3
Haptophyta	Coccolithophyceae	Noelaerhabdaceae	*Emiliania huxleyi*	0.12±0.05	43.1±3.2
		Isochrysidaceae	*Tisochrysis lutea*	0.15±0.04	126.8±34.8
Chlorophyta	Chlorophyceae	Dunaliellaceae	*Dunaliella* sp.	0.24±0.06	59.8±6.2
	Trebouxiophyceae	Coccomyxaceae	*Coccomyxa* sp.	0.22±0.03	46.0±5.3

Table 2.1.3. EPS chemical composition (Ara, arabinose; Fuc, fucose; Fru, fructose; Gal, galactose; GalA, galacturonic acid; GalN, galactosamine; Glc, glucose; GlcA, glucuronic acid; GlcN, glucosamine; Man, mannose; Rha, rhamnose; Rib, ribose; Xyl, xylose).

Microalgae strain	Monosaccharide composition (mol%)													Sulphate (wt.%)
	Xyl	Man	Fuc	Gal	Glc	Rha	GalN	GlcN	Ara	Rib	GlcA	GalA	Fru	
Coolia monotis	33.3	2.4	6.1	43.9	8.3	-	-	3.4	-	-	2.2	-	-	17.7
Amphidinium carterae	4.2	4.8	1.0	44.0	25.0	7.2	-	3.5	2.7	1.2	-	6.1	-	28.2
Heterocapsa sp. AC210	8.2	4.4	40.9	31.7	6.6	-	2.1	1.7	-	-	-	3.9	-	14.4
Emiliania huxleyi	14.6	5.1	2.0	10.2	3.4	15.3	-	-	20.4	8.4	-	5.9	14.6	33.5
Tisochrysis lutea	11.0	18.1	1.0	31.9	2.7	-	-	-	22.8	-	2.4	9.3	-	10.6
Dunaliella sp.	14.1	22.1	-	6.8	9.1	29.2	-	-	4.5	-	4.8	8.9	-	13.7
Coccomyxa sp.	1.2	10.0	3.8	76.5	2.4	6.0	-	-	-	-	-	-	-	15.6

2.1.4.2. Exopolysaccharide composition

The chemical composition of the EPS produced by the seven microalgae is presented in Table 2.1.3. Although all the EPS were heteropolysaccharides, their compositions were extremely variable. The EPS produced by three Dinophyceae strains was characterized. Although previously reported dinoflagellates' EPS were quite simple, composed of up to three different sugar monomers (Hasui, Matsuda, Okutani, et al., 1995; Hasui, Matsuda, Yoshimatsu, et al., 1995; Mandal et al., 2011), this was not the case for the EPS of *Coolia monotis*, *Heterocapsa* sp. AC210, and *Amphidinium carterae*, since they presented between 7 to 10 different monosaccharides in their composition (Table 2.1.3).

High contents of Gal were found for the EPS of the three dinoflagellates species, namely *C. monotis* (43.9 mol%), *A. carterae* (44.0 mol%) and *Heterocapsa* sp. AC210 (31.7 mol%). EPS with high Gal contents have been reported previously, including the EPS secreted by *Gymnodinium* A_3 OKU-1, a homopolysaccharide composed of Gal (Hasui, Matsuda, Yoshimatsu, et al., 1995), and that produced by *A. carterae*, which was composed of Gal and Glc (73 and 27 mol%, respectively) (Mandal et al., 2011). In this study, the EPS of *A. carterae* was also mainly composed of Gal and Glc (44 and 25 mol%), although Xyl, Man, Fuc, Rha, GlcN, Ara, Rib and GalA were detected but at concentrations bellow 7.2 mol% (Table 2.1.3). Interestingly, *C. monotis* EPS, besides Gal (43.9 mol%), had a high content of Xyl (33.3 mol%), a sugar that was not reported in dinoflagellates before. In addition to Gal, *Heterocapsa* sp. AC210 EPS also had a high content of Fuc, which accounted for 40.9 mol% of the polymer's sugar composition (Table 2.1.3). Fuc is a rare sugar often associated with biological activity (Concórdio-Reis et al., 2021; Roca et al., 2015), which so far had never been reported in dinoflagellates' EPS.

Although both tested Haptophyta microalgae, *Emiliania huxleyi* and *Tisochrysis lutea*, produced EPS rich in Ara (20.4 and 22.8 mol%, respectively), in accordance with previous reports for microalgae producers from this group (Gaignard et al., 2019; Laroche, 2022), *Tisochrysis lutea* presented a higher Gal content (31.9 mol%) (Table 2.1.3). *E. huxleyi* EPS composition also included a significant fraction (8.4–15.3 mol%) of the rare sugar Rha, as well as Rib and Fru (Table 2.1.3). Comparable amounts of Xyl (11.0 and 14.6 mol%), Fuc (1.0 and 2.0 mol%), Glc (2.7 and 3.0 mol%) and GalA (5.9 and 9.3 mol%) were detected in the composition of the EPS produced by both strains. *Isochrysis braarudii* (RCC3686) and *Isochrysis* sp. (RCC6688) were recently investigated as EPS producers by Gaignard et al. (2019). The EPS secreted by the two

strains also had high levels of Gal (23–46 mol%), but *I. braarudii* EPS also comprised Ara and Xyl (39–47 and 18–19 mol%, respectively), with traces of Rha, Glc, GlcA and Rib; whereas *Isochrysis* sp. EPS had a high content of Man and Rha (32–34 and 15–19 mol%, respectively), with traces of Ara and GlcA (Gaignard et al., 2019). Except for Rha and Rib, which were not detected in this study, the same sugar monomers were reported. It should be noted that the composition of the EPS strongly depends on the cultivation conditions, downstream processes and the analytical methodologies (Laroche, 2022).

Dunaliella sp. (RCC5) was recently reported to produce an EPS mainly composed of Gal, Rha, Xyl, Man and GalA (28,21,17,13 and 11 mol%, respectively) with traces of Glc, Ara and GlcA (Gaignard et al., 2019). In this study the EPS from *Dunaliella* sp. had the same sugar monomers, although different proportions were observed (Table 2.1.3). Rha, Man, Xyl, Glc and GalA were the monosaccharides found at higher concentrations (29.2, 22.1, 14.1, 9.1 and 8.9 mol%, respectively), whereas Gal, GlcA and Ara were detected at concentrations below 7 mol% (Table 2.1.3). Also belonging to the Chlorophyta phylum, *Coccomyxa* sp. produced an EPS mainly composed of Gal (76.5 mol%), which is a common feature of EPS from this phylum (Gaignard et al., 2019).

The presence of Rha, Fuc, Rib or uronic acids makes the EPS excellent candidates for various applications due to their potential to possess bioactive properties, such as anti-inflammatory, antioxidant antiviral activity (Concórdio-Reis et al., 2021). Rha can be used as precursor for the synthesis of aroma and flavors, and Fuc is found in the composition of anticarcinogenic and anti-inflammatory drugs, and in skin care formulations for its capacity to accelerate wound healing and moisturizing properties (Concórdio-Reis et al., 2021; Roca et al., 2015). Additionally, Rib has presented several benefits in clinical trials by promoting a more youthful, radiant, and healthy appearance to the skin (St.Cyr, 2009).

Of notice was the presence of high sulphate contents in all the microalgae's EPS (10.6–33.5 wt.%), which was previously detected only in *A. carterae* EPS (Mandal et al., 2011), but never quantified for any of these strains. Apart from contributing to the anionic character of the EPS, the presence of sulphate groups in polysaccharides is linked to many health beneficial effects, such as antioxidant, anticoagulant, anti-viral, antibacterial, and immunomodulatory activities (Freitas et al., 2021; Raposo et al., 2013). However, such biological properties might be dependent on other factors in addition to the sulphation level, such as the distribution of the sulphate group in the

polymer's chain, the sugar composition, and stereochemistry (Phélippé et al., 2019; Senni et al., 2013).

2.1.5. Conclusions

In this chapter, seven microalgae belonging to three different phyla were screened for EPS production. The chemical composition of the EPS was determined, including those produced by *Coolia monotis*, *Heterocapsa* sp. AC210, *Coccomyxa* sp., and *Emiliania huxleyi*, whose composition was never reported before. The results revealed the presence of unusual sugars, such as fucose, rhamnose and ribose, and high contents in sulphate. These features are often associated with interesting biological properties that are worth exploring in the future. Nonetheless, based on novelty, EPS yield and polymer's composition, *Heterocapsa* sp. AC210 was the microalgae EPS-producer chosen for further investigation.

Chapter | 2.2

Novel bioactive EPS produced by microalga *Heterocapsa* AC210: production and characterization

The results presented in this chapter were submitted to the following international scientific journal:

Concórdio-Reis, P., Cardeira, M., Macedo, A.C., Ferreira, S.S., Serra, A.T., Coimbra, M.A., Amorim, A., Reis, M.A.M. & Freitas, F. Marine dinoflagellate *Heterocapsa* AC210: exopolysaccharide production, characterization, and biological properties. Submitted to *Algal Research*.

Exopolysaccharide composition analysis was performed by Professor Manuel A. Coimbra from University of Aveiro. The biological assays were performed in collaboration with Dr. Ana Teresa Serra from Instituto de Biologia Experimental e Tecnológica.

2.2.1. Summary

Marine microalgae are promising sources of novel valuable biomolecules such as proteins, carotenoids, lipids, or polysaccharides. Among them, dinoflagellates are still understudied as sources of valuable products. In this study, the dinoflagellate *Heterocapsa* sp. AC210 was described as a new EPS producer. The cultivation and EPS production in bioreactor was evaluated for the first time in detail and was found to be partially growth associated. *Heterocapsa* sp. AC210 produced an EPS composed of seven different sugar monomers, including fucose and glucosamine, which are quite rare and have never been reported in dinoflagellates' EPS. Moreover, the EPS had a high content of sulphate (29.7 wt.%), which is often associated with biological properties. Cytotoxicity was accessed in human keratinocytes and fibroblasts, and the results showed that the EPS did not reduce cell viability of both cell lines for concentrations up to 1 g L^{-1}. Additionally, antioxidant and anti-inflammatory assays demonstrated that the EPS reduced by 18% the intracellular reactive oxygen species and decreased up to 79.3% and 46.2% the IL-8 and IL-6 secretion in keratinocytes, which supports its potential application in the cosmeceutical and biomedical fields.

2.2.2. Introduction

Microalgae are photoautotrophic microorganisms, with a key role in carbon sequestration since they convert CO_2 into organic carbon at a rate higher than organic breakdown (Gaignard et al., 2019; Jajesniak et al., 2014). In fact, microalgae account for nearly half of both CO_2 captured and O_2 produced by photosynthetic organisms annually (Freitas et al., 2021).

Currently, there are several thousands of known microalgae species (Gaignard et al., 2019) that are present in different evolutionary lines, have contrasting ecological requirements and an enormous metabolic diversity that makes them good candidates for biodiscovery (Freitas et al., 2021). High-value biomolecules produced by microalgae include natural pigments, polyunsaturated fatty acids (PUFAs), lipids, proteins, antioxidants, vitamins, and EPS, that are interesting to many industries, such as pharmaceutical, nutraceutical, food/feed production and skin-care (Ariede et al., 2017; Delattre et al., 2016; Gaignard et al., 2019; H.-M. D. Wang et al., 2017). Among these different compounds, microalgae EPS are very promising, since they have been reported to have many biological properties, including anti-inflammatory, immunomodulatory, antiviral, antibacterial, antitumor and antihyperlipidaemic activities, as well as anti-coagulant and/or anti-thrombotic properties (Ferreira et al., 2015; Jesus Raposo et al., 2015; Liu et al., 2016; Singh, Kant et al., 2019; Xiao & Zheng, 2016).

However, only recently the relevance of microalgae as producers of valuable polysaccharides has started to be considered (Delattre et al., 2016). Nevertheless, EPS producers have been identified in several microalgae, including prokaryotic cyanobacteria, within families Oscillatoriaceae, Nostocaceae and Microcoleaceae, and eukaryotic lineages, belonging to phyla Rhodophyta (Glaucosphaeraceae, Porphyridiaceae), Chlorophyta (Chlamydomonadaceae, Chlorellaceae), Charophyta (Desmidiaceae), and Bacillariophyta (Gaignard et al., 2019).

Within kingdom Chromista, dinoflagellates (Dinophyceae) are a particularly interesting group due to their distinctive ecological and metabolic properties. These unicellular planktonic microalgae are found in all types of aquatic ecosystems (freshwater, marine, sea ice) and have a high trophic diversity (autotrophs, mixotrophs, heterotrophs, parasites, and symbionts) (Assunção et al., 2017). Some dinoflagellates have been reported to produce EPS with valuable properties, namely *Margalefidinium polykrikoides* (cited as *Cochlodinium polykrikoides*), that synthesized a sulphated EPS composed of mannose, galactose and glucose with anti-viral activity (Hasui, Matsuda, Okutani, et al., 1995); and two *Gymnodinium* spp., both produced sulphated homopolysaccharides of galactose with immunomodulatory and antitumor activities (Bae et al., 2006; Hasui, Matsuda, Yoshimatsu, et al., 1995; Umemura et al., 2003; Yim et al., 2007; Yim, Kim, Ahn, et al., 2004). Surprisingly, the description of dinoflagellates' EPS with biological activity is, to our knowledge, limited to the examples provided above. Given this, the exploitation of dinoflagellates as sources of EPS holds great potential to develop a strategy to capture CO_2 while producing high-value products from currently underexploited microalgae sources.

In this context, the dinoflagellate *Heterocapsa* AC210 was evaluated for the first time as an EPS producer. Microalgae growth and EPS production were investigated, and the produced EPS was characterized in terms of its chemical and linkage composition, molecular mass distribution, and thermal properties. Moreover, *in vitro* studies were conducted to assess the EPS cytotoxicity and biological properties, namely antioxidant and anti-inflammatory activities.

2.2.3. Materials and methods

2.2.3.1. Microorganism, pre-cultivation, and cultivation media

The microalga used in this work, *Heterocapsa* strain AC210, originally isolated from the Balearic Sea (Spain), was obtained from the Roscoff Culture Collection (accession number RCC1514). The strain was cultured in sterile f/2 media (no added

Si) (pH 8.2), with the composition described in Table 2.2.1 (Guillard & Ryther, 1962), which was prepared using natural seawater (Naturitas, Spain), after salinity adjustment (30 g L^{-1}) and sterilization (121 ºC, 20 min, 2 bar). The culture was maintained at 20 ºC, 16:8 hour light/dark cycles, with frequent dilutions (1:2, 30 days) of the cultures in fresh F/2 medium. The inoculum was prepared by adding fresh f/2 medium (100 mL) to the microalga cultures (100 mL) and incubation at 20 ºC, with 16:8 hour light/dark cycles and a light intensity of 32 µmol s^{-1} m^{-2}, provided by external fluorescent lamps (4000 K), for 7 days. The incident light intensity was measured with a LI-COR light meter (LI-250 A), equipped with a pyranometer sensor LI-200 SA (LI-COR, USA).

Table 2.2.1. Composition of medium f/2 and medium NBP.

Nutrients	f/2 (mM)	NBP (mM)
Cyanocobalamin (vitamin B12)	3.69×10^{-7}	2.21×10^{-6}
Thiamine.HCl (vitamin B1)	2.96×10^{-4}	1.32×10^{-4}
Biotin (vitamin H)	2.05×10^{-6}	2.05×10^{-5}
$NaNO_3$	8.82×10^{-1}	2.00
NaH_2PO_4	3.62×10^{-2}	-
KH_2PO_4	-	1.00×10^{-1}
Na_2EDTA	1.17×10^{-2}	2.64×10^{-2}
$FeCl_3$	1.17×10^{-2}	2.00×10^{-2}
$CuSO_4$	3.93×10^{-5}	1.00×10^{-4}
$CoCl_2$	4.20×10^{-5}	1.00×10^{-4}
$MnCl_2$	9.10×10^{-4}	1.00×10^{-3}
Na_2MoO_4	2.60×10^{-5}	1.00×10^{-4}
$ZnSO_4$	7.65×10^{-5}	1.00×10^{-3}
$ZnCl_2$	-	1.00×10^{-3}
$MgSO_4$	-	2.00×10^{-3}

The photobioreactor experiments were conducted in NBP medium (NutriBloom Plus). NBP medium was prepared by supplementing natural seawater with 1 mL L^{-1} of commercial culture medium NutriBloom Plus (Necton S.A., Portugal) (Gao et al., 2021). The final composition (after dilution) of medium NBP is presented in Table 2.2.1. This medium was chosen since it had a higher nutrient content compared to f/2 medium and could enhance microalga growth. HEPES (4-(2-hydroxyethyl)piperazin-1-ethanesulphonic acid) (20 mM) was added as pH buffer and the pH was adjusted to 8.0 by addition of NaOH (1 M).

2.2.3.2. Photobioreactor experiments

Heterocapsa AC210 was cultivated in a cylindrical heat-sterilized 2 L bioreactor (BioStat B-plus, Sartorius, Germany) equipped with 4 sets of 30 LED lamps (4000 K) providing an incident light intensity of 98 µmol s^{-1} m^{-2} in a 16:8 h light/dark cycle. The bioreactor vessel was covered with a black acrylic structure to prevent the interference of natural light (Fig. 2.2.1). Filtered air (0.2 µm) was provided at a constant flow rate of 0.4 SLPM (standard liters per minute, of compressed air) and the off gas was cooled in a condenser. The temperature was controlled at 25 ºC and the stirring (70 rpm) was provided by two six blade impellers. In all experiments, the photobioreactor was inoculated with a 10% (v/v) inoculum prepared as described above, with a starting OD_{750} of 0.015 ± 0.003. Culture broth samples (15 mL) were recovered daily from the photobioreactor for quantification of cell growth, nutrients' concentration, and EPS production. Each experiment was performed in at least duplicate photobioreactor runs.

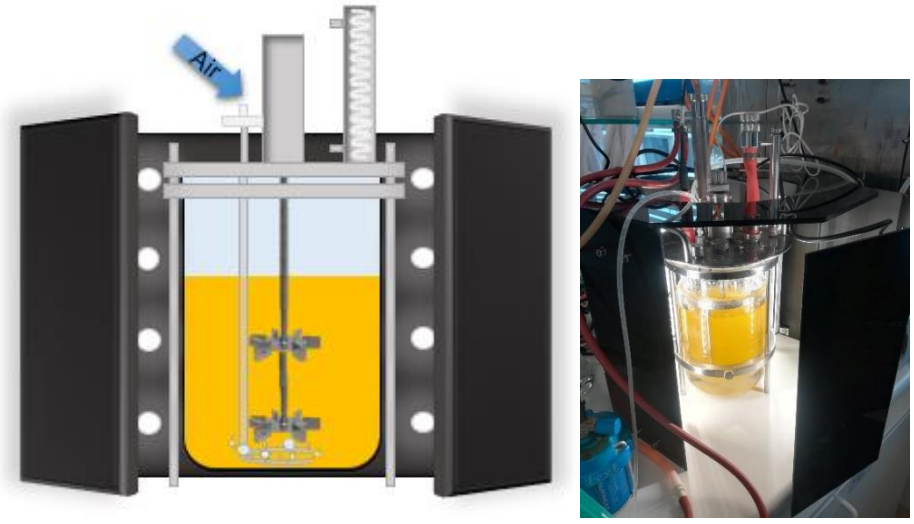

Figure 2.2.1. Experimental set-up used in the bioreactor cultivation of *Heterocapsa* AC210.

2.2.3.3. Analytical techniques

Cell growth was monitored during the photobioreactor runs, by measuring the culture broth's optical density (OD) at 750 nm, using a UV-Vis spectrophotometer (CamSpec M509T), in duplicate analysis. This wavelength was previously reported for determination of cell growth for different microalgae strains without pigment interference (Gaignard et al., 2019; Medina-Cabrera et al., 2020). For high cell concentrations (optical density higher than 1.0), samples were diluted in 0.5 M ammonium formate.

At the end of the runs, the cultivation broth was recovered from the photobioreactor and used for the gravimetric determination of the cell dry weight (CDW). Culture broth samples (240 mL) were centrifuged (11000 × *g*, 45 min, 10ºC) and the recovered cells were washed twice with ammonium formate (0.5 M) by re-suspension of the cell pellet and centrifugation (11000 × *g*, 45 min, 10ºC). The obtained pellets were freeze dried and weighted for determination of the final CDW. Triplicates were used for this analysis. The correlation between the OD_{750} and the CDW (R^2=0.997), used to estimate the CDW (g L^{-1}) of the samples withdrawn during the cultivation experiments, was determined to be as follows (Eq. 2.2.1):

$$\mathrm{CDW} = \frac{\mathrm{OD}_{750} - 0.0054}{1.7002} \quad (2.2.1)$$

The samples' cell-free supernatant was used for the quantification of nitrate and phosphate and EPS production. Nitrate and phosphate concentration was determined by colorimetry using a flow segmented analyzer (Skalar 5100, Skalar Analytical, The Netherlands) (Concórdio-Reis et al., 2018). EPS concentration was measured as glucose equivalent by a modified Anthrone method (Dutta & Bhadury, 2020). Anthrone (Sigma-Aldrich) solution (0.125% in 95% sulphuric acid, Honeywell Fluka™) was freshly prepared 2 h before use. The supernatant sample (0.5 mL) was added to a test tube containing 2.5 mL cold anthrone reagent, while the tube was kept immersed in cold water. The tubes were gently stirred to avoid heat generation and incubated for 14 min at 100 ºC. After cooling on ice, the optical density was measured at 625 nm in a UV-Vis spectrophotometer. Glucose (Scharlau) solutions (5–100 mg L^{-1}) were used as standards. All analyses were performed in duplicate. Elemental analysis was performed for the EPS and the biomass, using an elemental analyzer (Thermo Finnigan-CE Instruments, Flash EA 1112 CHNS series, Italy).

2.2.3.4. Kinetic parameters calculation

The maximum specific cell growth rate μ_{max} (d^{-1}) was calculated using the following equation (2.2.2):

$$\ln\left(\frac{x}{x_0}\right) = \mu_{max} \times t \quad (2.2.2)$$

where x_0 is the initial biomass concentration (g L^{-1}). The overall EPS volumetric productivity (r_p, mg L^{-1} d^{-1}) and the biomass volumetric productivity (r_x, g L^{-1} d^{-1}) were determined according to eqs. (2.2.3) and (2.2.4), respectively:

$$r_p = \frac{\Delta p}{\Delta t} \quad (2.2.3)$$

$$r_x = \frac{\Delta x}{\Delta t} \quad (2.2.4)$$

where Δp and Δx corresponds to the EPS (mg L^{-1}) and biomass (g L^{-1}) produced during the cultivation run, respectively, and Δt interval (days) corresponds to the duration of the cultivation run. The specific EPS productivity (q_p, g_{EPS} g_{CDW}^{-1} d^{-1}) was calculated using the following equation (2.2.5):

$$q_p = \frac{r_p}{\Delta x} \quad (2.2.5)$$

2.2.3.5. EPS extraction and purification

At the end of the cultivation runs, the culture broth was centrifuged (11000 × *g*, 45 min, 10ºC) and the supernatant was dialyzed using a 3.5 kDa NMWCO membrane (ZelluTrans/Roth) against deionized water, at room temperature, under constant stirring. The efficiency of the process (i.e., removal of low molecular weight compounds) was monitored by measuring the conductivity of the dialysis water until it reached a value bellow 10 µS cm^{-1}. Sodium azide (10 mg L^{-1}) was added to prevent any biological contamination and possible EPS degradation. The purified EPS solution was concentrated in a rotary evaporator (Büchi Rotavapor R-210, Switzerland) operating at a pressure of 19 mbar and a temperature of 50 ºC. Finally, the solution was freeze-dried, and the EPS was weighted and kept in a closed vessel.

2.2.3.6. EPS Physical and chemical characterization

Carbohydrate composition

The EPS was analyzed for its neutral sugar content after acid hydrolysis with 200 µL of 72% (w/w) H_2SO_4 for 3 h at room temperature, followed by 2.5 h at 100 ºC in 1 M H_2SO_4 (Blakeney et al., 1983; Selvendran et al., 1979), derivatization to alditol acetates, and analysis of individual neutral sugars by gas chromatography with flame ionization detector (GC-FID, Perkin Elmer–Clarus 400). The GC was equipped with a 30 m column DB-225 (J&W Scientific, Fol-som, CA, USA) with i.d. and film thickness of 0.25 mm and 0.15 µm, respectively (Pandeirada et al., 2019). The total sugars were determined by the sum of the amount of the individual sugars, considering that the hydrolysis of a glycosidic linkage results in an addition of a water molecule into the sugar structure.

Uronic acids (UA) were quantified by the *m*-phenylphenol colorimetric method (Blumenkrantz & Asboe-Hansen, 1973), using galacturonic acid (20 to 160 µg mL^{-1}) as standard in a microplate reader (Eon, BioTeK).

To identify amino sugars and uronic acids, the EPS was hydrolyzed with 2 M trifluoroacetic acid (TFA), at 120 ºC, during 1 h, acid evaporated and resuspended in MilliQ water to be analyzed by high-performance anion exchange chromatography with pulsed amperometric detection (HPAEC-PAD). HPAEC-PAD analysis was performed on a Dionex ICS-6000 system consisting of DC chromatography oven and SP pump. Carbohydrates were detected by an electrochemical detector in integrated amperometry mode with AgCl reference electrode and conventional permanent gold electrode, using Chromeleon 7.3 software (Thermoscientific Dionex) and the standard carbohydrate quadruple waveform recommended for use with CarboPac columns. Separation of compounds was carried out using a Dionex CarboPac PA100 guard column (50 mm × 4 mm) and a Dionex CarboPac PA100 analytical column (250 mm × 4 mm) using gradient elution at a 1 $ml.min^{-1}$ flow rate. Eluents used were as follows: eluent A – MilliQ water, eluent B – 500 mM NaOH, eluent C – 500 mM sodium acetate. The solvents were prepared using MilliQ water (18 MΩ.cm resistance or greater); 26.4 mL of 50% sodium hydroxide solution, MERCK, for 1L of eluent B; 41.015 g of sodium acetate, Thermo Scientific™ Dionex™ AAA-Direct Reagents, for 1L of eluent C, filtered through a 0.2 µm nylon filter afterwards. The eluents were used within one week. The working temperature of the column and the detector was 30 °C and initial equilibration was carried out with 0.1% solvent B. Following manual injection of 25 µL sample onto the column, the compounds were eluted with a 55 min programme based on optimization of Dionex CarboPac PA100 Column Product Manual methods as follows: a gradient of A:B:C 99.9:0.1:0 (v/v/v) to 99:1:0 from 0 to 30 min; then a gradient to 50:30:20 (v/v/v) within 5 min, maintained for 20 min. The eluents returned to the initial ratio after the ratio of 30:30:40 for 10 min to clean impurities. Equilibration time was 30 min. To quantify the monosaccharides, calibration curves were prepared for galactose (Gal), mannose (Man), xylose (Xyl), fucose (Fuc), galactosamine (GalN), glucose (Glc), glucuronic acid (GlcA), and galacturonic acid (GalA).

Glycosidic linkage composition

Glycosidic linkage composition of the EPS was analysed by methylation (Passos & Coimbra, 2013) and carboxyl reduction of methylated polysaccharides (Dourado et al., 2004) to detect uronic acids linkages and improve hydrolysis of methylated polysaccharides (Pettolino et al., 2012). The partially methylated alditol acetates were separated and analysed by gas chromatography quadrupole mass spectrometry

(GCqMS) (GC-2010 Plus, Shimadzu, Japan) using a non-polar column HT5 (30 m length, 0.25 mm internal diameter and 0.10 µm stationary phase, Trajan, Australia) as described by Hamed et al. (2022).

Sulphate esters composition

Sulphate esters in the EPS were determined by turbidimetry using the barium chloride method (Dodgson & Price, 1962; Pandeirada et al., 2019). The samples were submitted to a hydrolysis with 2 M TFA at 120 °C for 1 h. Then, 3.8 mL of 3% (w/v) trichloroacetic acid and 1 mL of barium chloride-gelatin reagent (0.5 g of barium chloride in 100 mL of 0.5% (w/v) gelatine solution) were added to 0.2 mL of the hydrolysate, which was kept at room temperature for 15-20 min. The solution was transferred to microplates and analysed at 360 nm (Eon, BioTeK) against reagent blank containing gelatin solution instead of barium chloride-gelatin reagent. The concentration of sulphate esters was determined using K_2SO_4 as standard as SO_4^{2-} (0.05–5 mM).

To evaluate the sulphate position, the EPS were desulphated and submitted to methylation analysis, as described previously (Ferreira et al., 2021).

Pyruvate and lactate composition

Pyruvate and lactate were determined by proton nuclear magnetic resonance (^{1}H NMR) after hydrolysis of 10 mg with 1 mL of 2 M trifluoroacetic acid (TFA), at 120 ºC, during 1 h, in specific speedvac tubes. After acid evaporation, the hydrolysed EPS was freeze-dried twice from 99.9% D_2O and finally dissolved in 500 µL of 99.9% D_2O, containing 1 % (w/w) of 3-(trimethylsilyl)-1-propanesulphonic acid sodium salt (DSS, Sigma-Aldrich, USA) and transferred to NMR tubes (NE-UL5-7, NEWERA, USA). ^{1}H NMR spectrum was acquired at 60 ◦C on Bruker 300 MHz spectrometer using zg30 sequence with 4.75 s of acquisition time and 56 number of scans. DSS was used as internal reference (22.3 µmol, 0.95 ppm) to quantify pyruvate (singlet, 2.55 ppm) and lactate (doublets, 1.55 and 1.58 ppm), according to Uhliariková et al. (2021). The relative areas of ^{1}H NMR resonances were quantified using MestReNova software (Mestrelab Research S.L., Version 14.0.0-23239). Results were expressed as dry weight percentage of EPS.

Fourier transform infrared spectroscopy

Fourier Transform Infra-Red (FTIR) Spectroscopy was recorded on a Perkin-Elmer Spectrum II spectrometer. The spectra were obtained between 500 and 4500 cm^{-1} after 10 scans, at room temperature.

Molecular mass distribution

Number and average molecular weights (Mn and Mw, respectively) of EPS, as well as the polydispersity index (PDI, Mn/Mw), were determined by Size Exclusion-High Performance Liquid Chromatography (SE-HPLC). The analysis was performed at 25ºC on a KNAUER Smartline HPLC equipped with a Phenomenex Phenogel Linear LC Column 300 x 7.8 mm (USA), using 0.1 M $LiNO_3$ as eluent, at a flow rate of 0.6 mL min^{-1}. 50 µL of EPS solution (0.5 w/v% in 0.1 M $LiNO_3$) were injected and a Water 2414 Refractive Index Detector was used for detection. The values of Mw and Mn were calculated using a calibration curve generated with pullulan standards (P50 to P80) (Paz-Samaniego et al., 2015).

Thermogravimetric (TG) analysis

EPS samples (~10 mg) were characterized by Thermogravimetry (TG) using a Thermogravimetric Analyzer Labsys EVO (Setaram, France), with a heating rate of 10 ºC min^{-1}, from 25 to 500 ºC. The maximal thermal degradation temperature (T_{deg}, °C) corresponds to the temperature value obtained for the maximum decreasing peak of the sample mass.

Elemental analysis

The elemental analysis of the EPS was performed using an elemental analyzer (Thermo Finnigan-CE Instruments, Flash EA 1112 CHNS series, Italy). The samples are subjected to a flash combustion in an oxygen environment and the resulting gases (N_2, CO_2, H_2O and SO_2) are separated by gas chromatography. Finally, the content of nitrogen, carbon, hydrogen, and sulphur was calculated using a thermal conductivity detector.

2.2.3.7. Biological assays

Cell culture

Biological assays were performed using the human immortalized keratinocyte cell line HaCaT, obtained from Deutsches Krebsforschungszentrum (DFKZ, Germany), and the human fibroblast cell line CCD-1079Sk obtained from American Type Culture Collection (ATCC, USA). HaCaT cells were cultured in Dulbecco's Modified Eagle medium (DMEM) supplemented with 10% (v/v) of heat-inactivated fetal bovine serum (FBS) and 1% (v/v) penincilin-strepmycin (PS). CCD-1079Sk cells were cultured in DMEM medium supplemented with 10% (v/v) FBS and 1% (v/v) non-essential amino acids (NEAA). Cells were maintained at 37ºC with 5% CO_2, as described by (Concórdio-Reis, Pereira, et al., 2020).

Cytotoxicity assays

The HaCaT and CCD-1079Sk cells were seeded into 96-well plates at a density of 4.5×10^5 cells mL^{-1} and 1.5×10^5 cells mL^{-1} and allowed to grow for 72 and 24 hours, respectively. Then, cells were incubated with the EPS diluted in the respective culture medium with 0.5% FBS (62.5–1000 mg L^{-1}). Cells incubated with only culture medium (0.5 % FBS) were included as control. After 24 hours, cells were washed once with PBS (Sigma-Aldrich, USA) and cell viability was assessed using CellTiter 96® AQueous One Solution Cell Proliferation Assay (Promega, USA) containing MTS reagent. The optical density was measured at 490 nm using a BioTek EPOCH2 Microplate Reader (BioTek, USA) and cell viability was expressed in terms of percentage of living cells relatively to the control. A minimum of three independent experiments were performed in triplicate.

Cellular antioxidant activity

Cellular antioxidant activity was evaluated following previously described methods (Matos et al., 2019; Serra et al., 2010), with some modifications. Briefly, HaCaT cells were seeded at a density of $1.4x10^5$ cells cm^{-2} in 96 well plates and the formation of intracellular reactive oxygen species (ROS) was monitored using 2′,7′-dichlorofluorescein diacetate (DCFH-DA) as a fluorescent probe. 72h after seeding, cells were washed with PBS and treated with selected non-toxic concentrations (62.5 µg mL^{-1}; 125 µg mL^{-1}; 250 µg mL^{-1}; 500 µg mL^{-1}; 1000 µg mL^{-1}) of the samples and 25 µM DCFH-DA in PBS for 1 h. Subsequently, cells were washed again with PBS and incubated with the stress inducer 2,2'-Azobis(2-amidinopropane) dihydrochloride (AAPH, 600 µM in PBS) for 1h. After that, fluorescence was measured in a FL800 microplate fluorescence reader (Bio-Tek Instruments, Winooski, VT, USA) (Ex/Em 485 ± 20/528 ± 20 nm). The results were expressed as ROS percentage relative to the untreated control (cells treated with DCFH-DA and AAPH). Three independent experiments were performed in triplicate.

Anti-inflammatory activity

HaCaT cells were seeded at a density of $1x10^5$ cell cm^{-2} in 12 well plates. After 3 days, cells were stimulated with 15 µg mL^{-1} of lipopolysaccharides (LPS) from *Escherichia coli* and co-incubated with different concentrations of each sample (62.5; 125; 250; 500; 1000 µg mL^{-1}) diluted in culture medium (DMEM medium containing 0.5 % FBS). Cells incubated only with LPS in culture media and with only culture media were used as positive and negative control, respectively. After 24h, supernatants were collected, centrifuged for 10 min at 2000 x g and stored at - 80 ^oC until further analysis. Interleukin-8 (IL-8) and Interleukin-6 (IL-6) level was assessed by enzyme-linked

immunosorbent assay (ELISA), using commercially available kits (PeproTech; London, UK), according to the manufacturer's instructions, with absorbance measured at 450 nm with wavelength correction set at 620 nm in a microplate spectrophotometer (EPOCH 2, BioTek Instruments).

2.2.4. Results and discussion

2.2.4.1. Microalgae growth and EPS production

Heterocapsa AC210 cell growth and EPS production on NBP medium was evaluated (Fig. 2.2.2), and the kinetic parameters obtained in the bioreactor cultivation were determined (Table 2.2.2). After a short adaptation period (first day), *Heterocapsa* AC210 grew exponentially for 5 days before entering a stationary growth phase (Fig. 2.2.2), reaching a maximum cell dry weight of 0.38±0.01 g L^{-1} at the end of the cultivation run (8 days). A maximum specific growth rate (μ_{max}) of 0.464±0.133 d^{-1} was attained between days 2 and 5 (Table 2.2.2). This value is within those reported for the dinoflagellate *Gymnodinium impudicum* strain KG03 (0.435–0.688 d^{-1}) (Yim et al., 2003).

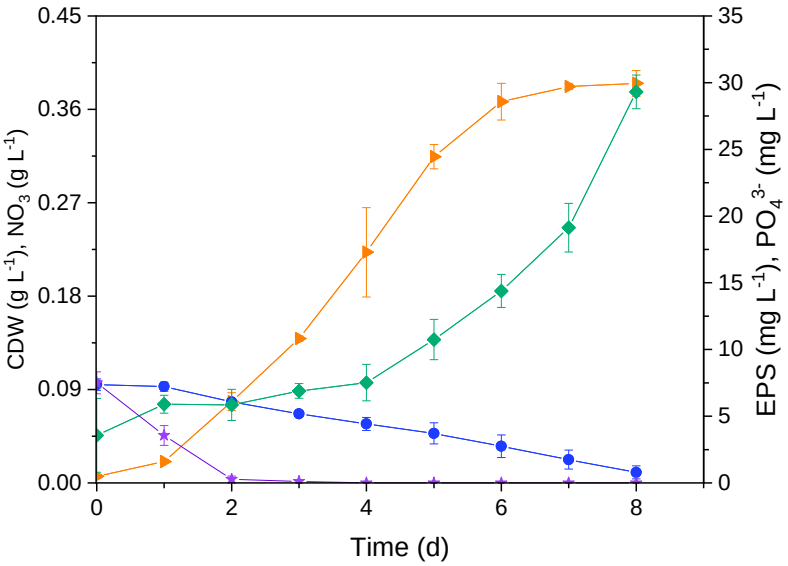

Figure 2.2.2. Cultivation profile (CDW (▶), EPS (◆), nitrate concentration (●) and phosphate concentration (★)) of *Heterocapsa* AC210 grown on NBP medium.

Table 2.2.2. Kinetic parameters (μ_{max}, maximum specific growth rate; r_p, EPS volumetric productivity; r_x, biomass volumetric productivity; q_p, EPS specific productivity) obtained in the bioreactor cultivation.

Parameters	
CDW (g L^{-1})	0.38±0.01
EPS (mg L^{-1})	25.7±3.0
μ_{max} (d^{-1})	0.464±0.133
r_p (mg_p L^{-1} d^{-1})	3.22±0.38
r_x (g_x L^{-1} d^{-1})	0.047±0.002
q_p (mg_p g_x^{-1} d^{-1})	8.50±1.04

Concomitant with cell growth, nutrient consumption was observed with phosphate and nitrate being completely consumed within 2 and 8 days of cultivation, respectively (Fig. 2.2.2). Phosphate depletion strongly affects microalgae cell generation, thus, affecting cell growth (Medina-Cabrera et al., 2020). Nitrogen has an essential role for cell proliferation and protein synthesis in microalgae (Medina-Cabrera et al., 2020). In some species, low nitrate concentrations favor the shift to the stationary phase and induce EPS production as a response to starvation (Delattre et al., 2016; Medina-Cabrera et al., 2020). This seemed to be the case for *Heterocapsa* AC210, since EPS production was initiated during exponential cell growth and increased concomitant with microalgae growth and nitrogen consumption (Fig. 2.2.2). When the culture reached the stationary cell growth phase, significant EPS production was observed, suggesting that the production of EPS is partially growth associated. At the end of the cultivation run, a maximum EPS concentration of 25.7±3.0 mg L^{-1} was reached, resulting in an overall EPS volumetric productivity (r_p) of 3.22±0.38 mg_p L^{-1} d^{-1} (Table 2.2.2). Similar results were reported for dinoflagellate *G. impudicum* strain KG03, where EPS production was growth associated. The EPS concentration was found to be between 17.5 mg L^{-1} (standard cultivation conditions) and 134.7 mg L^{-1} (optimized cultivation conditions), and the r_p values were in the range of 0.92–7.09 mg_p L^{-1} d^{-1} (Yim et al., 2003).

2.2.4.2. EPS characterization

Physicochemical composition

The EPS from microalga *Heterocapsa* AC210 had a heterogeneous composition, comprising neutral sugars, namely galactose (Gal, 20 mol%), mannose (Man, 16 mol%), xylose (Xyl, 14 mol%), fucose (Fuc, 9 mol%), galactosamine (GalN, 7 mol%), and glucose (Glc, 6 mol%); and uronic acids, namely, glucuronic acid (GlcA, 22 mol%) and galacturonic acid (GalA, 6 mol%). Lactate (0.34 mg g^{-1}) and pyruvate (0.14 mg g^{-1}) were found as substituents (Table 2.2.3). This chemical composition is different from that previously described for this microalga strain cultivated in shake flasks for 30 days (Chapter 2.1). In that study, the EPS was mainly composed of Fuc (40.9 mol%) and Gal (31.7 mol%), with smaller amounts of Xyl (8.2 mol%), Glc (6.6 mol%), Man (4.4 mol%), GlcA (3.9 mol%), GalN (2.1 mol%), and GlcN (1.7 mol%) (Chapter 2.1). These differences are probably due to variations in the cultivation conditions, namely irradiance, agitation, media, cultivation time, and/or aeration. Nonetheless, this opens the possibility that, by manipulating the cultivation conditions of *Heterocapsa* sp. AC210, new EPS can be discovered.

Although few examples are known, dinoflagellates were reported to synthesize galactose-rich EPS (Roux et al., 2021; Yim et al., 2007). A similar composition was found for the EPS produced by *Gymnodinium* A_3 OKU-1 strain, an EPS composed of galactose and sulphate in similar proportions (Hasui, Matsuda, Yoshimatsu, et al., 1995). Lactate was also detected in its composition (Hasui, Matsuda, Yoshimatsu, et al., 1995). On the other hand, the toxic dinoflagellate *Amphidinium carterae* secreted an EPS composed of Gal (73 mol%) and Glc (27 mol%) residues (Mandal et al., 2011); whereas the EPS from *M. polykrikoides* was mainly composed of Man, Gal, Glc and uronic acids (Hasui, Matsuda, Okutani, et al., 1995). Thus, to the best of our knowledge, our results report, for the first time, the presence of Fuc, Xyl and GlcN in dinoflagellates' EPS.

Table 2.2.3. Sugar and glycosidic linkage composition (mol%) of *Heterocapsa* AC210 EPS.

	Sugar composition (mol%)								Total sugars (mg/g)
	Fuc	**Xyl**	**Man**	**Gal**	**Glc**	**GalA**	**GlcA**	**GalN**	
EPS composition	9	14	16	20	6	6	22	7	**172**
Glycosidic Linkages									
t-linked	0.8 (0.6)	5.6 (4.5)	11.2 (14.9)	5.6 (4.9)	0.6 (0.7)	nd	✓	nd	
(1→2)-linked	nd	1.0 (1.3)	nd	2.5 (3.0)	nd	nd	nd	nd	
(1→4)-linked	1.3 (3.2)	5.8 (7.5)	2.1 (1.1)	2.5 (3.4)	3.0 (4.2)	nd	nd	nd	
(1→6)-linked	nd	nd	nd	3.5 (4.3)	nd	nd	nd	nd	
(1→2,3)-linked	nd	nd	nd	2.4 (2.6)	nd	nd	nd	nd	
(1→2,4)-linked	4.1 (4.3)	1.6 (0.7)	nd	nd	0.6 (0.1)	nd	nd	nd	
(1→2,6)-linked	nd	nd	nd	0.9 (1.2)	nd	nd	nd	nd	
(1→3,4)-linked	2.8 (0.9)	nd	2.7 (tr)	0.7 (0.6)	nd	✓	nd	nd	
(1→3,6)-linked	nd	nd	nd	1.9 (tr)	0.4 (0.3)	nd	nd	nd	
(1→2,3,6)-linked	nd	nd	nd	nd	0.7 (0.3)	nd	nd	nd	
(1→3,4,6)-linked	nd	nd	nd	nd	0.7 (0.4)	nd	nd	nd	

	Substituents composition (mg/g)		
EPS composition	**Sulphate**	**Pyruvate**	**Lactate**
	297	0.14	0.34

Values in brackets are from glycosidic linkage composition after desulphation nd – not detected; tr – traces; Sulphate – SO; Pyr – pyruvate; Lac – lactate.

Moreover, the EPS had a high content of sulphate (29.7±2.8 wt.%) (Table 2.2.3). The high content of sulphate may indicate that the salts were not completely removed from the polysaccharides, in accordance with the observed low sugar content of 172 mg g^{-1}. As the mol% ratio of sulphate to the carbohydrate residues is 3.6, it shows that not all the sulphate is linked to the polysaccharide. Nevertheless, the presence of sulphate substituents is a common feature of dinoflagellate EPS. In fact, the EPS produced by marine dinoflagellates such as *Gyrodinium impudicum* KG03 and *M. polykrikoides*, were found to comprise sulphate groups with contents of 10.3 and 7–8 wt.%, respectively (Hasui, Matsuda, Okutani, et al., 1995; Yim et al., 2007). Moreover, sulphate was also detected in the EPS produced by two *Lepidodinium chlorophorum* strains (Roux et al., 2021). Additionally, elemental analysis showed a low content in nitrogen (0.62 wt.%), which indicated that the EPS did not have a high protein content.

Glycosidic linkages

The EPS produced by *Heterocapsa* AC210 had a wide range of glycosidic linkages of Fuc, Xyl, Man, Gal, and Glc, as well as (1→3,4)-Glc*p*A and t-Gal*p*A, determined by a non-quantitative carboxyl reduction (Table 2.2.3). Fuc was found as *t*-Fuc*p* (0.8 mol%) or (1→4)-Fuc*p* (1.3 mol%) with substituents or ramifications at position 2 and 3 (4.1 and 2.8 mol%, respectively). Xyl was found as *t*-Xyl*p* (5.6 mol%), (1→2)-Xyl*p* (1.0 mol%), (1→4)-Xyl*p* (5.8 mol%), and (1→2,4)-Xyl*p* (1.6 mol%). Gal was mainly found as *t*-Gal*p* (5.6 mol%), followed by (1→6)-Gal*p* (3.5 mol%), (1→2)-Gal*p* (2.5 mol%), and (1→4)-Gal*p* (2.5 mol%), which were also substituted at positions 2 or 3 (2.4 mol% of (1→2,3)-Gal*p;* 1.9% of (1→3,6)-Gal*p*; 0.9% of (1→2,6)-Gal*p*; and 0.7% of (1→3,4)-Gal*p*). Glc was mainly observed as (1→4)-Glc*p* (3.0 %). *t*-Glc*p* (0.6 mol%), (1→2,4)-Glc*p* (0.6 mol%), (1→3,6)-Glc*p* (0.4 mol%), (1→2,3,6)-Glc*p* (0.7 mol%), and (1→3,4,6)-Glc*p* (0.7 mol%) were also found. Although highly substituted, the content of linkages is not enough to explain the high content of sulphate determined in the sample, showing the presence of salts.

To evaluate the sulphate esters positions and composition, the EPS was desulphated before glycosidic linkage analysis. The desulphation distinguishes if the substitution of a sugar residue is a branching point or a sulphate ester. When a substitution remains after desulphation, it indicates that this position contains a branching point. On the other hand, the decrease of substituted linkages indicates the presence of sulphate esters at those positions. After desulphation, an increase of (1→4)-Fucp occurred with a decrease of (1→3,4)- Fucp, indicating that 21% of Fuc residues were substituted at position 3 (Table 3). Desulphated EPS had an increase of (1→4)-Xylp occurred with a decrease of (1→2,4)- Xylp, indicating that 6% of Xyl residues were substituted at position 2. An increase of 23% of t-Manp residues occurred with a concomitant decrease of (1→4)-Manp and (1→3,4)-Manp, indicating the presence of Man mainly as t-Manp (93% of total Man) with sulphate esters at position 4 or at positions 3 and 4. Increase of (1→4)- Galp and (1→6)- Galp with decrease of (1→3,4)- Galp and (1→3,6)- Galp, indicates the presence of 10% of Gal with sulphate esters at position 3. Decrease of (1→2,4)-Glcp, (1→3,6)-Glcp, (1→2,3,6)-Glcp, (1→3,4,6)-Glcp residues occurred with increase of (1→4)-Glcp, indicating the presence of 22% of Glc substituted sulphate esters at position 2 and/or positions 3 and 6.

FTIR analysis

The FTIR spectrum of the EPS produced by *Heterocapsa* AC210 (Fig. 2.2.3) showed an intense broad band at around 3000–3500 cm^{-1} with a peak at 3334 cm^{-1}

that corresponds to the stretching vibration of hydroxyl groups (Concórdio-Reis et al., 2021; Farinha et al., 2015; Yim et al., 2007). This band partially overlaps the C-H stretching peak of CH_2 groups (2924 cm^{-1}), and the band at around 3250 cm^{-1} characteristic of the N-H stretching vibration (Concórdio-Reis et al., 2021; Farinha et al., 2015; Shao et al., 2014). The peaks at 1646 cm^{-1} and 1414 cm^{-1} are characteristic of the C=O asymmetric and symmetric stretching vibrations, respectively (Concórdio-Reis et al., 2021; Yim et al., 2007). The absorption region at around 1230 cm^{-1} can be attributed to the stretching vibration of S=O from sulphate groups and/or of C-O-C from acyl substituents (Concórdio-Reis et al., 2021; Parikh & Madamwar, 2006; Yim et al., 2007). The peak at 1078 cm^{-1} can be assigned to C-O and C-C vibrations of the glycosidic bonds and pyranose ring (Concórdio-Reis et al., 2021), and/or the vibration of S=O and C-O-S groups (Mandal et al., 2011). Finally, the peak at around 600 cm^{-1} could also result from the glycosidic linkage bond (Mandal et al., 2011).

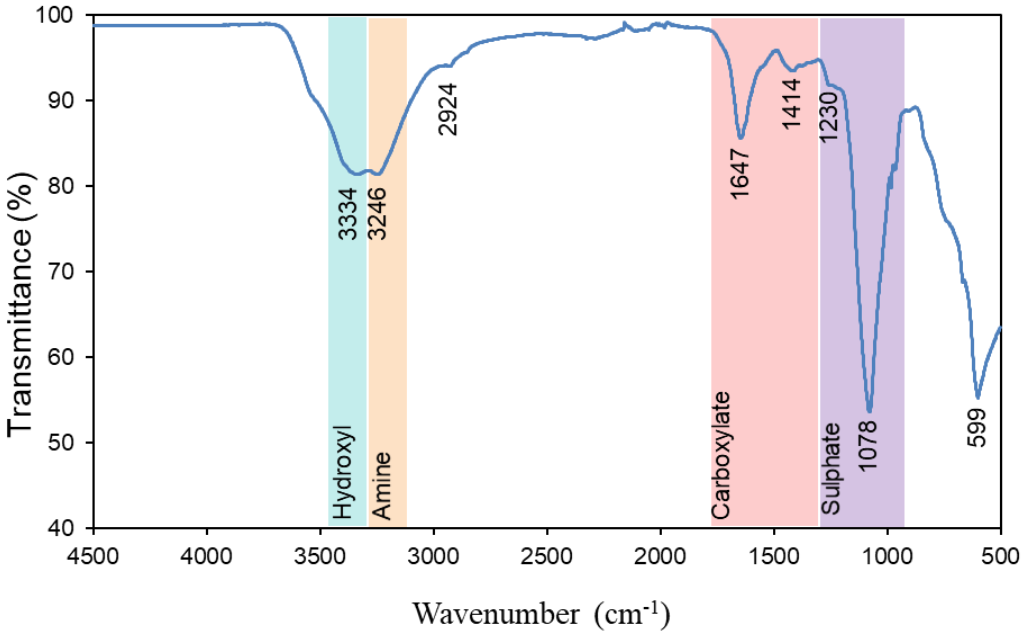

Figure 2.2.3. FTIR spectrum of the EPS produced by *Heterocapsa* AC210.

Molecular mass distribution

The molecular mass distribution analysis of *Heterocapsa* AC210 EPS revealed two distinct chromatographic peaks, suggesting that the sample comprised two high molecular weight saccharide fractions, with 7.55±0.97 x 10^5 and 4.50±0.73 x 10^4 Da, and PDI of 1.51±0.01 and 1.22±0.06, respectively. Similarly, the EPS synthesized by the dinoflagellates *A. carterae* and *M. polykrikoides* were composed of two polysaccharide fractions with Mw values of 2.2 x10^5 and 1.3 x10^3 Da, and of 1.3 x10^6 and 6.3 x10^5 Da, respectively (Hasui, Matsuda, Okutani, et al., 1995; Mandal et al., 2011). In contrast, the EPS produced by *G. impudicum* KG03 and *Gymnodinium A3*

OKU-1 presented only one polysaccharide fraction, with Mw values of 1.87 x10^6 and 1.3 x10^6, respectively (Hasui, Matsuda, Yoshimatsu, et al., 1995; Yim et al., 2007).

Thermal properties

The TG curve of *Heterocapsa* AC210 EPS displayed two main degradation steps (Fig. 2.2.4). An initial weight loss of 21% is observed between 37 and 194 ºC due to moisture loss (Concórdio-Reis et al., 2021; Mandal et al., 2011; Yim et al., 2007). High moisture content has previously been described for dinoflagellates' EPS and might be due to the high affinity of water molecules to carboxyl groups present in the polysaccharide (Mandal et al., 2011; Yim et al., 2007). Above this temperature, a second weight loss of 21% occurred, corresponding to the decomposition of the polysaccharide chains, in accordance with sugar analysis. The EPS T_{deg} was found to be 239 ºC, a value similar to that reported for the EPS produced by the dinoflagellate *G. impudicum* KG03 (250 ºC) (Yim et al., 2007) and within the range of values reported for other microbial EPS (111–300 ºC) (Ahmed et al., 2013; Concórdio-Reis et al., 2021; Kanamarlapudi & Muddada, 2017; Parikh & Madamwar, 2006). The EPS showed a high char yield (54.6%) that could be due to the high sulphate content, a complex molecular configuration and the presence cations that might bind to the different charged sugar moieties (Concórdio-Reis et al., 2021; Parikh & Madamwar, 2006).

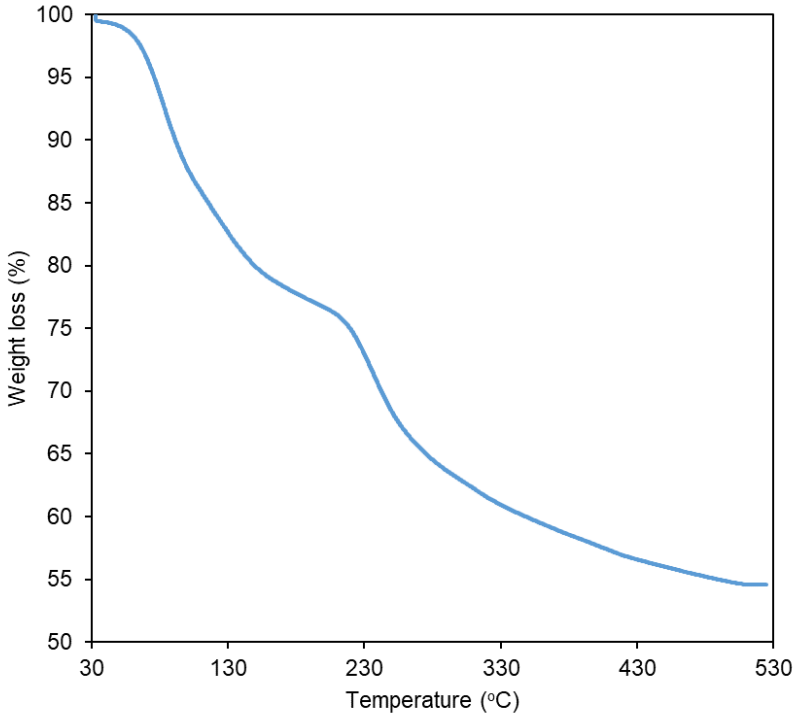

Figure 2.2.4. Thermogravimetric analysis (TGA) curve of the EPS produced by *Heterocapsa* AC210.

2.2.4.3. Biological assays

Cytotoxicity assessment

The potential cytotoxicity of the *Heterocapsa* sp. AC210 EPS was evaluated in both human keratinocytes (HaCaT) and human fibroblasts (CCD-1079Sk), which are the predominant cell types found in skin, representing the epidermal and dermal layers, respectively (Matos et al., 2019). These cell lines play a major role in the biological response for maintaining skin integrity (Concórdio-Reis, Pereira, et al., 2020; Matos et al., 2019) and are among the cell lines recommended by ISO 10993-5 international standard for cytotoxicity assessment. As shown in Fig. 2.2.5, the EPS did not induce any cytotoxic effect to either cell line since cell viability was not affected in the presence of EPS concentrations up to 1000 µg mL^{-1}. These results are consistent with literature, as the biocompatibility of several polysaccharides such as alginate, hyaluronic acid and xanthan gum were demonstrated for the same polymer concentration range (Gedikli et al., 2018; Pagano et al., 2021).

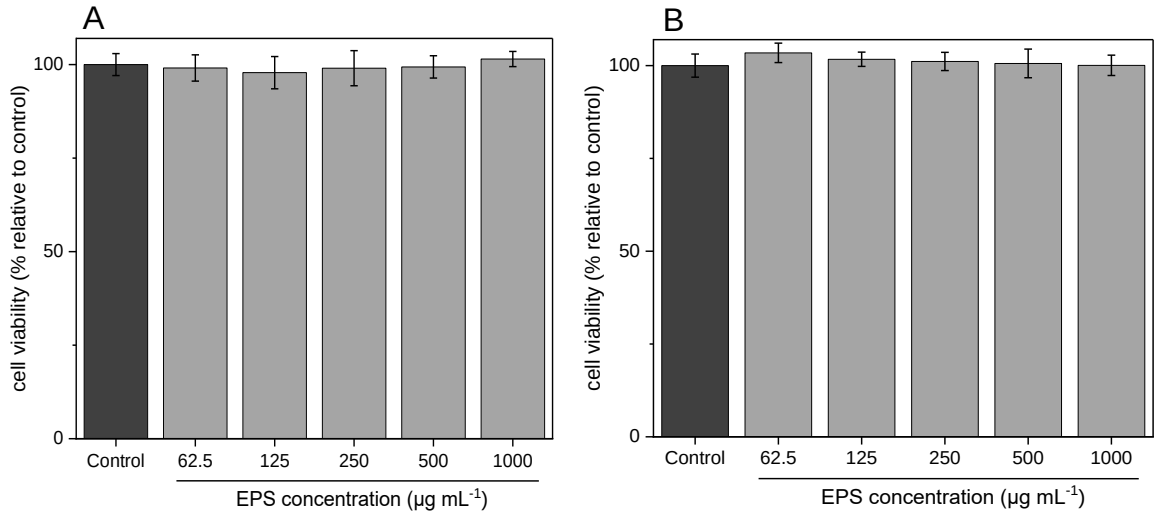

Figure 2.2.5. Effect of *Heterocapsa* AC210 EPS on the viability of HaCaT (A) and CCD-1079Sk cell lines after 24 h incubation. Results were expressed in terms of mean ±SD of three independent experiments performed in triplicates.

Cellular antioxidant activity

The capacity of *Heterocapsa* sp. AC210 EPS to inhibit ROS production in HaCaT cells was evaluated for polymer concentrations between 62.5 and 1000 µg mL^{-1} (Fig. 2.2.6). Compared to the control, a decrease of the ROS production was observed concomitant with an increasing EPS concentration, indicating that the EPS has antioxidant properties. In the presence of only 250 µg mL^{-1} of EPS, ROS production decreased by 14.3%. At the maximum concentration tested (1000 µg mL^{-1}), a 18.3%

reduction in the ROS level was observed. Similarly, several natural polysaccharides from different sources have been reported to reduce ROS production in a variety of cell lines after exposure to different oxidative agents. Examples include the plant polysaccharide (*Sophora subprosrate*) that, at concentrations between 100 and 400 µg mL^{-1}, significantly decreased the ROS level in mouse macrophage cell line (RAW264.7 cells) infected with porcine circovirus type 2 (PCV2) (Su et al., 2013). The polysaccharide extracted from *Cyclocarya paliurus* plant reduced ROS production in H_2O_2-induced RAW264.7 cells in a dose-dependent manner from 25 to 100 µg mL^{-1} (Xie et al., 2020). Additionally, the sulphated-polysaccharide extracted from the seaweed *Sargassum thunbergia*, at concentrations between 25 and 100 µg mL^{-1}, reduced H_2O_2-induced ROS production (~30 to ~40%) in African green monkey kidney (Vero) cells (M.-C. Kang et al., 2019). Also, treatment with different concentrations of arabinan-rich pectic polysaccharide from acerola (25–200 µg mL^{-1}), ROS concentration in H_2O_2-induced NIH 3T3 murine fibroblast cells decreased significantly (Klosterhoff et al., 2018). In the presence of the *Porphyridium* sp. Polysaccharide, ROS level in human coronary artery endothelial cells (HCAECs) decreased by ~30 % (Levy-Ontman et al., 2017). After only one hour of treatment with the fucose-rich EPS produced by *Bacillus megaterium* RB-05 (200 and 250 µg mL^{-1}), a significant reduction of ROS levels was observed in H_2O_2-induced human lung fibroblasts cells (WI38) (Roy Chowdhury et al., 2014).

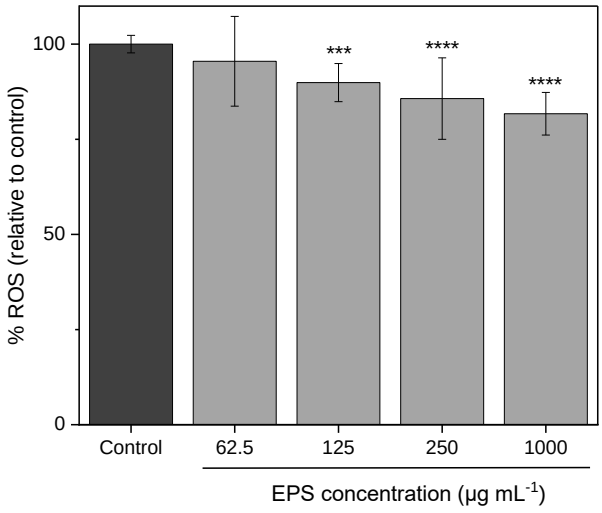

Figure 2.2.6. Effect of *Heterocapsa* AC210 EPS on the inhibition of AAPH-induced ROS production in HaCaT cells. The results were expressed as ROS percentage relative to the untreated control (cells treated with AAPH), in terms of mean ±SD of three independent experiments. Statistically significant differences between the samples and the control were calculated according to t-test (*** p≤0.001, **** p≤0.0001).

Free radicals such as reactive oxygen species (ROS) can cause oxidative stress in essential cellular structures (e.g., lipids, DNA, proteins) of living organisms, leading to altered functionality (Freitas et al., 2021; Matos et al., 2019). Even though ROS overproduction might occur due to environmental factors, cellular exposure to ROS is inevitable as these species are formed as a consequence of aerobic metabolism (Guerreiro et al., 2020; Matos et al., 2019). These oxidant species contribute to the skin ageing process, either directly by causing damages in the biomolecules, or indirectly by interfering with the signaling pathways of keratinocytes and fibroblasts (Matos et al., 2019). Moreover, ROS can severely affect the skin wound healing capacity, as they cause cell death, less flexibility of skin lipids, and proteases inhibitors oxidative damage (Maalej et al., 2014).

Anti-inflammatory activity

The anti-inflammatory activity of the EPS produced by *Heterocapsa* sp. AC210 was evaluated as the capacity to reduce the release of inflammatory cytokine IL-8 (Fig. 2.2.7 A) and IL-6 (Fig. 2.2.7 B) by HaCaT cells after an inflammatory stimulus induced by LPS. As Fig. 2.2.7 A shows, *Heterocapsa* sp. AC210 EPS presented an anti-inflammatory effect for all concentrations tested, with the IL-8 secretion reducing up to 79.3%. Interestingly, for concentrations higher than 500 µg mL^{-1}, *Heterocapsa* sp. AC210 EPS efficiency in reducing IL-8 secretion was comparable to that of IKK-2 and IKK-1 inhibitor BMS (5 µM), a commercial anti-inflammatory substance (no statistical difference for a 95% confidence level). Additionally, IL-6 levels decreased 46.2% for EPS concentrations above 500 µg mL^{-1} ($p \leq 0.01$) (Fig. 2.2.7 B).

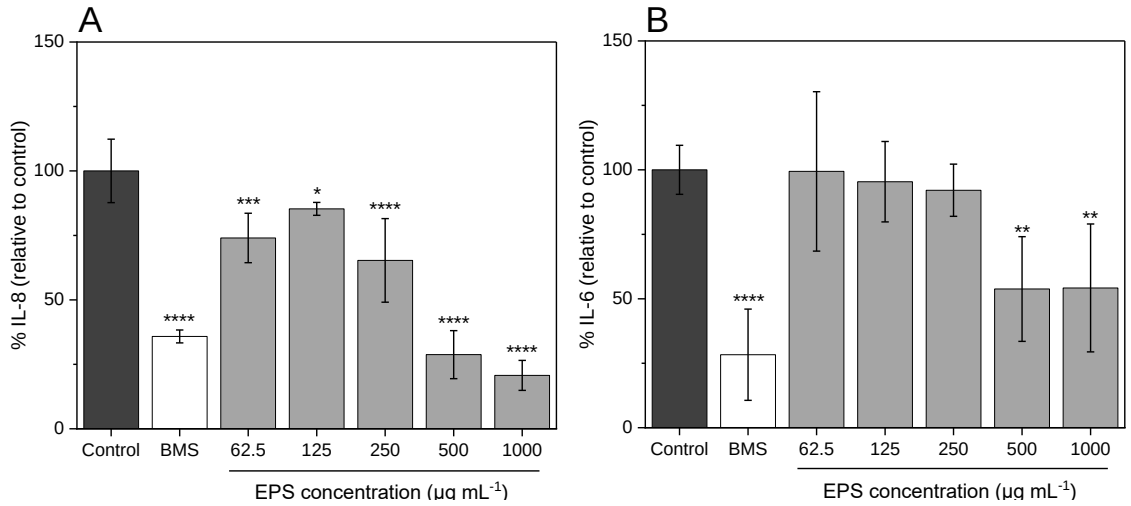

Figure 2.2.7. Effect of *Heterocapsa* AC210 EPS on the IL-8 (A) and IL-6 (B) cytokine secretion in HaCaT cells challenged by LPS. BMS (5 µM) was used as a comparative commercially available anti-inflammatory agent. Results were expressed in terms of mean ±SD of three independent experiments. Statistically significant differences between the samples and the control were calculated according to t-test (** $p \leq 0.01$, *** $p \leq 0.001$, **** $p \leq 0.0001$).

The biological properties of the polysaccharides, including their anti-inflammatory activity, seem to be related to the complex interaction of several factors such as their structure, composition, sulphation level, distribution of sulphate groups along the backbone of the polysaccharide, molecular weight, and stereochemistry (Choo et al., 2020). Therefore, contradictory results have been reported in literature. For instance, the heteroglycan isolated from cyanobacteria *Nostoc commune* significantly reduced secretion of IL-6 in LPS-stimulated human monocytes at concentrations above 10 µg mL^{-1}. On the contrary, it increased the production of pro-inflammatory cytokine IL-8, being more than three-fold at the highest concentration tested (100 µg mL^{-1}) (Olafsdottir et al., 2014). The sulphated polysaccharide from *Sargassum swartzii* (34% sulphate) exhibited anti-inflammatory activity by reducing IL-6 production in LPS-induced macrophages (RAW 264.7) for concentrations above 50 µg mL^{-1} ($p \leq 0.05$) (Jayawardena et al., 2020). Also, in monocytes challenged with LPS, heparin resulted in an increase of IL-6 production, whereas dextran and fucan (sulphate content of 29%) did not affect the production of this cytokine (Anastase-Ravion et al., 2002). In this study, only the semisynthetic dextran derivatives (DD) randomly substituted with carboxymethyl, benzylamide, sulphonate, and sulphate groups (21%), resulted in a decrease of 20–30% in IL-6 production (Anastase-Ravion et al., 2002). As for IL-8 production, an inhibition of 61 and 65% was observed in the presence of heparin and DD, respectively (Anastase-Ravion et al., 2002). These results suggest that *Heterocapsa* AC210 EPS had significant anti-inflammatory activity by reducing pro-inflammatory cytokines production. Such bioactive compound might be useful in the treatment of chronic wounds (Jesus Raposo et al., 2015) or skin inflammatory diseases such as atopic dermatitis or psoriasis (Choo et al., 2020).

2.2.5. Conclusions

The dinoflagellate microalga *Heterocapsa* sp. AC210 was investigated as an EPS producer. Monosaccharide analysis revealed the presence of seven different sugar monomers, including fucose, xylose and glucosamine, which have never been reported in dinoflagellates' EPS before. Additionally, the EPS had a high content of sulphate, which is associated with the biological properties often found for microalga's EPS. Up to 1000 µg mL^{-1} the EPS was not cytotoxic and *in vitro* bioactivity tests revealed its antioxidant and anti-inflammatory activities. These findings establish a valuable starting point for both the production of this high value EPS, and the development of new EPS-based bioactive materials with potential application in the cosmeceuticals and biomedicine fields.

3

Bacterial Exopolysaccharides

Chapter | 3.1

Bioprospecting for new exopolysaccharide-producing bacteria from unusual marine environments

The results presented in this chapter were published in the following peer-reviewed scientific journal:

Concórdio-Reis, P., Alves, V.D., Moppert, X., Guézennec, J., Freitas, F. & Reis, M.A.M (2021) Characterization and Biotechnological Potential of Extracellular Polysaccharides Synthesized by *Alteromonas* Strains Isolated from French Polynesia Marine Environments. *Marine Drugs* 19, 522. DOI: 10.3390/md19090522

Sample collection, bacterial isolation, EPS production and extraction, and EPS carbohydrate composition analysis were performed by Dr. Xavier Moppert from Pacific Biotech BP.

3.1.1. Summary

Marine environments comprise almost three quarters of Earth's surface, representing the largest ecosystem of our planet. The vast ecological and metabolic diversity found in marine microorganisms suggest that these marine resources have a huge potential as sources of novel commercially appealing biomolecules, such as EPS. Six *Alteromonas* strains from different marine environments in French Polynesia atolls were selected for EPS extraction. All the EPS were heteropolysaccharides composed of different monomers, including neutral monosaccharides (glucose, galactose, and mannose, rhamnose and fucose), and uronic acids (glucuronic acid and galacturonic acid), which accounted for up to 45.5 mol% of the EPS compositions. Non-carbohydrate substituents, such as acetyl (0.5–2.1 wt%), pyruvyl (0.2–4.9 wt%), succinyl (1–1.8 wt%), and sulphate (1.98–3.43 wt%); and few peptides (1.72–6.77 wt%) were also detected. Thermal analysis demonstrated that the EPS had a degradation temperature above 260 °C, and high char yields (32–53%). Studies on EPS functional properties revealed that they produce viscous aqueous solutions with a shear thinning behavior and could form strong gels in two distinct ways: by the addition of Fe^{2+}, or in the presence of Mg^{2+}, Cu^{2+}, or Ca^{2+} under alkaline conditions. Thus, these EPS could be versatile materials for different applications.

3.1.2. Introduction

Sea water covers more than 70% of the earth's surface and represents the largest ecosystem of the planet. Despite the enormous metabolic diversity and discovery potential, marine natural resources are still underexplored, understudied and underutilized in biotechnology (Casillo et al., 2018; Roca et al., 2016). From the shallow coastal waters to the deep ocean, marine habitats have a variety of unique ecological characteristics that prompted marine microbial communities to develop adaptation mechanisms in order to survive (Casillo et al., 2018; Chalkiadakis et al., 2013). This is especially true in extreme environments such as those found in deep-sea hydrothermal vents, volcanic and hydrothermal marine areas, marine salterns and sea ice in polar regions (Martin-Pastor et al., 2019).

Important molecules for cell survival are extracellular polysaccharides (EPS), high molecular weight carbohydrate polymers secreted by many microorganisms, particularly bacteria (Delbarre-Ladrat et al., 2017; Guezennec, 2002). Bacterial EPS make up a substantial part of the extracellular polymers that surround cells in microbial communities (Nichols et al., 2005). A variety of functions have been attributed to EPS,

including adhesion to surfaces, cell-cell recognition and aggregation, entrapment of nutrients, and protective barrier (Donot et al., 2012; More et al., 2014; Wang et al., 2019). EPS are especially important for marine bacteria to thrive under the extreme conditions characteristic of their environment, such as high pressure, high salinity, low nutrient concentration, low or high temperature, and heavy metal presence (Zhang et al., 2017). Moreover, bacterially synthesized EPS are commercially appealing due to their interesting physicochemical and functional properties, with potential applicability as biomaterials, rheology modifiers of aqueous solutions or bioactive therapeutic agents (Freitas et al., 2017; Wang et al., 2019). In fact, marine bacteria are currently a very promising source for the discovery of EPS with distinctive structures and unique properties, with applicability in several industrial sectors (Roca et al., 2016; Sahana & Rekha, 2019). These EPS often exhibit a high diversity in structure and composition, that might include rare sugars, such as fucose or rhamnose (Sahana & Rekha, 2019; Zarandona et al., 2020), which are known to confer the biopolymers' biological activity (Freitas et al., 2017). High content in uronic acids and sulphate groups are also found within marine bacteria derived EPS, which further contributes to their unique properties (Sahana & Rekha, 2019).

In the course of discovery of biomolecules of biotechnological interest, it is well accepted that microorganisms originating from unusual environments, such as deep-sea hydrothermal vents, Antarctica and microbial mats located in some Polynesian atolls, will provide a valuable source for novel biopolymers, including EPS with unique properties (Nichols et al., 2005; Roca et al., 2016). Microbial mats (locally called "Kopara" mats) are characterized by salt concentrations ranging from 5 to 42 g L^{-1}, pH values between 6 to 10.5 and temperatures ranging from 20 °C, during the night, up to 42 °C (Guézennec et al., 2011). To date, only five genera of EPS-producing bacteria were found in such environments i.e., *Pseudomonas*, *Pseudoalteromonas, Alteromonas, Paracoccus*, *and Vibrio*, with uronic acids and amino-sugars content up to 50% (w/w), as well as acyl and sulphate groups, in their secreted EPS composition, which render them unique properties and great potential for use in several applications, including in the cosmetic, biomedicine, pharmaceutical and therapeutics fields (Guézennec et al., 2011).

In this study, six *Alteromonas* strains originating from different locations in French Polynesia were screened for EPS production in an aerobic, carbohydrate-based medium. The resulting EPS were characterized in terms of chemical composition, molecular mass distribution and thermal properties. To investigate their potential as biomaterials in important biotechnological applications, the functional properties of the

biopolymers were assessed, including determination of their rheological properties and gel forming capacity.

3.1.3. Materials and Methods

3.1.3.1. Sample collection and bacterial isolation

During different sampling campaigns, samples were collected from different sources in three marine sites in French Polynesia, Southern Pacific Ocean, namely, Moorea Island lagoon (Society Archipelago) Fakarava atoll (Tuamotu Archipelago), and Tikehau atoll (Tuamotu Archipelago) (Table 3.1.1). In the laboratory, immediately upon retrieval, all samples were treated according to their nature. Enrichment cultures in appropriate marine medium led to a collection of up to 2000 isolates. Around 10% of the bacterial collection was screened for the ability to secrete EPS. The isolates were plated on 2216E (Oppenheimer & Zobell, 1952; Zobell, 1941) solid medium supplemented with glucose at a concentration of 30 g L^{-1} and incubated at ambient temperature. The bacteria were selected based on their ability to show a mucoid phenotype (Fig. 3.1.1). Six isolates belonging to *Alteromonas* genus were used in this study (Table 3.1.1). The strains were deposited at Collection Nationale de Cultures de Microorganismes (CNCM) of Pasteur Institute under the Budapest Treaty.

Table 3.1.1. Isolates' identification, sampling location and sample source of the EPS producing *Alteromonas* strains isolated from marine environments in French Polynesia.

EPS	Isolate strain designation	Sampling site	Sample source	Accession number
A	Mo 169	Moorea Island lagoon	Giant clam (*Tridacna maxima*)	CNCM I-5374
B	Mo 278	Moorea Island lagoon	Sea Anemone (*Actiniaria*)	CNCM I-5375
C	Fak 1576	Fakarava atoll	Coral	CNCM I-5376
D	Tik 650	Tikehau atoll	"Kopara" mat	CNCM I-5523
E	Fak 1386	Fakarava atoll	Pearl oyster mantle	CNCM I-5524
F	Mo 203	Moorea Island lagoon	"Kopara" mat	CNCM I-3970

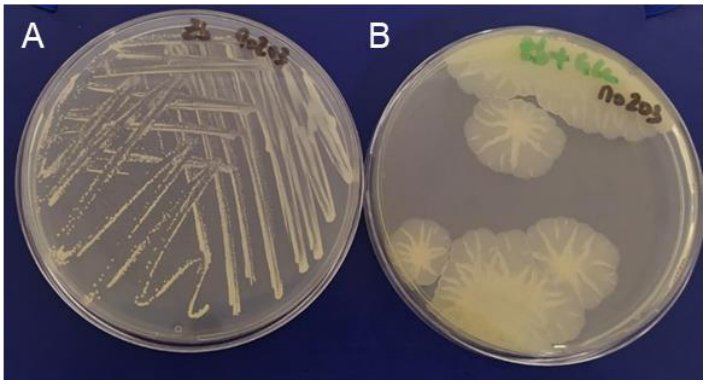

Figure 3.1.1. Culture of strain Mo 203 on Zobell-agar medium (A) and glucose-supplemented (30 g.L^{-1}) Zobell-agar medium (B).

3.1.3.2. EPS production and extraction

EPS production was performed at 30°C in a 1-liter fermenter (New Brunswick, Toulouse, France), containing 1 L of 2216E-glucose broth. A batch of the culture medium was inoculated at 10% (v/v) with a suspension of cells in exponential growth phase. The pH was adjusted and maintained at 7.6 by automatic addition of NaOH 2 mol L^{-1}. Foaming was avoided by addition of Pluronic-PE6100 oil and the agitation rate was controlled at 200–1200 rpm to maintain the dissolved oxygen concentration at 40% of the air saturation. Glucose supplementation was 6% (60 g L^{-1}) for all strains. Fermentations were stopped when glucose was consumed, between 24 up to 48 h, according to the strain (Cambon-Bonavita et al., 2002; Raguénès et al., 1996). Water-soluble EPS were recovered from the culture medium by high-speed centrifugation (20000 × *g* for 2 h), then purified by ultrafiltration against deionized water using a pellicon-2 Mini Holder equipped with a Biomax 100 K filter (Millipore Corporation, Bedford, MA). Supernatants were filtered on PolyEtherSulphone (PES) before ultimate concentration and lyophilized prior to further analysis.

3.1.3.3. EPS characterization

EPS composition

The total neutral carbohydrate and uronic acid contents were determined by the method proposed by orcinol-sulphuric method (Rimington, 1931; Tilmans & Philippi, 1929) and the meta-hydroxydiphenyl method (Blumenkrantz & Asboe-Hansen, 1973), respectively. The molar ratio of monosaccharides was determined according to Kamerling et al. (1975) and Montreuil et al. (1986). The monosaccharides were

analyzed after either aqueous hydrolysis or acidic methanolysis of the polymers and subsequent GC analysis as peracetylated derivatives or trimethylsilyl derivatives respectively. Each value is a mean of three determinations.

Protein content was quantified by a modified Lowry method, as described by Concórdio-Reis, Reis, et al. (2020). For the determination of inorganic content, lyophilized EPS samples (~40 mg) were placed at 100 ^{o}C until a constant weight was attained. The dried EPS samples were subjected to pyrolysis (550 ^{o}C, 24 h), and weighted for the gravimetric quantification of the inorganic content. The acid hydrolysates were also used for the quantification of acyl groups by HPLC with an Aminex HPX-87H 300×7.8 mm column (Biorad, Hercules, CA, USA) coupled with UV detector (210 nm), as described by Concórdio-Reis, Reis, et al. (2020). Acetate, pyruvate, and succinate (Sigma-Aldrich) were used as standards at concentrations between 0.015 and 1.0 g L^{-1}.

Sulphate concentration in the hydrolysates was determined by HPLC as described in section 2.1.3.4. All analysis were performed in duplicate.

Molecular mass distribution

The analyses were performed on a Prominence HPLC system from Shimadzu equipped with a flow refractive index detector (RID20A from Shimadzu), a UV detector (SPD40A from Shimadzu operating at 280 nm) and a DAWN HELEOS Light Scattering detector from Wyatt, operating at 18 scattering angles and at a wavelength of 660 nm. The samples were analyzed in water with 0.1 M $NaNO_3$ and 100 ppm of NaN_3 as a bacteriostatic agent, at room temperature, using a flow rate of 0.8 mL min^{-1}. All polymers were injected at a concentration of 0.6 mg ml^{-1} and with a volume of 100 µl. Separation was performed with a guard column SHODEX OH PACK SB-G-6B and two shodex columns OH PACK SB-806MHQ (13µm, 300x8mm) and SB-805 HQ (7µm, 300x8mm). The average molar masses (number-average molar mass M_n and weight-average molar mass M_w) and the dispersity index ($Đ = M_w/M_n$) were derived both from the RI and MALS signal using a specific refractive index increment dn/dC = 0,13 mL g^{-1}.

Elemental Analysis

The elemental analysis was performed as described in section 2.2.3.6.

Fourier Transform Infra-Red (FTIR) Spectroscopy

FTIR were performed as described in section 2.2.3.6.

Thermogravimetric (TG) analysis

TG analysis was performed as described in section 2.2.3.6.

3.1.3.4. EPS functional properties

Rheological properties

The apparent viscosity of the EPS aqueous solutions (1 wt.%) was measured at 25ºC using a controlled stress rheometer (Haake Mars III – Thermo Scientific, Germany), with a UTC – Peltier system to control temperature, and a cone-plate sensor system (angle 2°, diameter 35 mm). Measurements were carried out using a stationary shear flow, according to an adapted method from Freitas et al. (2011).

Gel forming capacity

The gel forming capacity of the EPS was tested by preparation of cation-mediated gels using monovalent cations ($ZnCl_2$, $AgNO_3$), divalent cations ($FeSO_4.7H_2O$, $CuSO_4.5H_2O$, $CaCl_2.2H_2O$, $MgSO_4.7H_2O$) and a trivalent cation ($FeCl_3.6H_2O$). The gelation studies were performed according to the procedure described by Shimada et al., (1997), with minor modifications: 5 mL of EPS solution (5 g L^{-1}) was added to the metal salt (10 mg of cation) and agitated until dissolution and gel formation was assessed (standard conditions). Afterwards, 1 mL of NaOH (2 M) was added and the solution was agitated to test gelation in alkaline conditions. Gel formation was assessed by visual inspection and the gels were categorized according to their strength and homogeneity: (+) for homogeneous gels that maintained their gel structure in a tube-inversion test, (-) for homogeneous gels that did not sustain their structure in the inversion test, and (--) for small non-homogeneous gels.

3.1.4. Results and discussion

3.1.4.1. Isolation and identification of EPS producing strains

The six *Alteromonas* isolates used in this study were selected based on their ability to show a mucoid phenotype (Fig. 3.1.1). Strains Mo 169, Mo 278 and Mo 203 were originally isolated from a giant clam, a sea anemone and a “Kopara” mat sample, respectively, collected at Moorea Island lagoon (Society Archipelago). Strains Fak 1576 and Fak 1386 were isolated from a coral and a pearl oyster mantle, respectively, at the Fakarava atoll, while strain Tik 650 was isolated from a “Kopara” mat sample collected at Tikehau atoll (Table 3.1.1). Upon taxonomical analysis, the strains were identified as belonging to the *Alteromonas macleodii* specie, except for strain Tik 650 identified as a *Alteromonas simiduii*.

3.1.4.2. EPS characterization

Chemical composition

The *Alteromonas* EPS were heteropolysaccharides composed of four to six different monomers, including neutral sugars (glucose, galactose, and mannose, rhamnose and fucose) and uronic acids (glucuronic acid and galacturonic acid) (Table 3.1.2).

Almost all biopolymers were rich EPS in uronic acids, with glucuronic acid (GlcA) and galacturonic acid (GalA) accounting for up to 45.5 mol%. Such high contents in uronic acids were also reported for EPS produced by deep-sea hydrothermal bacterium *A. infernus* GY 785 (Zykwinska et al., 2018), and *Alteromonas* sp. JL2810 collected from surface seawater (Zhang et al., 2017). Due to the uronic acids in their composition, both *Alteromonas* strains showed a high metal binding capacity, leading to a possible use in wastewater treatment and metal recovery (Loaëc et al., 1998; Zhang et al., 2017). On the other hand, no uronic sugars were detected in the EPS produced by *A. hispanica* F32 isolated from a hypersaline environment (Mata et al., 2008) and two strains of *A. stellipolaris*, namely, strains PQQ-42 and PQQ-44, isolated from a fish hatchery (Torres et al., 2019).

The rare sugar rhamnose (Rha) was also present in significant proportions in EPS C, E and F. Although Rhamnose was previously reported in EPS from *Alteromonas* strains (Le Costaouëc et al., 2012; Mata et al., 2008; Torres et al., 2019; Zhang et al., 2017; Zykwinska et al., 2018), only a few exhibited significant amounts of this sugar in their composition. Examples include the EPS produced by *A. macleodii* subsp. *fijiensis* biovar deepsane HYD 657 (Le Costaouëc et al., 2012), and the EPS from *Alteromonas* sp. JL2810 that consisted in a trisaccharide repeating unit composed of Rha, GalA and mannose (Man) (Zhang et al., 2017). EPS C also contained fucose (Fuc) in its composition, although at low quantities. The presence of rare sugars such as Rha and Fuc, or uronic acids makes these EPS excellent candidates for various applications, such as anti-inflammatory and antioxidant agents, or in the synthesis of nucleoside analogs used as antiviral substances (Roca et al., 2015). Moreover, these EPS can be used as sources of rare sugar monosaccharides with high value applications. For instance, rhamnose is used as precursor in the synthesis of aroma and flavors (Roca et al., 2015), whereas Fuc is often present in the composition of anticarcinogenic and anti-inflammatory drugs, and incorporated in skin care formulations for the acceleration of wound healing (Roca et al., 2015).

Table 3.1.2. Characterization of EPS produced by *Alteromonas* strains isolated from French Polynesia: monosaccharide (Fuc, fucose; Gal, galactose; GalA, galacturonic acid; Glc, glucose; GlcA, glucuronic acid; Man, mannose; Rha, rhamnose) and acyl groups (Ac, acetate; Pyr, pyruvate; Suc, succinate) composition; sulphate, uronic acids, protein, and inorganic salts content; average molecular weight (Mw); polydispersity index (PDI); and the maximal thermal degradation temperature (T_{deg}).

EPS	Monosaccharide composition (molar ratio)	Acyl groups (wt%)	Sulphate (wt%)	Protein (wt%)	Inorganic content (wt%)	M_w (MDa)	PDI	T_{deg} (°C)
A	Glc:GlcA:Man:Gal:GalA (2.5:2.5:1.5:1.5:1.5)	Ac (0.52 ± 0.05) Pyr (4.89 ± 0.13)	2.76 ± 0.11	2.82 ± 0.36	7.71 ± 1.48	1.6 4.6[1]	1.3 1.3[1]	269
B	Gal:GlcA:Glc:GalA (2:1.5:1:1)	Ac (0.53 ± 0.03) Pyr (0.19 ± 0.00) Suc (1.75 ± 0.07)	3.29 ± 0.25	3.51 ± 0.12	19.99 ± 1.72	4.6	1.4	265
C	Gal:Rha:Man:Glc:GlcA:GalA:Fuc (4.5:2:1.5:1:1:1:0.5)	Pyr (1.07 ± 0.15)	3.39 ±0.01	2.56 ± 0.97	34.68 ± 0.24	1.2	1.4	268
D	GlcA:Glc:Gal:Man:GalA (3:2:2:1.5:1.5)	Ac (2.05 ± 0.01)	1.98 ± 0.01	6.77 ± 0.23	11.42 ± 0.31	1.4	1.5	262
E	Gal:Man:Rha:Glc:GlcA:GalA (3:2:1:1:1:1)	Suc (0.99 ± 0.04)	2.90 ± 0.01	2.07 ± 0.31	15.01 ± 0.13	2.5 4.3[1]	1.1 1.5[1]	267
F	Glc:Gal:GlcA:Rha:GalA (2:2:2:1:1)	Ac (0.71 ± 0.02) Pyr (5.52 ± 0.30)	3.43 ± 0.02	1.72 ± 0.02	13.69 ± 0.34	3.2	1.2	260

[1] EPS presented two distinct peaks in the size exclusion chromatography plots

Non-sugar substituents, such as acetyl, pyruvyl, succinyl and sulphate, were determined in the *Alteromonas* EPS (Table 3.1.2). All the six EPS had at least one type of acyl substituent with a total acyl content accounting for 1 to 5.5 % of the EPS dry mass. EPS A and F were particularly rich in pyruvyl groups (4.9–5.5 wt%) while EPS E and B exhibited a higher content in succinyl substituents (1 and 1.75 wt%, respectively). EPS D only had acetyl groups, which accounted for 2.05 wt% of the EPS' mass. Acetyl and pyruvyl substituents, although rarely, have been reported in a few EPS produced by *Alteromonas* strains (Le Costaouëc et al., 2012; Mata et al., 2008). On the other hand, succinyl, to the best of our knowledge, has never been found in *Alteromonas* EPS. Additionally, sulphate substituents were found in all EPS but in low concentrations ranging from 1.98–3.43 wt% (Table 3.1.2). Although more commonly found in algae, sulphated EPS have been described to be produced by some marine bacteria (Casillo et al., 2018), including *A. hispanica* F32 (0.25 wt%) (Mata et al., 2008), *A. infernus* GY785 (3 wt%) (Zykwinska et al., 2018), *Alteromonas* HYD 657 (7.5 wt%) (Le Costaouëc et al., 2012). Sulphated polysaccharides are of great interest in the fields of biomedicine, pharmaceuticals, nutraceutical foods and cosmetics due to their biological activity (Casillo et al., 2018). Reported bioactive properties include anti-inflammatory, immunomodulatory, antioxidant, antiviral, antibacterial, antiulcer, antitumor and antihyperlipidaemic activity, as well as anti-coagulant and/or anti-thrombotic properties (Jesus Raposo et al., 2015; Liu et al., 2016; Singh, Kant, et al., 2019; Xiao & Zheng, 2016). In fact, Sahana and Rekha (Sahana & Rekha, 2019) recently reported that the EPS produced by *Alteromonas* HYD 657 was biocompatible, capable of promoting cell proliferation and contributed to wound healing *in vitro*.

The EPS samples also presented some content of protein and inorganic salts (Table 3.1.2). The presence of few peptides (1.72–6.77 wt%) in the EPS is well in agreement with values previously reported for other *Alteromonas* strains (0–8 wt%) (Le Costaouëc et al., 2012; Mata et al., 2008; Raguénès et al., 2003; Sahana & Rekha, 2019). The inorganic salts content of EPS B, C and E (15.01–34.68 wt%) was similar to those reported (15.5–40 wt%) for *A. hispanica* F32 (Mata et al., 2008) and *Alteromonas* sp. PRIM-28 (Sahana & Rekha, 2019), whereas EPS A, D and F had a comparatively lower content (7.71–13.69 wt%).

The elemental analysis of the EPS (Fig. 3.1.2) was in line with the results described above. Nitrogen and sulphur were detected in all EPS (0.16–1.43 wt% and 0.76–2.31 wt%, respectively), which could be due to the presence of few peptides and sulphate groups in the EPS, respectively (Table 3.1.2).

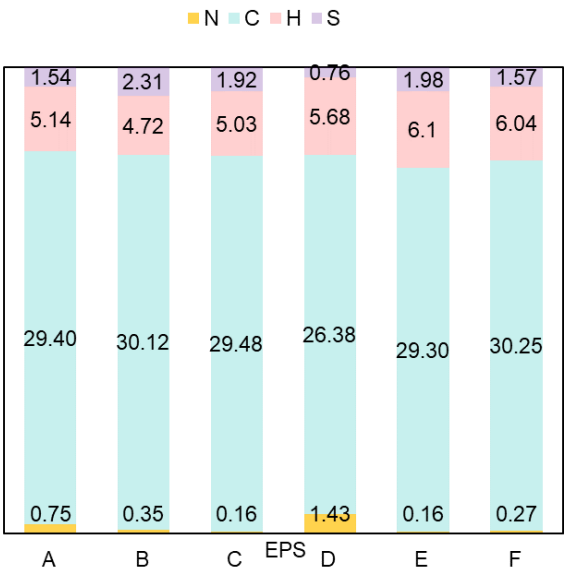

Figure 3.1.2. Elemental analysis (wt.%) of EPS A to F produced by *Alteromonas* strains isolated from French Polynesia**.**

Fourier Transform Infra-Red (FTIR) Spectroscopy

The FTIR spectra of the EPS, presented in Fig. 3.1.3, contained bands typically found in carbohydrates. The broad and intense band observed in the frequency range of 3500–3000 cm^{-1} corresponded to the O-H stretching vibration of hydroxyl groups, which partially overlaps the C-H stretching peak of CH_2 groups that appeared at around 2930 cm^{-1} (Chen et al., 2019; Concórdio-Reis, Pereira, et al., 2020). The absorption peak at approximately 1600 cm^{-1} and the adsorption region between 1300 and 1450 cm^{-1} are characteristic of the C=O asymmetric and symmetric stretching vibrations, respectively, of the carboxylates from the uronic acids (Chen et al., 2019; Concórdio-Reis, Pereira, et al., 2020; X. Liu et al., 2018). The band found at around 1245 cm^{-1} can be attributed to the stretching vibration of C-O-C from acyls, and/or of S=O from sulphate groups (Concórdio-Reis, Pereira, et al., 2020; X. Liu et al., 2018; Trabelsi et al., 2016). Finally, the bands in the frequency range of 1200–900 cm^{-1} can be assigned to C-O and C-C vibrations of the glycosidic bonds and pyranose carbohydrate ring (Concórdio-Reis, Pereira, et al., 2020; X. Liu et al., 2018).

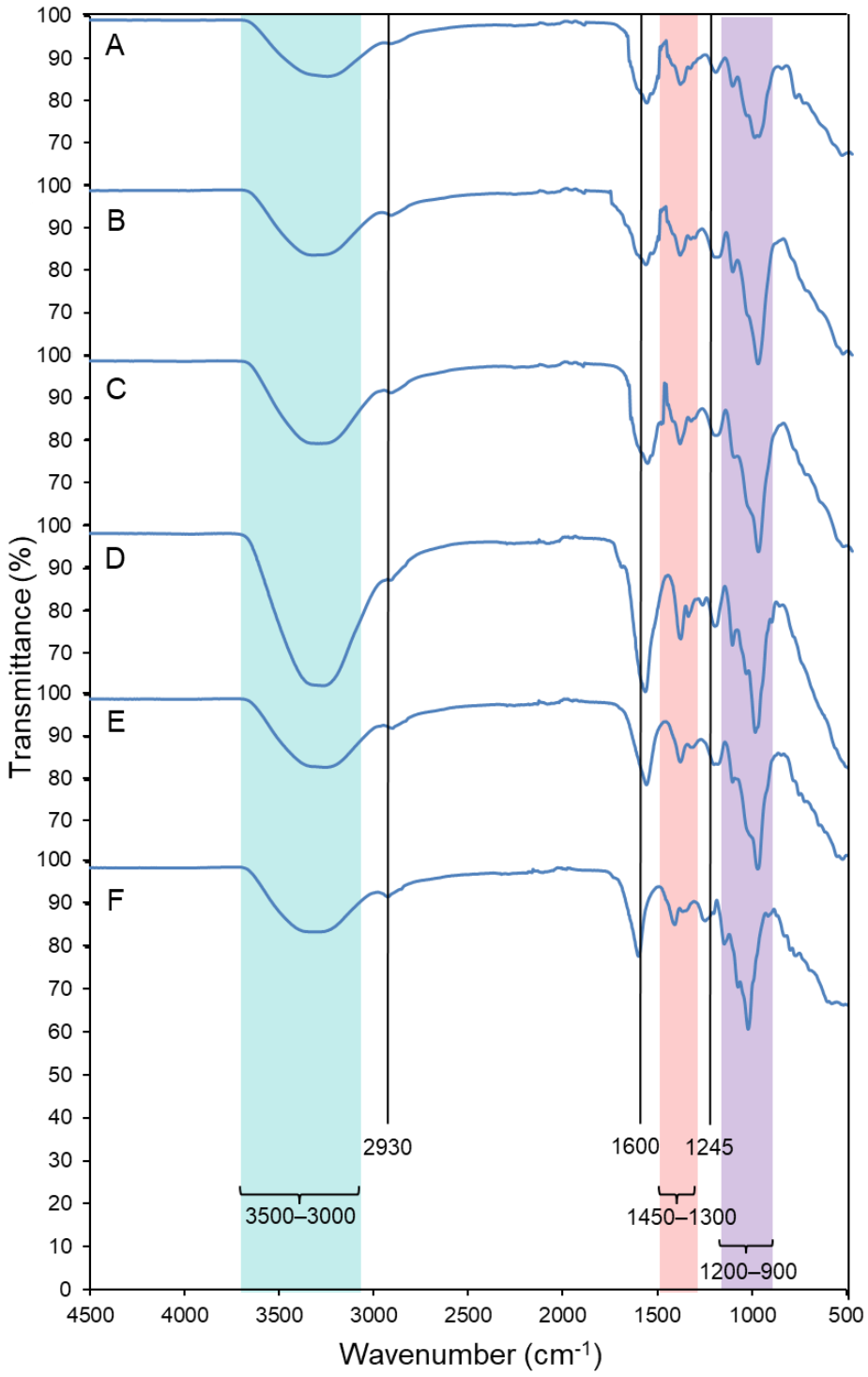

Figure 3.1.3. FTIR spectra of EPS A to F produced by *Alteromonas* strains isolated from French Polynesia**.**

Molecular mass distribution

EPS characterization in terms of composition and average molecular weight is presented in Table 3.1.2. Regarding the average molecular weights (M_w), all the EPS produced by *Alteromonas* strains presented a high Mw value, ranging from 1.2 – 4.6 MDa (Table 3.1.2). These Mw values are within the ranges reported for commercial EPS, such as xanthan, alginate and hyaluronic acid (0.3–50 MDa) (Freitas et al., 2017), and for other *Alteromonas* EPS (1.1–2 MDa), such as those produced by *Alteromonas infernus* GY785 (Zykwinska et al., 2018), *A. macleodii* subsp. *Fijiensis* HYD 657 (Le Costaouëc et al., 2012) and *A. macleodii* subsp. *Fijiensis* biovar *medioatlantica* (Raguénès et al., 2003). However, these values were higher than the Mw estimated for the EPS obtained from *Alteromonas* sp. PRIM-28 (Sahana & Rekha, 2019) and *Alteromonas* sp. JL2810 (Zhang et al., 2017), which were 780 kDa and 0.17 MDa, respectively, and lower than 19.7 MDa, the highest Mw reported so far for *Alteromonas* EPS (Mata et al., 2008). Interestingly, two distinct chromatographic peaks were detected in EPS A and EPS E, suggesting that strains Mo 169 and Fak 1386 might synthesize two types of high molecular weight EPS. Examples of the two distinctive HPSEC results, one and two chromatographic peaks, are presented in appendix A.1 (Fig. A.1). All EPS presented low PDI values, thus indicating their homogeneity in terms of molecules chain length (Table 3.1.2).

Thermogravimetric analysis

The applicability of materials is also dependent on their thermal characteristics; thus, the thermal stability of the six EPS was studied using thermogravimetric analysis (TGA) (Fig. 3.1.4). The thermal degradation of all the EPS occurred in three phases. In the first phase, an increase in temperature from 37–45 ^{o}C to 173–193 ^{o}C resulted in a decrease in weight of 12.1–17.5% (degradation steps are presented in appendix A.2, Table A.1), which was probably related to moisture loss (Concórdio-Reis, Pereira, et al., 2020; Insulkar et al., 2018). The highest mass loss value (17.5%) was observed for EPS E, which suggests a strong water binding capacity. Above this temperature, a significant weight loss of 30.2–45.1% occurred until 386–429^{o}C (Fig. 3.1.4 and Table A.1), which corresponded to the second degradation phase, probably related with the decomposition of the polysaccharide's side chains (Concórdio-Reis, Pereira, et al., 2020). The EPS's T_{deg} was similar in all EPS, varying between 260 ^{o}C and 269 ^{o}C (Table 3.1.2). Finally, as temperature rose above 386–429^{o}C, a gradual decrease in mass was observed for all EPS (2.5–6.4 %), identified as the third step of thermal degradation (Fig. 3.1.4), which is associated with polysaccharide's main-chain scission (Concórdio-Reis, Pereira, et al., 2020). All the EPS showed high char yields (32–53 %), with EPS C and B presenting the highest results (53% and 46%, respectively). This

trend is in agreement with previous results, since both EPS also presented the highest inorganic content in their composition (Table 3.1.2).

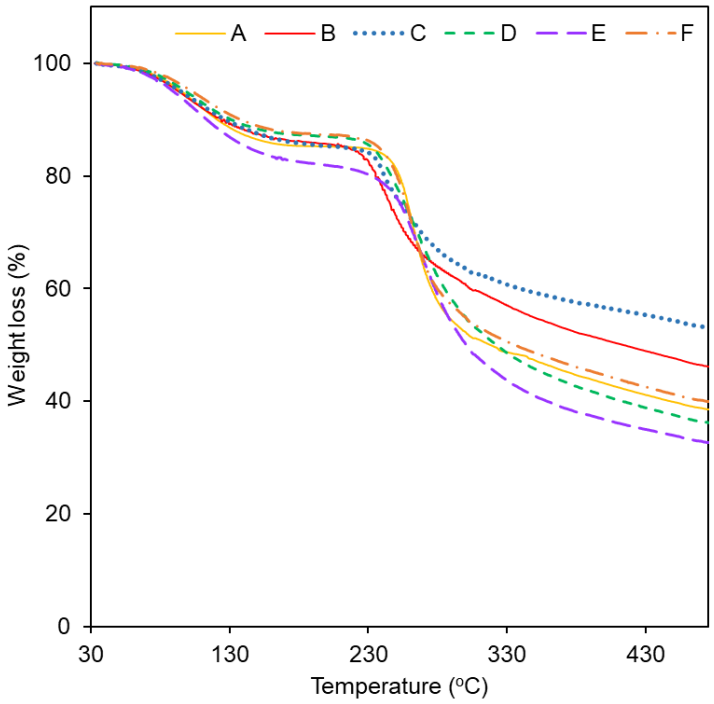

Figure 3.1.4. Thermogravimetric analysis (TGA) curves of EPS produced by *Alteromonas* strains isolated from French Polynesia**.**

3.1.4.3. EPS functional properties

Polysaccharides are excellent candidates for biomaterials with applications in several industries due to their valuable rheological properties, as well as the ability to form polymeric structures, such as films, gels, and emulsions (Roca et al., 2015).

Rheological properties

The flow curves obtained for purified EPS solutions (1 wt.%) are presented in Fig. 3.1.5. It can be observed that the EPS have diverse thickening capacities, since they show different values of apparent viscosity for the same shear rate, with the following order: A>E>B~C>D>F. This trend is clearly visible at the lower shear rate values tested, where the curves present or approach the first Newtonian plateau at which a high degree of polymer chains interactions (e.g. entanglements) is expected, and the molecules show high flow resistance and thereby higher viscosity (Ji et al., 2020; Rütering et al., 2018).

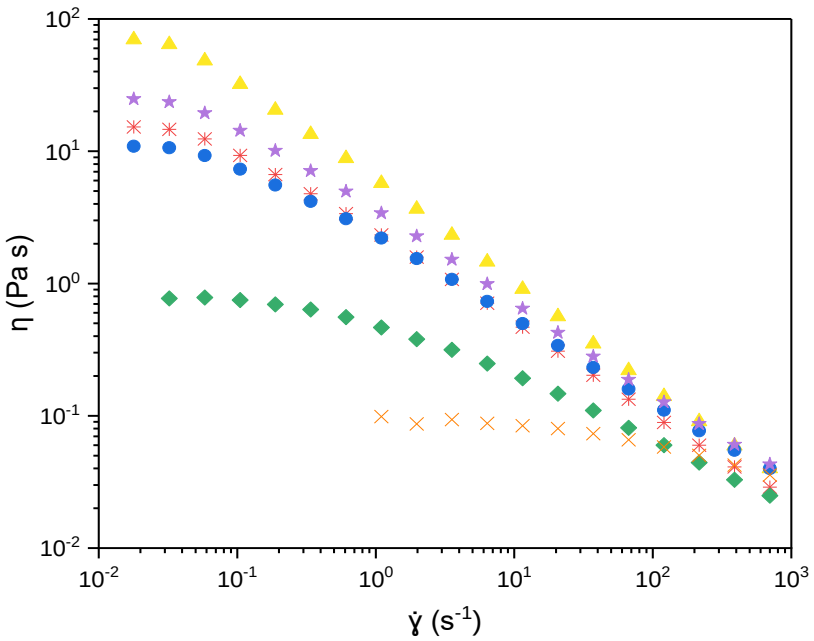

Figure 3.1.5. Apparent viscosity (η) as a function of shear rate (γ̇) for different aqueous solutions (1 wt.%) prepared with EPS A (▲), B (✳), C (●), D (◆), E (★), F (×), produced by *Alteromonas* strains isolated from French Polynesia.

The Newtonian plateau at low shear rates followed by a shear thinning behavior observed for all *Alteromonas* sp. EPS solutions is in line to that reported for other polysaccharide aqueous solutions (Alves, Freitas, Costa, et al., 2010; Cruz et al., 2011, p. 011; Freitas et al., 2011; Ji et al., 2020; Rütering et al., 2018). This viscosity dependence with the shear rate is commonly described by mathematic models, such as the Carreau model (Carreau, 1972):

$$\eta = \eta_\infty + \frac{\eta_0 - \eta_\infty}{[1 + (\lambda\,\dot{\gamma})^2]^{\frac{1-n}{2}}} \qquad (3.1.1)$$

where η is the apparent viscosity (Pa s), $\dot{\gamma}$ is the shear rate (s^{-1}), λ is a time constant (s), η_0 (Pa s) is the zero-shear rate viscosity, η_∞ is the viscosity of the second Newtonian plateau (Pa s), and n is the viscosity exponent. Equation (3.1.1) was simplified assuming η_∞ values much lower than η_0 and η, fitted to the data of Fig. 3.1.5 and the estimated parameter values are presented in Table 3.1.3.

Table 3.1.3. Carreau model parameters estimated for different aqueous solutions (1 wt.%) prepared with EPS produced by *Alteromonas* strains isolated from French Polynesia

EPS	η_0 (Pa s)	*n (-)*	λ (s)	R^2	MRE* (%)
A	76.2±2.1	0.181±0.051	24.6±2.8	0.999	13.6
B	16.1±0.3	0.361±0.024	19.7±1.5	0.999	9.8
C	11.3±0.2	0.437±0.021	17.7±1.5	0.999	14.9
D	0.74±0.02	0.549±0.034	2.26±0.27	0.998	5.6
E	26.3±0.4	0.338±0.025	21.2±1.6	0.999	5.9
F	0.09±0.01	0.772±0.056	0.07±0.04	0.998	3.1

$$*MRE = \sum_{i=1}^{j} \left| \left(x_{\exp i} - x_{\mathrm{model}\, i} \right) / x_{\exp i} \right| / j \text{ x } 100$$

EPS A is the one showing a higher thickening effect, with an estimated η_0 of 76.2±2.1 Pa s, followed by a quick transition to a strong shear thinning illustrated by the low viscosity exponent (*n* = 0.181±0.051). This behavior can be compared with that demonstrated by 1 wt.% xanthan solution (Freitas et al., 2011). As the viscosity decreases, by the order indicated above, the time constant values also decrease. Since the time constant is a relaxation time, it means that under lower viscosity values the rate of formation of new interactions between molecules increases over the rate of their disruption. Consequently, the transition from Newtonian plateau to shear-thinning regimes moves to higher shear rate values, as observed (Fig. 3.1.5) (Alves, Freitas, Costa, et al., 2010; Cruz et al., 2011). Polysaccharides with shear thinning behavior are commercially relevant in specific areas such as cosmetics, food products, pharmaceuticals, oil drilling fluids and paints (Torres et al., 2015).

It is not detected an evident correlation between the viscosity properties and the average molecular weight and chemical composition of the EPS presented in Table 2. The interactions between polymer chains in solution are strongly dependent, not only of such factors, but also on the on the polymers chemical structure. As such, deeper studies are needed to evaluate the effect of single factors (e.g. chemical composition and structure, average molecular weight, charge density, polymer concentration, temperature, ionic strength) and their interaction, on the observed apparent viscosity.

Gel forming capacity

The presence of negatively charged groups (uronic acids, sulphate and acyl substituents) render EPS a polyelectrolyte character that allows the formation of physical cross-linking interactions with cations, leading to gel formation (Casillo et al., 2018; Hu & Xu, 2020). The EPS gelation ability was tested using different polyvalent cations (Mg^{2+}; Cu^{2+}, Ca^{2+}; Fe^{2+}, Fe^{3+}), under standard and alkaline conditions (Table 3.1.4). Gel formation was assessed according with their strength and homogeneity: (+)

for homogeneous gels that maintained their gel structure in an inversion test (Fig. 3.1.6), (-) for homogeneous gels that did not sustain their structure in the inversion test, and (--) for small non-homogeneous gels. Images of gels (-) and (--) are presented in Appendix A.3 (Fig A.2). As shown in Table 3.1.4, under standard conditions, only EPS C and E were able to form strong homogenous gels with Fe^{2+} (Fig. 3.1.6). Interestingly, both EPS were majorly composed of galactose (Gal) and, with the exception of Fuc in EPS C, presented the same sugar monomers but in different ratios (Table 3.1.2). Moreover, both had the lowest uronic acid content (around 17 and 22 mol%, respectively) of the six EPS tested. Cu^{2+} and Fe^{3+} were capable of promoting gelation of EPS A and C; and A and D, respectively. Although homogenous, these gels were weaker and did not maintain their structure upon inversion. Nonetheless, the Fe^{3+}-cross-linked polysaccharide hydrogels are particularly interesting since they often show improved properties such as stimuli-responsiveness abilities, redox properties, photosensitivity, higher mechanical stability, or enhanced absorptivity (Massana Roquero et al., 2022).

Table 3.1.4. Gel formation under standard and alkaline conditions was assessed according to their strength and homogeneity: (+) for homogeneous gels that maintained their gel structure in an inversion test, (-) for homogeneous gels that did not sustain their structure in the inversion test, (--) for small non-homogeneous gels, and blank for no gelation observed.

Standard conditions						
Cation	A	B	C	D	E	F
Mg^{2+}						
Cu^{2+}	-		-		--	
Ca^{2+}						
Fe^{2+}			+		+	
Fe^{3+}	-				--	-
Alkaline conditions						
Cation	A	B	C	D	E	F
Mg^{2+}	+	-	-	--	-	+
Cu^{2+}		+	--		--	
Ca^{2+}	+		-	--	--	+
Fe^{2+}	-	-	--	--	--	-
Fe^{3+}	--		--	--	--	

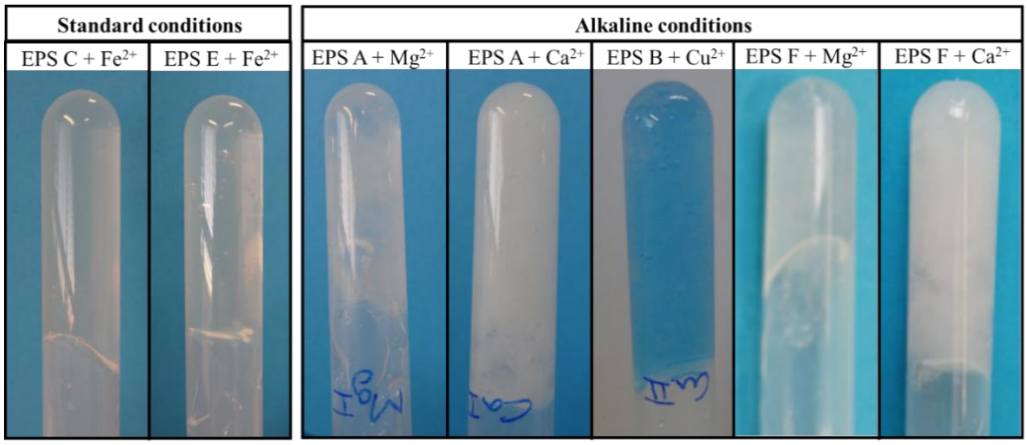

Figure 3.1.6. Results from gel formation type (+) with different cations, under standard and alkaline conditions.

Overall, alkaline conditions seemed to improve gelation since five combinations originated strong gels (Table 3.1.4, Fig 3.1.6). For EPS A and F, strong gelation occurred in the presence of Mg^{2+} and Ca^{2+}, and a weak gel was formed in the presence of Fe^{2+}. In terms of their compositions, EPS A and F had high uronic acid content (42.1 and 37.5 mol%, respectively) and similar acyl compositions, namely both were rich in pyruvate and had acetate in smaller amounts (Table 3.1.2). Moreover, EPS B formed a strong gel only with Cu^{2+} cations (Table 3.1.4, Fig 3.1.6). EPS B is composed of Gal, GlcA, Glc and Gal A and, compared with the other polymers, had the highest uronic acid content (45.5 mol%) (Table 3.1.2). Similarly, the two *Vibrio* EPS, HE800 and MO245, formed strong gels with Cu^{2+} but not with other cations, such as Ca^{2+} (Martin-Pastor et al., 2019; Zykwinska et al., 2016). The authors suggested that these results were due to the stronger affinity of uronic acid rich polysaccharides for Cu^{2+} compared to Ca^{2+} (Martin-Pastor et al., 2019), which is in accordance to our findings. The presence of cations, such as Ca^{2+}, Mg^{2+}, Cu^{2+}, might grant valuable biological properties to the gels, since these metals have antibacterial properties, are capable of promoting cell proliferation and differentiation, increase growth factors expression, and stimulate angiogenesis (Hoppe et al., 2011; Zykwinska et al., 2016). Thus, these cation-mediated gels might have a promising future in wound management and tissue engineering.

3.1.5. Conclusions

The EPS from six *Alteromonas* strains collected from French Polynesia marine environments were characterized and investigated for their functional properties. The *Alteromonas* strains produced high molecular weight heteropolysaccharides, with high contents in uronic acids and rare sugars in their composition. These monomers, together with the sulphate groups also detected in their composition, indicate that these EPS could have interesting biological properties that are worthy to explore. Moreover, the EPS showed a good thermal stability, interesting rheological properties, and gel forming capacity, envisaging their potential in applications such as biomedicine, pharmaceuticals, cosmetics, or food industry. Based on the higher thickening effect and the capacity to form gels with Fe^{3+}, *A. macleodii* Mo169 (EPS A producer) was the bacterium chosen for further investigation.

Chapter | 3.2

Films based on bacterial EPS from unusual marine environments

The results presented in this chapter were published in the following international scientific journal:

Concórdio-Reis, P., Pereira J.R., Alves, V.D., Nabais, A. R., Neves, L. A., Marques, A.C., Fortunato, E., Moppert, X., Guézennec, J., Reis, M.A.M. & Freitas, F. Characterisation of films based on exopolysaccharides from *Alteromonas* strains isolated from French Polynesia marine environments. *Polymers* 14, 102876. DOI: 10.3390/polym14204442.

3.2.1. Summary

This work assessed the film-forming capacity of EPS produced by six *Alteromonas* strains recently isolated from different marine environments in French Polynesia atolls. The films were transparent and resulted in small color alterations when applied over a colored surface (ΔE_{ab} below 12.6 in the five different colors tested). Moreover, Scanning Electron Microscopy showed that the EPS' films were dense and compact, with a smooth surface. High water vapour permeabilities were observed (2.7–6.1 x 10^{-11} mol m^{-1} s^{-1} Pa^{-1}), which are characteristic of hydrophilic polysaccharide films. The films were also characterized in terms of barrier properties to oxygen and carbon dioxide. Interestingly, different behaviors in terms of their mechanical properties under tensile tests were observed: three of the EPS films were ductile with high elongation at break (ε) (35.6–47.0 %), low tensile strength at break (Ƈ) (4.55–11.7 MPa) and low Young's modulus (εm) (10–93 MPa), whereas the other three were stiffer and more resistant with a higher Ƈ (16.6–23.6 MPa), lower ε (2.80–5.58 %) and higher εm (597–1100 MPa). These properties demonstrate the potential of *Alteromonas* sp. EPS' films to be applied in different areas, such as, biomedicine, pharmaceuticals, or food packaging.

3.2.2. Introduction

Petrochemical-based plastics have widespread use in nowadays society due to their low-cost and useful characteristics, that include good mechanical and thermal properties, heat molding capacity, suitable gas barrier properties and high transparency (Alves et al., 2011; Ferreira et al., 2014). However, due to their limited biodegradability that imposes a serious environmental and human health threat, those synthetic plastics are expected to be replaced by novel biodegradable materials (Zhao et al., 2021). Biopolymers, such as polysaccharides, are a promising substitute since they are biodegradable, biocompatible and non-toxic, being obtained from renewable resources (Alves et al., 2011; Kaewprachu et al., 2022; Li et al., 2020). Applications of polysaccharide-based films include food packaging (Zhao et al., 2021), drug delivery systems (Laubach et al., 2021; Tabernero & Cardea, 2020), coatings for medical devices (Freitas, Alves, Reis, et al., 2014) and wound dressings (Shen et al., 2021). Most of such applications were investigated using polysaccharides extracted from plants (e.g. starch), algae (e.g. alginate), or animal resources (e.g. chitosan). Only recently, microbial polysaccharides, due to their improved properties, started to arise as competitive alternatives to other natural polymers as well as synthetic products (Freitas, Alves, Reis, et al., 2014).

Polysaccharides-based films are considered effective barriers against gases, including oxygen and carbon dioxide, when exposed to low relative humidity conditions (Freitas, Alves, Reis, et al., 2014). This property is relevant for maintaining the food's nutritional and sensory properties in food packaging applications (Zhao et al., 2021) and the stability of bioactive molecules in drug delivery systems (Laubach et al., 2021). However, their hydrophilic nature renders them poor barrier properties against water vapour, which limits their application as water barriers in food packaging (Freitas, Alves, Reis, et al., 2014; Zhao et al., 2021). In other hand, they constitute interesting materials to produce film pads with good water absorption capacity to be used in active packages (Vieira et al., 2022). In addition, due to their hydrophilicity, polysaccharides can form non-covalent bonds with growth factors to support bioadhesion (Shen et al., 2021) and can absorb the exudate produced during the wound healing process, which are important aspects for wound dressing materials (Gruppuso et al., 2021). However, to meet the requirements of most applications, the mechanical properties of polysaccharide-based films still need to be improved (Freitas, Alves, Reis, et al., 2014; Zhao et al., 2021). To that end, several strategies have been studied, including blending with other polymers, the addition of hydrophobic materials and plasticizers, or chemical modifications of the film-forming polysaccharide (Freitas, Alves, Reis, et al., 2014; Zhao et al., 2021). Another strategy is to look for novel polymers with different molecular structures and functional properties that might result in improved films' properties.

In this context, the potential of microbial polysaccharides is limitless as newly isolated EPS-producing bacteria can be considered as sources of polysaccharides with novel or improved properties. In addition, marine environments, which represent the largest ecosystem of the planet, are an underexplored source of novel microorganisms characterized by high ecological and metabolic diversity with great biodiscovery potential (Concórdio-Reis et al., 2021; Guezennec et al., 2012). EPS from marine bacteria display great structural and compositional diversity, including the presence of atypical sugar monomers (e.g. fucose, fructose, rhamnose), and high contents in uronic acids and sulphate groups (Concórdio-Reis et al., 2021; Zarandona et al., 2020).

Recently, the EPS from six different *Alteromonas* strains were isolated from unique French Polynesia marine environments, namely Moorea Island lagoon, Fakarava atoll and Tikehau atoll (Concórdio-Reis et al., 2021). The six EPS are high molecular weight heteropolysaccharides composed of neutral monosaccharides (glucose, galactose, and mannose, rhamnose and fucose), and with high content of uronic acids (glucuronic acid and galacturonic acid) that contribute to their anionic

character (Concórdio-Reis et al., 2021). The EPS solutions revealed an interesting shear thinning behavior and could form gels by the addition of Fe^{2+} or in the presence of Mg^{2+}, Cu^{2+}, or Ca^{2+} under alkaline conditions, which supports their potential as biomaterials in biotechnological applications (Concórdio-Reis et al., 2021). In this work, these *Alteromonas* sp. EPS were used to prepare biodegradable films, which were then characterized in terms of their optical, morphological, mechanical and barrier properties, envisaging their potential application in packaging, wound management, or drug delivery.

3.2.3. Materials and methods

3.2.3.1. Exopolysaccharide production

The EPS (A–F) were produced by six *Alteromonas* strains isolated from different locations in French Polynesia, as described in Chapter 3.1.

3.2.3.2. Preparation and rheological characterization of filmogenic solutions

Aqueous solutions were prepared by dissolving the freeze-dried EPS in deionized water (1.5 wt.%) under constant stirring, at temperatures up to 60 ºC. Sodium azide (10 mg L^{-1}) was added to prevent microbial growth. After dissolution, glycerol was added as a plasticizer (60 and 30 $wt._{glycerol}.wt._{polymer}^{-1}$ % for EPS A, and EPS B–E, respectively), and the solution was stirred for complete homogenization. Finally, air bubbles were removed under vacuum.

Rheological characterization of the film-forming solutions was performed on a MCR92 modular compact rheometer (Anton Paar, Graz, Austria) equipped with a cone-plate geometry (angle 2º, diameter 35 mm, 0.145 mm gap). The flow curves were obtained at 25 ºC, using a steady state flow ramp in the shear rate range of 0.01 s^{-1} to 700 s^{-1}. The Carreau model (Eq. (3.2.1)) was employed, assuming η_∞ values much lower than η_0 and η (Carreau, 1972; Concórdio-Reis et al., 2021):

$$\eta = \eta_\infty + \frac{\eta_0 - \eta_\infty}{[1 + (\lambda\,\dot{\gamma})^2]^{\frac{1-n}{2}}} \qquad (3.2.1)$$

where η is the apparent viscosity (Pa s), $\dot{\gamma}$ is the shear rate (s^{-1}), λ is a time constant (s), η_0 (Pa s) is the zero-shear rate viscosity, η_∞ is the viscosity of the second Newtonian plateau (Pa s), and n is the viscosity exponent.

3.2.3.3. Films' preparation

The films were obtained by casting the filmogenic solutions (30 mL) into polystyrene Petri dishes (diameter 88 mm) and left to dry at 30 ºC for 48 h. Afterwards, the films were peeled from the Petri dishes, and conditioned at a controlled relative humidity (RH) of 53% by placing the films inside a desiccator that contained a saturated $Mg(NO_3)_2$ solution. RH was monitored using a thermohygrometer (Vaisala, Finland). Films' thickness was measured in at least six points using a digital micrometer (Mitutoyo, UK).

3.2.3.4. Optical characterization

The films' optical and UV barrier properties were evaluated by measuring the absorbance spectrum (200–600 nm) using a CamSpec M509T spectrophotometer (United Kingdom). In addition, the films transparency was determined as the ratio between absorbance at 600 nm (Abs_{600}) and film thickness (mm) and was expressed as Abs_{600} mm^{-1} (López & García, 2012). The alteration of color on objects due to the application of the films was assessed by measuring the color parameters of colored paper, with and without the films. A Minolta CR-400 (Konica Minolta, Japan) colorimeter was used, and the CIEL*a*b* color space was applied with the calculation of color differences (ΔE_{ab}), chroma (C_{ab}) and hue (h_{ab}), using the following equations:

$$\Delta E_{ab} = [(\Delta L^*)^2 + (\Delta a^*)^2 + (\Delta b^*)^2]^{1/2} \quad (3.2.2)$$

$$C_{ab} = (a^{*2} + b^{*2})^{1/2} \quad (3.2.3)$$

$$h_{ab} = arctan\ \frac{b^*}{a^*} \quad (3.2.4)$$

where L^* is the lightness, a^* defines the red/green value and b^* the yellow/blue value.

3.2.3.5. Morphological characterization

The morphology of the EPS films was assessed by Scanning Electron Microscopy (SEM) using a SEM Hitachi TM 3030Plus Tabletop. The samples were mounted on a SEM stub and coated with a thin layer of Iridium.

3.2.3.6. Mechanical properties

Tensile tests were performed using a texture analyzer (Food Technology Corporation, England) equipped with a 250 N loading cell. The samples were cut into rectangular shape pieces (15 mm x 50 mm), attached on tensile grips, and stretched at 0.5 mm s^{-1} in tension mode until break. Young's modulus (εm, MPa) was determined within the elastic deformation of the stress–strain curve, as the initial slope of stress as a function of strain. The tensile strength at break (Ƈ, MPa) was calculated as the ratio of the maximum force to the films' initial cross-sectional area. The elongation at break (ε, %) was determined as the ratio of the extension of the sample upon rupture by its initial length. Five replicates of each sample were analyzed.

3.2.3.7. Water vapour permeability

For the water vapour permeability (WVP) tests, the films were sealed on the top of a glass cell, with a diameter of 35 mm, which contained a saturated NaCl solution (RH=75.3%). The cells were placed inside a desiccator that contained a saturated $MgCl_2$ solution (RH=34.7%). The desiccator was equipped with a fan to promote air circulation, and the temperature and RH inside the desiccator were measured throughout the experiment using a thermohygrometer (Vaisala, Finland). The water vapor flux was measured by weighing the cell at regular time intervals over a period of 8 h, and the WVP (mol m s^{-1} Pa^{-1}) was calculated by the following equation:

$$WVP = \frac{N_w \times \delta}{\Delta P_{w.eff}} \quad (3.2.5)$$

where N_w is the water vapour molar flux (mol m^{-2} s^{-1}), δ (m) is the film thickness and $\Delta P_{w,eff}$ (Pa) is the effective driving force, calculated as the water vapour pressure difference between both sides of the film (Alves et al., 2011). Two film replicas were analyzed for each EPS.

3.2.3.8. Gas permeability

The gas permeability measurements were performed using a stainless-steel cell with two identical chambers separated by the film. The permeability was evaluated by pressurizing the feed chamber up to 0.7 bar with pure gas, namely carbon dioxide (99.998%) or oxygen (99.999%) (Praxair, Portugal), followed by the measurement of the pressure change in both chambers over time, using pressure transducers (JUMO, Model404327, Germany). The temperature was maintained at 30 ºC using a

thermostatic bath (Julabo, Model EH, Germany). The permeability was calculated using Eq. (3.2.6):

$$\frac{1}{\beta}\left(\frac{\Delta p0}{\Delta p}\right) = P\,\frac{\mathrm{t}}{\delta} \qquad (3.2.6)$$

where Δp (bar) is the pressure difference between the feed and permeate compartment, P ($m^{-2}\,s^{-1}$, where 1 barrer = 1×10^{-10} cm^3 (STP) cm cm^{-2} s^{-1} cm Hg^{-1} = 8.3×10^{-13} $m^2\,s^{-1}$) is the gas permeability, t (s) is the time, δ (m) is the film thickness, and β (m^{-1}) is the geometric parameter of the cell, as described by Alves, Costa et al. (2010).

3.2.4. Results and discussion

3.2.4.1. Rheology of filmogenic solutions

All filmogenic solutions had the same EPS concentration (1.5 wt%) and glycerol was added as plasticizer. Glycerol, a low molecular weight molecule, acts as a plasticizer since its presence weakens the intermolecular interactions between the polysaccharide chains, resulting in a less compact structure with enhanced flexibility (Piermaria et al., 2009; Vivek et al., 2021). Moreover, glycerol is also an effective humectant that can retain moisture, improving the films' plasticity (Ferreira et al., 2016; Li et al., 2020). For the preparation of the films, glycerol was added as a plasticizer agent at a concentration of 30 $wt._{glycerol}\ wt._{pol.}{}^{-1}$ %. However, the film obtained with EPS A was brittle, fragile and easily breakable, making it very difficult to handle. This result is characteristic of polysaccharide films where no plasticizer was added, or the proportion of plasticizer:polysaccharide is not sufficient (Ferreira et al., 2016; Rodriguez et al., 2017). Therefore, a higher plasticizer concentration was used (60 $wt._{glycerol}\ wt._{pol.}{}^{-1}$ %) for this EPS, enabling the production of films easily handled without breaking.

As illustrated in Fig. 3.2.1, all the filmogenic solutions prepared with the *Alteromonas* sp. EPS presented a non-Newtonian shear thinning behaviour characteristic of most polysaccharides' solutions, in accordance with a previous rheological evaluation of these EPS solutions (Concórdio-Reis et al., 2021). Additionally, the filmogenic solutions immediately recovered their original apparent viscosity upon elimination of the shear force, resulting in overlapping flow curves for all EPS samples. A rapid recoverability is a desired feature, as it prevents dripping and guarantees films' homogeneity after the application procedure.

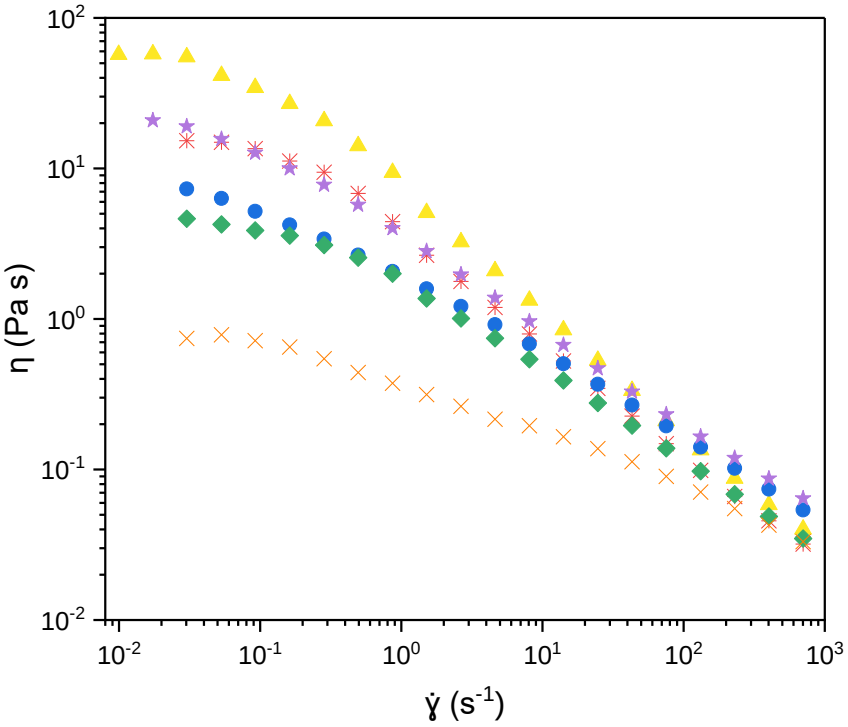

Figure 3.2.1. Apparent viscosity (η) as a function of shear rate ($\dot{\gamma}$) for the filmogenic solutions prepared with EPS A (▲), B (✳), C (●), D (◆), E (★), F (×), produced by *Alteromonas* strains isolated from French Polynesia (1.5 wt.% EPS, 30 wt.% glycerol for all solutions, except EPS A that was prepared with 60 wt.% glycerol).

The obtained flow curves were fitted to the Carreau model and the estimated parameters are presented in Table 3.2.1. For EPS A solution, even though the EPS concentration was higher in this work (1.5 wt.%) when compared to 1 wt.% EPS studied in Chapter 3.1, a lower η_0 value (59.2 Pa s) was observed, in comparison with that previously reported (76.2 Pa s). In addition, regarding the filmogenic solutions prepared with EPS B, C, and E, their η_0 values were similar to those reported previously for 1 wt.% EPS (16.4 and 16.1 Pa s, 8.06 and 11.3 Pa s, 21.9 and 26.3 Pa s, respectively), despite an expected increase due to the higher EPS concentration used in the present work (1.5 compared with 1 wt.%) (Concórdio-Reis et al., 2021). These facts may be attributed to the presence of glycerol (60 wt.% polymer basis for EPS A and 30 wt.% polymer basis for EPS B, C and E), acting as lubricant and decreasing polymer-polymer interactions. On the other hand, the η_0 values of EPS D and EPS F filmogenic solutions increased despite the addition of glycerol (from 0.74 to 4.40 Pa s, and 0.09 to 0.79 Pa s, respectively). Differences on molecular structure between the various EPS is a possible explanation for the diverse behavior of the filmogenic solutions viscosity when increasing polymer concentration in the presence of glycerol. Decreasing the filmogenic solutions' viscosity is advantageous since it

facilitates homogenization of the filmogenic solution and the escape of air bubbles, which would result in defects in the film matrix (e.g., presence of pores, holes or differences in thickness).

Table 3.2.1. Carreau model parameters (η_0, zero-shear rate viscosity; n, viscosity exponent; λ, time constant) estimated for the filmogenic solutions prepared with the different EPS produced by *Alteromonas* strains isolated from French Polynesia.

EPS	η_0 (Pa s)	n (-)	λ (s)	R^2
A	59.2±1.1	0.374±0.036	22.6±2.5	0.996
B	16.4±0.3	0.329±0.050	8.30±1.00	0.995
C	8.06±0.15	0.549±0.008	25.3±1.9	0.999
D	4.40±0.08	0.474±0.028	5.95±0.69	0.996
E	21.9±0.3	0.463±0.014	27.2±1.9	0.999
F	0.79±0.01	0.667±0.010	9.79±1.04	0.998

The rheology of filmogenic solutions is an important factor for the production of films by casting and drying at an industrial scale, since it strongly affects the type of equipment to be used and the processing conditions (Piermaria et al., 2009). This information is relevant not only to produce stand-alone films, but also for the application of coatings into products by dipping, brushing, or spraying (Piermaria et al., 2009). The shear thinning behavior of EPS filmogenic solutions and the recovery of the original apparent viscosity upon elimination of the shear force, envisage suitable properties to produce films by casting using automatic film application on a flat support.

3.2.4.2. Film appearance, morphology, and optical characterization

As can be seen in Fig. 3.2.2 (left panel), all the *Alteromonas* sp. EPS formed homogeneous transparent films that were flexible but resistant when handled. Except for film C that appeared to have a rougher surface, the SEM images showed that all the films had a smooth and homogenous surface, without pores or holes (Fig 3.2.2, center panel). The cross-section images confirmed the roughness of EPS C film and showed that the remaining films prepared with EPS A to F had a more compact and homogenous structure with no porosity inside the membrane (Fig. 3.2.2).

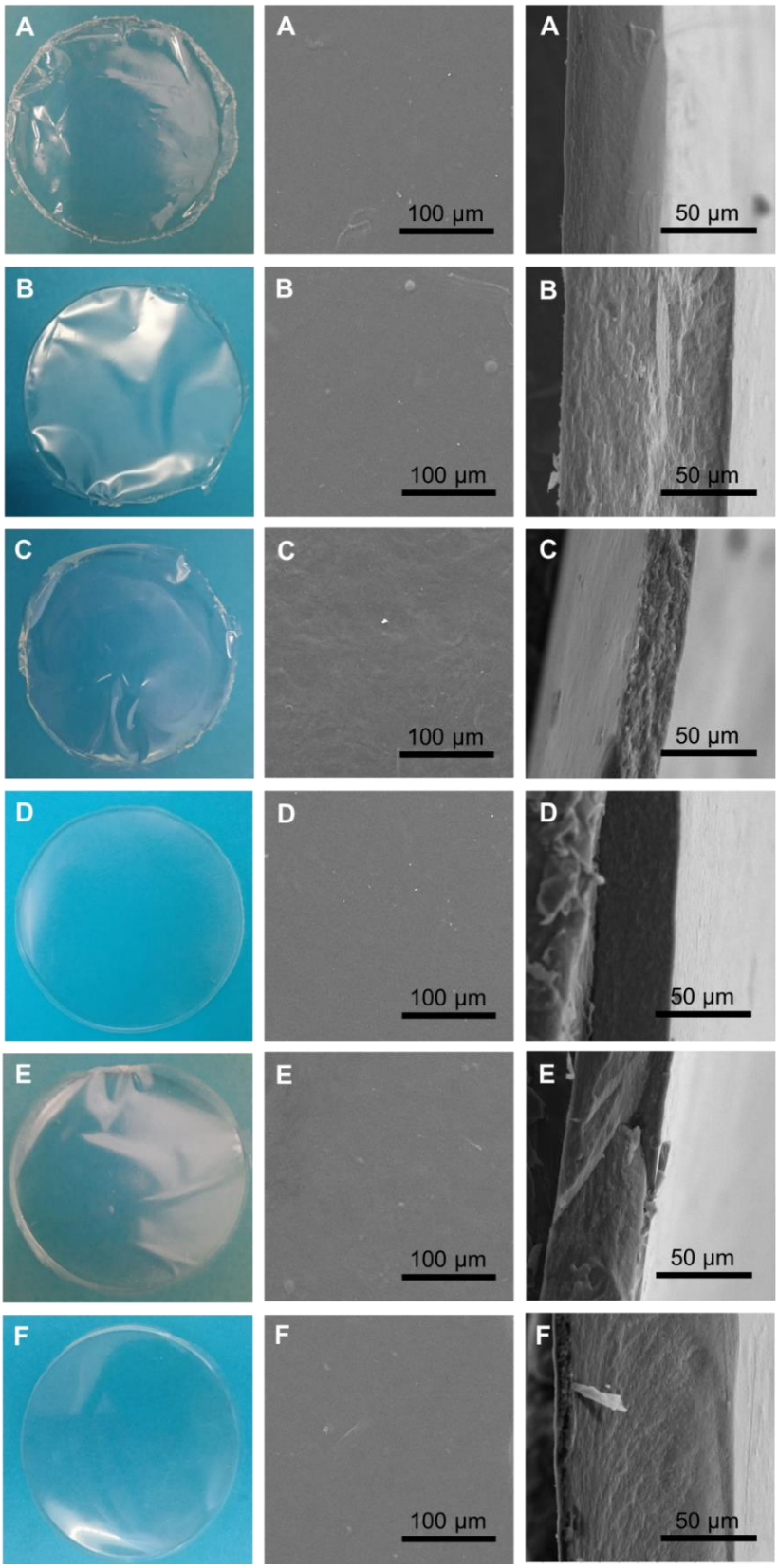

Figure 3.2.2. Photographs of the films prepared with *Alteromonas* EPS A–F (left panel) and Scanning Electron Microscopy images: top view (center panel) and cross section view (right panel).

As presented in Fig. 3.2.3, no significant optical bands were found in the spectra from 400 to 600 nm, thus showing the films were transparent. In this range, the optical density of the film prepared with EPS C was higher, suggesting that this film was opaquer (Fig. 3.2.3). Nonetheless, the films' transparency values were within the range of those reported for other biopolymer films, namely chitosan (1.9) (Ferreira et al., 2016), gelatin (0.67) (Ferreira et al., 2014), and Kefir microflora EPS (2.71) (Piermaria et al., 2009); and lower than those reported for cassava starch (4.7), corn starch (4.6) (López & García, 2012), and *Enterobacter* A47 EPS films (3.67) (Ferreira et al., 2014). Commonly used synthetic plastics films, such as low-density polyethylene (LDPE), oriented polypropylene and polyvinyl dichloride, also presented similar transparency values (3.05, 1.67 and 4.58, respectively) (López & García, 2012; Piermaria et al., 2009). Moreover, the absorption band observed between 200 and 300 nm suggests that the EPS films show barrier properties to UV radiation (López & García, 2012) (Fig. 3.2.3), that might be further improved by increasing the thickness of the films.

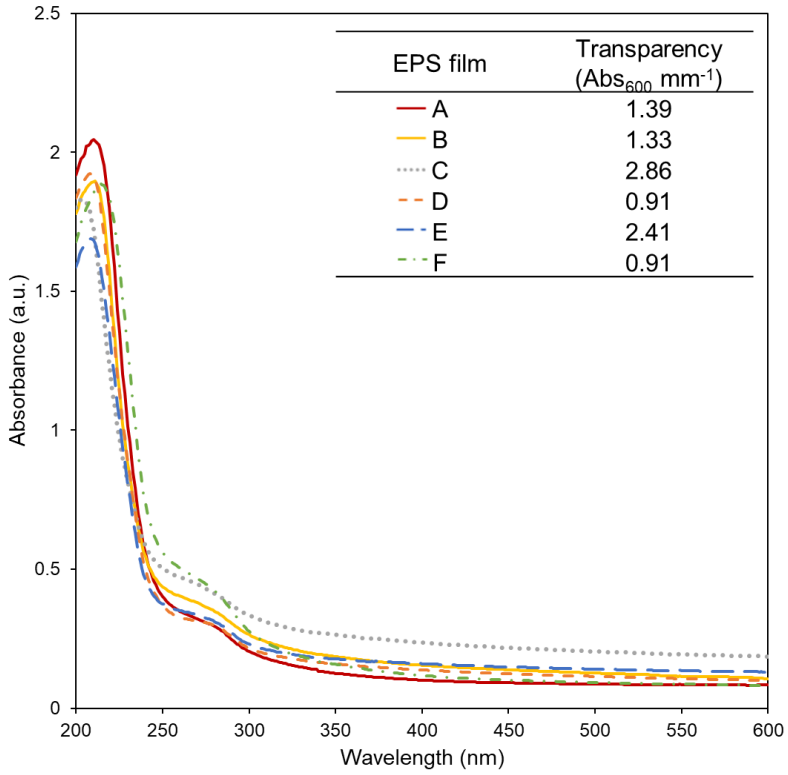

Figure 3.2.3. UV-vis absorption spectra and transparency (insert) of the films prepared with EPS A–F produced by *Alteromonas* strains isolated from French Polynesia.

The color changes in objects was investigated by comparing the color parameters of colored paper sheets uncovered and covered by the films. The CIEL*a*b* color parameters for five different colors are presented in Fig. 3.2.4 and Table 3.2.2. For all EPS films, the hue (h^*_{ab}, angle towards the horizontal axes) did not change with the application of the film (Fig. 3.2.4). However, there was an approximation towards the origin, indicating that color saturation (chroma, C^*_{ab}) decreased (Fig. 3.2.4). Considering the color alteration (ΔE_{ab}) (Table 3.2.2), for all *Alteromonas* sp. EPS films, the values were low (1.7–12.6), and the lowest changes were observed for white and blue colors (ΔE_{ab}<5). Even low, these alterations may be perceived by the human eye, since color differences with ΔE_{ab} values below 1.5 are classified as small, and only ΔE_{ab} values below 0.2 are not perceptible (Silva & Silva, 1999).

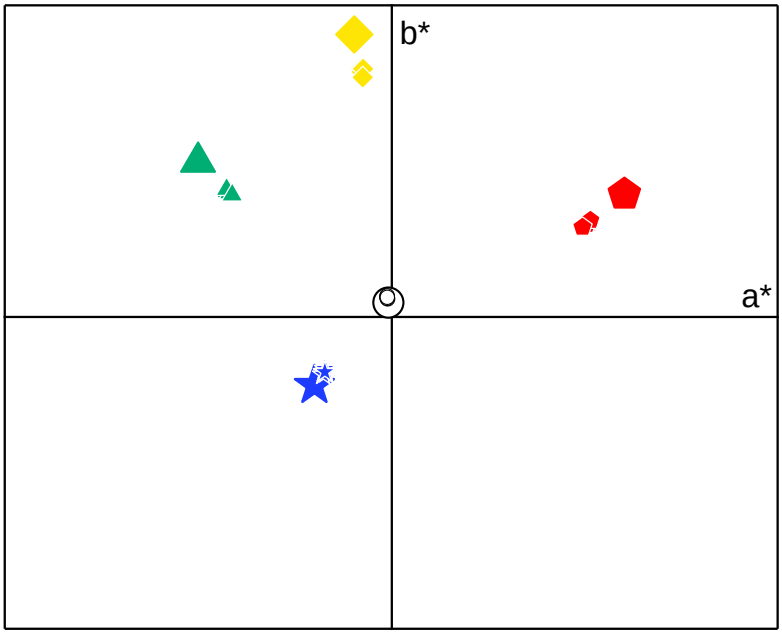

Figure 3.2.4. Parameters a* and b* of the CIELAB system for colored paper sheets uncovered (large symbols) and covered (small symbols) by the EPS films.

Higher ΔE_{ab} values were found for the films prepared with *Enterobacter* A47 EPS in all colors (9.2–19.8) (Ferreira et al., 2016). Chitosan films also presented higher ΔE_{ab} values in blue and white colored surfaces (11.6 and 9.7, respectively), but similar values for the other colors tested (9.9–12.5) (Ferreira et al., 2016).

Table 3.2.2. Parameters a*, b* and L* of the CIELAB system and calculated color alteration (ΔE_{ab}) that resulted by the covering of colored paper sheets with the different EPS films.

Color	Parameter	EPS					
		A	**B**	**C**	**D**	**E**	**F**
White	a*	-0.80±0.01	-0.72±0.02	-0.80±0.01	-0.86±0.05	-0.84±0.01	-0.89±0.07
	b*	5.4±0.1	4.6±0.0	5.0±0.0	5.0±0.5	4.8±0.1	5.4±0.4
	L*	92.8±0.1	93.1±0.1	93.3±0.1	93.4±0.4	93.4±0.0	92.9±0.5
	ΔE_{ab}	**2.5±0.1**	**1.8±0.1**	**1.9±0.0**	**1.8±0.7**	**1.7±0.0**	**2.4±0.7**
Green	a*	-34.1±0.0	-33.9±0.1	-32.9±0.3	-33.8±0.2	-33.4±0.0	-33.7±0.2
	b*	32.7±0.0	32.2±0.0	31.3±0.3	32.1±0.2	31.9±0.1	32.3±0.1
	L*	69.2±0.0	69.7±0.0	70.1±0.1	69.9±0.1	70.2±0.0	69.4±0.1
	ΔE_{ab}	**9.1±0.0**	**9.6±0.1**	**11.0±0.4**	**9.8±0.3**	**10.3±0.1**	**9.7±0.2**
Blue	a*	-14.1±0.1	-13.5±0.1	-13.7±0.0	-13.9±0.0	-13.5±0.1	-13.7±0.1
	b*	-14.8±0.3	-14.4±0.1	-14.1±0.1	-14.2±0.0	-14.0±0.1	-13.3±0.1
	L*	58.7±0.0	58.9±0.0	58.7±0.2	58.2±0.3	59.2±0.4	57.7±0.4
	ΔE_{ab}	**3.3±0.3**	**4.0±0.1**	**4.1±0.1**	**3.9±0.0**	**4.4±0.2**	**4.8±0.1**
Yellow	a*	-5.8±0.1	-6.1±0.0	-5.9±0.0	-6.3±0.1	-6.1±0.0	-6.0±0.2
	b*	63.7±0.0	63.1±0.0	61.5±0.1	63.5±0.2	62.9±0.1	63.3±0.5
	L*	88.4±0.2	89.0±0.1	89.0±0.1	89.2±0.1	89.3±0.0	88.7±0.2
	ΔE_{ab}	**9.2±0.1**	**9.6±0.0**	**11.2±0.1**	**9.2±0.2**	**9.8±0.1**	**9.5±0.5**
Red	a*	41.3±0.2	40.7±0.1	39.6±0.1	40.9±0.6	40.5±0.2	40.7±0.1
	b*	24.8±0.1	24.1±0.0	23.1±0.1	24.0±0.3	23.8±0.1	24.4±0.2
	L*	59.3±0.0	59.9±0.0	60.5±0.0	60.7±0.8	60.4±0.1	59.7±0.2
	ΔE_{ab}	**10.0±0.2**	**11.0±0.1**	**12.6±0.2**	**11.2±1.1**	**11.5±0.2**	**10.8±0.3**

The optical properties, namely transparency and UV light absorption capacity of polysaccharide films are relevant for some of their applications. For example, for food packaging, transparency is an important feature for consumer's acceptability, while UV barrier properties are useful to prevent the oxidative degradation of fatty foods, increasing the shelf life of food products (López & García, 2012). Moreover, for medical applications, UV barrier properties could be advantageous for skin therapeutics (e.g., in transdermal drug delivery systems), and transparency is useful to control the wound healing process without the need to remove the membrane, or for bioactive coatings of products and devices (Tomé et al., 2015).

3.2.4.3. Mechanical properties

Mechanical characterization is essential for the application of the films as biomaterials, for example, in wound dressings, synthetic tissues or food packaging (Gruppuso et al., 2021; Li et al., 2020; Pagano et al., 2021; Rodriguez et al., 2017). Therefore, the films prepared with *Alteromonas* EPS were subjected to tensile tests and the obtained mechanical parameters are presented in Table 3.2.3. It is noticed that the EPS films displayed different mechanical behaviors. EPS A, B and C presented typical mechanical characteristics of flexible films, with lower stiffness, showed by the lower tensile strength (Ƈ) (4.55–11.7 MPa), higher elongation at break (ε) (35.6–47.0%) and lower Young's modulus (εm) (10–93 MPa). On the opposite, EPS D, E and F seemed to form more rigid films, characterized by higher Ƈ values (16.6–23.6 MPa), lower ε (2.80–5.58%) and higher εm (597–1100 MPa) (Table 3.2.3). Interestingly, the Ƈ of these films is higher to that of LDPE (0.9–14 MPa), poly(ε-caprolactone) (14 MPa) and polyvinyl chloride (PVC, 15 MPa) films (Fan et al., 2021; Zhao et al., 2021). These differences in mechanical behavior between *Alteromonas* sp EPS films could not be correlated with their differences in chemical composition or molecular weight (Chapter 3.1, Table 3.1.2). Nonetheless, the EPS might present variations on their polymer chain structures that impact the inter-chain interactions and, therefore, their mechanical characteristics (Freitas, Alves, Gouveia, et al., 2014).

The large range of variables involved in the mechanical behavior of films might compromise comparison between polymer films, since not only the mechanical characteristics are strongly influenced by the factors stated above, but also by the film preparation techniques (e.g., type and concentration of the plasticizer) and conditioning conditions (e.g., RH values) (Ferreira et al., 2014; Piermaria et al., 2009; Rodriguez et al., 2017). Despite this, both the Ƈ and ε values (4.55–23.6 MPa and 2.80–47.0%, respectively) are within those found for several polysaccharide-based films (3.1–75.1 MPa and 2.5–116.7%, respectively) (Table 3.2.3). Of notice were the high ε values determined for the films prepared with EPS A, B and C (Table 3.2.3), which were superior to those reported for several commercialized films such as polystyrene (2–3%), poly(3-hydroxybutyrate) (5–8%), cellophane (14.4%) and poly(L-lactic acid) (9%) (Tomé et al., 2011; Zhao et al., 2021). Such high ε values suggests that those EPS films have potential for applications where a high elasticity is required, such as for wound dressings, since the high flexibility allows the films to easily adapt to the wound shape and deform according to the skin movements (Gruppuso et al., 2021). Moreover, the higher ε values found for the *Enterobacter* A47 EPS film prepared with citric acid (50%) as plasticizer (Ferreira et al., 2014), and the increased in ε values found for Kefir

microflora EPS films prepared with increasing glycerol concentrations (Piermaria et al., 2009), seem to indicate that the plasticity of the *Alteromonas* sp. films might be optimized by adding more glycerol or by using a different plasticizer.

Also, the tensile strength of the EPS films might be improved by blending the EPS with other biopolymers (e.g., gelatin, chitosan, or bacterial cellulose) (Freitas, Alves, Reis, et al., 2014), or by the addition of reinforcing materials (e.g., starch nanocrystals, nano/microfibrils of bacterial cellulose or chitin whiskers) (Freitas, Alves, Reis, et al., 2014; Rodriguez et al., 2017). For example, the *Nostoc commune* colonies EPS films were successfully reinforced by the addition of starch nanoparticles and chitin whiskers (Rodríguez et al., 2018).

3.2.4.4. Water vapour permeability

WVP is a crucial factor for the application of films and is dependent on several factors, including hydrophobicity, diffusion rate, solubility coefficient, crystalline and amorphous regions ratio, film density, and polymer chain mobility (Li et al., 2020). As presented in Table 3.2.3, all *Alteromonas* sp. EPS films had high WVP values (2.7–6.1 x 10^{-11} mol m^{-1} s^{-1} Pa^{-1}) for a driving force of 75.3–34.7% RH. These values were higher than those found for other polysaccharide films (1.0–2.3 x 10^{-11} mol m^{-1} s^{-1} Pa^{-1}) tested for similar driving forces (Table 3.2.3). It is known that WVP is a very important property for wound management applications. Providing the accurate moist environment for correct healing is a major feature demonstrated by some commercially available dressings, such as Tegaderm and OpSite (Niculescu & Grumezescu, 2022). Moreover, the transparency observed in *Alteromonas* sp. EPS films allows easy wound monitorization which suggests that these films might have a potential in this field (Niculescu & Grumezescu, 2022; Tomé et al., 2015).

Table 3.2.3. Mechanical properties, water vapour permeability (WVP), and gas (oxygen and carbon dioxide) barrier properties of films prepared with different *Alteromonas* EPS and of other carbohydrate-based films reported in literature (Gly, glycerol; RH, relative humidity; n.a., not available; n.d. non detected).

Film composition	Mechanical properties			Plasticizer (wt. $wt._{polymer}^{-1}$% or g L^{-1})	RH (%)	Permeabilities				Reference
	Tensile strength at break (Ƈ, MPa)	Elongation at break (ε, %)	Young modulus (εm, MPa)			WVP (10^{-11} mol m^{-1} s^{-1} Pa^{-1})	Driving force (ΔRH%)	Gases (10^{-16} mol m^{-1} s^{-1} Pa^{-1}) O_2	Gases (10^{-16} mol m^{-1} s^{-1} Pa^{-1}) CO_2	
EPS A	4.55±0.36	47.0±1.1	10±0	Gly (60% or 9 g L^{-1})	53	5.8±0.7	75.3–34.7	43.1±10.1	62.6±11.0	This study
EPS B	11.7±1.1	37.7±0.5	93±12	Gly (30% or 4.5 g L^{-1})		2.7±0.1		7.5±0.4	24.0±1.2	This study
EPS C	10.8±1.1	35.6±5.5	65±5			6.1±1.0		30.0±1.5	28.5±1.4	This study
EPS D	23.6±2.8	5.58±0.83	1100±110			3.7±0.4		n.d.	n.d.	This study
EPS E	21.1±0.1	4.40±0.42	597±62			2.9±0.0		n.d.	n.d.	This study
EPS F	16.6±0.4	2.80±0.46	885±125			5.8±0.2		n.d.	n.d.	This study
***Enterobacter* A47 EPS**	3.8–15.5	5.4–22.1	14.5–457.8	Gly (30%)	45	1.7–2.3	80.9–53.4	n.a.	n.a.	Freitas, Alves, Gouveia, et al. (2014)
	3.1	54.9	2.8	Citric acid (50%)	44.3	1.0	76.9–22.5	0.7	42.7	Ferreira et al. (2014)
***Pseudomonas oleovorans* EPS**	51	9.5	1738	None	44.3	1.1 5.4	64.8–22.0 92.0–64.8	n.a.	2.0	Alves et al. (2011)
Kefir microflora EPS	40.9 15.2	2.70 116.7	n.a. n.a.	None Gly (25%)	75	0.32 0.23	75–0	n.a.	n.a.	Piermaria et al. (2009)
Gellan	30	34	n.a.	Gly (4%)	54	2.0	54–0	n.a.	n.a.	Yang et al. (2010)

Table 3.2.3. Mechanical properties, water vapour permeability (WVP), and gas (oxygen and carbon dioxide) barrier properties of films prepared with different *Alteromonas* EPS and of other carbohydrate-based films reported in literature (Gly, glycerol; RH, relative humidity; n.a., not available; n.d. non detected) (cont.).

Film composition	Mechanical properties			Plasticizer (wt. $wt._{polymer}^{-1}$% or g L^{-1})	RH (%)	Permeabilities				Reference
	Tensile strength at break (Ƈ, MPa)	Elongation at break (ε, %)	Young modulus (εm, MPa)			WVP (10^{-11} mol m^{-1} s^{-1} Pa^{-1})	Driving force (ΔRH%)	Gases (10^{-16} mol m^{-1} s^{-1} Pa^{-1}) O_2	Gases (10^{-16} mol m^{-1} s^{-1} Pa^{-1}) CO_2	
Chitosan	31.1	10.6	n.a.	None	n.a.	n.a.	-	n.a.	n.a.	Vivek et al. (2021)
	41.6	24.7	1193	Gly (15%)	n.a.	n.a.	-	n.a.	n.a.	Zarandona et al. (2020)
Chitosan/dextran-like EPS	43.3	20.7	n.a.	1,3-propanediol (50%)	n.a.	n.a.	-	n.a.	n.a.	Vivek et al. (2021)
Chitosan/ *Alteromonas* sp. EPS	39.5–42.7	16.6–23.7	1008–1186	Gly (15%)	n.a.	n.a.	-	n.a.	n.a.	Zarandona et al. (2020)
Alginate crosslinked with calcium	64.7	2.8	n.a.	Gly (40%)	56	n.a.	-	n.a.	n.a.	Olivas & Barbosa-Cánovas (2008)
	24.1	7.6	n.a.		98	2.6	100–0	n.a.	n.a.	
	65.9	2.5	n.a.	Sorbitol (40%)	56	n.a.	-	n.a.	n.a.	
	18.4	6.6	n.a.		98	1.7	100–0	n.a.	n.a.	
Pectin/ alginate/ xanthan	29.7	19.0	n.a.	Gly (18 g L^{-1})	50	1.01	100–0	n.a.	n.a.	Fan et al. (2021)
Hyaluronic acid (HA)	70.7	5.6	n.a.	none	58	n.a.	-	n.a.	n.a.	Kim et al. (2020)
HA/carboxymethyl cellulose (CMC)	68.8–75.1	7.9–13.6	n.a.	none	58	n.a.	-	n.a.	n.a.	
Cassava starch/CMC	13.3	65.7	n.a.	Gly (15 g L^{-1})	55	0.92	100–0	n.a.	n.a.	Li et al. (2020)

On the contrary, low WVP values are preferable for food packaging in order to maintain the moisture content of the food (Fan et al., 2021). For example, synthetic polymers used as packaging materials, such as LDPE and polyethylene terephthalate (PET), both had a WVP of 0.01 x 10^{-11} mol m^{-1} s^{-1} Pa^{-1} for a driving force of 90–0% RH (Lagaron et al., 2004), and cellophane that presented a WVP of 0.47 x 10^{-11} mol m^{-1} s^{-1} Pa^{-1} with 72–0% RH (Tomé et al., 2011). Nonetheless, different strategies could be employed to increase the films barrier properties to water vapor, such as promoting crosslinking reactions between the polymer's chains, or the addition of lipids (e.g. olive oil, rice wax, or beeswax) to the filmogenic solutions or in multilayer films (Freitas, Alves, Reis, et al., 2014; Salvada et al., 2022; Vieira et al., 2021).

3.2.4.5. Gas permeability

For transdermal drug delivery, oxygen barrier properties might be important in maintaining the stability of the entrapped bioactive molecules (Laubach et al., 2021). Polysaccharides films are effective gas barriers at low RH due to their hydrogen-bonded dense polymer matrix (Freitas, Alves, Reis, et al., 2014). However, it increases significantly for increasing ambient moisture due to the plasticizing effect of water (Ferreira et al., 2016). *Alteromonas* sp. EPS A film presented the highest permeability value for both gases (43.1±10.1 and 62.6±11.0 x 10^{-16} mol m^{-1} s^{-1} Pa^{-1} for O_2 and CO_2, respectively), followed by the films prepared with EPS C (30.0±1.5 and 28.5±1.4 x 10^{-16} mol m^{-1} s^{-1} Pa^{-1} for O_2 and CO_2, respectively) and EPS B (7.5±0.4 and 24.0±1.2 x 10^{-16} mol m^{-1} s^{-1} Pa^{-1} for O_2 and CO_2, respectively). The permeability of EPS A film was also superior to other polysaccharide films such as those prepared with FucoPol, chitosan, and galactomannans (0.13–2.3 and 14.7–42.7 x 10^{-16} mol m^{-1} s^{-1} Pa^{-1} for O_2 and CO_2, respectively) in similar RH conditions (32.4–50%) (Ferreira et al., 2014). Permeability to gases is a main issue in wound management. Being able to provide the correct exposure of the wound to oxygen or carbon dioxide to enhance the healing process is a major feature of commonly used dressings such as Hyalosafe and Hydrofilm (Niculescu & Grumezescu, 2022).

For EPS D, E and F it was not possible to measure the gas permeability since no pressure alterations were found after 48 h, suggesting that these films are excellent barriers to oxygen and carbon dioxide. For food packaging applications low gas permeation to oxygen or carbon dioxide is very important for food preservation (Bastarrachea et al., 2011). In fact, these EPS had better gas barrier properties compared with synthetic polymers usually used as packaging materials, such as LDPE

(10.03 and 42.2 x 10^{-16} mol m^{-1} s^{-1} Pa^{-1} for O_2 and CO_2, respectively) or PET (0.12 and 0.38 x 10^{-16} mol m^{-1} s^{-1} Pa^{-1} for O_2 and CO_2, respectively) (Ferreira et al., 2014).

3.2.5. Conclusions

Six *Alteromonas* sp. EPS were investigated for the preparation of biodegradable films by casting, using glycerol as plasticizing agent. The films were transparent, and their application caused small color alterations when applied over colored surfaces. Considering their mechanical properties, two distinct behaviours were found: three EPS formed flexible films, with high elongation at break and low tensile strength at break, whereas the other three EPS films were stiffer and more resistant, with low elongation at break, and high tensile strength at break. The higher elongations values here described were superior to those found in literature for other EPS films prepared with the same content in glycerol, suggesting their potential for applications that require flexible films. EPS A, B and C presented high carbon dioxide and oxygen permeabilities, whereas EPS D, E and F proved to be excellent gas barriers. In addition, the films had high water vapour permeabilities due to their hydrophilic character. These features are very important for wound management applications since it is of great importance to maintain water balance and good contact in the wound-dressing interface with the possibility to absorb wound exudate. Given this, the flexible transparent and permeable films produced using EPS A, B and C revealed to be great candidates for the development of dressing materials to cover and protect wounds, while monitoring the wound healing process. On the other hand, EPS D, E and F, by being stiffer and due to their great barrier properties could be used in food packaging applications, alone or as one layer of multilayer polymeric films. Nonetheless, different strategies, such as changing the type and concentration of plasticizer, incorporation of additives or blending the EPS with other biopolymers, must be studied to meet the requirements for those applications.

Chapter | 3.3

Alteromonas macleodii Mo169 EPS production using agro-industrial wastes

The results presented in this chapter resulted in the following manuscripts:

Concórdio-Reis, P., Serafim, B., Pereira, J.R., Moppert, X., Guézennec, J., Reis, M.A.M. & Freitas, F. Exopolysaccharide production by marine bacterium *Alteromonas macleodii* Mo169 using fruit pulp waste as sole carbon source. In preparation.

Concórdio-Reis, P., Serafim, B., Pereira, J.R., Moppert, X., Guézennec, J., Reis, M.A.M. & Freitas, F. Production of a new glucosamine/ribose rich exopolysaccharide by *Alteromonas macleodii* Mo169 grown on glycerol. In preparation.

3.3.1. Summary

Glycerol, a by-product from the biodiesel industry, and the sugar-rich apple pulp waste generated from fruit processing for juice production were used as sole carbon sources for the cultivation of *Alteromonas macleodii* Mo169 to produce high-value EPS. There was a noticeable impact of the different tested feedstocks on the bioprocess, as evidenced by different cell growth and EPS synthesis profiles, as well as on the secreted polymers' composition. The highest EPS productivity (0.190±0.013 g L^{-1} h^{-1}) and biomass concentration (9.20±0.61 g L^{-1}) were obtained from the glucose- and fructose-rich apple pulp waste. The EPS was mainly composed of glucose (31.1±0.2 mol%), arabinose (23.9±0.1 mol%) and mannose (17.3±0.1 mol%). Although glycerol resulted in a lower EPS productivity (0.166±0.010 g L^{-1} h^{-1}), the secreted EPS presented high contents of glucosamine (36.2±1.0 mol%) and ribose (20.4±0.7 mol%), two sugar monomers that are not commonly found among the *Alteromonas* genus and are known to confer wound healing and anti-aging properties. Therefore, EPS enriched is such monosaccharides have potential interest for human health and well-being applications.

3.3.2. Introduction

Owing to their wide ecological and environmental characteristics, marine habitats are the widest source of biological and chemical diversity, including not only unexplored and/or unknown microorganisms, but also new biomolecules with unique features and properties that might find extensive biotechnological applications (Casillo et al., 2018; Finore et al., 2014). Among those different metabolites, marine bacterial EPS, high molecular weight polysaccharides secreted by the organisms, have emerged as innovative biomaterials with significant industrial importance (Sahana & Rekha, 2019). Marine EPS exhibit a high diversity in terms of structure and composition, and are often found to have biological activity, exploitable by the pharmaceutical and medical industries (Casillo et al., 2018; Concórdio-Reis et al., 2021). Moreover, their improved thickening, stabilizing, gelling, and/or emulsifying capacities suggest their potential for a wide range of biotechnological applications in a variety of areas, such as the food, pharmaceutical, cosmetics or petroleum industries (Casillo et al., 2018; Roca et al., 2016).

Despite the potential of marine EPS, these polysaccharides represent only a small fraction of the current polymer's market, mainly due to the low productivities and high production costs of their production bioprocesses (Casillo et al., 2018; Roca et al.,

2015). EPS yield is greatly influenced by the fermentation conditions, including the carbon source (Casillo et al., 2018; Finore et al., 2014; Poli et al., 2010). Besides, the commonly used carbon sources, such as glucose, fructose or sucrose, also represent a high fraction of the overall production expenses (Freitas, Alves, Pais, et al., 2009; Pereira et al., 2021; Roca et al., 2015). Therefore, it becomes crucial to explore novel and less expensive carbon sources for the cultivation of EPS-producing marine bacteria. In this perspective, agro-industrial wastes and by-products can be considered relevant alternative feedstocks for the production of these value-added biomolecules (Joulak et al., 2022).

Glycerol, a byproduct of many industrial processes (e.g., biodiesel production), is generated in large quantities (10 wt.% of the biodiesel product), with limited application in high-value products (Abdul Raman et al., 2019). Nonetheless, glycerol byproduct was successfully implemented in bacterial EPS production bioprocesses. Examples include the galactose-rich and the fucose-rich EPS produced by *Pseudomonas oleovorans* (Freitas, Alves, Carvalheira et al., 2009) and *Enterobacter* A47 (Alves, Freitas, Torres, et al., 2010), respectively. Except for four EPS-producing *Halomonas* strains that were recently cultivated in glycerol-containing media, in shake flasks assays (Joulak et al., 2022), EPS production by marine bacteria using this carbon source has still not been investigated. Similarly, the wastes generated by the fruit juice industry might be suitable feedstocks to produce EPS. Upon manufacturing apple juice, 25–35% (w/w) of the apple mass is not used (Pereira et al., 2021). The fruit pomace, mainly composed of peels, pulp and seeds, has a high sugar content (21–31 g L^{-1}) that might be useful substrates for bacterial cultivation (Pereira et al., 2021; Rebocho et al., 2019).

Alteromonas macleodii Mo169 was isolated from a giant clam collected in Moorea Island lagoon, French Polynesia (Concórdio-Reis et al., 2021). This strain, when cultivated in glucose enriched medium, produced an EPS with potential for utilization in different industrial fields, particularly in the food, pharmaceutical, biomedical, and cosmetic industries (Chapter 3.4). The EPS had a high content of sulphate (2.8 wt.%) (Concórdio-Reis et al., 2021) and was mainly composed of (1→4)-linked glucuronic acid (39.3 mol%), mannose (12.8 mol%), glucose (11.2 mol%) and galactose (4.0 mol%) (Chapter 3.4). *A. macleodii* Mo169 EPS had interesting rheological properties, namely a thickening and weak gel forming capacities that were rapidly recovered after exposure to either high shear rates or temperatures up to 95 ºC (Chapter 3.4). Additionally, the EPS could form hydrogels with different strengths in the presence of iron(III) (Chapter 3.4), and bioactive bio-nanocomposites with silver, gold,

and selenium (Chapter 3.5). Envisaging a cost-effective EPS production process, in this chapter, *A. macleodii* Mo169 was cultivated using low-cost carbon sources, namely glycerol and apple pulp waste. To the best of our knowledge, this is the first time such feedstocks are used for the cultivation of an *Alteromonas* strain. The study aimed at evaluating the strain's ability to utilize the two feedstocks as substrate for cell growth and EPS synthesis. First, shake flask experiments were performed with four different media. Once a suitable medium was selected, the bacterium was cultivated in bioreactor using glucose as carbon source for comparison, and the two agro-industrial wastes, glycerol and apple pulp waste. The impact of the substrates tested on the synthesized polymers' composition and molecular mass distribution was also assessed.

3.3.3. Materials and methods

3.3.3.1. Apple pulp processing

Apple pulp waste was supplied by SUMOL+COMPAL, S.A. (Portugal) (Fig 3.2.1). For the cultivation experiments, the apple pulp waste was processed as described by Pereira et al. (2021). The waste was diluted with deionized water (3:1, v/v) for viscosity reduction, centrifuged (13000 × *g*, 15 min, 4 ºC) for the removal of insoluble solids, and autoclaved (121 ºC, 1 bar, 30 min) for sterilization (Fig. 3.2.1).

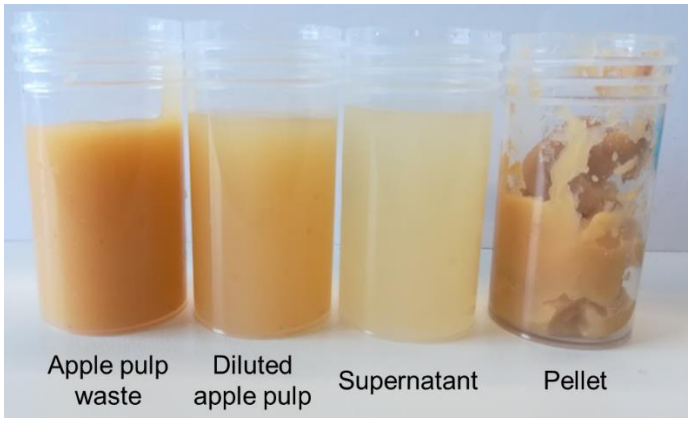

Figure 3.3.1. Picture of the different stages of the apple pulp waste process.

3.3.3.2. Characterization of the sugar-rich apple pulp supernatant

The diluted apple pulp supernatant was characterized in terms of viscosity, density, pH, conductivity, total dry mass, moisture, elemental composition, and the

content in salts, ammonium, phosphate, sugars, acyls, and high molecular weight soluble compounds. The sample's apparent viscosity was determined at room temperature using a viscometer (Fungi Lab S.A., Alpha series, Spain). The density was determined gravimetrically by weighing tree different volumes (10, 20 and 30 mL) of the sample. The total dry mass was determined gravimetrically by freeze drying the sample (~5 g) and weighing the obtained dry material. For the moisture content determination, the sample (~5 g) was subjected to a temperature of 100 ^{o}C and weighted once a constant weight was attained. Afterwards, the dried sample was placed at a temperature of 550 ^{o}C for 24 h, and the inorganic salts content was determined gravimetrically by weighing the resulting ashes. Elemental analysis (C, H, S, N) was performed on the freeze-dried sample as described in section 2.2.3.6. Ammonium and phosphate concentrations were determined by colorimetry using a flow segmented analyzer (Skalar 5100, Skalar Analytical, The Netherlands). Standard solutions of phosphorus (KH_2PO_4) and ammonium (NH_4Cl) were prepared at concentrations between 4 and 20 mg L^{-1}. Sugars, organic and inorganic acyls contents and composition were determined according to section 2.1.3.4. For the determination of the sample's high Mw compounds content, a sample (5 mL) of the apple pulp supernatant was dialyzed with a 12000 MWCO membrane (ZelluTrans/Roth) against deionized water at room temperature, under constant stirring. The efficiency of the process (i.e., removal of low molecular weight compounds) was monitored by measuring the conductivity of the dialysis water until it reached a value bellow 10 µS cm^{-1}. Sodium azide (10 mg L^{-1}) was added to prevent any biological contamination and possible degradation. After lyophilization, the content in high molecular weight compounds was determined gravimetrically and analyzed in terms of chemical composition and molecular weight as described in sections 2.1.3.4 and 2.2.3.6, respectively.

3.3.3.3. Microbial cultivation

Microorganism

Alteromonas macleodii Mo169 was obtained as previously described in section 3.1.3.1. The culture was cryopreserved at -80 ^{o}C in 20% (v/v) glycerol and was reactivated in an agar plate according to section 3.1.3.1. For inoculum preparation, an isolated colony from the agar plate was inoculated into a 250 mL baffled shake flask containing 100 mL of marine 2216 medium (Millipore, Merck KGaA) (Oppenheimer & Zobell, 1952; Zobell, 1941) supplemented with glucose (30 g L^{-1}, 99%, Fluka). After

incubation for 24 h at 30 ºC in an orbital shaker, the culture (10%, v/v) was used as inoculum for the shake flask and bioreactor experiments.

Shake flasks assays: cultivation media

The marine 2216 medium (Oppenheimer & Zobell, 1952; Zobell, 1941) previously used for the cultivation of this bacterium (Concórdio-Reis et al., 2021), was not compatible with the cultivation using the sugar-rich apple pulp (precipitation occurred). Therefore, it was used as standard reference conditions in the shake flasks experiments carried out to find a suitable medium. The following four different media were evaluated:

1) modified Schatz medium containing (g L^{-1}): NaCl, 30 g; KH_2PO_4, 1 g; NH_4NO_3, 1 g; $MgSO_4 \cdot 7H_2O$, 0.2 g; $FeSO_4 \cdot 7H_2O$, 0.01 g; $CaCl_2 \cdot 2H_2O$, 0.01 g (Fondi et al., 2015).

2) modified semi-complex medium (SCM) composed of (g L^{-1}): NaCl, 30; $MgCl_2 \cdot 6H_2O$, 13; $MgSO_4 \cdot 7H_2O$, 9; KCl, 1.3; $CaCl_2 \cdot 2H_2O$, 0.2; NaBr, 0.15; $NaHCO_3$, 0.05; yeast extract, 0.3; and peptone, 0.2 (Joulak et al., 2022).

3) salted Medium E* with the following composition (per liter): NaCl, 30 g; $(NH_4)_2HPO_4$, 3.3 g; K_2HPO_4, 5.8 g; KH_2PO_4, 3.7 g; 10 mL of a 100 mM $MgSO_4$ solution and 1 mL of a micronutrients' solution. The micronutrients solution was composed of (per liter of 1 N HCl): $FeSO_4 \cdot 7H_2O$, 2.78 g; $MnCl_2 \cdot 4H_2O$, 1.98 g; $CoSO_4 \cdot 7H_2O$, 2.81 g; $CaCl_2 \cdot 2H_2O$, 1.67 g; $CuCl_2 \cdot 2H_2O$, 0.17 g; and $ZnSO_4 \cdot 7H_2O$, 0.29 g (Concórdio-Reis et al., 2018).

4) liquid A1 medium containing per liter (750 mL natural sea water (Naturitas, Spain) and 250 mL deionized water): yeast extract, 4 g; peptone, 2 g (Roca et al., 2016).

The pH value of all media was adjusted to 7.6 with 1 M NaOH prior to autoclaving. The experiments were performed in 500 mL baffled shake flasks containing 200 mL of the appropriate medium, supplemented with glucose (30 g L^{-1}). The assays were performed in an orbital shaker at 200 rpm and 30 ºC, for 24 h. Samples were collected at times 0 and 24 h for CDW and EPS quantification.

Bioreactor cultivation

Three sets of experiments were performed: standard cultivation (Std) using glucose as carbon source for comparison, and the cultivation with the agro-industrial residues glycerol (Gly) and apple pulp waste (AP). Salted Medium E* was supplemented with 60 g L^{-1} of glucose (Std.) or glycerol (Gly), or with the sugar-rich apple pulp supernatant, obtained as described above (section 3.3.3.1). All experiments were carried out in a BioStat B-Plus bioreactor (Sartorius, Germany) with a working

volume of 2 L. A constant aeration rate (2 SLPM) was kept during the cultivation, and the dissolved oxygen concentration was controlled at 40% by the automatic variation of the stirring speed (200–1200 rpm). The bioreactors were operated at 30±0.2 ºC and the pH was maintained at 7.6±0.1 by the automatic addition of NaOH 5 M. Foam formation was avoided by the automatic addition of Antifoam A (Sigma-Aldrich). Samples (15 mL) were withdrawn during the cultivation runs for the culture's broth apparent viscosity measurement, and for the quantification of the CDW, carbon source, ammonium, phosphate, and EPS.

Analytical techniques

Samples' viscosity was determined at 25ºC using a MCR92 modular compact rheometer (Anton Paar, Graz, Austria) equipped with a cone-plate geometry (angle 2º, diameter 35 mm, 0.145 mm gap). Culture broth samples were centrifuged (13000 × *g*, 15 min, 4 ºC) for cell separation. Samples with high viscosity were diluted in deionized water (1:2 or 1:3, v/v) prior to centrifugation for viscosity reduction. The cell-free supernatant was used for quantification of carbon source, ammonium, and EPS. The bacterial pellet was used for the quantification of CDW and for evaluation of polyhydroxyalkanoates (PHA) production. For CDW determination, the pellets were washed twice with a 30 g L^{-1} NaCl solution (resuspension in the solution followed by centrifugation at 13000 × *g* and 4 ºC, for 15 min) and lyophilized to gravimetrically quantify the CDW For detection of intracellular PHA granules, the pellets were resuspended in 0.5 mL of a 30 g L^{-1} NaCl solution, and Nile Blue (0.5 µL) were added. After incubation at 100 ºC for 5 min, slides were prepared and observed in the microscope (Olympus BX51 epifluorescence) under fluorescent light. The carbon source (glucose, glycerol, and fructose) concentration in the cell-free supernatant was determined by HPLC with a VARIAN Metacarb column (BioRad) coupled to an infrared (IR) detector. The analysis was performed at 50 ºC, using H_2SO_4 (0.01 N) as eluent at a flow rate of 0.6 mL min^{-1}. Glucose, glycerol, and fructose were used as standards at concentrations between 0.016 and 1.0 g L^{-1}. Ammonium concentration was determined as described in section 3.3.3.2. The concentration of EPS in the cell-free supernatant was determined gravimetrically after dialysis, using the same protocol as for the determination of high molecular weight compounds in the apple pulp supernatant (section 3.3.3.2).

Kinetic parameters

The maximum specific cell growth rate μ_{max} (h^{-1}) was calculated using the following equation (3.3.1):

$$\ln\left(\frac{x}{x_0}\right) = \mu_{max} \times t \quad (3.3.1)$$

where x_0 is the initial biomass concentration (g L^{-1}). The EPS volumetric productivity (r_p, mg L^{-1} h^{-1}) and the biomass volumetric productivity (r_x, g L^{-1} h^{-1}) were determined according to eqs. (3.3.2) and (3.3.3), respectively:

$$r_p = \frac{\Delta p}{\Delta t} \quad (3.3.2)$$

$$r_x = \frac{\Delta x}{\Delta t} \quad (3.3.3)$$

where Δp and Δx corresponds to the EPS (g L^{-1}) and biomass (g L^{-1}) produced during the cultivation time Δt (h). The specific EPS productivity (q_p, g_{EPS} g_{CDW}^{-1} d^{-1}) was calculated using the following equation (3.3.4):

$$q_p = \frac{r_p}{\Delta x} \quad (3.3.4)$$

The yields on biomass ($Y_{x/s}$, g_{CDW} $g_{substrate}^{-1}$) and on EPS ($Y_{p/s}$, g_{EPS} $g_{substrate}^{-1}$) on substrate were determined using Eqs. (3.3.5) and (3.3.6), respectively:

$$Y_{x/s} = \frac{\Delta x}{\Delta s} \quad (3.3.5)$$

$$Y_{p/s} = \frac{\Delta p}{\Delta s} \quad (3.3.6)$$

where Δs is the substrate uptake during the cultivation run.

3.3.3.4. Polymer characterization

The polymers composition in terms of sugars and acyls substituents (organic and inorganic) was performed as described in section 2.1.3.4. Average Mw and PDI determination were performed as reported in section 2.2.4.2.

3.3.3.5. Statistical analysis

All experiments were performed in duplicate, and their values were expressed as the mean ± standard deviation. Student's *t*-test was used to determine statistical differences ($p < 0.05$) among averages at a confidence level of 95%.

3.3.4. Results and discussion

3.3.4.1. Characterization of the sugar-rich apple pulp supernatant

Sugar-rich apple pulp supernatant was previously used for the bioreactor cultivation of microorganisms (Pereira et al., 2021). Nonetheless, due to possible differences between waste batches, the physical-chemical characteristics of the apple pulp supernatant were determined (Table 3.3.1). The pH (3.59) of the apple pulp supernatant used in this study was within the values (3.59–4.16) reported for different apple varieties (Wu et al., 2007). The low viscosity (0.004 Pa s) and density (0.95 g cm^3) of the apple pulp supernatant, similar to that of water indicated that the processing method was adequate for its utilization as feedstock for the cultivation experiments. It had a moisture content of 93.5±2.5 wt.% and total dry mass of 3.13±0.09 wt.% (Table 3.3.1). The inorganic salts content (0.09±0.02 wt.%) was lower than that previously described in literature (1.65 wt.%) (Pereira et al., 2021). The elemental analysis revealed that the apple pulp supernatant was mainly composed of carbon (36.8±0.6 wt.%), with a small sulphur content (0.09±0.00 wt.%) which was probably related to the presence of salts. No nitrogen was detected, contrary to Pereira et al. (2021) that reported traces of this element in the apple pulp. Additionally, a minor phosphate content (38.9±0.0 mg L^{-1}) was detected.

Table 3.3.1. Physical-chemical characterization of the sugar-rich apple pulp supernatant (n.d., not detected).

Parameter	value
pH	3.59±0.01
Conductivity (µS cm^{-1})	759.4±0.5
Density (g cm^{-3})	0.95±0.04
Viscosity at 1.67 s^{-1} (Pa s)	0.004±0.000
Total dry mass (wt.%)	3.13±0.09
Moisture content (wt.%)	93.5±2.5
Salts content (wt.%)	0.09±0.02
Carbon (wt.%)	36.8±0.6
Hydrogen (wt.%)	6.91±0.25
Sulphur (wt.%)	0.09±0.00
Nitrogen (wt.%)	n.d.
High Mw soluble compounds content (g L^{-1})	1.60±0.04

A high molecular weight fraction (1.60±0.04 g L^{-1}), with a Mw of 5.73±0.16x10^5 Da and a PDI of 4.22±0.94 was detected in the apple pulp supernatant. It was mainly composed of galacturonic acid (42.9±1.3 mol%), arabinose (33.1±2.0 mol%) and

galactose (13.7±0.6 mol%), with minor contents of glucose (3.75±0.47 mol%), xylose (3.68±0.41 mol%) and rhamnose (2.42±0.05 mol%). This high molecular weight soluble fraction was probably composed of different polysaccharides, including pectins. Pectins have a high molecular weight (~2 x 10^5 Da) and are composed of up to 81 wt.% galacturonic acid, with minor contents of arabinose, galactose, glucose, xylose and/or rhamnose (Antunes et al., 2017; Dranca et al., 2020).

The apple pulp supernatant was rich in glucose and fructose, with contents of 29.1±0.8 and 11.5±0.4 g L^{-1}, respectively. In comparison with the apple pulp supernatant used by Pereira et al. (2021), it had approximately twice the sugar content, which demonstrates the feedstock's variability. Traces (bellow 1.5 g L^{-1}) of sucrose, rhamnose, and arabinose were also noticed. Organic acyl groups, namely pyruvate and acetate, were detected, but at low concentrations (bellow 0.1 wt.%). *A. macleodii* Mo169 was previously cultivated using glucose as carbon source (Concórdio-Reis et al., 2021), but fructose was not previously tested.

3.3.4.2. Cultivation media

Four different media, namely Schatz medium, SCM, salted Medium E*, and A1 medium, were evaluated for the cultivation of *A. macleodii* Mo169 (Fig 3.3.2). The CDW and EPS produced are presented in Table 3.3.2. Marine 2216 medium was used as a control.

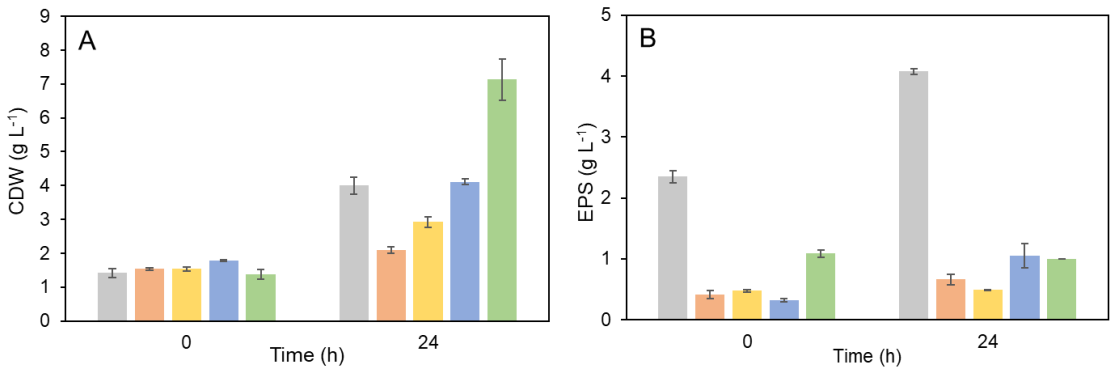

Figure 3.3.2. *A. macleodii* Mo169 growth (A) and EPS production (B) in different media: control (2216 medium,), Schatz ( ), SCM ( ), salted Medium E* ( ), and A1 ( ) media.

As Fig. 3.3.2 A demonstrates, the strain was able to grow in all the media tested, although with some differences. In comparison to the control medium (2.58±0.12 g L^{-1}), the Schatz and SCM media resulted in significantly lower biomass

production (0.55±0.05 and 1.38±0.10 g L^{-1}, respectively) (Table 3.3.2). On the contrary, no statistically significant difference was observed in the CDW between the control medium and the salted Medium E* (p>0.05), in which 2.33±0.07 g L^{-1} of CDW were produced. The use of A1 medium resulted in the highest CDW production (5.75±0.75 g L^{-1}). However, no EPS production was observed with this medium (Table 3.2.2). As depicted in Fig. 3.3.2 B, the highest EPS concentration was obtained with the control medium. Nonetheless, the presence of a significant amount of high molecular weight compounds was noticed in this medium (Fig. 3.3.2 B), probably associated with its content in yeast extract and peptone (Roca et al., 2016), resulting in overestimating EPS production. Out of the other four media, the salted Medium E* presented the highest EPS production value (0.72±0.22 g L^{-1}) (Table 3.3.2), thus, it was chosen for conducting the bioreactor experiments.

Table 3.3.2. *A. macleodii* Mo169 biomass (Δx) and EPS production (Δp) using different media: control (2216 medium), Schatz, SCM, salted Medium E*, and A1 media (n.d., not detected).

Media	Δx (g L^{-1})	Δp (g L^{-1})
Control	2.58±0.12	1.50±0.05
Schatz	0.55±0.05	0.25±0.025
SCM	1.38±0.10	n.d.
Salted Medium E*	2.33±0.07	0.72±0.22
A1	5.75±0.75	n.d.

3.3.4.3. Bioreactor cultivation

After a suitable medium was found, *A. macleodii* Mo169 was cultivated in a bioreactor using salted Medium E* supplemented with glucose (Std, standard conditions). This carbon source was previously used for the cultivation of this strain (Concórdio-Reis et al., 2021). Therefore, this assay was performed as a starting point to assess the impact of the different carbon sources on *A. macleodii* Mo169 growth and EPS production. Once the typical cultivation profile was evaluated for the standard conditions, the culture was grown on glycerol (Gly) and apple pulp waste (AP) as sole carbon sources.

Standard conditions – Glucose supplemented medium

The cultivation profile and kinetic parameters for *A. macleodii* Mo169 growth and EPS production using glucose as carbon source is presented in Fig. 3.3.3 A and Table 3.3.3, respectively. For 16 h of cultivation, the culture grew at a maximum

specific cell growth rate of 0.130±0.009 h^{-1} and a CDW of 5.22±0.03 g L^{-1} was achieved (Fig 3.3.3 A). Afterwards, the cell growth rate decreased due to ammonium-limiting conditions (<0.08 g L^{-1}), and a biomass concentration of 6.13±0.04 g L^{-1} was obtained at the end of the cultivation run (24 h) (Fig. 3.3.3 A). A similar profile was observed for EPS production, which was initiated during the exponential phase of growth and reached a plateau (average value of 2.13±0.21 g L^{-1}) when the culture entered the stationary growth phase, indicating its synthesis was growth associated (Fig. 3.3.3 A). Concomitant with cell growth and EPS production, glucose consumption was observed (32.9±4.6 g L^{-1}) (Fig. 3.3.3 A, Table 3.3.3). Nonetheless, glucose was not completely consumed and 16.9±1.2 g L^{-1} of this carbon source were still available at the end of the assay. When cell growth rate decreased (16–24 h), glucose consumption rate was not affected, suggesting that this nutrient was probably being used for cell maintenance and/or the production of other metabolites besides EPS. Some *Alteromonas* strains were described as PHA producers (Martínez-Checa et al., 2005; Shi et al., 2017), suggesting that this strain might be consuming glucose for PHA production. Thus, Nile Blue staining was performed to assess the possible intracellular accumulation of PHA granules (Fig. 3.3.4 A). The lack of fluorescence (Fig. 3.3.4 A) indicated that no PHA accumulation was detected. However, PHA production might have been initiated a short time before the end of the assay, and it was not detected by this technique. During the last 8 h, EPS concentration in the culture broth remained almost constant, suggesting that EPS production was growth associated and ceased upon cell growth arrest. Similarly, for *Halomonas caseinilytica* K1 and *Salipiger mucosus* A3T, EPS production occurred during the exponential growth phase (Joulak et al., 2022; Llamas et al., 2010). On the other hand, EPS production by *Halomonas elongata* K4, *Halomonas halophila* S4, *Pseudoalteromonas* sp. MD12-642, and *Pseudoalteromonas* sp. AM seemed to be partially growth associated (Al- Nahas, 2011; Joulak et al., 2022; Roca et al., 2016).

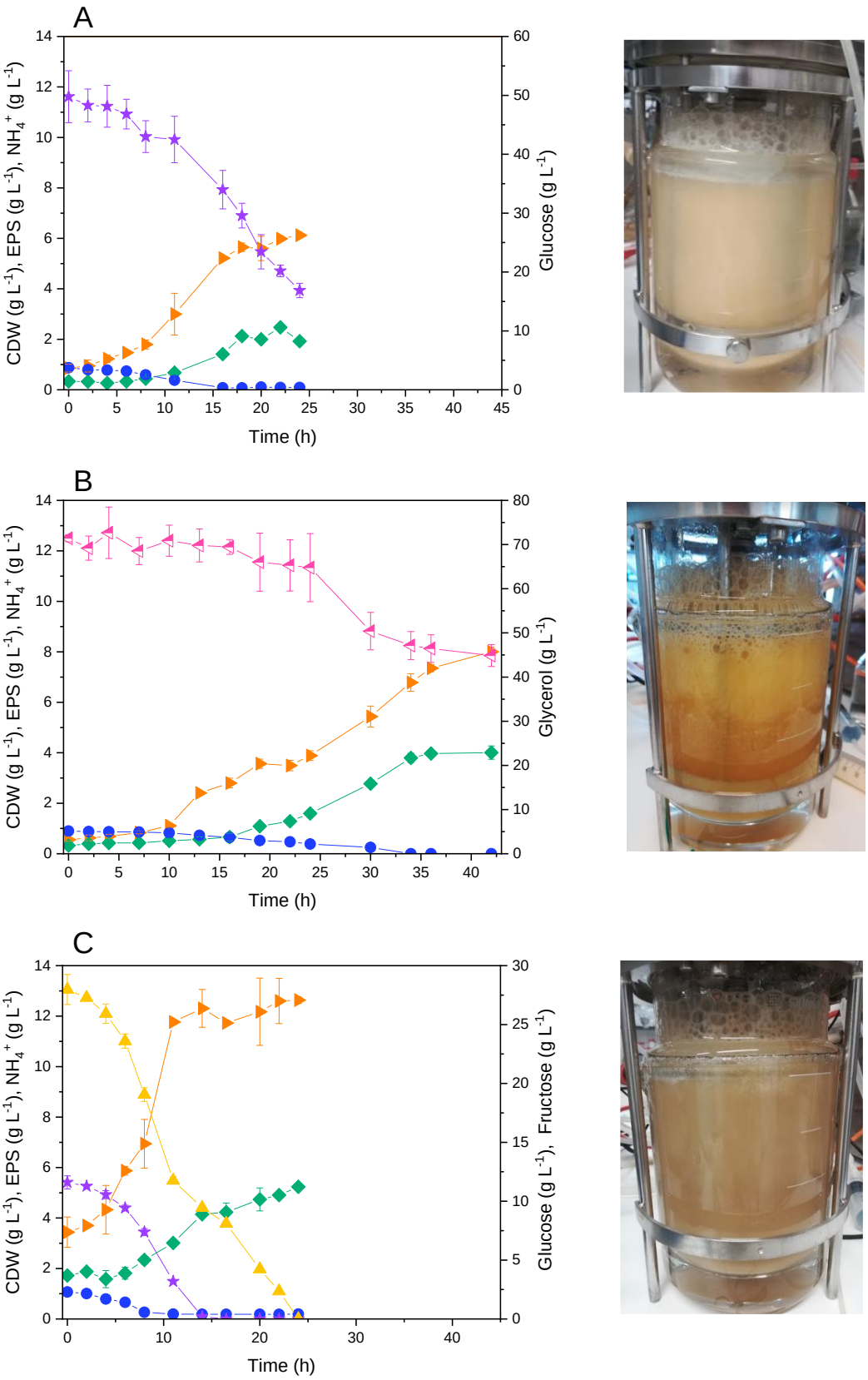

Figure 3.3.3. Cultivation profiles and pictures of *A. macleodii* Mo169 cultivation with different carbon sources: (A) Std, (B) Gly, and (C) AP. CDW (▶), EPS (◆), glucose (★), fructose (▲), glycerol (◀), and ammonium (●) concentrations.

Table 3.3.3. Kinetic parameters obtained in the bioreactor cultivation experiments using different carbon sources (if not stated otherwise, the parameters were calculated between times 0 and 24 h for runs Std and AP, and between 0 and 42 h for run Gly).

Parameter	Run			
	Std	Gly	AP	
Δx (g L^{-1})	5.27±0.16	7.45±0.19	9.20±0.61	
Δp (g L^{-1})	2.14±0.15	3.68±0.27	3.51±0.08	
μ_{max} (h^{-1})	0.130±0.009 (6–16 h)	0.048±0.002 (13–36 h)	0.139±0.012 (4–11 h)	
r_p (g L^{-1} h^{-1})	0.150±0.008 (6–18 h)	0.166±0.010 (16–36 h)	0.190±0.013 (6–24 h)	
r_x (g L^{-1} h^{-1})	0.219±0.007	0.177±0.005	0.383±0.026	
q_p (g g^{-1} h^{-1})	0.017±0.001	0.012±0.001	0.016 ±0.001	
Substrate	glucose	glycerol	glucose	fructose
Δs (g L^{-1})	32.9±4.6	26.6±2.6	11.6±0.6	28.0±1.3
$Y_{p/S}$ (g g^{-1})	0.065±0.010	0.139±0.017	0.089±0.003	
$Y_{X/S}$ (g g^{-1})	0.160±0.023	0.280±0.028	0.232±0.016	

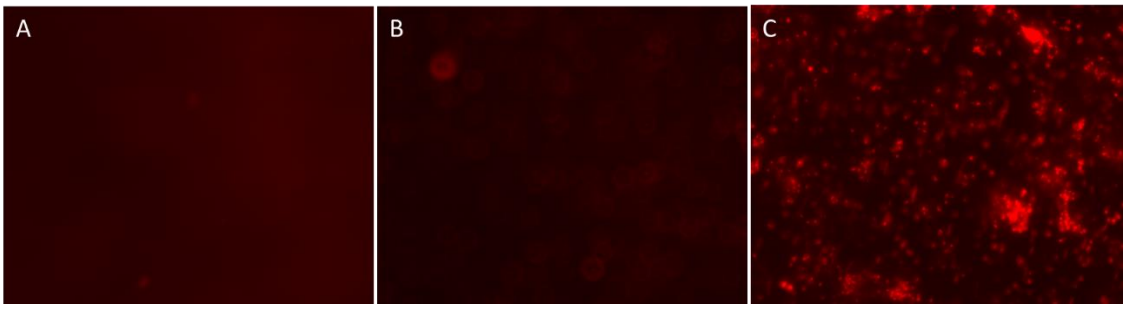

Figure 3.3.4. Microscopic images of the samples of *A. macleodii* Mo169 cultivation with different carbon sources, (A) Std, (B) Gly, and (C) AP, stained with Nile Blue solution (magnification 100 x).

Considering that the effective EPS production occurred between 6 and 18 h of cultivation, 1.80±0.09 g L^{-1} of EPS were produced, corresponding to a maximum volumetric productivity of 0.150±0.008 g L^{-1} h^{-1} (Table 3.3.3). These values were relatively high compared to those reported for other marine EPS-producers using glucose as carbon source (0.008–0.25 g L^{-1} h^{-1}) (Table 3.3.3). Although higher EPS concentrations were obtained for several bacteria (2.5–9.5 g L^{-1}), their productivity was lower than that presented by *A. macleodii* Mo 169 (Table 3.3.4). Examples include *Alteromonas macleodii* subsp. *Fijiensis* (Raguénès et al., 1996), *Alteromonas macleodii* MS907 (Raguénès et al., 2003), *Pseudoalteromonas* sp. AM (Al- Nahas, 2011), and *Vibrio diabolicus* (G. Raguénès et al., 1997), whose reported EPS volumetric productivity ranged between 0.052 and 0.125 g L^{-1} h^{-1} (Table 3.3.4). Only *Pseudoalteromonas* sp. MD12-642 presented a higher performance, with an EPS

production of 2.50–4.40 g L^{-1}, that corresponded to volumetric productivity of 0.17–0.25 g L^{-1} h^{-1} (Roca et al., 2016).

Table 3.3.4. EPS production and volumetric productivity obtained in the cultivation of different marine bacteria using glucose, glycerol, and fructose as carbon sources.

Bacteria	Carbon source	Cultivation method	EPS (g L^{-1})	Productivity (g L^{-1} h^{-1})	Reference
A. macleodii Mo169	Glucose	Bioreactor	1.80–2.14	0.150	This study
	Glycerol	Bioreactor	3.31–3.68	0.166	This study
	Apple pulp (glucose, fructose)	Bioreactor	3.42–3.51	0.190	This study
Alteromonas macleodii subsp. *Fijiensis*	Glucose	Bioreactor	6.00	0.1	Raguénès et al. (1996)
Alteromonas macleodii MS907	Glucose	Bioreactor	9.00	0.125	Raguénès et al. (2003)
Alteromonas sp. strain 1644	Fructose	Bioreactor	7.50	0.107	Samain et al. (1997)
Alteromonas gracilis sp.	Glucose	Shake flask	1.82	0.019	Matsuyama et al. (2015)
Alteromonas infernus GY785	Glucose	Bioreactor	5.5	0.102	G.H.C. Ragénès et al. (1997)
Halomonas caseinilytica K1	Glucose	Shake flask	0.044	0.011	Joulak et al. (2019)
	Glycerol	Shake flask	0.074	0.018	Joulak et al. (2022)
Halomonas elongata K4	Glucose	Shake flask	0.061	0.015	Joulak et al. (2019)
	Glycerol	Shake flask	0.280	0.070	Joulak et al. (2022)
Halomonas smyrnensis S3	Glucose	Shake flask	0.100	0.033	Joulak et al. (2019)
	Glycerol	Shake flask	0.054	0.018	Joulak et al. (2022)
Halomonas halophila S4	Glucose	Shake flask	0.030	0.010	Joulak et al. (2019)
	Glycerol	Shake flask	0.040	0.013	Joulak et al. (2022)
Pseudoalteromonas sp. MD12-642	Glucose	Bioreactor	2.50–4.40	0.17–0.25	Roca et al. (2016)
Pseudoalteromonas ruthenica	Glucose	Shake flask	1.80	0.025	Saravanan & Jayachandran (2007)
Pseudoalteromonas sp. AM	Glucose	Shake flask	9.50	0.06	Al- Nahas (2011)
Pseudoalteromonas SM20310	Glucose	Shake flask	0.567	0.008	Liu et al. (2013)
Vibrio diabolicus	Glucose	Bioreactor	2.5	0.052	G. Raguénès et al. (1997)

Due to the increase in EPS concentration, the apparent viscosity of the cultivation broth increased dramatically by two orders of magnitude, displaying a non-Newtonian fluid behavior (Fig. 3.3.5). This viscosity build up is a common characteristic to many microbial fermentations for EPS production and usually dictates the end of the cultivation run due to the loss of bulk homogeneity (i.e., mixing, mass and oxygen) (Alves, Freitas, Torres, et al., 2010; Freitas et al., 2011; Poli et al., 2010).

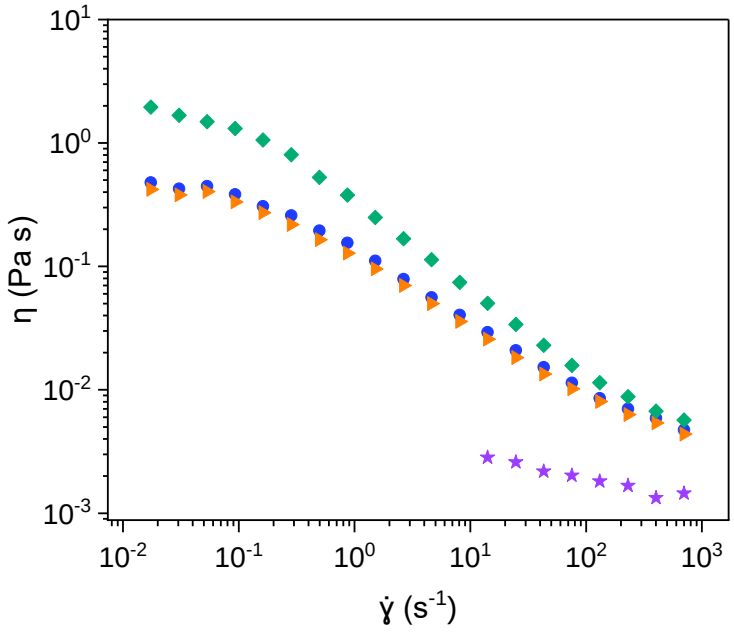

Figure 3.3.5. Apparent viscosity (η) as a function of shear rate ($\dot{\gamma}$) for the cultivation medium (★) and the fermentation broth obtained in the Std (●), Gly (▶), and AP (◆) assays.

Agro-industrial wastes as carbon source: Glycerol

As large amounts of glycerol byproduct are generated by many industrial processes (Abdul Raman et al., 2019), *A. macleodii* Mo 169 growth and EPS production were evaluated using glycerol as sole carbon source (Fig. 3.3.3 B). After an initial adaptation phase (~7 h), the culture entered the exponential growth phase, consuming almost all the ammonium available within ~30 h of cultivation. During this phase, the culture grew at a maximum specific cell growth rate of 0.048±0.002 h^{-1}, producing 7.45±0.19 g L^{-1} of biomass at the end of the cultivation run (42 h) (Table 3.3.3). Cell growth with glycerol was slower than with glucose (Std run), but a higher biomass concentration was reached at the end of the Gly cultivation run (Table 3.3.3). Additionally, the yield of substrate on biomass ($Y_{p/S}$) was higher in run Gly (0.280±0.028 g g^{-1} compared with 0.160±0.023 g g^{-1} for run Std). Similarly, for four *Halomonas* strains, higher CDW and $Y_{p/S}$ values were reported using glycerol (2.21–

3.20 g L^{-1} and 0.789–0.864 g g^{-1}) instead of glucose (0.74 –1.12 g L^{-1} and 0.172–0.280 g g^{-1}) (Joulak et al., 2022). Since the inoculum was prepared using glucose as carbon source, it is possible that the culture needed more time to adapt to the new carbon source, therefore, a slower cell growth rate was observed. Nonetheless, glycerol seemed to be efficiently used for biomass production. Similar results were reported for *Escherichia coli* JM101, with lower μ_{max} and higher biomass values obtained with glycerol compared to the cultivation using glucose (Martínez-Gómez et al., 2012). Upon transcriptional-proteomic analysis, the authors found that the strain induced a carbon stress and carbon scavenging response when growing on glycerol as the sole carbon source, indicating that glycerol is an energy-poor carbon source (Martínez-Gómez et al., 2012). These metabolic mechanisms allowed a more adequate response to growth on these non-favorable conditions that resulted in a reduction of the μ value, and a 2 hours delay in growth (Martínez-Gómez et al., 2012). Also, a more efficient carbon utilization was observed, with less carbon lost as CO_2 (Martínez-Gómez et al., 2012).

Similar to the Std run, EPS production from glycerol was also enhanced during the exponential growth phase and ceased when the cell growth rate decreased (36 h) (Fig. 3.3.3 B). At that point, 3.31±0.19 g L^{-1} of EPS had been produced, corresponding to a maximum volumetric productivity of 0.166±0.010 g L^{-1} h^{-1} (Table 3.3.3). This value was slightly higher compared with that of the Std run (0.150±0.008 g L^{-1} h^{-1}). Nonetheless, similar values were obtained for the overall specific productivities (0.012±0.001 and 0.017±0.001 g g^{-1} h^{-1} for runs Gly and Std, respectively). Although a higher EPS concentration was obtained with glycerol, the broth's viscosity increased to similar values as those reported for the fermentation broth of run Std (Fig. 3.3.5). However, the viscosity of microbial culture broths are influenced by several factors in addition to EPS concentration, such as the biomass concentration, the size of both the cells and cell aggregates formed, or differences in the composition and conformation of the EPS molecules (Alves, Freitas, Torres, et al., 2010; Roca et al., 2016).

As observed in Fig. 3.3.3 B, the broth of run Gly became increasingly more orange, which might suggest that the bacterium is able to produce an orange-colored pigment. Pigment synthesis occurs in several microorganisms, including bacteria belonging to the *Alteromonas* genus (Gauthier, 1977; Gauthier & Breittmayer, 1979; Ivanova et al., 1996; Norton & Jones, 1969), and can be dependent on the fermentation conditions (Venil et al., 2020). Apart from serving as food colorants, bacterial pigments have several pharmacological activities like anti-microbial, anti-cancer, antioxidant, anti-inflammatory and anti-allergic properties with large economic

potential (Venil et al., 2020). Therefore, *A. macleodii* Mo169 pigment production might be worth exploring in the future.

Agro-industrial wastes as carbon source: Apple pulp

The glucose- and fructose-rich supernatant obtained from waste apple pulp (AP) was used as the sole feedstock for the cultivation of *A. macleodii* Mo169 and EPS production (Fig. 3.3.3 C). After inoculation, the culture started growing at a maximum specific growth rate of 0.139±0.012 h^{-1}, with no noticeable adaptation phase. The observed specific cell growth rate was similar to that obtained using glucose as carbon source (0.130±0.009 h^{-1}) (Table 3.3.2). The available ammonium was consumed within 11 h of cultivation, and the culture reached the stationary growth phase at this time. At the end of the cultivation run, a CDW of 9.20±0.61 g L^{-1} was attained, corresponding to a biomass volumetric productivity of 0.383±0.026 g L^{-1} h^{-1}. As depicted in Fig. 3.3.3 C, the two sugars present in the apple pulp, glucose and fructose, were successfully used by the culture. Both sugars were consumed simultaneously after inoculation, with glucose being exhausted first within 14 h, and fructose at the end of the cultivation (24 h) (Fig. 3.3.3 C). The fluorescence observed after coloration with Nile Blue indicated that PHA was accumulated intracellularly (Fig. 3.3.4 C), showing that part of the carbon consumed was used for PHA production. Both *Alteromonas lipolytica* and *Alteromonas hispanica* were reported to accumulate poly-β-hydroxybutyrate (PHB), a short-chain-length PHA, as intracellular reserve product (Martínez-Checa et al., 2005; Shi et al., 2017). The monomeric composition of PHAs is dependent on the bacterial strain and the carbon source supplied (Guézennec et al., 2011), thus, further analysis is required. Nonetheless, PHA have been increasingly studied as ecological alternatives to non-degradable plastics produced from fossil oils and have attracted a substantial industrial interest (Guézennec et al., 2011; Silva et al., 2021).

A high molecular weight fraction, accounting for 1.72±0.08 g L^{-1}, was detected in the cultivation medium at the beginning of the run, which was associated with the presence of the soluble apple pulp polysaccharide, as described above. Nonetheless, an increase in EPS concentration was observed concomitant with cell growth (Fig. 3.3.3 C). Interestingly, EPS production continued after the culture reached the stationary phase, which was not observed using only glucose as carbon source (run Std). These results suggest that the culture can effectively use fructose for EPS production during the stationary growth phase. Between 6 and 24 h of cultivation, a maximum EPS volumetric productivity of 0.190±0.013 g L^{-1} h^{-1} was observed. This value was superior to those reported for other marine bacteria (0.008–0.125 g L^{-1} h^{-1}) (Table 3.3.4). Only *Pseudoalteromonas* sp. MD12-642 presented a higher value when

cultivated under fed-batch mode (0.25 g L^{-1} h^{-1}), but a lower value for batch experiments (0.17 g L^{-1} h^{-1}) (Roca et al., 2016). Additionally, the specific productivity of 0.016±0.001 g g^{-1} h^{-1} was similar to that obtained in run Std (0.017±0.001 g g^{-1} h^{-1}), suggesting that the higher EPS concentration obtained with apple pulp waste was related to its capacity to enhance biomass production.

3.3.4.4. EPS characterization

Chemical composition

The different cultivation media, as well as the different tested feedstocks, impacted on the polymers' composition, as highlighted on Table 3.3.5. Contrary to the EPS obtained using marine 2216 medium supplemented with glucose (Chapter 3.4), no uronic acids (glucuronic and galacturonic acid) were detected in the EPS synthesized in run Std with salted Medium E*, thus resulting in a polymer with lower anionic character. Additionally, both EPS had the same neutral monosaccharides (mannose, galactose, glucose, and glucosamine) but at different molar proportions (Table 3.3.5). The most significant difference was the higher glucosamine content in Std EPS (21.9±1.3 mol%), which was approximately equimolar to mannose (23.2±0.4 mol%), and the high content in glucose (46.2±1.1 mol%). It should be considered that, as described above (section 3.3.4.2), marine 2216 medium had a high content of high molecular weight soluble compounds that, if not totally degraded, might be present in the broth at the end of the cultivation run. Due to their high molecular weight, such compounds were probably extracted together with the EPS secreted by *A. macleodii* Mo169. Consequently, their presence in the extracted sample impacted on the analyzed sugar composition, increasing some monomers concentration (e.g., glucose, mannose, and galactose, which are commonly present in yeast extract) (Roca et al., 2016).

Table 3.3.5. Characterization of the EPS produced by *A. macleodii* Mo169 in the bioreactor cultivation experiments using different carbon sources (Ara, arabinose, Gal, galactose; GalA, galacturonic acid; Glc, glucose; GlcA, glucuronic acid; GlcN, glucosamine; Man, mannose; and Rib, ribose; Mw, average molecular weight; and PDI, polydispersity index).

	Reported in		Run					
	Chapter 3.1 and 3.4		Std		Gly		AP	
Monosaccharide composition (mol%)								
Man	12.8		23.2±0.4		12.3±0.5		17.3±0.1	
Gal	4		8.7±0.1		4.4±0.1		8.7±0.1	
Glc	11.2		46.2±1.1		26.7±0.1		31.1±0.2	
GlcN	2.4		21.9±1.3		36.2±1.0		10.3±0.5	
Rib	n.d.		n.d.		20.4±0.7		n.d.	
Ara	n.d.		n.d.		n.d.		23.9±0.1	
GlcA	39.3		n.d.		n.d.		n.d.	
GalA	10.4		n.d.		n.d.		8.7±0.0	
Acyl content (wt.%)								
Sulphate	2.8–5.3		6.1±0.1		6.0±0.5		6.0±0.5	
Pyruvate	0.063–4.9		0.6±0.0		0.5±0.2		0.5±0.1	
Lactate	0–0.63		n.d.		n.d.		n.d.	
Acetate	0–0.5		1.0±0.0		0.9±0.0		1.2±0.0	
Molecular mass distribution								
Mw (MDa)	1.6	4.6	1.8±0.1	0.83±0.09	1.9±0.0	0.76±0.02	1.7±0.0	0.74±0.0
PDI	1.3	1.3	1.0±0.0	1.3±0.1	1.0±0.0	1.1±0.1	1.0±0.0	1.1±0.0

Similarly, uronic acids were also not found for the EPS produced in run Gly (Table 3.3.5). Interestingly, this EPS had an even higher content in glucosamine (36.2±1.0 mol%), being the main monosaccharide in its composition. Of notice was the presence of ribose, that accounted for 20.4±0.7 mol% of the EPS composition.

The chemical composition of the EPS produced with AP was similar to that of the EPS from run Std (Table 3.3.5), with the exception of having galacturonic acid (8.7±0.0 mol%) and arabinose (23.9±0.1 mol%) in its composition. However, galacturonic acid and arabinose were the main monosaccharides in the high molecular weight fraction of AP, with the relative percentages of 42.9±1.3 and 33.1±2.0 mol%, respectively (section 3.3.4.1). Therefore, it should be considered that the content of these monosaccharides in the EPS might be related to the presence of such high molecular weight contaminants (e.g., pectins), and further analysis might be required (e.g., determination of the EPS chemical linkages and structure).

Considering the acyl content, lactate and pyruvate were within the ranges previously described for the EPS produced by *A. macleodii* Mo169 (Table 3.3.5). On the contrary, higher contents of acetate and sulphate were detected (0.9–1.2 wt.% and 6.0–6.1 wt.% compared with 0–0.5 wt.%, and 2.8–5.3 wt.%, respectively). However, no significant alterations were found between the different carbon sources (Table 3.3.5).

Glycosaminoglycans (GAG), which include polysaccharides rich in glucosamine, have been reported to have anticoagulant, antitumor and antioxidant effects (Gao et al., 2022). Marine EPS are particularly attractive for the development of innovative GAG-mimetic compounds for human health (Delbarre-Ladrat et al., 2017). However, bacteria belonging to the *Alteromonas* genus usually produce EPS composed of glucose, mannose, galactose and their uronic acid derivatives (Delbarre-Ladrat et al., 2017; Sahana & Rekha, 2019), whereas amino-sugars are not commonly found within this group (Delbarre-Ladrat et al., 2017). Nonetheless, *Alteromonas* sp. PRIM-28 produced an EPS composed of glucose, mannuronate and N-acetyl glucosamine (1:3.67:0.93), which was biocompatible and capable of modulating various cellular events during *in vitro* wound healing, suggesting its potential as a multifunctional bioactive material for wound care (Sahana & Rekha, 2019). Due to the EPS' high content in glucosamine, particularly when cultivated using glycerol as carbon source, *A. macleodii* Mo169 might be a potential source of novel and improved biomaterials with health applications. Additionally, as far as the authors know, this is the first report of a ribose-containing EPS produced by a bacterium belonging to the *Alteromonas* genus. D-ribose has presented several benefits in cultured fibroblasts' metabolic activity, as well as in clinical tests by promoting a more youthful, radiant, and healthy appearance to the skin (St.Cyr, 2009). Considering the high content in ribose (20.4±0.7 mol%) and its rheological properties, the EPS from run Gly might also have a potential application in skin care. Moreover, this flexibility in the EPS' composition allows the optimization of the cultivation process towards the production of tailor-made polysaccharides with improved properties.

Molecular mass distribution

The polymer's average molecular weight (Mw) and polydispersity index (PDI) are presented in Table 3.3.5. Independently of the cultivation conditions, two high molecular weight fractions were synthesized by *A. macleodii* Mo 169. Moreover, the Mw values obtained were all within the range reported for other *Alteromonas* EPS (0.17–2 MDa) (Le Costaouëc et al., 2012; Raguénès et al., 2003; Sahana & Rekha, 2019; Zhang et al., 2017; Zykwinska et al., 2018). All the EPS obtained with salted Medium E* presented similar Mw values for all the tested feedstocks (1.7–1.9 and

0.74–0.83 MDa) (Table 3.3.5). Nonetheless, these values were lower than those previously reported with marine 2216 medium (1.6 and 4.6 MDa) (Concórdio-Reis et al., 2021) (Table 3.3.5). All the EPS were found to be homogenous polymers, as shown by their low PDI values (1.0–1.1) (Table 3.3.5).

3.3.5. Conclusions

In this work, the bioreactor cultivation of EPS-producer *A. macleodii* Mo169 was investigated, revealing a growth associated EPS production from glucose. Moreover, this work describes the ability of *A. macleodii* Mo169 to grow and synthesize EPS using low-cost feedstocks, namely glycerol and apple pulp waste, as sole substrates. Results showed that both the cultivation medium and the carbon source influenced bacterial growth, EPS productivity, and the polymer's composition. Cell growth and EPS production were enhanced using both glycerol and the glucose- and fructose-rich apple pulp waste. Additionally, the EPS produced using glycerol included high contents of glucosamine and ribose, which is not a common feature in EPS from the *Alteromonas* genus. This opens the possibility to design polymers with diverse compositional characteristics, through engineering and manipulation of different cultivation factors, including the mineral media and the carbon source. Hence, tailored polysaccharides with improved functional properties can be developed for specific applications in human health. Interestingly, PHA accumulation was detected in the cells grown on apple pulp waste, which might be worth exploring in the future since PHA are alternatives to non-degradable plastics of fossil fuel origin.

Chapter | 3.4

Alteromonas macleodii Mo169 EPS potential as structuring biomaterial: thickening and gelling capacity

The results presented in this chapter resulted in the following manuscripts:

Concórdio-Reis, P., Ferreira, S.S., Alves, V.D., Moppert, X., Guézennec, J., Coimbra, M.A., Reis, M.A.M. & Freitas, F. Rheological characterization of the exopolysaccharide produced by *Alteromonas macleodii* Mo 169. Submitted to *International Journal of Biological Macromolecules*.

Concórdio-Reis, P., Araújo, D., Moppert, X., Guézennec, J., Reis, M.A.M. & Freitas, F. Iron(III) cross-linked hydrogels based on *Alteromonas macleodii* Mo 169 exopolysaccharide. In preparation.

Exopolysaccharide carbohydrate analysis was performed by Professor Manuel A. Coimbra from University of Aveiro.

3.4.1. Summary

Rheology modifiers and gelling agents are essential additives in numerous products in a variety of industries. Due to environmental awareness, consumer-oriented industries are interested in novel natural rheological agents that can replace synthetic chemicals. The chemical composition and rheological properties of the novel EPS produced by *Alteromonas macleodii* Mo 169 (EPS A) were investigated, revealing that it was mainly composed of uronic acids (50 mol%). The EPS viscosity increased exponentially with its concentration in solution, and a non-Newtonian shear thinning behavior was found for concentrations above 0.1 wt.%. The elastic and viscous moduli indicated a weak gel-like structure above 0.4 wt.%. It maintained its shear thinning behavior and viscoelastic properties in the presence of NaCl and $CaCl_2$ for pH range 5–7 and temperatures up to 55 ^{o}C. Though the apparent viscosity decreased at pH 3 and 9 and temperatures above 65 ^{o}C, the shear thinning behavior was retained. The viscous and viscoelastic properties were recovered after heating (95 ^{o}C) and cooling (0 ^{o}C), indicating a good thermal stability and recoverability. After high shear force, the solution recovered original rheological properties within few seconds, demonstrating self-healing properties. Moreover, the gel forming capacity of EPS A in the presence of Fe^{3+} was investigated. The impact of Fe^{3+} (0.05–9.95 g L^{-1}) and EPS (0.3–1.7 %) concentration on the hydrogel strength was evaluated through a modelling approach. The Fe^{3+}-EPS A hydrogels present a range of strength of 0.3–44 kPa, which can meet the requirements for several specific applications (e.g., drug delivery or tissue engineering).

3.4.2. Introduction

Recently, due to the growing social and environmental awareness, natural polymers, such as polysaccharides, are the focus of increasing commercial interest since they are promising ecological and safe materials with application in cosmetics, food products, medical field, oil recovery, and agricultural industries, among other areas (Rana & Upadhyay, 2020; Rütering et al., 2018). The utilization of polysaccharides in such areas is mainly related with their rheological properties, such as gelling, stabilizing, texturizing, emulsifying and thickening capacities (J. Li et al., 2017). Nonetheless, only few natural rheological additives are competitive today due to the high functionality and profitability of synthetic products (Rütering et al., 2018). Among natural polymers, bacterial EPS stand out due to the high productivities independent of season and location, high structure reproducibility and simple downstream procedure (Martin-Pastor et al., 2019; Rütering et al., 2018). Examples of

well-known EPS include xanthan gum, bacterial alginate, hyaluronic acid and gellan gum that have reached commercialization and are utilized in a wide range of products and processes (J. Li et al., 2017; Rana & Upadhyay, 2020). Thus, bacterial EPS are considered important molecules for the development of new products with improved structural and rheological properties.

In line with this, exploring new EPS microbial sources might lead to the discovery of novel structuring biomaterials with improved properties (J. Li et al., 2017). Marine habitats are considered exceptional sources of biological diversity given the variety of environmental conditions found in the sea (Casillo et al., 2018; Concórdio-Reis et al., 2021). In this context, microorganisms isolated from unique marine environments, such as deep-sea hydrothermal vents, sea ice in polar regions, and microbial mats located in some Polynesian atolls, are valuable sources of distinctive EPS (Concórdio-Reis et al., 2021; Martin-Pastor et al., 2019). Although diverse marine EPS were found promising candidates to be employed in the biotechnological field (Casillo et al., 2018), very few are commercially available. One example is Hyalurift, a hyaluronic acid-like EPS produced by *Vibrio diabolicus* that presents tissue regeneration properties (Roca et al., 2016).

In Chapter 3.1., the EPS from six *Alteromonas* strains isolated from unique marine environments in French Polynesia were characterized and assessed for their potential as biomaterials in biotechnological applications (Concórdio-Reis et al., 2021). From the preliminary rheological studies, the EPS from *Alteromonas macleodii* strain Mo 169 (EPS A) stood out, showing a pseudoplastic behavior with a high thickening effect comparable to commercially employed xanthan gum (Concórdio-Reis et al., 2021). Moreover, this EPS formed hydrogels in the presence of Fe^{3+} cations (Concórdio-Reis et al., 2021). Fe^{3+}-cross-linked polysaccharide hydrogels are attracting considerable attention due to their improved properties compared with other ionotropic polysaccharide hydrogels (Massana Roquero et al., 2022). The unique chemistry of Fe^{3+} cations (e.g., coordination chemistry, photochemistry) provide novel features to the hydrogels, including stimuli-responsiveness abilities, redox properties, photosensitivity, higher mechanical stability, or enhanced absorptivity (Massana Roquero et al., 2022).

In this chapter, the chemical structure of EPS A was proposed and its rheological behavior in aqueous solutions was investigated, with special emphasis given to the effects of several important industrial parameters, such as concentration, presence of salts (NaCl and $CaCl_2$), pH, and temperature on the steady flow viscosity and viscoelastic properties. In addition, the ability of the EPS to recover its structure after high-shear events and its thermal stability under temperature fluctuations were

investigated. Also, the EPS A-Fe^{3+} hydrogel preparation conditions were investigated. The impact of Fe^{3+} and EPS concentrations on the hydrogels' strength was evaluated through response surface methodology (RSM). This modelling approach has the advantage to establish the dependency of hydrogel properties not only on each parameter, but also on the interaction between them (Azarifar et al., 2019). These studies are essential to assess the potential of EPS A to be used as structuring or thickening agents in drug delivery, tissue engineering, food products, cosmetic formulations, and oil drilling fluids.

3.4.3. Materials and Methods

3.4.3.1. Materials and sample preparation

The EPS was produced by *Alteromonas macleodii* Mo 169 (CNCM I-5374) and purified as previously described in section 3.1.3.2.

3.4.3.2. Exopolysaccharide carbohydrate analysis

Carbohydrate, glycosidic linkage, pyruvate and lactate composition were determined as described in section 2.2.3.6.

3.4.3.3. Rheological properties

The rheological characterization of the EPS in solution was performed on a MCR92 modular compact rheometer (Anton Paar, Graz, Austria) equipped with a cone-plate geometry (angle 2º, diameter 35 mm, 0.145 mm gap). The rheological characterization of the hydrogels was performed with a parallel plate geometry (diameter 50 mm, gap 2 mm). Temperature was controlled at 25 ºC (except for the temperature dependency tests) with a Peltier system and solvent evaporation was minimized by covering the sample's edge with low viscosity paraffin oil.

Apparent viscosity

Flow curves were determined using a steady state flow ramp in the shear rate range of 0.01 s^{-1} to 700 s^{-1}. Steady-state tests were carried out for EPS solutions with different polymer concentrations (0.01–1.25 wt.%). The effect of pH (3–9) and the presence of salts (1 M), namely NaCl (AppliChem Panreac, Barcelona, Spain) and $CaCl_2$ (Fisher Scientific, Leicestershire, United Kingdom), on the apparent viscosity of a 0.75 wt.% EPS solution were assessed. The Carreau model (Eq. (3.1.1)) (Chapter 3.1)

was employed to describe the flow curves of EPS solutions, as described in section 3.1.4.3.

Oscillatory shear tests

Amplitude sweep experiments (0.01 – 100%, 1 Hz) were performed to determine the linear viscoelastic region (LVE) of the EPS solutions. Frequency sweep tests were carried out between 0.01 and 10 Hz using a constant strain of 1%, within the LVE region. Storage modulus (G') and loss modulus (G") were determined for EPS solutions under different concentrations (0.1–1.25%). Moreover, the effect of pH (3–9) and the presence of salts (NaCl and $CaCl_2$) on both moduli were investigated (0.75 wt. % EPS solution).

Effect of temperature

Both oscillatory and steady-state tests were performed on a 0.75 wt.% EPS solution at different temperatures (0 – 95 ^oC). Temperature ramp flow analysis was performed at a constant shear rate (10 s^{-1}) between 0 and 95 ^oC with a heating rate of 6 ^oC min^{-1}. Afterwards, the sample was cooled down to to 0^oC at the same rate. Moreover, dynamic temperature sweep tests were performed at a constant strain and frequency (1% and 1 Hz, respectively) between 0 and 95^oC. The sample was heated up to 95 ^oC at a rate of 6 ^oC min^{-1}, kept at this temperature for 10 minutes, and then cooled down to 0^oC at the same rate, and a new oscillatory time sweep was carried out at that temperature.

Thixotropy

To assess structure degradation and recovery, a thixotropic loop test was performed by increasing the shear rate from 0.01 s^{-1} to 1000 s^{-1}, fixing the shear rate at 1000 s^{-1} for 60 s, and decreasing from 1000 to 0.01 s^{-1} (Abid et al., 2021). Moreover, the impact of high shear on the viscoelastic parameters was investigated at a frequency of 1 Hz by a three-stage oscillatory-rotational-oscillatory tests: (1) 120 s at LVE region; (2) 60 s at 1000 s^{-1}; and (3) 200 s at LVE region (Ayyash et al., 2020; Medina-Cabrera et al., 2021).

3.4.3.4. Hydrogels

Hydrogels preparation

EPS A hydrogels were prepared thought cation-mediated gelation using Fe^{3+} as the crosslinking agent. Fig. 3.4.1 illustrates the preparation steps for hydrogel disc preparation. The lyophilized EPS was dissolved in deionized water and left stirring overnight for complete dissolution. The EPS solution was poured inside a cylindrical

silicone mold (diameter 50 mm, height 3 mm) and the excess was removed with a spatula, so the height of the solution was homogenous and equal to the height of the mold. Then, the silicone mold with the EPS solution was immerged in the crosslinking solution by adding $FeCl_3$ solution (250 mL) into the container. After 2 h, the $FeCl_3$ solution was removed, and deionized water was added (250 mL) into the container to remove the excess of Fe^{3+} ions from the hydrogel. One hour later, the hydrogel disc was removed from the mold and characterized by oscillatory shear measurements (Fig. 3.4.1).

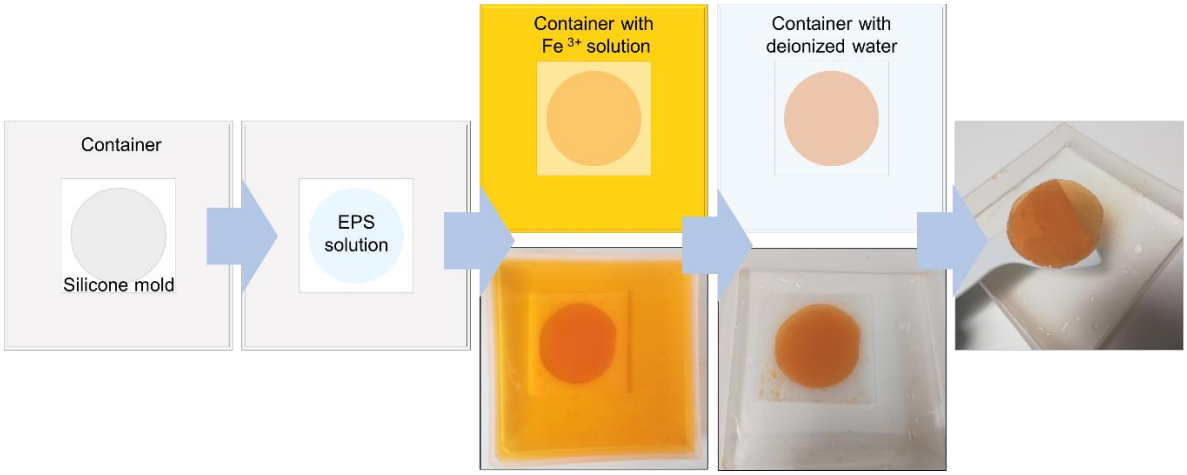

Figure 3.4.1. Schematic representation of the hydrogel discs preparation with EPS A.

Experimental design

A central composite rotatable design (CCRD) based on RSM was applied to evaluate the impact and interaction between the experimental variables (X_i): Fe^{3+} concentration (X_1, g L^{-1}) and EPS concentration (X_2, wt.%), on the observed response (Y): the hydrogel strength, represented by the G' value obtained at 1 Hz (Dehghan-Baniani et al., 2020). This design was composed of 11 runs: four factorial design experiments at levels ±1; four axial experiments at level α=±1.414; and a central point with three replicas which enabled the determination of both the experimental error and the reproducibility of the data (Azarifar et al., 2019; Torres et al., 2012). The list of experiments and corresponding settings for X_1 and X_2 is presented in Table 3.4.1. The experimental data was fitted to a quadratic equation model presented in Eq. (3.4.1).

$$Y_p = \beta_o + \beta_1 X_1 + \beta_2 X_2 + \beta_{11} X_1^2 + \beta_{22} X_2^2 + \beta_{12} X_1 X_2 \quad (3.4.1)$$

where Y_p is the predicted response and β_i are the model coefficients, namely, the intercept (β_0), linear (β_1, β_2), interaction (β_{12}) and quadratic coefficients (β_{11}, β_{22}) (Torres et al., 2012; Yang et al., 2020). The significance of each source of variation was

obtained from the statistical analysis of variance (ANOVA) provided by the statistical software (Design of Experiment 11). After validation, the model was used to analyze and predict the rheological properties of the EPS A hydrogel.

Table 3.4.1. Central composite rotatable design (CCRD) with two independent variables, X_1 (Fe^{3+} concentration, g L^{-1}) and X_2 (EPS concentration, %), and the response Y (G', Pa).

Experiment	X_1 Fe^{3+} (g L^{-1})	X_2 EPS (%)	Y G' (Pa)	
			Actual value	Predicted value
A	1.5	0.5	3202.1	3058.9
B	8.5	0.5	3084.8	352.65
C	1.5	1.5	20880	20389
D	8.5	1.5	44482	41402
E	0.05	1	304.93	85.592
F	9.95	1	9588.4	13030
G	5	0.3	1571.1	5403.2
H	5	1.7	42361	46684
I	5	1	25173	26044
J	5	1	25528	26044
K	5	1	32363	26044

3.4.4. Results and Discussion

3.4.4.1. Carbohydrate analysis

The carbohydrate analysis confirmed that EPS A was mainly composed of glucuronic acid (GlcA, 39.3 mol%, Table 3.4.2). The compositional analysis also revealed the presence of mannose (Man, 12.8 mol%), glucose (Glc, 11.2 mol%) and galacturonic acid (GalA, 10.4 mol%), and lower contents of galactose (Gal, 4.0 mol%) and glucosamine (GlcN, 2.4 mol%, derived from GlcNAc after acid hydrolysis). EPS A also possessed sulphate (17.2 mol%), lactate (2.2 mol%), and pyruvate (0.2 mol%) substituents. The presence of these charged groups can increase the EPS solution's viscosity due to the intramolecular repulsion force (Xu et al., 2018). This composition shows that the EPS is highly negatively charged at physiological pH. Except for glucosamine, the same sugar monomers were reported in a previous study, although with a different relative molar ratio, with much less GlcA (Concórdio-Reis et al., 2021). It is possible that these differences are due to the different hydrolysis used, as uronic acid residues component of glucuronans are resistant to hydrolysis and not

quantitatively determined (De Ruiter et al., 1992). For this reason, in the present study, *m*-phenylphenol colorimetry assay, a specific method for quantification of uronic acids (Blumenkrantz & Asboe-Hansen, 1973) was used to evaluate their total amount and their identification and the relative content of GlcA and GalA in the sample has been obtained by HPAEC and also by GC-MS after carboxyl-reduction with a deuterated reducing agent. Anyway, it cannot be excluded that differences can be found in different batches.

According to the glycosidic-linkage composition, GlcA, Man, Glc, and Gal were present as (1→4)-linked residues. Ramifications or substitutions were found at positions 2 and/or 3 (Table 3.4.2). This linkage composition is similar with the reported for other *A. macleodii* strains (Le Costaouëc et al., 2012; Rougeaux et al., 1998). Glycosidic linkages of uronic acids only allowed to identify the main linkages involved, as carboxyl reduction is not quantitative. Therefore, it cannot be excluded the existence of uronic acids substituted with sulphate ester (Le Costaouëc et al., 2012), that would explain the high mol% of sulphate esters determined. It was not possible to detect the glycosidic linkages of GlcN, inferring its linkage to uronic acids, as aldobiouronic derivatives are not quantitatively hydrolyzed in the conditions used (Ferreira et al., 2011).

Table 3.4.2. Sugar and glycosidic linkage composition (mol%) of EPS A.

EPS composition		**Glycosidic linkages***		
		(1→4)-linked	**(1→2,4)-linked**	**(1→3,4)-linked**
Man	12.8	10.6	0.8	1.4
Gal	4.0	0.6	2.8	0.6
Glc	11.2	10.8	0.3	0.2
GlcA	39.3	✓	nd	nd
GalA	10.4	nd	nd	nd
GlcN	2.4	nd	nd	nd
Sulphate	17.2			
Pyruvate	0.2			
Lactate	2.2			
Total (mg/g)	**600**			

* molar percentage of glycosidic linkages was adjusted to sugar composition values; ✓ - Only (1→4)-GlcA were detected in glycosidic linkage analysis. nd - not detected.

3.4.4.2. Rheological properties of EPS A in solution

Effect of polymer concentration

The steady shear behavior of EPS A aqueous solution was assessed for concentrations ranging from 0.01 to 1.25 wt.% (Fig. 3.4.2 A). For all concentrations tested, the EPS solutions showed a non-Newtonian shear thinning behavior. This shear thinning behavior, frequently described for other polysaccharide solutions (Abid et al., 2021; Grinev et al., 2020; Ji et al., 2020; Torres et al., 2015), is attributed to the disruption of molecular interactions (e.g. entanglements, hydrogen bonds, electrostatic or hydrophobic interactions) with increased shear rate, that results in the ordered alignment of the polymer molecules in the flow direction, and, consequently, a decrease in viscosity (Abid et al., 2021; Alves, Freitas, Costa, et al., 2010; Gu et al., 2020; Ji et al., 2020). This behavior is characteristic of entangled macromolecules and was already described in a preliminary rheological evaluation of this EPS (Concórdio-Reis et al., 2021).

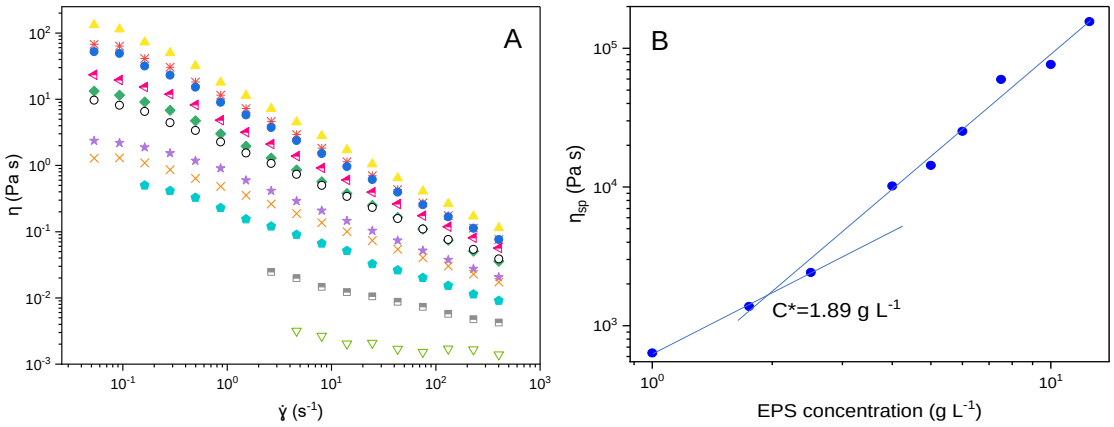

Figure 3.4.2. Apparent viscosity (η) as a function of shear rate ($\dot{\gamma}$) for different EPS concentrations: 0.01 wt.% (▽); 0.05 wt.% (■); 0.1 wt.% (⬟); 0.18 wt.% (✕); 0.25 wt.% (★); 0.4 wt.% (○); 0.5 wt.% (◆); 0.6 wt.% (◀); 0.75 wt. % (●); 1 wt.% (✳); and 1.25 wt.% (▲) (A). Concentration dependence of zero-shear specific viscosity (η_{sp}) of EPS A (B).

The flow curves (Fig. 3.4.2 A) obtained for concentrations above 0.1 wt.% were fitted to the Carreau model and the estimated parameter values are presented in Table 3.4.3. An accurate determination of viscosity below this concentration was difficult, therefore limiting the fitting of the Carreau model. Nevertheless, the results show that increasing the EPS concentration from 0.10 to 1.25 wt.% led to an increase of the η_0 from 0.64±0.01 to 156±4 Pa s (Table 3.4.3). For high concentration solutions, the distance between polysaccharide molecules decreases, thus more interactions and entangled aggregates are formed, causing higher flow resistance and therefore higher viscosity (Gu et al., 2020; Ji et al., 2020). Additionally, the relaxation time (λ) increased

from 6.57±0.57 to 11.7±1.1 s for higher EPS concentrations, due to the higher number of overall entanglements, the rate of formation of new interactions is slower compared with less concentrated EPS solutions. Accordingly, the transition from Newtonian to shear-thinning regime shifted to lower shear rates as the EPS concentration increases (Concórdio-Reis et al., 2021; Torres et al., 2015).

Table 3.4.3. Carreau model parameters estimated for different EPS concentrations, and 0.75 wt.% EPS in the presence of different salts and under different pH solutions.

EPS (wt.%)	Salt (1 M)	pH	Temperature (ºC)	η_0 (Pa s)	*n* (-)	λ (s)	r^2	MRE[a] (%)
1.25				156±4	0.083±0.045	11.7±1.1	0.998	14.0
1.00				76.5±2.7	0.095±0.068	9.32±1.23	0.996	15.3
0.75				59.6±2.2	0.131±0.064	9.88±1.35	0.996	14.3
0.60				25.2±0.6	0.266±0.029	9.98±0.85	0.998	7.4
0.50	-	7	25	14.3±0.1	0.266±0.014	9.37±0.36	0.999	3.8
0.40				10.8±0.2	0.350±0.017	12.2±0.8	0.999	7.0
0.25				2.42±0.03	0.400±0.015	6.65±0.37	0.999	5.8
0.18				1.38±0.02	0.420±0.021	6.89±0.02	0.998	5.5
0.10				0.64±0.01	0.423±0.018	6.57±0.57	0.999	6.9
0.75	NaCl	7	25	31.5±1.2	0.149±0.018	7.88±0.64	0.999	14.4
	$CaCl_2$			33.8±1.1	0.177±0.027	9.43±0.83	0.999	9.0
		9		2.03±0.02	0.453±0.024	3.16±0.27	0.998	9.8
0.75	-	5	25	26.1±0.3	0.198±0.045	8.00±0.67	0.998	5.1
		3		3.61±0.05	0.410±0.015	4.67±0.28	0.999	8.7
			0	86.9±1.6	0.206±0.053	22.3±2.3	0.996	14.7
			5	54.9±0.9	0.209±0.041	14.0±1.2	0.998	12.6
			15	45.8±1.5	0.205±0.062	12.9±1.8	0.994	10.5
			35	50.2±2.5	0.249±0.069	17.1±3.3	0.991	13.9
			45	35.7±3.2	0.205±0.056	11.0±2.4	0.995	5.5
0.75	-	7	55	34.8±1.6	0.260±0.045	13.0±1.9	0.996	14.2
			65	15.5±2.3	0.205±0.034	6.18±1.67	0.998	11.8
			75	12.4±1.5	0.257±0.028	6.06±1.45	0.999	6.0
			85	10.6±0.1	0.317±0.020	7.00±0.42	0.999	8.9
			95	2.69±0.04	0.466±0.017	3.56±0.27	0.998	13.1

[a] $MRE = \sum_{i=1}^{j} \left| \left(x_{\exp i} - x_{\text{model } i} \right) \Big/ x_{\exp i} \right| / j \text{ x } 100$

To gain more information on the concentration regimes of EPS A, the concentration dependence of zero-shear rate specific viscosity (η_{sp}) was represented in Fig. 3.4.2 B. In this study, the η_{sp} was calculated from η_0 values estimated by the

Carreau model (Table 3.4.3) (Martin-Pastor et al., 2019; Torres et al., 2015). As displayed in Fig. 3.4.2 B, two distinct linear zones are observed, characterized by the different slope values (1.45±0.05 and 2.43±0.19). The transition between the two concentration regimes can be determined as the intercept of both lines, corresponding to a concentration of 1.89 g L^{-1}. A rough estimate for the overlap concentration, which defines the onset of the semi dilute non entangled regime is given by the concentration at which $\eta_{sp} \cong 1$ (Hilliou et al., 2009). As such, further studies are needed for lower polymer concentrations than 1 g L^{-1} (0.1%), using capillary viscometry, in order to assess all possible concentration regimes, as the lowest η_{sp} value that was possible to measure with accuracy with the rheometer was quite higher than 1.

The impact of polymer concentration (0.1 – 1.25%) on the storage (G') modulus and the loss (G'') is presented in Fig. 3.4.3. G' is a measurement of the energy stored in a material, thus representing the elastic component of the overall material stiffness; and G'' is a measurement of the energy lost by viscous dissipation (Gu et al., 2020). For the lowest concentration tested (0.1 wt.%), the EPS solution exhibited a typical liquid-like behavior, with G'' higher than G' over the whole frequency range (Fig. 3.4.3 A). As the EPS concentration increased to 0.25 wt.% (Fig. 3.4.3 B and C), G' increased more rapidly than G'' with increasing frequency. Consequently, a crossover occurred at around 0.1 Hz, and the EPS solutions started to exhibit a predominant elastic behavior at frequencies higher than the crossover point, which suggests that the EPS A has potential to be employed as thickening agent (Abid et al., 2021). Interestingly, once the EPS concentration surpassed 0.4 wt.% (Fig 3.4.3 D–I), the elastic contribution is dominant and both dynamic moduli are dependent on the frequency in all the frequency range studied, suggesting that the EPS formed a weak gel-like structure. A similar gel behavior was reported for *Rhizobium radiobacter* S10 EPS (Zhou et al., 2014), *Sagittaria sagittifolia* polysaccharide (Gu et al., 2020), *Leuconostoc citreum* SK24.002 α-D-glucan (Miao et al., 2015), and *Weissella confusa* R003 dextran (Netsopa et al., 2018), for concentrations above 0.75, 1.5, 3 and 5 wt.%, respectively. In contrast, a variety of microbial EPS reported in literature did not exhibit gel behavior. Examples include the EPS from *Sporidiobolus pararoseus* JD-2 (Han et al., 2016), *Lactobacillus plantarum* C70 (Ayyash et al., 2020), *Streptococcus thermophiles* S-3 (Xu et al., 2018), *Vibrio* strain MO245 (Martin-Pastor et al., 2019), or *Leuconostoc citreum*-BMS strain (Abid et al., 2021). These differences in the rheological properties between polysaccharides are likely related with their distinct monosaccharide composition, glycosidic bond types, charge density, and molecular mass distribution (Ayyash et al., 2020; Concórdio-Reis et al., 2021).

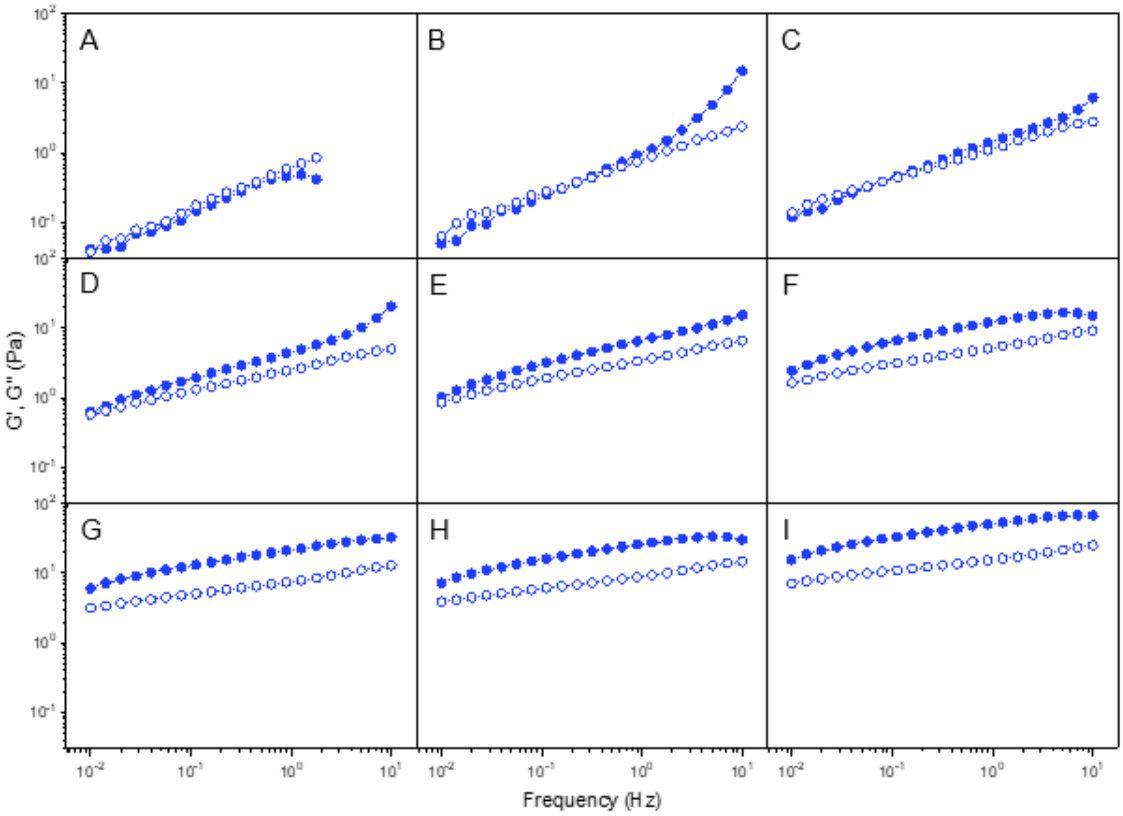

Figure 3.4.3. Angular frequency dependencies of storage G' (●) and loss G'' (○) moduli for the aqueous solutions of EPS A at different concentrations: 0.1 wt.% (A); 0.18 wt.% (B); 0.25 wt.% (C); 0.4 wt.% (D); 0.5 wt.% (E); 0.6 wt.% (F); 0.75 wt. % (G); 1 wt.% (H); and 1.25 wt.% (I).

Although both moduli presented a frequency dependence, which is typical of weak gels (Zhou et al., 2014), it decreases for the higher concentrations tested (above 0.75 wt.%). The weakening of frequency dependency might be a consequence of stronger intermolecular interaction associated with high concentration systems, resulting in gel systems with higher strength and stability (Miao et al., 2015). Moreover, as the concentration increases, the difference between G' and G'' also increases, thus indicating that the stability and strength of the gel structures was enhanced (Zhou et al., 2014). In fact, the absolute gel strength (G' values at 0.01 Hz) increased from 0.62 Pa to 15.5 Pa, as the EPS concentration increased from 0.4 to 1.25 wt.%. These values are similar to those reported for weak gels obtained with paenan, an EPS produced by *Paenibacillus polymyxa* (G' values between 3 and 14 Pa at 0.01 Hz) (Rütering et al., 2018).

The Cox-Merz rule is an empirical relationship between the steady shear flow and the dynamic tests that can be used to obtain qualitative information on the interactions of the polymer chains (Kontogiorgos et al., 2012). As depicted in Fig. 3.4.4, for lower concentrations (0.1–0.25 wt.%) the data deviated from the Cox-Merz rule with the

complex viscosity ($|\eta^*(\omega)|$) values higher than η ($\dot{\gamma}$) as the shear rate or frequency increased. Moreover, with an increase in concentration, $|\eta^*(\omega)|$ deviation from η ($\dot{\gamma}$) also increased. Divergence from the Cox-Merz rule was expected as it is often associated with the formation of intermolecular chain aggregates, hyperentanglements and gel-like systems (Cruz et al., 2011; Kontogiorgos et al., 2012). Deviations from the rule have been reported for polysaccharides such as xanthan (1 wt.%) (Richardson & Ross-Murphy, 1987), pectin (30 wt.%) (Dimopoulou et al., 2021), curdlan (2–8 wt.%) (Lo et al., 2003) or *Aeromonas* gum (2.5–4.9 wt.%) (Xu et al., 2006). In contrast, the rule was valid for polysaccharide solutions with non-interacting chains (Dimopoulou et al., 2021), such as galactomannan (0.6–1 wt.%) (Sittikijyothin et al., 2005), alginate (0.6 wt.%) (Storz et al., 2010), *Enterobacter* A47 EPS (0.81 wt.%) (Cruz et al., 2011), or *Pseudomonas oleovorans* EPS (0.85 wt.%) (Alves, Freitas, Costa, et al., 2010).

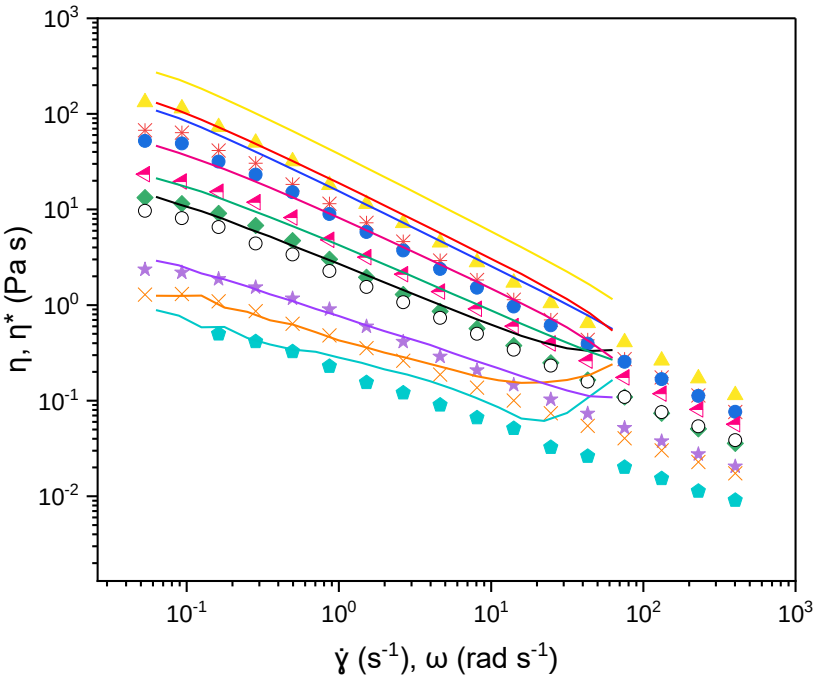

Figure 3.4.4. Cox-Merz plot for different EPS concentrations: 0.1 wt.% (⬟); 0.18 wt.% (✕); 0.25 wt.% (★); 0.4 wt.% (○); 0.5 wt.% (◆); 0.6 wt.% (◀); 0.75 wt. % (●); 1 wt.% (✳); and 1.25 wt.% (▲) Apparent viscosity η (symbols) and complex viscosity $|\eta^*|$ (lines), as a function of shear rate ($\dot{\gamma}$) and angular frequency (ω), respectively.

Effect of salts

The addition of salts to polysaccharide's solutions is reported to alter the rheological behavior, which affects their applicability as rheology modifiers. Therefore, the impact of the presence of salts, namely, 1 M NaCl or 1 M $CaCl_2$, was assessed in 0.75 wt.% EPS solutions (Fig. 3.4.5). For both salts, the EPS solutions maintained their

shear thinning behaviour, displaying identical viscosity, but their apparent viscosity was reduced compared to the EPS solution with no salts' addition (Fig. 3.4.5 A). The flow curves were fitted to Carreau equation, and the estimated parameters (Table 3.4.3), namely n<1, confirmed the shear thinning behavior of the EPS solutions. The presence of inorganic ions is often associated with a viscosity reduction of polyelectrolyte systems, such as polysaccharides rich in carboxylic groups. The charged ions can interact with the polyelectrolyte charges, reducing electrostatic repulsion between the EPS chains. Moreover, the charge shielding caused by the high counter-ions concentration might cause the EPS to fold up and acquire a more compact structure. Consequently, the smaller hydrodynamic volume resulted in a decreased viscosity (Dimopoulou et al., 2021; Freitas, Alves, Carvalheira 2009; Ji et al., 2020). Interestingly, no significant difference between the two salts was observed (Fig. 3.4.5 A, Table 3.4.3), even though divalent ions, such as Ca^{2+}, usually have a more pronounced effect on polysaccharide's apparent viscosity than monovalent ions like Na^{+} (Ji et al., 2020; Medina-Cabrera et al., 2021). Xanthan gum, for example, kept a high viscosity when Na^{+} was added (~1 M). However, in the presence of Ca^{2+} (~1 M), the viscosity of the xanthan solution decreased drastically (from approximately 12 to 1.5 Pa s) (J. Li et al., 2017).

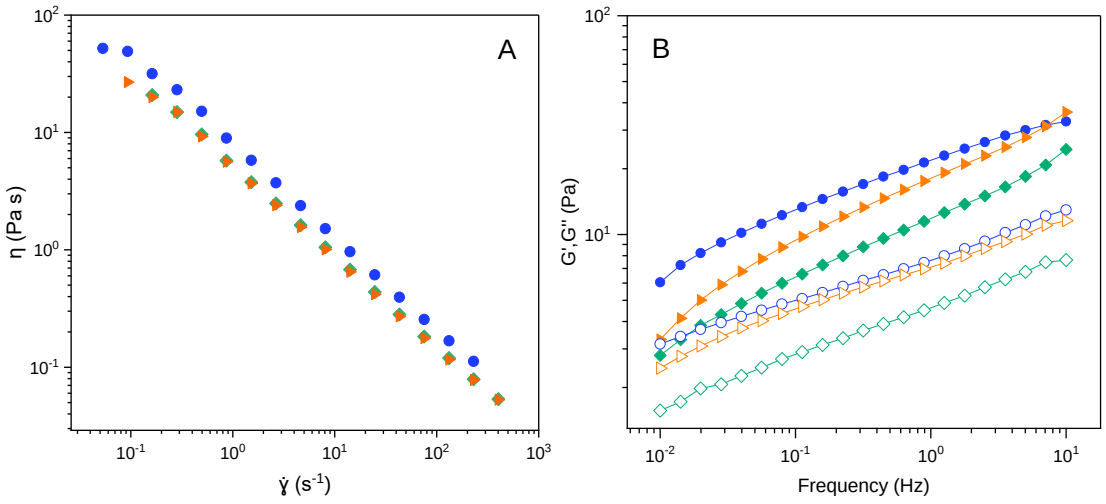

Figure 3.4.5. Effect of salt addition on EPS A aqueous solutions (0.75 wt.%) (without salt addition (●); in 1 M NaCl (◆) and in 1 M $CaCl_2$ (▶)) on the apparent viscosity (A); and viscoelastic properties (B), namely, storage modulus G' (full symbols) and loss modulus G'' (open symbols).

The effect of the presence of 1 M $CaCl_2$ and 1 M NaCl on the viscoelastic properties of a 0.75 wt.% EPS solution was also evaluated and the results are presented in Fig. 3.4.5 B. Regardless of the salt added, G' was higher than G''

throughout the entire frequency range, suggesting that the addition of inorganic salts did not disrupt the EPS weak gel-like structure. Despite this, both cations altered the viscoelastic moduli of the EPS solution. Na^+ caused a significant reduction on both G' and G'', whereas with Ca^{2+}, G'' remained identical, and a decrease was observed only for G' at low frequencies. These results indicate that, despite the loss in strength, the EPS can still sustain its weak gel-like structure under high salt conditions.

Effect of pH

The effect of pH in the steady shear flow behavior of EPS A (0.75 wt.% solution) was investigated at different pH values, namely 3, 5, 7 and 9. The flow curves are depicted in Fig. 3.4.6 A and the estimated Carreau model parameters are presented in Table 3.4.3. Although the shear thinning behavior was maintained for all EPS solutions, both acidic and alkaline conditions induced a decrease in the apparent viscosity (Fig. 3.4.6 A). The EPS showed maximal viscosity values at neutral pH, with an estimated η_0 of 59.6±2.2 Pa s, whereas alkaline pH caused a severe effect on the rheological properties, decreasing the η_0 to 2.03±0.02 Pa s. Alkaline conditions might cause a reduction of intermolecular associations or a shielding effect that reflected in changes of the hydrodynamic volume of the molecules, leading to a decrease in viscosity (Abid et al., 2021; J. Li et al., 2017). Similarly, the EPS rheology was significantly affected at pH 3 (Fig. 3.4.6 A), with the η_0 decreasing to 3.61±0.05 Pa s. Nonetheless, under mild acidic conditions (pH 5), the impact on rheology was not as pronounced as for pH 3, since the η_0 was found to be 26.1±0.3 Pa s. As the pH decreases, the charged carboxylic groups of the EPS get protonated, which due to their abundance, might lead to a weakening of the electrostatic repulsions, mainly negative due to the presence of unprotonated sulphates under these acid conditions. Thus, the EPS might adopt a more compact conformation as the pH drops, resulting in a decrease in viscosity (Abid et al., 2021; Dimopoulou et al., 2021; Li & Hou, 2011; J. Li et al., 2017).

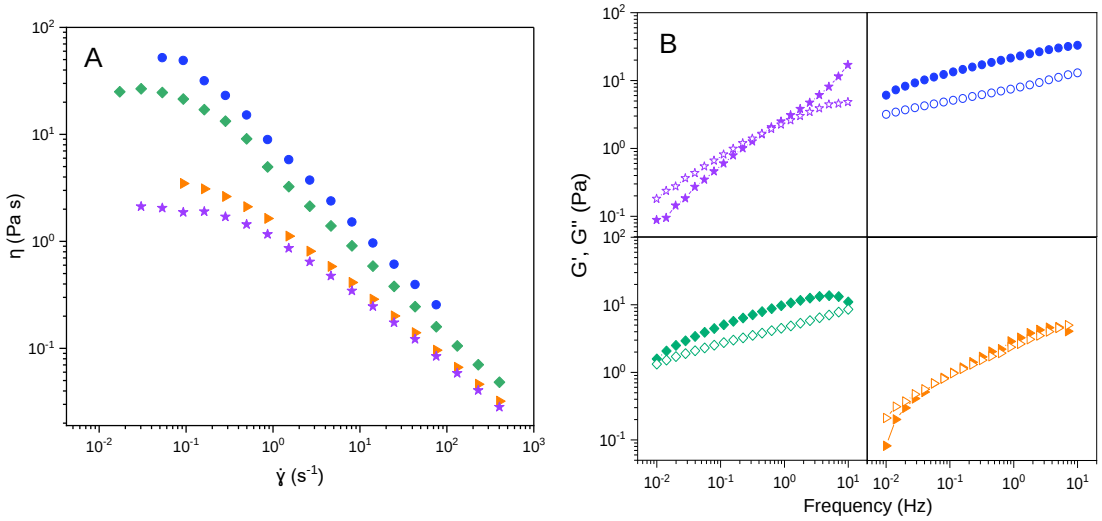

Figure 3.4.6. Apparent viscosity (η) of EPS A solutions (0.75 wt.%) as a function of the shear rate ($\dot{\gamma}$) (A) and angular frequency dependencies of storage G' (full symbols) and loss G'' (open symbols) moduli (B), under different pH values: pH 9 (★), pH 7 (●); pH 5 (◆) and pH 3 (▶).

A behavior similar to that observed for *A. macleodii* Mo169 EPS was observed for the aqueous solutions of the EPS produced by *Paenibacillus edaphicus* NUST16 (J. Li et al., 2017) and by *Enterobacter* A47 (Torres et al., 2015), for which the highest viscosity values were obtained near neutral conditions, decreasing in both acidic and alkaline conditions. Interestingly, both EPS had glucuronic acid in their composition in similar quantities (around 9 mol%). Different results were found for EPS composed of neutral sugars. For example, the aqueous solutions of the neutral EPS produced by *Lactobacillus plantarum* C70 (Ayyash et al., 2020) and *L. kefiranofaciens* ZW3 (Ahmed et al., 2013). Moreover, the viscosity of the solutions of the EPS of *Leuconostoc citreum*-BMS was not affected by increasing the pH from 7 to 9, but acidic conditions induced a decrease in viscosity, which may be attributed to the higher content in acid groups (Abid et al., 2021). On the other hand, for the EPS secreted by *Pseudomonas oleovorans* (Freitas, Alves, Carvalheira, et al., 2009), the solutions' viscosity was only affected by alkaline pH values.

Comparable to the results from the steady state tests, the viscoelastic properties were considerably affected by pH variations (Fig. 3.4.6 B). Although both moduli were affected by pH variation, G' seemed more sensitive to pH alteration than G''. At pH 5, G' was higher than G'', suggesting that the EPS maintained the gel-like structure. However, a significant loss of gel strength was observed, particularly at low frequencies. This response to pH variation might be interesting for the development of drug delivery systems suitable for the treatment of conditions associated with local

acidosis such as sites of tumor, wound infection, and ischemia (Bolla et al., 2018; Wu et al., 2020). At pH 3 and pH 9, G'' became higher than G', indicating a dominant viscous behavior at lower shear rates and, consequently, a loss of the gel-like structure. Moreover, the curves showed a strong frequency dependence, characteristic of entangled viscoelastic chains (Dimopoulou et al., 2021). The viscoelastic properties of most polysaccharides are significantly affected by the pH, particularly at values below 4 and above 10 (Abid et al., 2021). For the EPS produced by *W. profunda* SM-A87, G' was higher than G'' between 3 and 11, but strong alkaline conditions (pH >11), favored a viscous behavior (Li & Hou, 2011). Also, gellan gum capacity to form a gel-like structures decreases as the pH drops below certain values (Fagioli et al., 2018).

Effect of temperature

Temperature is a crucial factor that impacts polysaccharide rheology, since it affects the strength of intra- and intermolecular hydrogen bonds and the speed of molecular chain movement, therefore affecting the conformation and the gel characteristics of the macromolecule (Cai et al., 2021). The impact of temperature (0 to 95 ^{o}C) on the viscosity of the EPS A solution (0.75 wt.%) was assessed. The flow curves and the fitted Carreau model parameters are presented in Fig. 3.4.7 A and Table 3.4.3, respectively. As depicted in Fig. 3.4.7 A, the apparent viscosity decreased as the temperature increased from 0 to 95 ^{o}C, but the shear thinning behavior was maintained even at the highest temperature tested. Moreover, the transition from the Newtonian regime to shear-thinning regime moved to higher shear rates as the temperature increased, which indicates that the formation of new interactions is faster at higher temperatures (Alves, Freitas, Costa, et al., 2010). This is in agreement with the estimated parameters of the Carreau model (Table 3.4.3), given that as temperature increases from 0 to 95 ^{o}C, the relaxation time (λ) decreased from 22.3 to 3.56 s. However, despite the temperature impact on the apparent viscosity of the solutions, the results presented in Fig. 3.4.7 A and Table 3.4.3 show that the rheological behavior of the EPS was maintained when the temperature was within the range of 5 to 55 ^{o}C (η_0 between 34.8 and 59.6 Pa s), suggesting that the EPS could maintain its entangled structure. Higher temperatures, between 65 and 85 ^{o}C, led to a slight decrease in viscosity (η_0 in the range of 10.6 to 15.5 Pa s), but upon rising to 95 ^{o}C, the apparent viscosity decreased significantly (η_0 of 2.69 Pa s) (Fig. 3.4.7 A, Table 3.4.3). High temperatures can facilitate the molecules' movement, reducing the intermolecular entanglements, resulting in a reduction of the apparent viscosity of the solutions (Cai et al., 2021). These results are similar to those reported for the *L.*

citreum-BMS EPS, which was not significantly affected by temperatures up to 45 ºC and maintained its shear thinning behavior at 90 ºC (Abid et al., 2021).

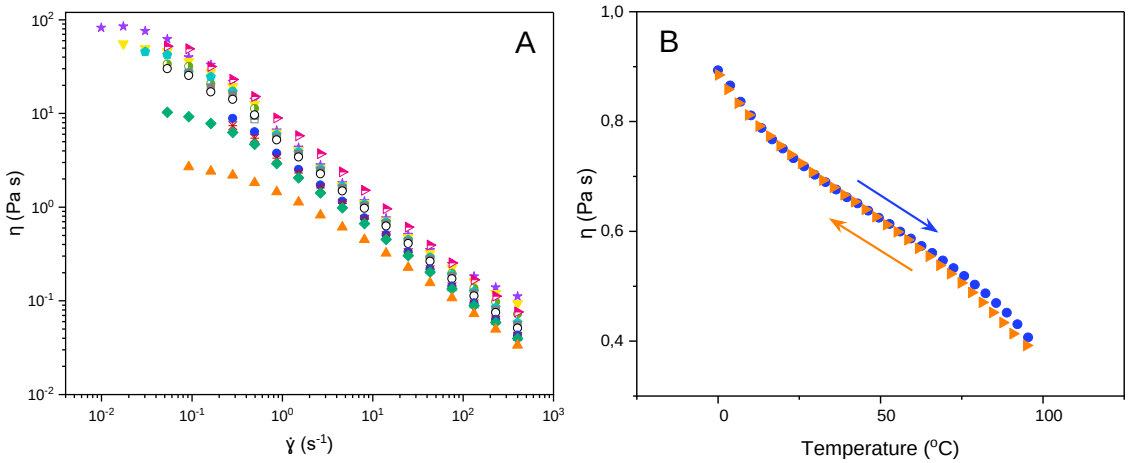

Figure 3.4.7. (A) Apparent viscosity (η) of EPS A solution (0.75 wt.%) as a function of the shear rate ($\dot{\gamma}$) under different temperatures: 0 ºC (★), 5 ºC (▼), 15 ºC (◑), 25 ºC (▶), 35 ºC (⬟), 45 ºC (■), 55 ºC (○), 65 ºC (●), 75 ºC (✳), 85 ºC (◆), and 95 ºC (▲). (B) Temperature sweeps, heating (●) and cooling (▶), of the 0.75 wt.% EPS solution at a fixed shear rate of 10 s^{-1}.

To understand the reversibility of the observed viscosity decrease resulting from exposure to high temperatures, the sample was heated from 0 to 95 ºC, and cooled back to 0 ºC (Fig. 3.4.7 B). As illustrated in Fig. 3.4.7 B, the viscosity decreased as the sample was heated. Nevertheless, upon cooling, the EPS solution recovered its initial viscosity, suggesting that that EPS A can be employed in products that are exposed to high temperatures during their processing, such as pasteurization of food products (Abid et al., 2021). In addition, the effect of heating was studied according to the Arrhenius equation (Eq. 3.4.2):

$$\eta = A\, exp\left(\frac{E_a}{RT}\right) \qquad (3.4.2)$$

where η is the apparent viscosity (Pa s), A is the pre-exponential factor (Pa s), E_a is the activation energy (J mol^{-1}), R is the gas constant (8.314 J mol^{-1} K^{-1}) and T is the absolute temperature (K). At a shear rate of 10 s^{-1}, the E_a was 5.55±0.93 kJ mol^{-1} and A was 0.077±0.003 Pa s (R^2 0.993). This E_a value was lower than those found for *S. thermophiles* S-3 EPS (7.34 kJ mol^{-1}) (Xu et al., 2018), *L. plantarum* C70 EPS (6.86 – 27.45 kJ mol^{-1}) (Ayyash et al., 2020), *L. citreum*-BMS EPS (17.35 – 18.72 kJ mol^{-1}) (Abid et al., 2021), levan (13.53 – 24.07 kJ mol^{-1}) (Bae et al., 2008), and *Lignosus rhinocerotis* polysaccharide (12.52-13.99 kJ mol^{-1}) (Cai et al., 2021).

Similarly, the mechanical spectra of the EPS solution were affected by temperature, and four different behaviors could be identified (examples are depicted in Fig. 3.4.8 A). When the temperature was between 0 and 55 ºC, G' was higher than G'', indicating that the weak gel-like behavior was maintained for this temperature range. At 65 ºC, a cross-over was detected at low frequencies, which can be attributed to the loss of the gel structure, although the elastic contribution was still predominant throughout most of the frequency range. As the temperature rose to 85 ºC, the cross-over moved to higher frequencies, with the viscous contribution predominating at lower frequencies. At the highest temperature tested (95 ºC), G'' was higher than G' during the whole frequency range, reflecting a liquid-like behavior (Fig. 3.4.8 A). This viscoelastic behavior is distinct from that found for *Pseudomonas stutzeri* AS22 EPS, for which both moduli presented a "plateau" region with G'>G'', followed by an increase for temperatures higher than 60 ºC, and a liquid-like behavior (G''<G') at 70 ºC attributed to the swelling and breakage of inter- and intra-molecular hydrogen bonds (Maalej et al., 2016).

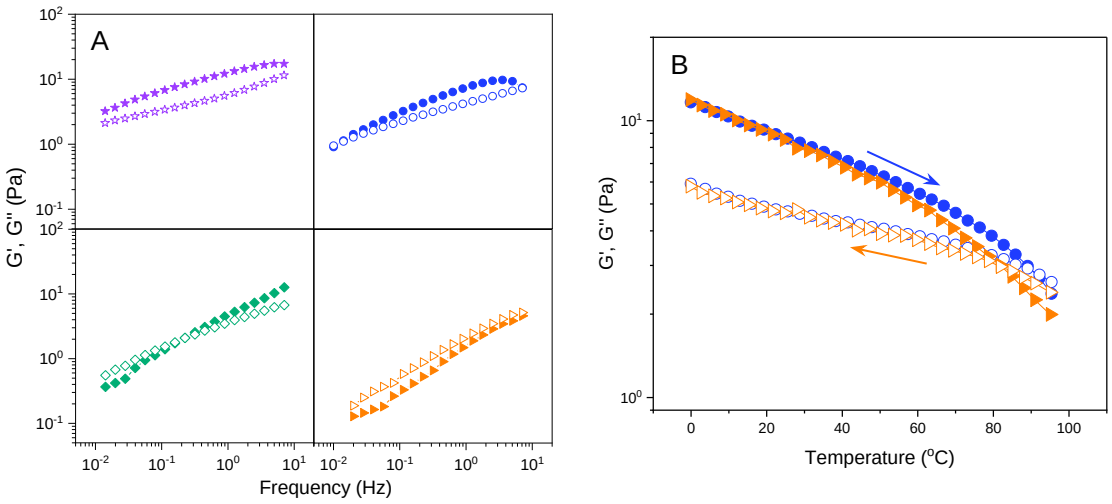

Figure 3.4.8. Storage G' (full symbols) and loss G'' (open symbols) moduli of EPS A solution (0.75 wt.%) under different temperatures (A): 0 ºC (★), 65 ºC (●), 85 ºC (◆), and 95 ºC (▶). Temperature dependence of storage G' (full symbols) and loss G'' (open symbols) moduli during heating from 0 to 95 ºC (blue) and cooling from 95 to 0 ºC (orange) (B).

To understand the reversibility of the impact of temperature on the viscoelastic properties, a temperature cycle was conducted by increasing the temperature from 0 to 95 ºC, and subsequently cooling down to 0 ºC (Fig. 3.4.8 B). At the frequency tested (1 Hz), G' was higher than G'' from 0 to 90 ºC, however, for higher temperatures, the viscous modulus G'' was dominant. Nevertheless, when the sample was cooled down, the EPS solution completely recovered its initial viscoelastic properties. In addition,

these results suggest that the gel formed by EPS A had good thermal reversibility when submitted to temperatures up to 95 ºC. Similarly, *R. radiobacter* S10 EPS was reported to regain its gel structure after exposure to temperatures up to 75 ºC (Zhou et al., 2014). However, thermal reversibility was not found for other gel-like polysaccharides, such as *P. stutzeri* AS22 EPS (Maalej et al., 2016) and *L. rhinocerotis* polysaccharide (Cai et al., 2021).

Thixotropy

The ability of EPS A to recover its rheological properties after high-shear stress was assessed for a polymer concentration of 0.75 wt.% (Fig. 3.4.9). As presented in Fig. 3.4.9 A, the forward and backward curves were overlapped, indicating that EPS A had no significant thixotropic properties at this concentration for the conditions tested. Regarding the mechanical properties, the EPS completely recovered its gel structure within 4 seconds after mechanical stress removal (Fig. 3.4.9 B), suggesting that the EPS has a strong self-healing capacity. This is an important rheological feature since high stress might occur during the application and manufacturing of many products, or due to unintended shaking (Rütering et al., 2018). A rapid recoverability and reversibility are desirable to prevent the product from dripping after its application and to guarantee product homogeneity (Rütering et al., 2018). This is an important aspect for different applications such as, for example, gelling agents in skincare products (Maalej et al., 2014). These products should have high viscosity at low shear forces to maintain the products' desired texture, and low viscosity at high shear force, when applied, to be easily absorbed by the skin. After the application, a rapid return to the original viscosity allows the topical product to remain on the skin (Maalej et al., 2014). Moreover, these self-healing properties are also an important indicator for the quality of gels employed in biomedicine and wearable devices, since the integrity of the gel network is not compromised under stress induction (e.g., upon injection) (Cai et al., 2021).

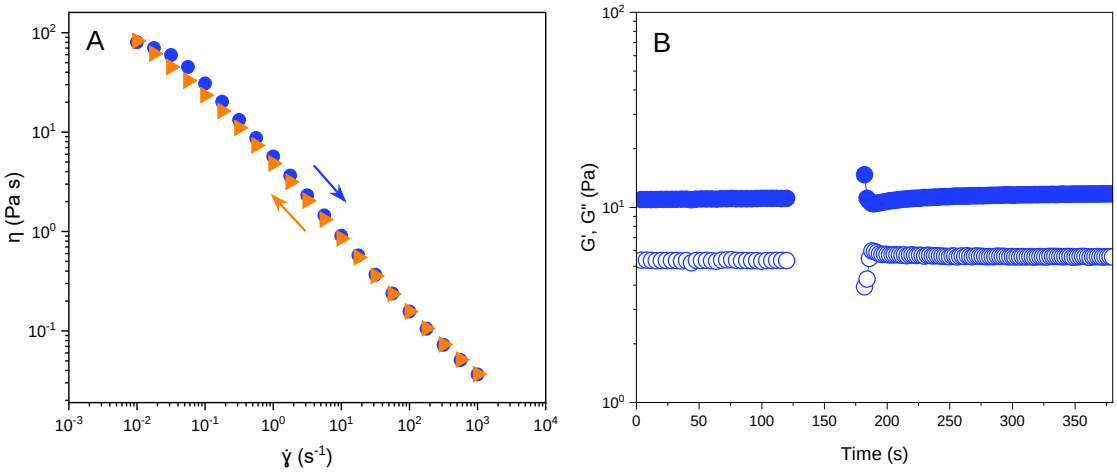

Figure 3.4.9. Thixotropic behavior of EPS A solutions (0.75 wt.%): A shows the effect of high shear stress on the apparent viscosity (η), with the shear rate ($\dot{\gamma}$) increasing from 0.01 to 1000 s^{-1} (●), kept at 1000 s^{-1} for 60 s, and decreased from 1000 to 0.01 s^{-1} (▶); and B shows the storage G' (full symbols) and loss G'' (open symbols) moduli before and after exposure to high shear conditions (1000 s^{-1} between time 120 and 180 s).

3.4.4.3. EPS hydrogels

Effect of Fe^{3+} and EPS concentrations: response analysis

As described in Chapter 3.1, EPS A forms homogeneous hydrogels in the presence of Fe^{3+} under neutral pH (Concórdio-Reis et al., 2021). Nonetheless, the hydrogels did not sustain their structure in the inversion test, therefore, the preparation conditions, i.e., Fe^{3+} and EPS concentration, were optimized. The Fe^{3+} concentration range tested (0.05–9.95 g L^{-1}) was chosen based on previous studies that aimed at optimizing *Enterobacter* A47 EPS (FucoPol) gelation with Fe^{3+} (0.05–10 g L^{-1}) (Rodrigues, 2021). The EPS concentration range tested (0.3–1.7 %) was defined based on the central point (1%) that was the concentration reported for FucoPol gelation tests (Fialho et al., 2019). Also, the maximum EPS concentration tested was 1.7% since higher concentrations did not form homogenous solutions due to the EPS' high viscosity.

The results obtained under different Fe^{3+} and EPS concentrations are presented in Fig. 3.4.10 and Table 3.4.1. As presented in Fig. 3.4.10, for all the conditions tested, G' was one order of magnitude higher than G'' in the whole frequency range. In addition to the higher moduli values compared to the EPS in solution, no frequency dependance was observed, suggesting a higher strength and stability (Miao et al., 2015). A similar behavior was found for Fe^{3+}-FucoPol (Rodrigues, 2021), Ca^{2+}-gellan (Ambebila et al., 2019), and Fe^{3+}-succinoglycan (Hu et al., 2020).

The maximum G' value was obtained at experiment D, with 8.5 g L^{-1} of Fe^{3+} and 1.5% EPS (44 kPa), and experiment H, with 5 g L^{-1} of Fe^{3+} and 1.7% EPS (42 kPa). These values were similar to those obtained for Fe^{3+}-xanthan hydrogels (~30/40 kPa) (M. Kang et al., 2019) and much higher than those obtained for the hydrogels prepared with Fe^{3+}-FucoPol (G' between 0.82–1.4 kPa) (Rodrigues, 2021), Ca^{2+}-gellan (G'~0.2–0.3 kPa) (Ambebila et al., 2019), K^{+}- and Na^{+}-carrageenan (0.01–0.6 kPa) (Martínez-Ruvalcaba et al., 2007; Morris & Chilvers, 1983) and Ca^{2+}-alginate (~1 kPa) (Martínez-Ruvalcaba et al., 2007; Segeren et al., 1974). Nonetheless, the experiments with the lowest Fe^{3+} (experiment E) and EPS concentrations (experiment G) resulted in the G' values (0.3 and 1.6 kPa, respectively) in the range of values found for the hydrogels reported above. These results indicate that EPS A hydrogels can have a wide range of strengths and, therefore, a wide range of applications. Examples of possible applications for Fe^{3+}-polysaccharide hydrogels include drug delivery, sensors manufacturing or tissue engineering. Fe^{3+}-succinoglycan hydrogels were successfully used for controlled drug delivery based on gel-sol conversion in the presence of reducing agents and visible light (Hu et al., 2020). Fe^{3+}-alginate hydrogels were used as "smart" sensing interface for improved electrochemical immunosensor for a tumor marker (Yin & Ma, 2019). Fe^{3+}-cross-linked carboxylates/sulphonates hydrogels were a promising candidate material in cartilage tissue engineering (Yu et al., 2022). Interestingly, these hydrogels presented a similar range of strength (G' between 10^2 and 10^4 Pa) (Yu et al., 2022) to that of Fe^{3+}-EPS A hydrogels (10^1 –10^5 Pa, Fig. 3.4.10). In fact, Fe^{3+}-EPS A hydrogels present a range of strength (0.3–44 kPa) that mimics several soft tissues, including brain (~0.1–1 kPa), cornea (~2 kPa), liver (0.5–5 kPa), adipose (~2.5–3.5 kPa) and muscle (~8 –17 kPa) tissues, and stiffer matrices such as the crosslinked collagen of osteoids (~25–40 kPa) (Engler et al., 2006; Hui et al., 2019; Wu et al., 2020; Zuidema et al., 2014). Moreover, the incorporation of bioceramics (e.g., bioglass, nano hydroxyapatite) can reinforce the hydrogel and increase the G' (Vishnu Priya et al., 2016), thus, expanding the possibilities for tissue engineering applications.

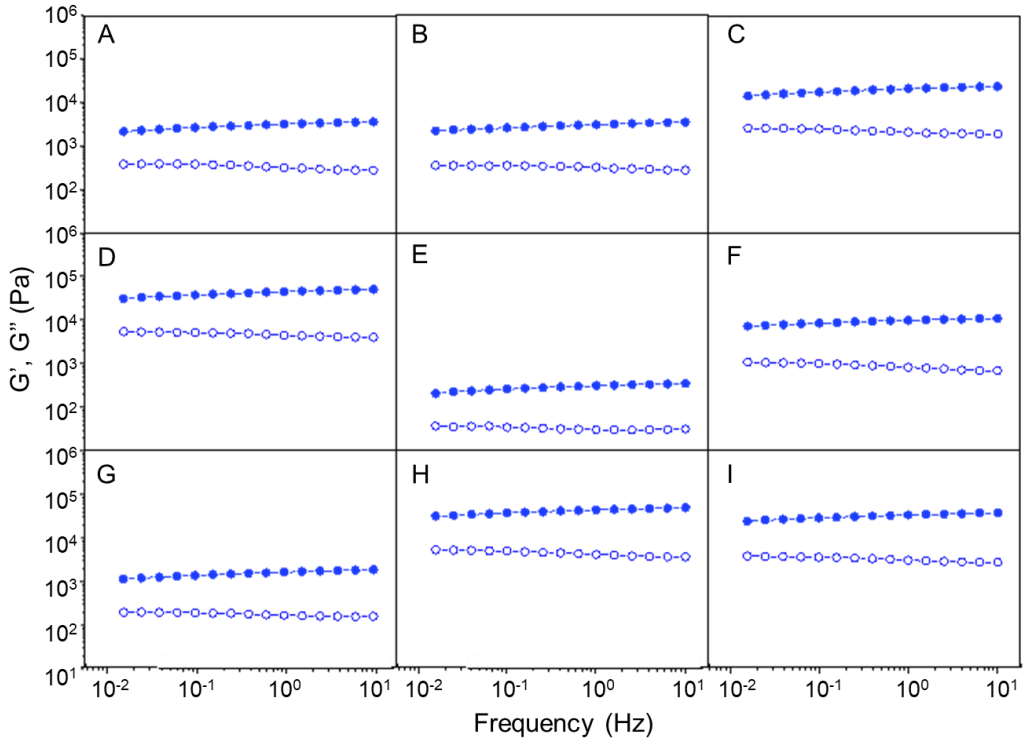

Figure 3.4.10. Angular frequency dependencies of storage G' (●) and loss G'' (○) moduli for EPS A hydrogels prepared with conditions A–I.

Model fitting and statistical validation

Based on statistical and mathematical methods, RSM provides a lot of information using limited number of experiments, thus, reduces the time and costs compared with classical methodologies (Dehghan-Baniani et al., 2020). In this study, RSM approach was used to evaluate the effect of Fe^{3+} and EPS concentration, as well as their combined effect on EPS A hydrogels strength. The quadratic model was evaluated by ANOVA to assess if it could be validated (Appendix A.4, Table A.2). The model was considered an accurate predictive tool if the maximum error of the prediction was within the experimental deviation range. Nonetheless, the quadratic effect of EPS concentration (X_2^2) was found to be non-significant for a 95% confidence level (*p*-value=0.36>0.05) (Appendix A.4, Table A.2), therefore, this term was eliminated from the model and a new ANOVA (Table 3.4.4) was performed for the reduced quadratic model (Eq. (3.4.3)) (Ahmadi et al., 2005; Azarifar et al., 2019; Ghelich et al., 2019).

$$Y_p = -12626 + 5872.5X_1 + 12248X_2 + 3388.5X_1X_2 - 795.34X_1^2 \quad (3.4.3)$$

Table 3.4.4 shows that the model was significant (*p*-value=0.0002<0.001) at the 99.9% probability level, with only 0.02% chance that the model *f*-value was due to

noise (Baptista et al., 2022). The lack of fit of the model, which indicates the impact of discrepancy between the actual and predicted values to the pure error between the replicates (Ghelich et al., 2019), was found to be not significant relative to the pure error (*p*-value=0.53>0.05). The determination coefficient (R^2) indicated that 96.17% of the variation in the response is related with the independent variables and can be elucidated by the model (Ghelich et al., 2019; Sharifi et al., 2018). The predicted R^2 (0.8718) was in reasonable agreement (i.e., the difference is less than 0.2) with the adjusted R^2 (0.9362), which demonstrates that the experimental and predicted values for G' are in good agreement (Ghelich et al., 2019). Also, the high observed precision (signal-to-noise ratio=16.65) indicated an adequate signal (value>4 is desirable) in the model for the navigation of the design space (Baptista et al., 2022; Sharifi et al., 2018; Yang et al., 2020).

Table 3.4.4. Analysis of variance (ANOVA) for the reduced quadratic model describing EPS A hydrogels strength as function of Fe^{3+} and EPS concentration.

Source of variation	Sum of squares	Degrees of freedom	Mean square	*f*-value	*p*-value
Model	2.599×10^9	4	6.498×10^8	37.69	0.0002
X_1 – Fe^{3+}	1.676×10^8	1	1.676×10^8	9.72	0.0206
X_2 – EPS	1.704×10^9	1	1.704×10^9	98.85	<0.0001
$X_1 X_2$	1.407×10^8	1	1.407×10^8	8.16	0.0289
X_1^2	5.868×10^8	1	5.868×10^8	34.04	0.0011
Lack of Fit	7.059×10^7	4	1.765×10^7	1.07	0.5343*
Pure Error	3.285×10^7	2	1.642×10^7		

* Not significant (*p*-value>0.05).

For model validation, diagnostic plots (Fig. 3.4.11), such as normal probability of residuals plot, predicted versus actual values, residual versus predicted values and standardized residuals versus run plot, should be evaluated (Ghelich et al., 2019). Fig. 3.4.11 A shows that the plotted residuals form a roughly straight line. Hence, the residuals followed the normal probability distribution, which confirmed the residuals independency and normality (Ghelich et al., 2019; Sharifi et al., 2018; Vining, 2010; Yang et al., 2020). The predicted versus actual values plot (Fig. 3.4.11 B) showed a random scatter, confirming that no data transformation was required (Vining, 2010), and that the obtained values are in close agreement with the predicted values (Ghelich et al., 2019). Similarly, the plots from the residuals versus fitted values plot (Fig. 3.4.11

C) should look like random scatter located close to zero-axis, confirming the assumption of constant variance (Ghelich et al., 2019; Sharifi et al., 2018; Vining, 2010). Finally, the residual versus the experimental run order graph (Fig. 3.4.11 C) shows a random scatter without any trend, which indicated that there were no time-related variables influencing the response during the experiment (Ghelich et al., 2019; Vining, 2010). Therefore, the analysis suggested that the proposed quadratic model was found to be adequate for describing EPS A hydrogel strength as a function of the Fe^{3+} and EPS concentrations in the design space.

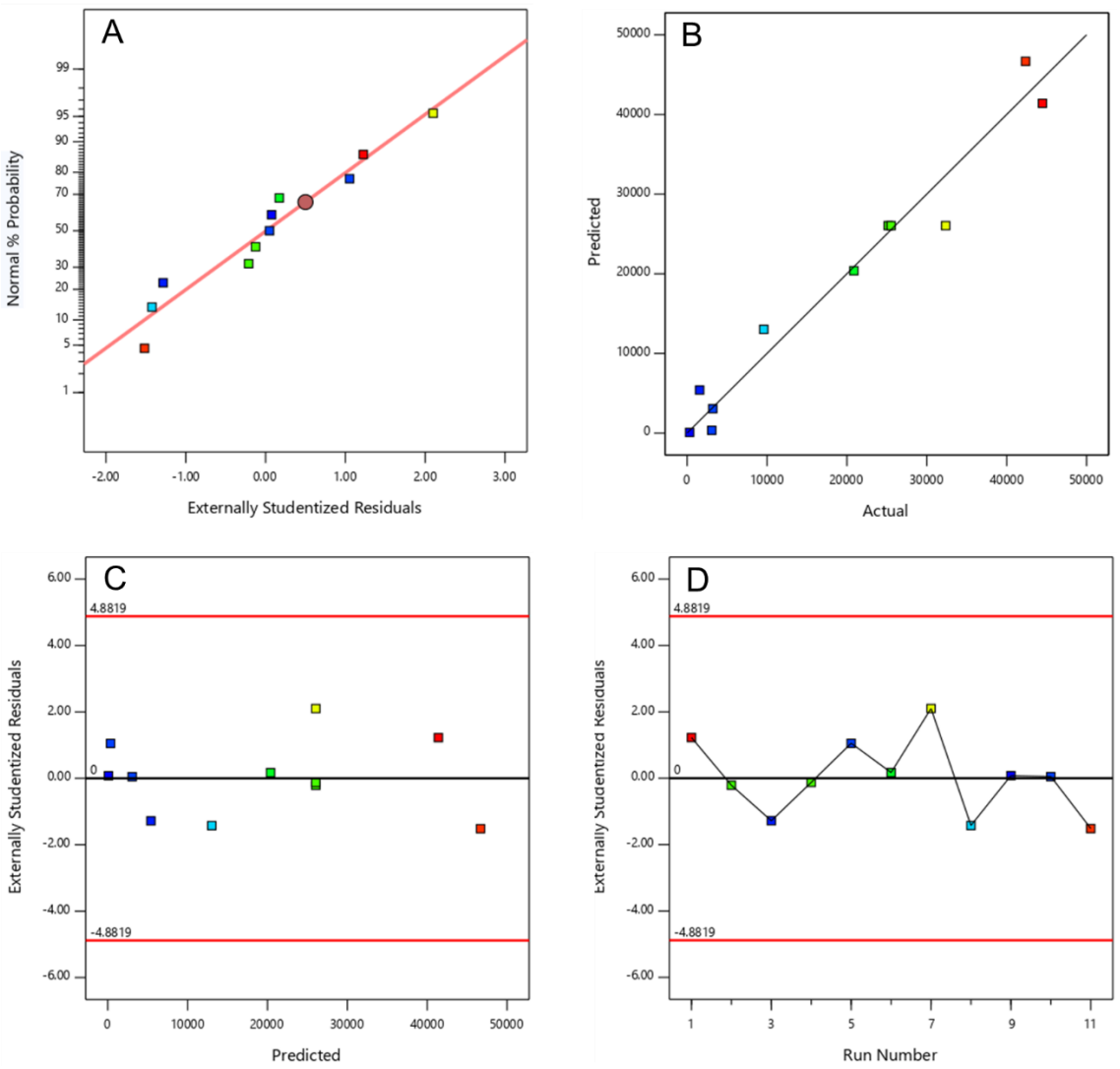

Figure 3.4.11. Diagnostic plots for the reduced quadratic model: normal probability plot (A), predicted versus actual values plot (B), studentized residuals versus predicted values plot (C) and studentized residuals versus run number plot (D).

RSM modelling

After validation, the proposed model was used to evaluate the impact of the linear, quadratic and interaction effects of Fe^{3+} and EPS concentration on the response. The G' value of the hydrogel was affected mostly by the linear term of EPS concentration (X_2) (*f*-value of 98.85) (Table 3.4.4). The positive β_2 value obtained (+12248, Eq.(3.4.3)) indicated that this effect is positive: an increase in EPS concentration results in an increase in the response, which was also confirmed by the response surface plots (Fig. 3.4.12). Contrary to the quadratic effect of EPS concentration (X_2^2) that was found to be non-significant, the quadratic Fe^{3+} term (X_1^2) affected the response significantly (*f*-value of 34.04) (Table 3.4.4). Such quadratic effect, together with the effect of the interaction ($X_1 X_1$) resulted in the curvature found in both surface graphs (Fig. 3.4.12). Comparison with literature is difficult since only few studies focused on the optimization of natural polysaccharide-based hydrogels using RSM (Safarzadeh Kozani et al., 2021), and the conventional methods do not take into consideration the effect of the parameters' interaction on the response.

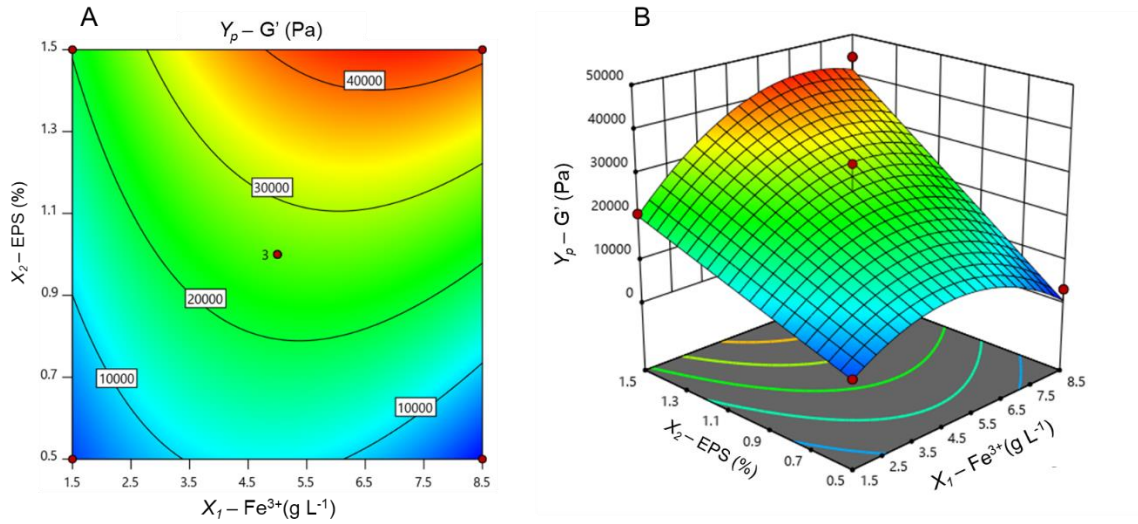

Figure 3.4.12. Contour (A) and three-dimensional response surface (B) plots for the effect of Fe^{3+} and EPS concentrations on EPS A hydrogel strength (G').

The proposed model offers the possibility to predict the performance of the hydrogel in terms of its strength. Moreover, different tailored hydrogel formulations can be developed to meet the requirements for specific applications (e.g., drug delivery or tissue engineering) by changing the process conditions.

3.4.5. Conclusions

This chapter reported the glycosidic composition and bonds of the EPS from *Alteromonas macleodii* Mo 169 (EPS A), a marine bacterium isolated in French Polynesia. The potential of the EPS to be used as a structuring agent, i.e., thickening and gelling agent, was also investigated. Compositional studies indicated the presence of acidic EPS, mainly composed of glucuronic acid, mannose, glucose, and galactose, all 1,4 linked, with 5.3 wt.% (17 mol%) sulphate, 0.63 wt.% (2.2 mol%) lactate, and 0.063 wt.% (0.2 mol%) pyruvate substituents, showing to be a negatively charged polysaccharide. Rheological characterization indicated that EPS A exhibited relevant non-Newtonian shear thinning behavior and a weak gel behavior under steady state and dynamic oscillatory measurements, respectively. Both behaviors were maintained under various conditions, such as in the presence of salts, at various pH values and temperatures. Moreover, EPS A showed outstanding recoverability after exposure to high temperatures and high shear stress. Also, the gel forming capacity of EPS A in the presence of Fe^{3+} was evaluated. RSM methodology was employed to investigate the impact of Fe^{3+} and EPS concentration on the hydrogel strength. Depending on the process conditions implemented, EPS A hydrogels can present various strength values that might be suitable for distinct applications. These results envisage the potential of marine bacteria as producers of novel high-value EPS that can, not only improve the rheological and structuring characteristics of products, but also contribute to the competitiveness of biobased products in different industrial fields, particularly in the food, pharmaceutical, biomedical, and cosmetic industries. Nevertheless, further studies to assess the EPS safety and the rheological behavior in formulations are required for the implementation of the EPS in such fields.

Chapter | 3.5

Alteromonas macleodii Mo169 EPS potential in nanotechnology: bioactive nanoparticle/EPS bio-nanocomposites

The results presented in this chapter resulted in the following manuscripts:

Concórdio-Reis, P., Ramos, K., Cardeira, M., Macedo, A.C., Serra, A.T., Moppert, X., Guézennec, J., Sevrin, C., Grandfils, C., Reis, M.A.M. & Freitas, F. Bioactive exopolysaccharide-composites based on gold and silver nanoparticles tailored for wound healing. Submitted to *Materials Today Communications*.

Concórdio-Reis, P., Macedo, A.C., Cardeira, M., Serra, A.T., Moppert, X., Guézennec, J., Sevrin, C., Grandfils, C., Reis, M.A.M. & Freitas, F. Selenium bio-nanocomposite based on *Alteromonas macleodii* Mo169 exopolysaccharide: Synthesis, characterization and *in vitro* bioactivity. In preparation.

The biological assays were performed in collaboration with Dr. Ana Teresa Serra from Instituto de Biologia Experimental e Tecnológica.

3.5.1. Summary

The marine isolate *Alteromonas macleodii* Mo 169 secretes an EPS mainly composed of glucuronic acid and containing sulphate, pyruvate, and lactate as acyl substituents (EPS A). The high density of negatively charged functional groups of the EPS renders it the ability to function as a stabilizing and reducing agent for the synthesis of metallic nanoparticles (NP). In this study, EPS A was used as stabilizing and reducing agent for the synthesis of gold and silver nanoparticles (AuNP and AgNP, respectively). Moreover, EPS A was shown to stabilize selenium nanoparticles (SeNP) synthesized using ascorbic acid as a reducing agent. The synthesized nanoparticles were spherical with an average particle size of 16, 15 and 32 nm for AuNP, AgNP and SeNP, respectively, displaying a polysaccharide layer that apparently contributed to reduce their aggregation. The cytotoxicity of the EPS and the bio-nanocomposites was evaluated on human keratinocyte (HaCaT) and fibroblast (CCD-1079Sk) cell lines. No cytotoxicity was found for the EPS alone or the bio-nanocomposites prepared with AuNP and AgNP for concentrations up to 1000 mg L^{-1}. A decrease in cell viability was only noticed for the EPS/SeNP composite at the highest concentrations tested (0.5 and 1 g L^{-1}). *In vitro* wound healing experiments demonstrated that the bio-nanocomposites EPS/AgNP and EPS/AuNP promoted cell migration for concentrations above 100 mg L^{-1}, thus contributing for a faster wound recovery. Moreover, the EPS/SeNP composite had a significant cellular antioxidant effect on the HaCaT cell line at concentrations above 125 mg L^{-1}. These findings demonstrated for the first time the potential of EPS A to synthesize and stabilize nanoparticles that possess promising physical-chemical and biological characteristics that render them valuable for the development of novel biomaterials for several applications, including wound care.

3.5.2. Introduction

Bio-nanotechnology plays an increasingly significant role in drug discovery and therapeutic development (Khurana et al., 2019; Li et al., 2019). NP, thanks to their unique properties such as small size, high surface to volume ratio, high surface reactivity, solubility, and multi-functionality, are of great value for various advanced application fields (Escárcega-González et al., 2018; Khurana et al., 2019). For example, NP have demonstrated a remarkable potential as carriers for drug delivery since they can facilitate the penetration of water-soluble therapeutic compounds. They can also improve the drugs' efficiency, and can be easily modified for drug targeted delivery (Khurana et al., 2019; Sathiyanarayanan et al., 2017). NP, in particular noble-metal NP, are excellent candidates for topical use in wound care due to their enhanced

mechanical strength, controlled release ability, and antimicrobial activity (Parani et al., 2016). Moreover, NP can be used in biological labelling, gene delivery, immunology, tissue engineering, and phagokinetic studies (Sathiyanarayanan et al., 2017).

NP's application is strongly associated with their characteristics, such as physicochemical properties, size, morphology, and dispersibility, which are defined by their synthesis method (C. Wang et al., 2017), which can involve physical, chemical, or biological procedures (Ahmed et al., 2014; Escárcega-González et al., 2018; Sathiyanarayanan et al., 2017). Contrary to conventional methods, biological, or green synthesis, is being increasingly explored given its cost-effective and environmentally friendly nature, based on the use of nontoxic reagents and procedures (Escárcega-González et al., 2018; Sathiyanarayanan et al., 2017; C. Wang et al., 2017). The concept of green NP synthesis was first described by Raveendran et al. (2003), who prepared silver NP using glucose and starch as reducing and capping agents, respectively. Since then, green synthesis has been employed for the development of many different metal nanomaterials, including Ag, Au, Zn, Ti, TiO_2, Fe_3O_4, Cu, Co, Pd, Ba, CdS, and Pt NP (Escárcega-González et al., 2018; Sathiyanarayanan et al., 2017).

Currently, natural materials derived from animals, plants, and microorganisms (bacteria, fungi, and algae) are under investigation to discover effective reducing and stabilizing agents for NP synthesis. In this context, polysaccharides are the most promising ecological solution due to their biocompatibility and biodegradability (C. Wang et al., 2017). These biomolecules are rich in functional groups, including hydroxyl groups and the hemiacetal reducing end, which might be essential for the reduction and stabilization of metallic particles, resulting in a great control of the synthesized NP' shape, size, and particle dispersion (Concórdio-Reis, Pereira, et al., 2020; Escárcega-González et al., 2018; Scala et al., 2019). Polysaccharides, such as xanthan (Pooja et al., 2014), dextran (Remya et al., 2016), levan (Ahmed et al., 2014; González-Garcinuño et al., 2019), chitosan (Zeng et al., 2018) and pullulan (Kanmani & Lim, 2013), have already been successfully used for this purpose. Besides stabilizing the synthesized NP, the presence of the polysaccharide can improve the biological activity of the NP (Li et al., 2019; C. Wang et al., 2017). Chitosan-stabilized SeNP exhibited a higher antidiabetic activity than other selenium compounds for the same selenium concentration (Zeng et al., 2018). Moreover, the polysaccharide can act as a carrier of the NP and a hydrophobic drug (e.g., doxorubicin, levofloxacin, or ceftriaxone) for targeted drug delivery (C. Wang et al., 2017). For example, gold NP coated with xanthan and loaded with doxorubicin demonstrated enhanced cytotoxic

activity against lung cancer cells due to xanthan functional groups (Tabernero & Cardea, 2020).

Marine habitats, given the unique environmental conditions found in the sea, which are often considered abiotic stress factors for bacteria (e.g., temperature, light intensity, pH, salinity), are considered valuable sources of novel polysaccharides with improved properties (Concórdio-Reis et al., 2021; Shen et al., 2021). Bacterial EPS secreted by marine bacteria to ensure cell adhesion and protection during unfavorable growth conditions (Rana & Upadhyay, 2020) have far more complex and diverse structures and, therefore, biological activities, than EPS produced by terrestrial microorganisms (Concórdio-Reis et al., 2021; Shen et al., 2021). These macromolecules are often characterized by interesting biological properties (anti-microbial, anti-inflammatory, antioxidant, wound healing, immunomodulatory), as well as functional properties (high viscosity, mechanical stability, ability to form films and/or gels), that support the interest in using them as advanced functionalized materials in different areas of application, including biomedicine (Concórdio-Reis, Pereira, et al., 2020; C. Wang et al., 2017).

Recently, the marine bacterium *Alteromonas macleodii* Mo 169 isolated from Moorea Island lagoon in French Polynesia was investigated as an EPS producer (Chapter 3.1). Previous studies revealed that this strain produced a high molecular weight (1.6 and 4.6 MDa) EPS (EPS A) that had a good thermal stability, interesting rheological properties, and gel and film forming capacities, supporting its use as structuring or thickening agents in wound management, tissue engineering or drug delivery (Chapter 3.1, 3.2 and 3.4). The EPS is mainly composed of glucuronic acid (GlcA, 39.3 mol%), with minor contents of mannose (Man, 12.8 mol%), glucose (Glc, 11.2 mol%), and galactose (Gal, 4.0 mol%), all (1→4)-linked (Chapter 3.4). Non-carbohydrate substituents were also detected, including sulphate, lactate and pyruvate (Chapter 3.1 and 3.4). Such high density in negatively charged functional groups (i.e., glucuronic acid, sulphate, pyruvate, and lactate) suggests a potential to reduce inorganic cations to NP and stabilize the synthesized NP (Concórdio-Reis, Pereira, et al., 2020). Thus, in this study, EPS A was evaluated for the first time as stabilizing and reducing agent in the synthesis of gold and silver nanoparticles (AuNP and AgNP, respectively). Moreover, the EPS has been shown to stabilize selenium nanoparticles (SeNP) synthesized using ascorbic acid as a reducing agent. The synthesized EPS/NP bio-nanocomposites were fully characterized in terms of their morphology, size, zeta potential, and metal content. Furthermore, aiming to explore the future application of

the obtained NP stabilized by the EPS, their safety and biological activity were assessed through *in vitro* cytotoxicity, antioxidant, and wound healing assays.

3.5.3. Materials and methods

3.5.3.1. Materials

The EPS was produced by *Alteromonas macleodii* Mo 169 (CNCM I-5374) and purified as previously described in section 3.1.3.2. Silver nitrate ($AgNO_3$) (≥99.8%), sodium selenite (Na_2SeO_3) (≥95.0%), chloroauric acid ($HAuCl_4$) (≥99.99%), and ascorbic acid were obtained from Sigma-Aldrich.

3.5.3.2. Preparation of the bio-nanocomposites

For AuNP synthesis, the procedure described by Ramos (2021) was followed. Briefly, 300 µL of a $HAuCl_4$ stock solution (20 mM) were added to 5 mL EPS solution (1 g L^{-1}, pH~5) for a final Au^{3+} concentration of 1.2 mM. The mixture was incubated at 100 ^oC for 6 h in the dark. After that period, the solution turned purple, which was indicative of the reduction of Au^{3+} to AuNP.

AgNP synthesis was performed as described by Ramos (2021). The EPS was dissolved in deionized water (1 g L^{-1}, 5 mL) and the pH was adjusted to ~9 with NaOH (0.1 M). Then, 550 µL of a stock $AgNO_3$ solution (100 mM) were added to the EPS solution for a final Ag^{2+} concentration of 11 mM. This mixture was incubated at 80 ^oC for 6 h, protected from light. The appearance of a yellowish-brown color indicated the reduction of Ag^+ into AgNP.

SeNP were synthesized according to the procedure described by Yan et al. (2018), with minor modifications. A 2 g L^{-1} EPS solution was prepared (5 mL), and the pH was adjusted to ~8 with NaOH (0.1 M). A quantity of 500 µL of a 100 mM Na_2SeO_3 stock solution was added to the EPS solution, to achieve a Se^{4+} concentration of 10 mM. After stirring, 1 mL of an ascorbic acid solution (200 mM) was mixed, and the tubes were incubated at room temperature, for 1 h, protected from the light. SeNP synthesis was indicated by the appearance of a red color.

Control samples were prepared using deionized water instead of the EPS solution. Additionally, all reactions were repeated at least three times to insure reproducibility. The formation of the NP was monitored by visual inspection of color change and confirmed by UV-visible spectra measurements (CamSpec M509T

spectrophotometer) in the wavelength range of 200–800 nm. After NP synthesis, the EPS/NP bio-nanocomposites were dialyzed using a 12 kDa MWCO (molecular weight cut off) membrane (ZelluTrans/Roth) against deionized water for 48 h. For further analysis, the purified bio-nanocomposites were maintained at 4 ºC or lyophilized.

3.5.3.3. Characterization of the bio-nanocomposites

The bio-nanocomposites' content in gold, silver, or was determined by Inductively Coupled Plasma – Atomic Emission Spectroscopy (ICP-AES) (Ultima, Horiba Jobin-Yvon, France, equipped with a 40.68 MHz RF generator, Czerny-Turner monochromator with 1.00 m (sequential) and autosampler AS500). The Zeta potential of the nanosuspensions of Ag, Au, and Se was determined using a Zetasiser Nano ZS, model ZEN (Malvern Panalytical), adopting electrophoretic cells (disposable folded hair cells, reference DTS1070). The analysis was carried out at 25 ºC and the zeta potential was calculated according to the Smoluchowski equation (Concórdio-Reis, Pereira, et al., 2020). The particle size of the bio-nanocomposites (diluted 10 times) was determined by dynamic light scattering (DLS). The analysis was performed at 25 ºC using a Photocor equipment (helium-neon laser, 633 nm, 20 mW, 90 ºC) and a Brookhaven BI9000 autocorrelator. All measurements were performed at least three times and the raw data was analyzed with Dynals Software (SoftScientific, Israel). The morphology and size distribution of the synthesized NP were determined by transmission electron microscopy (TEM) (JEM 1400, JEOL Europe, Belgium), as described by Concórdio-Reis, Pereira, et al. (2020). FTIR were performed as described in section 2.2.3.6. To determine the phase composition and crystalline structure of the NP, X-ray diffraction (XRD) analysis was performed using a benchtop MiniFlex II X-ray diffractometer from Rigaku (Tokyo, Japan) with a Cu X-ray tube (30KV/15 mA). The 2Θ scans were performed from 5º to 60º, with a step size of 0.01°.

3.5.3.4. Biological assays

Cytotoxicity assays

Cytotoxicity assays of the EPS and the NP/EPS bio-nanocomposites were performed as previously described in section 2.2.3.7.

Wound healing assays

Wound healing assays were performed as previously described by Concórdio-Reis, Pereira, et al. (2020). HaCaT cells were seeded at a density of 1.0×10^5 cell cm^{-2} in a 12-well plate and let to grow until 100% confluence (48 hours). A wound was created with a 200 µL pipette tip and each well was washed twice with warm Phosphate-buffered saline (PBS) to remove non-adherent cells. Then, the cells were incubated with the EPS and the EPS/NP bio-nanocomposites diluted in culture medium with 0.5% FBS (100 and 500 $mg_{EPS}.L^{-1}$) for 24 hours. Cells incubated with only culture medium with 0.5% FBS were included as negative control, while cells incubated with culture medium supplemented with high concentration of FBS (10%) were used as positive control. Photos of the same scratch region were taken with an inverted phase contrast microscope (Olympus CKX41, Japan) at two different time points: before and 24 hours after the addition of the samples. The wound area was measured using the ImageJ 1.47v software (USA) as the distance between borderlines. The wound area recovered was calculated following the equation:

$$\text{Wound area recovered} = \frac{(\text{Inital area})-(\text{Final area})}{\text{Initial area}} \times 100 \qquad (3.5.1)$$

Cellular antioxidant activity

Cellular antioxidant assays of the EPS and the NP/EPS bio-nanocomposites were performed as previously described in section 2.2.3.7.

3.5.3.5. Data analysis

Three independent experiments were performed in at least duplicate experiments, and the results were expressed in terms of mean ± SD (standard deviation). The statistical analysis was performed by Student's *t*-test and differences resulting in $p < 0.05$ were considered statistically significant. For the particle size determination, the equivalent diameter of at least 300 NP was determined from TEM micrographs and, from the cumulative size distributions established in number, the corresponding percentiles were determined: 10, 50, 90 and 99.

3.5.4. Results and Discussion

3.5.4.1. NP synthesis

Due to the high content in negatively charged functional groups, the EPS produced by the marine bacterium *A. macleodii* Mo169 was explored as a reductant and stabilizer for the green synthesis of NP.

AuNP

The EPS-mediated production of AuNP was visually observed by the solution's color change from colorless to purple, as depicted in Fig. 3.5.1 A. Considering the control experiments where no EPS was added, no color alteration was detected (Fig. 3.5.1 A). Upon UV-vis analysis of the EPS containing solution, the typical surface plasmon resonance (SPR) absorption band of AuNP was detected at 544 nm (Fig. 3.5.1 A). Similar observations were made for the AuNP prepared with levan (530–539 nm) (Ahmed et al., 2014), *Lactobacillus plantarum* EPS (525 nm) (Pradeepa et al., 2016), κ-carrageenan, (556 nm) (Marques et al., 2019), and two thermophilic marine bacteria EPS (538 and 565 nm) (Scala et al., 2019). Nonetheless, red AuNP solutions were obtained with *Bacillus megaterium* MSBN04 EPS (560 nm) (Sathiyanarayanan et al., 2014), xanthan (525 nm) (Pooja et al., 2014), chitosan (522 nm) (Huang & Yang, 2004) and carrageenan oligosaccharide derived from marine red algae (530 nm) (Chen et al., 2018). These differences in color and band wavelength might be related with differences on the AuNP synthesis protocol that have probably impacted the synthesized AuNP characteristics (size and shape) and, consequently, their UV-vis spectra (Marques et al., 2019). For example, the colloidal solutions of the AuNP synthesized with the polysaccharide gum acacia had different color depending on the gum concentrations used (0.25–3%). Also, the synthesized AuNP presented different particle sizes and zeta potential values (Devi et al., 2020). Similarly, the AuNP solutions prepared with liquid modified apple polysaccharide displayed a different color depending on the polysaccharide concentration: low concentrations (0.5%) originated light blue solutions, whereas the highest concentration (5%) tested was ruby red. Although the spectra obtained with the different concentrations had absorption peaks at similar wavelengths, the absorbance increased as the polysaccharide concentration increased, indicating a higher reduction of $HAuCl_4$ into AuNP (Kumari et al., 2020).

AgNP

AgNP formation was noticed by the change of the solution's appearance from colorless to a yellowish-brown color (Fig. 3.5.1 B) (Chen et al., 2016; Concórdio-Reis, Pereira, et al., 2020; Saravanan et al., 2017; Sivasankar et al., 2018). The effective AgNP synthesis was confirmed by the the UV-visible absorption spectra (Fig. 3.5.1 B), wherein the SPR band characteristic of AgNP formation could be detected at 430 nm (Anjugam et al., 2018; Chen et al., 2016; Concórdio-Reis, Pereira, et al., 2020; Manivasagan et al., 2015; Navarro Gallón et al., 2019; Saravanan et al., 2017).

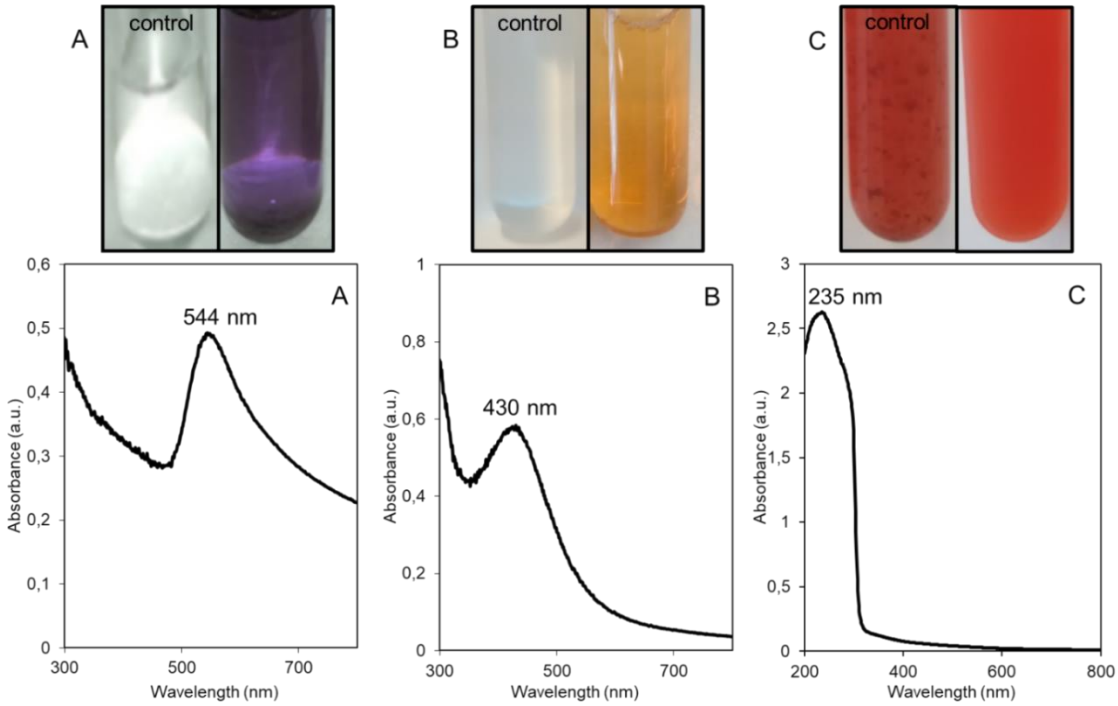

Figure 3.5.1. Digital photography (top) and corresponding UV-vis absorption spectra (bottom) of the EPS/NP bio-nanocomposites with AuNP (A), AgNP (B), SeNP (C).

SeNP

For SeNP synthesis, ascorbic acid was added into the mixture as a reducing agent and the EPS was investigated for the stabilization of the SeNP. Ascorbic acid was previously used as reducing agent in the synthesis of SeNP stabilized by *C. sinensis* fungus Cs-HK1 EPS (Xiao et al., 2017), carboxylic curdlans (Yan et al., 2018), β-D-glucan (Cai et al., 2018), chitosan (Zeng et al., 2018), arabinogalactans (Tang et al., 2019), lectinan (Jia et al., 2015), gum arabic (Kong et al., 2014), pectin (Qiu et al., 2018), and by the polysaccharides of *Gracilaria lemaneiformis* (Tang et al., 2021), *Grateloupia Livida* (Cao et al., 2021), *Oudemansiella raphanipies* (Jiang et al., 2022), *Lycium barbarum* (Liu et al., 2021), and *Catathelasma ventricosum* (Y. Liu et al., 2018). Within 1 h of incubation at room temperature with 10 mM of Se^{4+}, the solution's color changed from colorless to light yellow and, finally, to red (Fig. 3.5.1 C), indicating the

formation of amorphous or monoclinic SeNP (Liu et al., 2021; Tang et al., 2019; Xiao et al., 2017; Yan et al., 2018). This alteration in color may be ascribed to the excitation of SPR of SeNP, resulting in the SPR band observed in the UV-vis spectra of SeNP (235 nm) (Fig. 3.5.1 C). The SeNP synthesized by other polysaccharides presented a SPR band at a slightly higher wavelength (260–273 nm) (Cai et al., 2018; Liu et al., 2021; Qiu et al., 2018; Tang et al., 2021; Yan et al., 2018). Nonetheless, differences on the absorption peak were reported when the synthesis conditions were altered (Tang et al., 2019; Xiao et al., 2017), and might be related with differences in SeNP' crystallinity and particle size (Tang et al., 2019).

Although the control experiment without the addition of EPS also changed color to red, the presence of precipitates was noticed (Fig. 3.5.1 C). Similarly, previous studies reported the formation of brown/black aggregates that precipitated after Se^{4+} incubation with ascorbic acid in the absence of the stabilizer agent (Liu et al., 2021; Tang et al., 2019; Xiao et al., 2017; Yan et al., 2018). The authors suggested that this effect could be due to the high surface energy of SeNP that resulted in their aggregation and precipitation (Liu et al., 2021; Xiao et al., 2017; Yan et al., 2018). These results suggest that the addition of the EPS was essential for the synthesis of stable and well dispersed SeNP since NP synthesis occurred in the polysaccharide's molecular microenvironment. Natural polysaccharides, such as EPS A, act as soft templates to stabilize the SeNP by controlling the crystal nucleation and growth processes (Li et al., 2019). Moreover, the functional groups of the polysaccharide would facilitate the interaction of the SeNP with the target cells and their lipidic barriers (Li et al., 2019).

3.5.4.2. Characterization of NP

Composition

After purification by dialysis, the EPS/AuNP bio-nanocomposite had a gold content of 26.4 mg L^{-1}. The presence of gold in the form of NP was confirmed by XRD that showed two Bragg peaks characteristic of metallic gold at 38.3º and 44.5º in the 2θ region (Fig. 3.5.2 B), matching the (111) and (200) planes of face-centered cubic crystal (fcc) structure (Alle et al., 2020; Chen et al., 2018; Sathiyanarayanan et al., 2014). The highest intensity detected for the crystallographic (111) plane indicates the preferable growth direction of the AuNP (Alle et al., 2020; Sathiyanarayanan et al., 2014). Similarly, the diffractogram of the EPS/AgNP bio-nanocomposite (Fig. 3.5.2 C) exhibited two peaks (38.3º and 44.6º) that appear due to the presence of the face-

centered cubic (fcc) structure of silver nanocrystals (Concórdio-Reis, Reis, et al., 2020; Manivasagan et al., 2015; Sivasankar et al., 2018; Zhang et al., 2018). These features indicate that the 11.8 mg L^{-1} silver detected on the purified bio-nanocomposite were present as AgNP, also predominantly orientated to plane (111) (Concórdio-Reis, Pereira, et al., 2020). Moreover, the diffractogram of the EPS/SeNP bio-nanocomposite, which contained 183.8 mg L^{-1} of selenium, did not present the typical Bragg peaks of crystalline Se. These results suggest that the SeNP in the polysaccharide matrix did not transform into crystalline phase and remained in amorphous (Qiu et al., 2018; Tang et al., 2021). Similar results were observed in previous reports (Cai et al., 2018; Cao et al., 2021; Jia et al., 2015; Jiang et al., 2022; Qiu et al., 2018; Tang et al., 2021; Yan et al., 2018). A large band at about 20º was detected in all diffractograms (Fig. 3.5.2), including for EPS A, which can be attributed to the polysaccharide's amorphous nature.

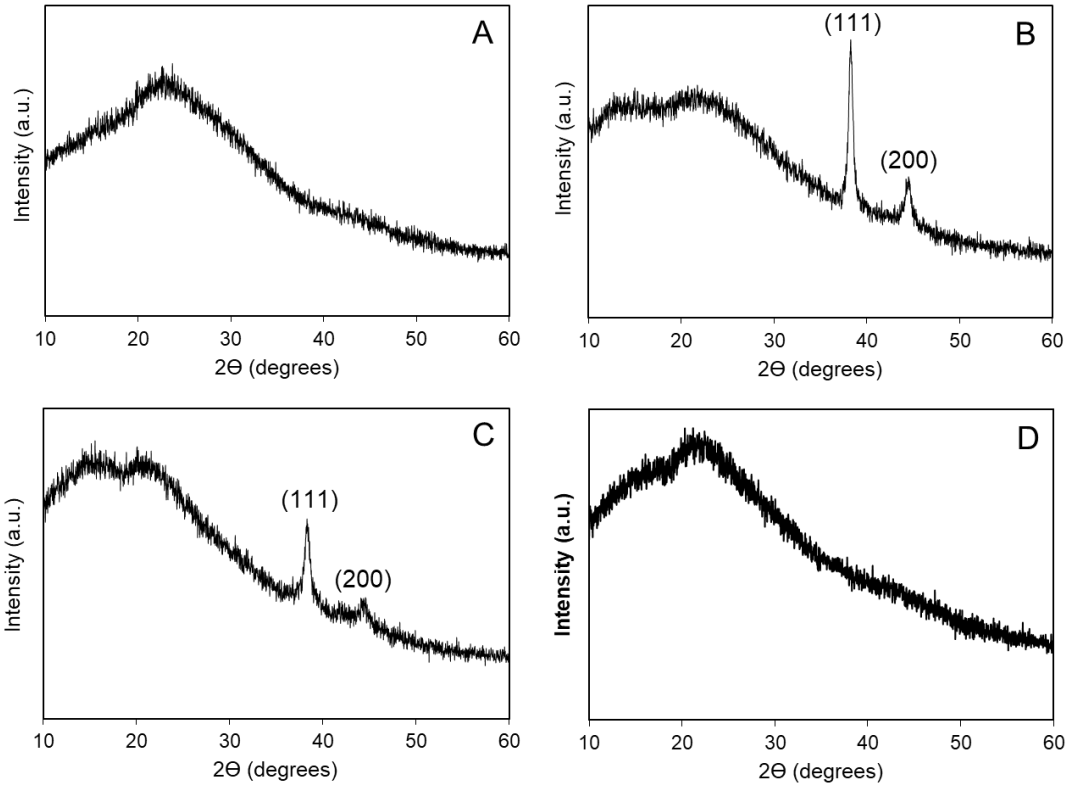

Figure 3.5.2. Diffractograms of EPS A (A) and its bio-nanocomposites with AuNP (B), Ag/NP (C) and SeNP (D).

Colloidal stability

Zeta potential measurements were performed to confirm the colloidal stability of the synthesized NP. According to the DVLO theory, stable particles present values higher than ± 25 mV (Concórdio-Reis, Pereira, et al., 2020), which seemed to be the

case of the EPS/AuNP bio-nanocomposite (-42.37±1.27 mV). The values found for the bio-nanocomposites indicate that the interactions between the NP are weak and, therefore, the chance of aggregation is negligible, suggesting that the particles are stable and well dispersed (Singh, Sran, et al., 2019). Similar values were obtained for AuNP synthesized and stabilized with xanthan gum (-42.2 mV) (Pooja et al., 2014), with carboxymethyl xanthan gum (-49.3 mV) (Alle et al., 2020), and with *L. plantarum* EPS (-41 mV) (Pradeepa et al., 2016). Lower values were obtained for the AuNP-capped with apple polysaccharide (-18.8 mV) (Kumari et al., 2020), *B. megaterium* MSBN04 EPS (-29.1 mV) (Sathiyanarayanan et al., 2014), levan (-13.9 to -22.1 mV) (Akturk, 2020), gum acacia (-29.4 mV) (Devi et al., 2020), and carrageenan oligosaccharide (-20 mV) (Chen et al., 2018). The high negative zeta potential value of the AuNP produced with EPS A, not only demonstrated the stability of the AuNP, but also the surface's high negative charge, which might be beneficial for the delivery of positively charged drugs (Pradeepa et al., 2016).

The value (-42.00±1.18 mV) obtained for the EPS/AgNP bio-nanocomposite was also indicative of the AgNP stability. Similarly, negative values were reported for AgNP synthesized with the EPS of *Bacillus licheniformis* strain B3-15 (-32.6 nm) (Scala et al., 2019), *Bacillus licheniformis* T14 (-20.2 mV) (Scala et al., 2019), *Enterobacter* A47 (-33.5 to -44.3 mV) (Concórdio-Reis, Pereira, et al., 2020), and *Bacillus subtilis* (-21 to -35 mV) (Selvakumar et al., 2014), *B. braunii* (-51.81 mV) (Navarro Gallón et al., 2019) and *C. pyrenoidosa* (-12.16 mV) (Navarro Gallón et al., 2019).

The EPS/SeNP bio-nanocomposite also presented a negative zeta potential (-46.43±1.36 mV), consistent with that found for the bio-nanocomposites with AuNP and AgNP, and with the values found in literature for polysaccharide-stabilized SeNP, namely polysaccharides from *G. lemaneiformis* (-47.1 mV) (Tang et al., 2021) and *G. Livida* (-46.77 mV) (Cao et al., 2021). Lower values were reported for SeNP prepared with carboxylic curdlans (-17 to -28 mV) (Yan et al., 2018), *O. raphanipies* polysaccharide (-14.1 mV) (Jiang et al., 2022), and *L. barbarum* polysaccharides (-37 mV) (Liu et al., 2021), which might be related with differences in composition (e.g., content in uronic acids) and molecular weight between polysaccharides (Liu et al., 2021; Yan et al., 2018). Nonetheless, all the EPS/NP bio-nanocomposites prepared with EPS A presented high negative zeta potential values, which indicated the high stability of the monodispersed NP.

NP morphology

Representative TEM micrographs of the purified EPS/NP bio-nanocomposites are shown in Fig. 3.5.3. The NP prepared with EPS A were dominantly spherical and mostly individual particles were noticed in all the micrographs. Nonetheless, some of the AuNP (Fig. 3.5.3 A) and AgNP (Fig. 3.5.3 B) seemed to appear in small clusters surrounded by a larger faint layer that can be assigned to the EPS. In the EPS/SeNP bio-nanocomposite sample, the EPS can be observed as a fainted sphere-like layer with smaller dimensions (Fig. 3.5.3 C, insert). A polysaccharide layer coating the NP was also observed in previous studies found in literature, and can be the main mechanism responsible for the stabilization of the NP (Chen et al., 2018; Concórdio-Reis, Pereira, et al., 2020; Sathiyanarayanan et al., 2014; Scala et al., 2019), and suggests that the EPS coating is mainly responsible for the stabilization of the NP (Sathiyanarayanan et al., 2014).

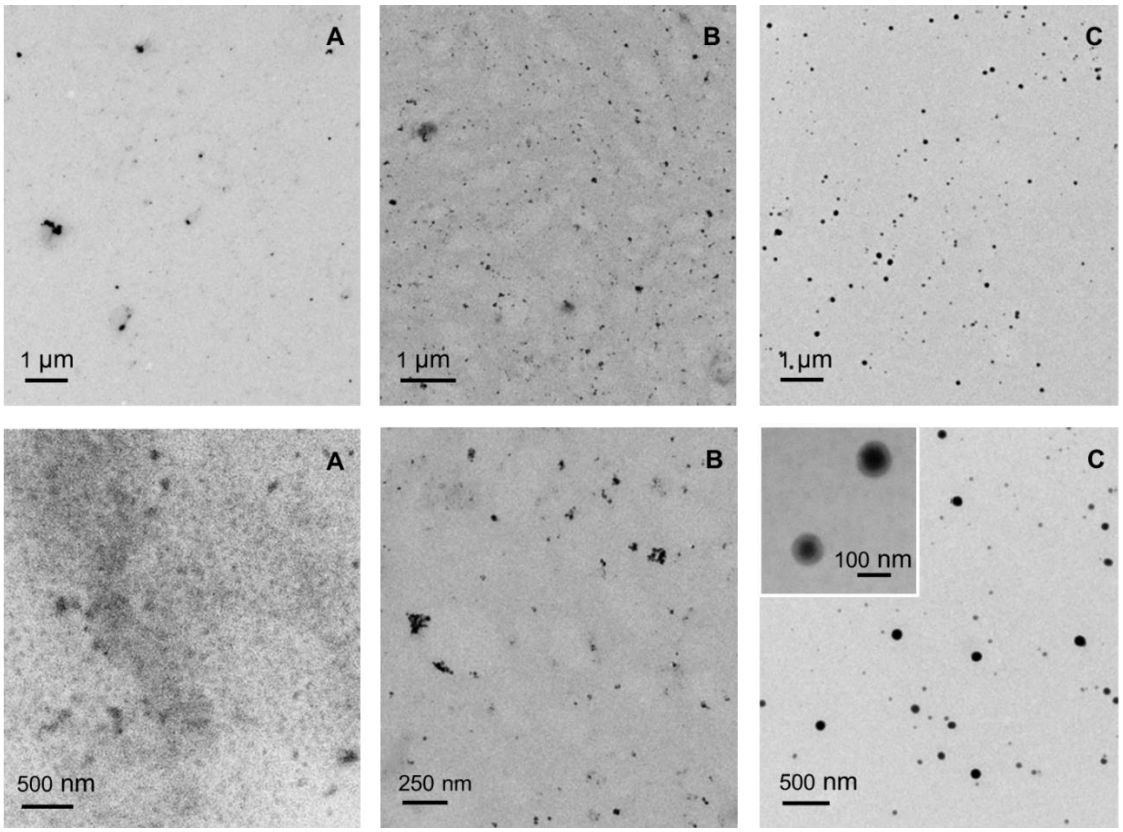

Figure 3.5.3. TEM images of the EPS/NP bio-nanocomposite suspensions with AuNP (A), AgNP (B), SeNP (C).

NP and EPS/NP bio-nanocomposite's size

As presented in Fig. 3.5.4, the particle size distribution was quite homogenous for all the NP, though SeNP seemed to be more polydisperse in size, with a broader size distribution. In fact, SeNP ranged from 22 to 76 nm for percentile 50 and 90, respectively, whereas AuNP and AgNP presented a size variation of 8 to 33 nm, and 11 to 28 nm, respectively, for the same percentiles. Also, the average particle size of the SeNP (32 nm) was higher to those found for the synthesized AuNP and AgNP (16 and 15 nm, respectively). These particle sizes fall within the ranges reported in literature for NP stabilized by other polysaccharides, as presented in Table 3.5.1.

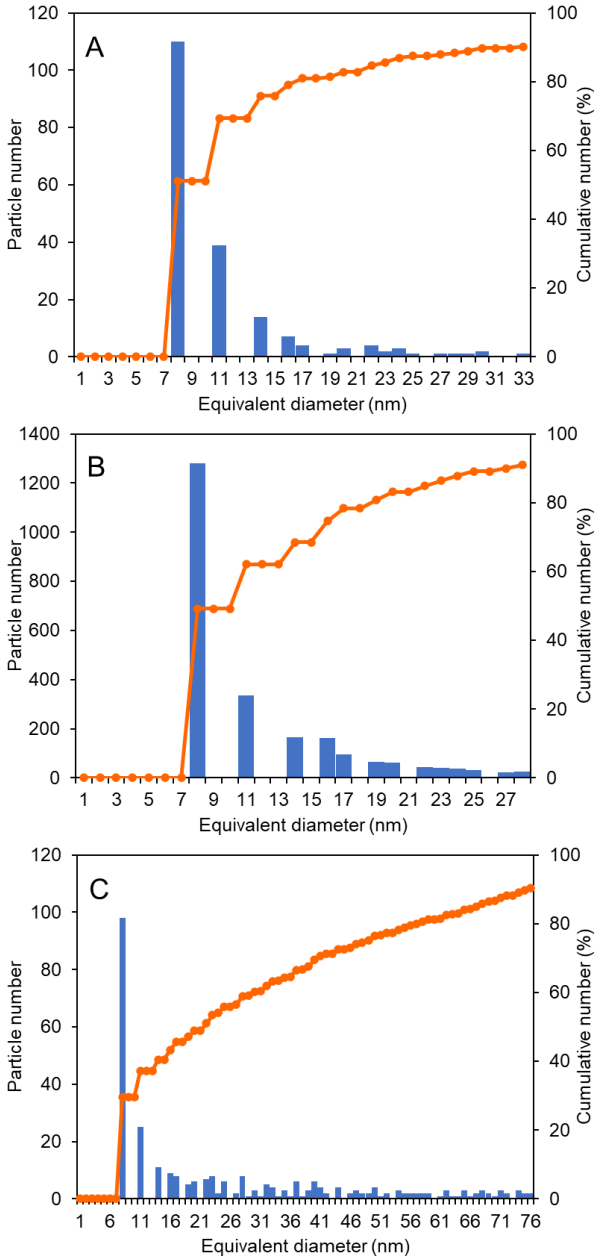

Figure 3.5.4. Histogram of the particles size distribution, particle number (bar) and cumulative number (line), of the AuNP (A), AgNP (B), and SeNP (C) prepared with the EPS produced by EPS A obtained by TEM.

The differences in terms of particle size are probably related with both the polysaccharides' physical and chemical properties (composition, molecular weight, viscosity in aqueous medium), as well as the synthesis parameters (pH, temperature, time, metal concentration, reducing agent concentration) used in each study (Concórdio-Reis, Pereira, et al., 2020; Tang et al., 2019; Xiao et al., 2017; Yan et al., 2018).

Table 3.5.1. Particle size of the NP (determined by TEM analysis) and their polysaccharide-based bio-nanocomposites (determined by DLS) (PS, polysaccharide; n.a., not available).

Polysaccharide	Size (nm)		Reference
	TEM	DLS	
AuNP			
EPS A	8–33/16	468	This study
B. megaterium MSBN04 EPS	5–20/10	n.a.	Sathiyanarayanan et al. (2014)
L. plantarum EPS	10–20	n.a.	Li et al. (2017); Pradeepa et al. (2016)
Natronotalea sambharensis sp. nov *EPS*	n.a.	55	Singh, Sran, et al. (2019)
Acacia gum	n.a.	96	Devi et al. (2020)
Carboxymethyl xanthan gum	8–10	n.a.	Alle et al. (2020)
Carrageenan oligosaccharide	35	n.a.	Chen et al. (2018)
Chitosan	7–20	n.a.	Huang & Yang (2004)
Dextran	13	n.a.	Medhat et al. (2017)
Gellan gum	13	n.a.	Dhar et al. (2008)
levan	n.a.	95–142	Akturk (2020)
xanthan gum	15–20	41.2	Pooja et al. (2014)
AgNP			
EPS A	11–28/15	191	This study
Arthrobacter sp. B4 EPS	9–72	n.a.	Yumei et al. (2017)
Bacillus licheniformis T14 EPS	40	170	Scala et al. (2019)
B. braunii EPS	13.8	n.a.	Navarro Gallón et al. (2019)
Bradyrhizobium japonicum 36 EPS	5–50	n.a.	Rasulov et al. (2015)
C. pyrenoidosa EPS	9.2	n.a.	Navarro Gallón et al. (2019)
C. sinensis Cs-HK1 EPS	40	450	Chen et al. (2016)
Enterobacter A47 EPS	13–30/17	n.a.	Concórdio-Reis, Pereira, et al. (2020)
Lactobacillus rhamnosus EPS	2–50	n.a.	Kanmani & Lim (2013)
Leuconostoc lactis EPS	30–200/35	n.a.	Saravanan et al. (2017)
L. plantarum EPS-605	20	n.a.	Li et al. (2017)

Table 3.5.1. Particle size of the NP (determined by TEM analysis) and their polysaccharide-based bio-nanocomposites (determined by DLS) (PS, polysaccharide; n.a., not available).

Polysaccharide	Size (nm)		Reference
	TEM	DLS	
Streptomyces sp. EPS	10–60/35	n.a.	Manivasagan et al. (2015)
Heparin	9–28	n.a.	Huang & Yang (2004)
Levan	19.47	n.a.	Zhang et al. (2018)
SeNP			
EPS A	22–76/32	297	This study
C. sinensis Cs-HK1 EPS	50	n.a.	Xiao et al. (2017)
G. lemaneiformis PS	83.6	93–138	Tang et al. (2021)
G. Livida PS	100	115	Cao et al. (2021)
Larix principis-rupprechtii PS	n.a.	94–173	Tang et al. (2019)
L. barbarum PS	n.a.	105	Liu et al. (2021)
O. raphanipies PS	60	n.a.	Jiang et al. (2022)
Carboxylic curdlan	56–65	118–243	Yan et al. (2018)
Gum arabic	34.9	145–170	Kong et al. (2014)
Lectinan	33–52	100	Jia et al. (2015)
Pectin	41	n.a.	Qiu et al. (2018)

The mean hydrodynamic diameter of the colloidal NP coated by the EPS was determined by DLS (Fig. 3.5.5). Interestingly, the EPS/AuNP bio-nanocomposite was found to have the highest diameter (468±27 nm), followed by the bio-nanocomposite prepared with SeNP (297±4 nm) and, finally, the EPS/AgNP bio-nanocomposite (191±15 nm). Additionally, a significant difference between the particle size determined by DLS and by TEM was found for all the bio-nanocomposites, which was also reported previously for other polysaccharides (Akturk, 2020; Cao et al., 2021; Chen et al., 2016, 2018; Pooja et al., 2014; Scala et al., 2019; Tang et al., 2021; Xiao et al., 2017). Such discrepancies might be explained by the differences in the detection method and the conditioning of the samples in each technique (Akturk, 2020). Moreover, the hydrodynamic diameter includes the hydration layer and polymer coating, resulting, therefore, in larger values (Cao et al., 2021; Scala et al., 2019; Yan et al., 2018). Additionally, interaction forces that occur in solution (e.g., Van der Waals forces) might contribute to the larger size observed with DLS (Chen et al., 2018).

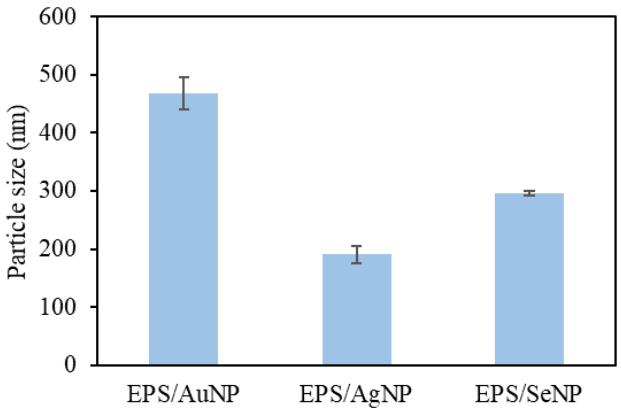

Figure 3.5.5. Hydrodynamic diameter of the EPS/NP bio-nanocomposites by DLS.

Compared with previous reports (Table 3.5.1), the EPS/AuNP bio-nanocomposite hydrodynamic diameter (468±27 nm) was much higher than those reported for AuNP bio-nanocomposites prepared with xanthan gum (41.2 nm) (Pooja et al., 2014), levan (95–142 nm) (Akturk, 2020), acacia gum (96 nm) (Devi et al., 2020), and with the EPS produced by marine bacterium *Natronotalea sambharensis* sp. nov. (55 nm), an EPS was composed of mannose, glucose, and glucuronic acid (Singh, Sran, et al., 2019). On the contrary, the EPS/AgNP bio-nanocomposite had a hydrodynamic diameter (191±15 nm) similar to that observed for the EPS composed of glucose and mannose synthesized by *Bacillus licheniformis* strain B3-15 (170 nm) (Scala et al., 2019); and lower to that of the bio-nanocomposite prepared with *C. sinensis* Cs-HK1 EPS (450 nm), which was a glucan with glucose side chains and about 27% (w/w) galactomannan-protein complexes (Chen et al., 2016). SeNP prepared with different polysaccharides have a wide range of sizes, which might be related to the viscosity and/or molecular weight (M_w) differences between the polysaccharides used (Tang et al., 2019). In this study, the SeNP stabilized by EPS A presented a higher value (297±4 nm) compared with those reported in literature. As examples, those prepared with the galactose-rich polysaccharides of *G. lemaneiformis* (92.5–137.7 nm) (Tang et al., 2021) and *G. Livida* (115.4 nm) (Cao et al., 2021), *Larix principis-rupprechtii* arabinogalactans (94.24–173.2 nm) (Tang et al., 2019), lectinan (100 nm) (Jia et al., 2015), gum arabic (145–170 nm) (Kong et al., 2014), and the *L. barbarum* polysaccharide composed of arabinose, xylose, glucose, and galactose (105.4 nm) (Liu et al., 2021). Interestingly, all these polysaccharides presented a lower Mw (0.092–18.4 kDa) than that found for EPS A (1.6 and 4.6 MDa) (Concórdio-Reis et al., 2021). The closest value was found for SeNP prepared with carboxilic curdlan Cur-4 with a Mw of 0.57 MDa (243.4 nm) (Yan et al., 2018), suggesting that the large Mw

found for EPS A could cause the larger particle size of the EPS/SeNP bio-nanocomposite.

EPS-NP interaction

FTIR analysis was carried out to investigate the interactions between the surface functional groups of EPS A and the NP. The shape and intensity of the broad band found between 3000–3500 cm^{-1}, corresponding to the stretching frequencies of hydroxyl groups (O-H) (Chen et al., 2018; Concórdio-Reis et al., 2021; Tang et al., 2019), was altered in all bio-nanocomposites (Fig. 3.5.6 B–D) compared with the EPS sample (Fig. 3.5.6 A). A shift of this band to higher wavenumbers (3281–3354 cm^{-1}) was noticed for the bio-nanocomposites compared with the EPS (3260 cm^{-1}). Significant alterations were also found in the adsorption region characteristic of the C=O asymmetric (1596 cm^{-1}) and symmetric (1300–1450 cm^{-1}) stretching vibrations of the carboxylates from the uronic acids (Concórdio-Reis et al., 2021; Navarro Gallón et al., 2019), which are indicative of the interaction between these groups of the EPS macromolecule and the NP. Alterations on the intensity of the band at 1237 cm^{-1} (Fig. 3.5.6 A), were found for all the bio-nanocomposites (Fig. 3.5.6 B–D), especially on the EPS/SeNP bio-nanocomposite spectrum (Fig. 3.5.6 D). This band was attributed to the stretching vibration of C-O-C from acyls, and/or of S=O from sulphate groups (Chen et al., 2018; Concórdio-Reis et al., 2021), suggesting the importance of these groups on the stabilization of the NP. Also, alterations were noticed on the absorption bands found at ~1720 cm^{-1} and in the frequency range of 900–1200 cm^{-1} that can be assigned the C=O stretching of the acyl substituents (Concórdio-Reis, Pereira, et al., 2020) and to C-O and C-C vibrations of the glycosidic bonds and pyranose carbohydrate ring (Akturk, 2020; Concórdio-Reis et al., 2021). These results suggest that the interaction of the EPS with the NP could be mainly attributed to the hydroxyl, carboxylate, and sulphate groups of the biopolymer.

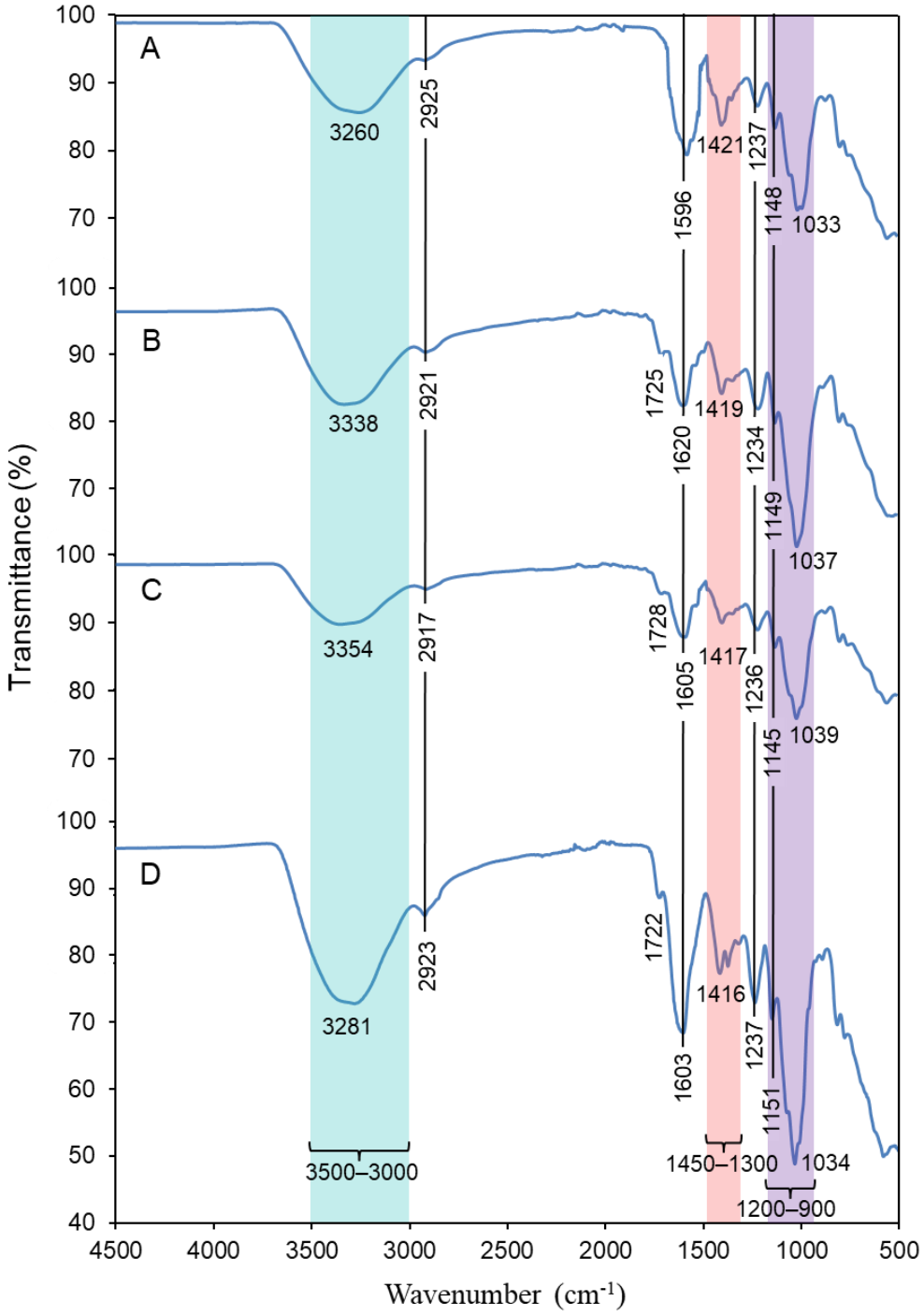

Figure 3.5.6. FTIR spectra of purified EPS A (A), and its bio-nanocomposites with AuNP (B), AgNP (C), and SeNP (D).

Similar results were found in literature for other polysaccharide/NP bio-nanocomposites. The OH and COO^- functional groups were found to be involved in the reduction and stabilization of AuNP by carboxymethyl xanthan gum (Alle et al., 2020), and of AgNP by *Enterobacter* A47 EPS (Concórdio-Reis, Pereira, et al., 2020), *Arthrobacter* sp. B4 EPS (Yumei et al., 2017), *B. braunii* EPS (Navarro Gallón et al.,

2019), *C. pyrenoidosa* EPS (Navarro Gallón et al., 2019), and by *Bacillus subtilis* EPS (Selvakumar et al., 2014). For the carrageenan oligosaccharide, the functional groups OH and SO^{3-} were apparently responsible for the reduction of Au^{3+} and the stabilization of the AuNP (Chen et al., 2018). FTIR analysis of levan indicated that the hydroxyl groups and the (C-O-C) glycosidic bonds shifted due to the possible interaction with AgNP/AuNP (Ahmed et al., 2014; Akturk, 2020). The capping and stabilization of AuNP by *B. megaterium* MSBN04 EPS seemed to be related with the carboxyl, hydroxyl and methoxyl groups of the EPS (Sathiyanarayanan et al., 2014). SeNP aggregation seemed to be avoided through the interactions between the NP and the hydroxyl groups of the polysaccharide. This interaction was previously reported for SeNP prepared with lectinan (Jia et al., 2015), arabinogalactan (Tang et al., 2019), pectin (Qiu et al., 2018), gum arabic (Kong et al., 2014), curdlan (Yan et al., 2018), and *C. sinensis* EPS (Xiao et al., 2017), *L. barbarum* (Liu et al., 2021) and *L. rhinocerotis* (Cai et al., 2018) polysaccharides. In addition to the hydroxyl groups, the imino groups of *G. Livida* and *G. lemaneiformis* polysaccharides also seemed to be involved in SeNP stabilizarion (Cao et al., 2021; Tang et al., 2021).

3.5.4.3. Biological assays

Assessment of cytotoxicity

Considering the potential of presently synthesized NP in the biomedical applications, their *in vitro* biocompatibility was investigated on human skin cell lines, namely CCD-1079Sk fibroblasts (Fig. 3.5.7 A) and HaCaT keratinocytes (Fig. 3.5.7 B). Cytotoxic effect was considered when cell viability decreased below 70% as according to ISO 10993-5. As presented in Fig. 3.5.7, the maximum EPS and EPS/NP bio-nanocomposite concentration tested was 1000 mg L^{-1} due to the limitation of solvent application at the assay, a consequence of EPS A high viscosity (Concórdio-Reis et al., 2021). Results showed that the EPS alone did not induce any cytotoxic effects on either cell line within the concentration range tested (Fig. 3.5.7). Also, no cytotoxicity was found for the EPS/AuNP and EPS/AgNP bio-nanocomposites, even at NP concentrations up to 26.4 and 11.8 mg L^{-1}, respectively. These results are in line with cytotoxicity data reported previously. Although at lower concentrations (500 $mg_{bio\text{-}nanocomposite}$ L^{-1}, 2.76 mg_{Ag} L^{-1}), similar results were found for the Fucopol/AgNP bio-nanocomposite, that did not present any cytotoxic effect towards HaCaT keratinocytes (Concórdio-Reis, Pereira, et al., 2020). Moreover, RAW 264.7 macrophages had a cell viability higher above 75% for levan coated AgNP (19.47 nm) at a concentration of 20

mg L^{-1} (Zhang et al., 2018). AuNP, 8–10 nm-sized, prepared with the same polymer exhibit cytotoxicity towards L-929 mouse fibroblasts only at the highest concentration tested (1000 mg L^{-1}) (Akturk, 2020). Cell viability of human dermal fibroblasts was only slightly affected by the EPS/AgNP bio-nanocomposite prepared with *C. pyrenoidosa* EPS at the highest concentration tested (40 mg L^{-1}). On the contrary, the AgNP stabilized with the *B. braunii* EPS did not affect cell viability (0.5–40 mg L^{-1}), leading the authors to suggest that these differences might be due to the larger size of the former (9.2 and 13.8 nm, respectively) (Navarro Gallón et al., 2019). Not only the cytotoxicity of NP is dependent on size, but also the shape, surface coating, and synthesis route could impact the safety of the bio-nanocomposites (Navarro Gallón et al., 2019). Moreover, the NP content of the EPS/NP bio-nanocomposite, which is often not quantified, can be responsible for these differences on cytotoxicity.

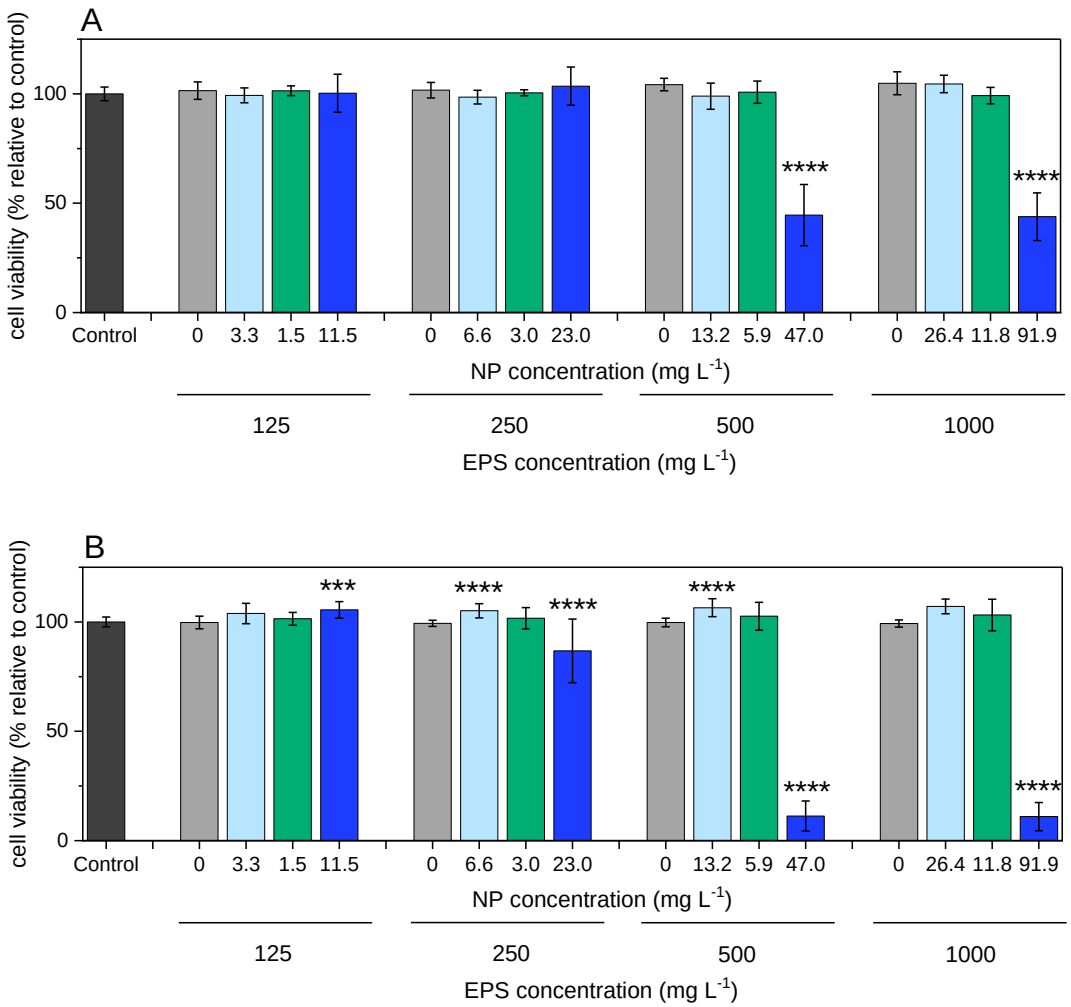

Figure 3.5.7. Cytotoxicity effect of EPS A (□), and its bio-nanocomposites with AuNP (□), AgNP (□), and SeNP (□) on CCD-10795k (A) and HaCaT (B) cell lines after 24 h incubation. Statistically significant differences comparing samples with the control were calculated according to t-test (***, p≤0.001, **** p≤0.0001).

Interestingly, the presence of the AuNP bio-nanocomposite slightly increased ($p<0.05$) HaCaT cell viability at concentrations above 250 $mg_{bio\text{-}nanocomposite}$ L^{-1}, that corresponded to a NP concentration of 6.6 mg_{Au} L^{-1} (Fig, 3.5.7 B). Lu et al. (2010) also found that the incubation of keratinocytes in the presence of low concentrations of chemically synthesized AuNP (5 mg L^{-1}) promoted a faster surface cell adhesion, high proliferation rates and significantly higher cell viability. However, in that study, AuNP concentrations above 10 mg L^{-1} were toxic to the cells (Lu et al., 2010), which was not observed in our findings. Also, no significant statistical difference was found on keratinocytes proliferation when different-sized AuNP were used (16, 24, 31, 42 and 51 nm) (Lu et al., 2010). This AuNP size range was slightly higher compared to our study (8 to 33 nm for percentile 50 and 90, and average size 16 nm). Nonetheless, there is a strong possibility that the EPS coating might contribute to the positive effect of AuNP on keratinocytes viability, suggesting the potential of the EPS/AuNP bio-nanocomposite to be used as a biomedical material in skin regeneration.

Regarding the cell viability of cells exposed to the EPS/SeNP bio-nanocomposite, concentrations of 500 mg L^{-1} (containing 47 mg_{Se} L^{-1}) caused a reduction on CCD-1079Sk and HaCaT cell viability superior to 55% (Fig. 3.5.7 B) and 89% (Fig. 3.5.7 B), respectively. Nonetheless, in the presence of 250 mg L^{-1} of EPS/SeNP bio-nanocomposite (23 mg_{Se} L^{-1}), no cytotoxic effect was considered since cell viability of both cell lines exceeded 87% (Fig. 3.5.7). A cytotoxic effect was considered when cell viability decreased below 70% as according to ISO 10993-5. Similar results were found for SeNP (83.6 nm) coated with *G. lemaneiformis* polysaccharides, where RAW 264.7 cells viability was maintained above 77% for concentrations up to 20 mg_{Se} L^{-1} (Tang et al., 2021). Moreover, RWPE-1 cells maintained their viability in the presence of 400 mg L^{-1} of pectin-coated SeNP (Qiu et al., 2018), a concentration superior to that found in this study (250 mg L^{-1}). In addition to the differences in cell lines' sensitivity towards metals (Concórdio-Reis, Pereira, et al., 2020), the size of those SeNP was superior (41 nm, compared with 32 nm for EPS A), and the content in Se of the bio-nanocomposite might also be different, resulting in the differences observed.

Evaluation of wound healing ability

Wound healing ability was investigated by assessing cell migration 24 h post scratch in the presence of EPS A and the EPS/NP bio-nanocomposites (Fig. 3.5.8). The wound healing ability was assessed through visual observation of the cells (Fig.

3.5.9) and the wound area recovered was calculated based on image measurements determined using Image J software.

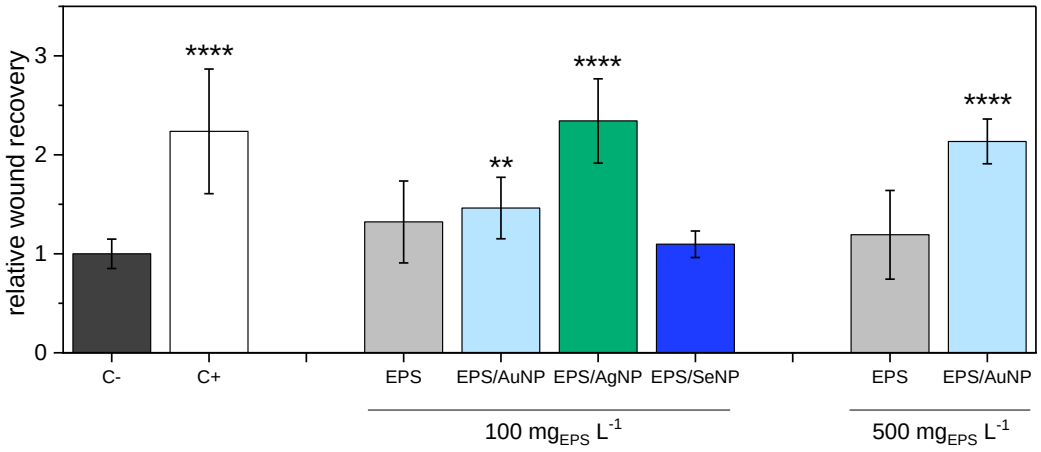

Figure 3.5.8. Wound healing assay. Migration assessment of HaCaT cells after treatment with EPS A (□), and its bio-nanocomposites with AuNP (□), AgNP (□), and SeNP (□) for 24 h post scratch. Negative control (□) consists of cells incubated in culture medium supplemented with 0.5% FBS and 1% PS and positive control (□) include cells incubated in culture medium with 10% FBS. Statistically significant difference comparing samples with the negative control were calculated according to t-test (**, p≤0.01, ** ** p≤0.0001).

As presented in Fig. 3.5.8, no significant differences (p ≥ 0.05) were found in wound recovery for EPS A and the EPS/SeNP bio-nanocomposite in comparison with the negative control, suggesting that these samples do not have wound healing potential. Nonetheless, in the presence of 100 mg L^{-1} of EPS/AgNP bio-nanocomposite (1.2 mg$_{Ag}$ L^{-1}), cell migration was 2.3-fold higher than that in the negative control (p≤0.0001), and comparable to that found for the positive control (no significant difference for α=5%) (Fig. 3.5.8). Also, at 100 mg L^{-1} (2.6 mg$_{Au}$ L^{-1}), the EPS/AuNP bio-nanocomposite promoted a significant increase in cell migration (p≤0.01, Fig. 3.5.8), although to a lesser extent than that observed for the AgNP and for the positive control (p≤0.001). However, increasing the EPS/AuNP concentration to 500 mg$_{EPS}$ L^{-1} (13.2 mg$_{Au}$ L^{-1}) resulted in a wound closure similar to that obtained with the positive control (no significant difference for α=5%), as cell migration increased 2.1-fold increase in comparison to the negative control (p≤0.0001, Fig. 3.5.8).

It is believed that both NP contribute to a faster wound healing process thanks to their antimicrobial, antioxidant, and anti-inflammatory properties (Naraginti et al., 2016). In fact, the potential for wound treatment of AgNP and, to a lesser extent, AuNP formulations has been previously reported (Kumar et al., 2018; Marques et al., 2019; Naraginti et al., 2016). For example, the topical application of AuNP and AgNP

synthesized and stabilized by the root extract of *Coleus forskohlii* (green synthesis) successfully reduced the healing period in Winstar rat model in comparison to the control and to the standard drug Soframycin (Naraginti et al., 2016). In that study, both NP significantly induced the formation of granulation tissue, the deposition of collagen and re-epithelialization, thus, accelerating wound closure (Naraginti et al., 2016).

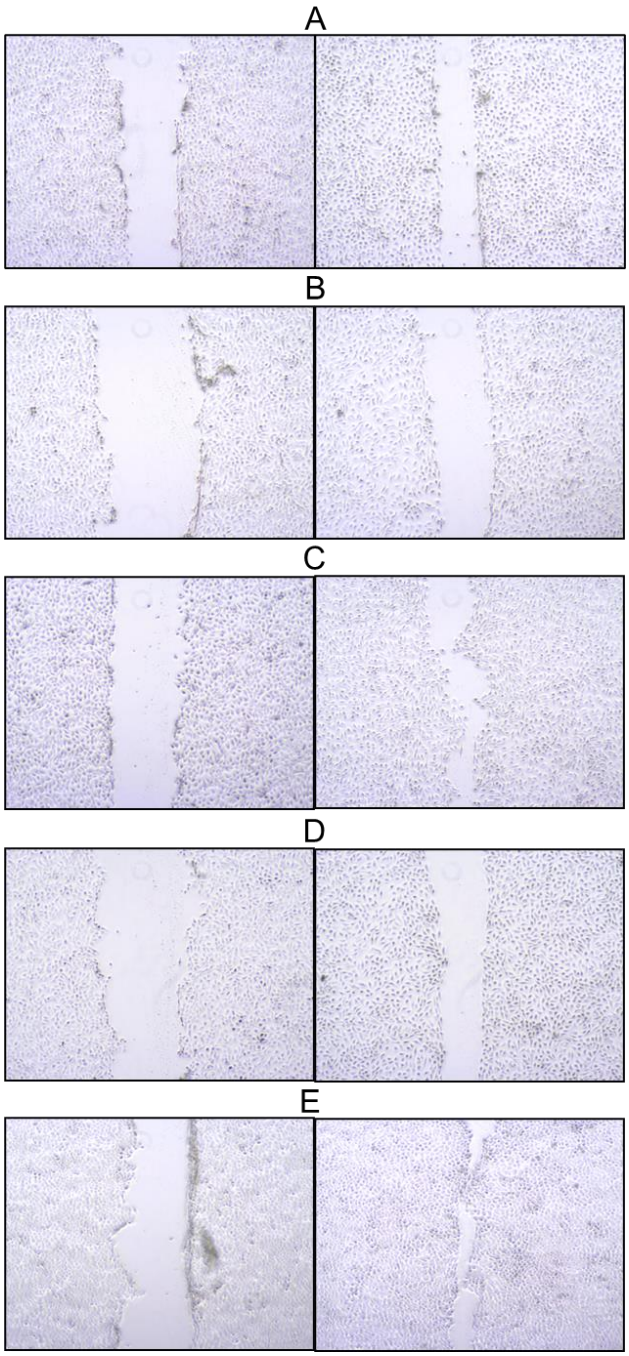

Figure 3.5.9. Representative images presenting cell migration of HaCaT cells. Images were taken before (left) and after (right) 24 h incubation without sample (Control, A), and with the addition of 100 mg L^{-1} EPS (B), 100 mg L^{-1} EPS/AgNP bio-nanocomposite (C), 500 mg L^{-1} EPS (D), and 500 mg L^{-1} EPS/AuNP bio-nanocomposite (E).

Evaluation of cellular antioxidant activity

Free radicals such as reactive oxygen species (ROS) can cause oxidative stress in essential cellular structures of living organisms, leading to altered functionality (Freitas et al., 2021; Matos et al., 2019). Many oxidative stress related diseases, such as cardiovascular and immunity diseases, type-II diabetes, cancer, or aging, are related with the accumulation of excessive ROS (Xiao et al., 2022). Antioxidants, by reducing the level of ROS, can be effective on the protection of the cells against oxidative stress (Xiao et al., 2022). The capacity of the EPS A and its NP bio-nanocomposites to reduce AAPH-induced ROS production in HaCaT cells was evaluated (Fig. 3.5.10). The EPS alone, and the bio-nanocomposites prepared with AuNP and AgNP did not reduce ROS generation at a cellular level. Nonetheless, EPS/SeNP bio-nanocomposite concentrations above 125 mg L^{-1} (11.5 mg_{Se} L^{-1}) significantly reduced ROS production ($p \leq 0.001$) (Fig. 3.5.10), suggesting a dose-dependent cellular antioxidant capacity. Comparably, ROS production in H_2O_2-induced HepG2 cells was also significantly decreased in the presence of SeNP coated with *C. sinensis* EPS (Xiao et al., 2022). Moreover, the inhibition of ROS production seemed to occur in a dose-dependent matter and was more intense as the SeNP's size decreased from 150 to 50 nm (Xiao et al., 2022). SeNP capped with *Bacillus paralicheniformis* SR14 EPS were more efficient in reducing the H_2O_2-induced ROS production by IPEC-J2 cells than chemically synthesized SeNP (Cheng et al., 2017), suggesting that the polysaccharide coating might be beneficial for antioxidant activity.

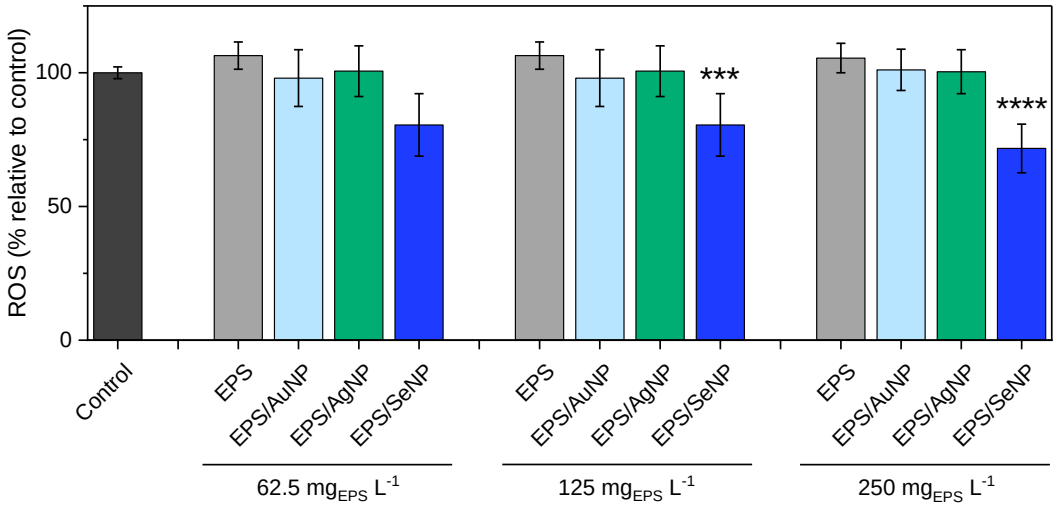

Figure 3.5.10. Antioxidant assay. Effect of EPS A (□), and its bio-nanocomposites with AuNP (□), AgNP (□), and SeNP (□) on the inhibition of AAPH-induced ROS production in HaCaT cells. Statistically significant differences comparing samples with the negative control were calculated according to t-test (***, $p \leq 0.001$, **** $p \leq 0.0001$).

3.5.5. Conclusions

The present study showed that the EPS produced by the marine bacterium *A. macleodii* Mo169 can be used in the preparation of NP with interesting biological activities, thus providing the fundamental evidence that marine EPS have potential in the nanotechnology and biomedical fields. The EPS was successfully employed for the reduction of silver and gold to AgNP and AuNP, respectively, through a simple, and green method. Moreover, the EPS was also used as stabilizer and dispersing agent in the formation of stable SeNP via the redox system of selenite and ascorbic acid. The synthesized NP were spherical in shape with a homogenous particle size distribution. The bioactivity potential of the EPS and the synthesized EPS/NP bio-nanocomposites was investigated for the first time. *In vitro* experiments demonstrated the safety of the EPS/AuNP and EPS/AgNP bio-nanocomposites on human keratinocytes (HaCaT) and fibroblast (CCD-1079Sk) cell lines, and their potential wound healing capacity. The SeNP coated with the EPS exhibited cellular antioxidant capacity *in vitro* and low cytotoxicity. These findings demonstrate that the *A. macleodii* Mo 169 EPS can be used as a reducing and/or stabilizing agent in the synthesis of NP with improved properties. Therefore, the EPS/NP bio-nanocomposites can be suitable for the development of novel biomaterials or formulations with biomedical applications. Nonetheless, additional research into the wound healing and antioxidant capacities of the EPS/NP bio-nanocomposites *in vivo,* along with their mechanisms, is needed in the future.

4

Conclusions and Future Work

4.1. General conclusions

In this thesis, both marine microalgae and marine bacteria were investigated as sources of EPS with improved properties. EPS production and the polymers' chemical composition were investigated for seven microalgae belonging to three different phyla. For the first time, the composition of the EPS secreted by *Coolia monotis*, *Heterocapsa* sp. AC210, *Coccomyxa* sp., and *Emiliania huxleyi* was reported. Although all the EPS had interesting composition, which included rare sugars and high sulphate contents, based on novelty and EPS yield, *Heterocapsa* sp. AC210 was chosen for photobioreactor cultivation. The dinoflagellate was cultivated in seawater-based medium and EPS production was apparently partially growth associated. Compositional analysis revealed the presence of seven different sugar monomers, including fucose, xylose and glucosamine, which have never been reported in dinoflagellates' EPS before. The high sulphate content in the EPS composition might be related with its *in vitro* biological activity, which included relevant antioxidant and anti-inflammatory properties. These results suggested that *Heterocapsa* sp. AC210 might be a source of high value EPS with potential application in the cosmeceuticals and biomedicine fields.

Additionally, the EPS produced by six bacteria isolated from unusual marine environments were characterized. The *Alteromonas* strains synthesized EPS with high uronic acids contents and rare sugars in their composition. These EPS presented interesting functional properties, including thickening, gel and film forming capacities. Upon the characterization of the EPS films, two different applications might be suggested: the flexible transparent films can be great candidates for the development of wound dressing materials, whereas the stiff films with outstanding barrier properties might be employed in food packaging. Based on its superior thickening and film properties, and the capacity to form gels with Fe^{3+}, the EPS produced by *Alteromonas macleodii* Mo 169 was selected and its properties were further investigated.

A. macleodii Mo 169 was cultivated with four different media and both cell growth and EPS production were used for the selection of a suitable medium. Then, in an attempt to reduce the EPS production costs, two low-cost feedstocks, namely glycerol and apple pulp waste, were used as sole substrates. Both cell growth and EPS production were enhanced using the two feedstocks. The EPS produced with glycerol had high contents of glucosamine and ribose, which is not a common feature in EPS from the *Alteromonas* genus. These results suggested that, based on the cultivation conditions, tailored EPS might be produced with improved properties.

The potential of the EPS to be used as a structuring agent, namely as a thickening and gelling agent, was evaluated. The EPS rheological characterization suggested a relevant shear thinning and weak gel-like behavior, that was sustained under different conditions, such as in the presence of salts, at various pH values and temperatures. Also, the EPS regained almost instantaneously its rheological properties after exposure to high temperatures and high shear stress. A modelling approach was employed for the preparation of EPS-Fe^{3+} hydrogels. The results showed that depending on the preparation conditions, the hydrogels had different strength values that might be suitable for drug delivery or tissue engineering applications.

The potential of *A. macleodii* Mo169 EPS on bio-nanotechnology was also investigated through the development of EPS/NP bio-nanocomposites. The polymer was successfully employed for the synthesis and/or stabilization of gold, silver and selenium nanoparticles. EPS/AuNP and EPS/AgNP bio-nanocomposites did not induce any cytotoxic effects on human keratinocyte and fibroblast cell lines, and presented a remarkable capacity to promote cell migration, suggesting their potential in wound healing management. The EPS/SeNP showed low cytotoxicity and a good antioxidant capacity.

Overall, the results from this PhD work clearly indicate the potential of EPS of marine origin to be employed as biomaterials or bioactive compounds in high-value areas, including the pharmaceutical, biomedical and cosmetic fields. The application of the EPS in products with such high market value might increase to the economic viability of the production process, thus, contributing to the arising of novel bio-based economic solutions.

4.2. Future work

This PhD work leaves unfinished aspects that should be investigated in the future. The following suggestions might be considered for future improvements:

EPS production by *Heterocapsa* sp. AC210 should be optimized through the assessment of medium composition and nutrient concentration, including the possibility of using organic carbon sources (heterotrophic cultivation). Aeration rate, CO_2 supply, light intensity and the light:dark cycles can also affect cell growth and EPS production and, therefore, should be studied. Additionally, different bioreactor operation modes and feeding strategies might be tested (e.g., continuous feeding, pulse feeding, two step autotrophic/heterotrophic cultivation, addition of CO_2 for pH control), as well as

different photobioreactor designs. The impact of these cultivation parameters on the EPS composition should also be investigated.

The mechanical and barrier properties of the *Alteromonas* EPS films might be improved for specific applications by changing the type and concentration of plasticizer, incorporate additives or blend the EPS with other biopolymers.

EPS production by *A. macleodii* Mo 169 using the tested agro-industrial wastes can be optimized in terms of the operational parameters (dissolved oxygen, aeration, stirring rate, pH). The impact of different nutrient sources and concentrations, as well as different bioreactor cultivation strategies (e.g., feeding or using ammonium hydroxide for pH control) should be considered. Additionally, industrial glycerol by-product, which often includes possible growth-inhibitory compounds (e.g., methanol) in its composition, should be tested as carbon source. Since the cultivation parameters affected the EPS characteristics, the functional and biological properties of the polymers produced using agro-industrial wastes should be evaluated.

The rheological behavior of the *A. macleodii* Mo169 EPS in specific formulations should be studied. Also, further characterization is required for the EPS-Fe^{3+} hydrogels, including compression tests and the determination of the water content, swelling, Fe^{3+} content, Fe^{3+} release, porosity, stability in different environments, thermal stability, and cytotoxicity. Additionally, sol-gel conversion tests using UV-vis light and reducing agents (e.g., citric acid or lactate) should be performed. The application of these hydrogels in scaffolds for tissue engineering and drug delivery should be explored. EPS gelation in the presence of Cu^{2+} might also be worth to explore.

The cellular mechanisms behind the *in vitro* biological activities (wound healing, antioxidant, and anti-inflammatory) of the microalga EPS and the bio-nanocomposites might be studied. Additional *in vivo* experiments are also suggested.

A structural characterization of both bacterial and microalgal EPS should be performed in order to understand their biological and functional properties. Moreover, other EPS applications may be investigated, namely as emulsifier, antiviral, antibacterial, cryoprotectant, and/or flocculant agents. Additionally, a combined biomaterial can be developed and explored using the bacterial EPS as the structuring agent (formulation, hydrogel, or film) and the microalgal EPS as the bioactive compound. A co-cultivation strategy might be explored to produce this combined biomaterial.

Bibliography

Abdul Raman, A. A., Tan, H. W., & Buthiyappan, A. (2019). Two-Step Purification of Glycerol as a Value Added by Product From the Biodiesel Production Process. *Frontiers in Chemistry*, *7*, 774. https://doi.org/10.3389/fchem.2019.00774

Abid, Y., Azabou, S., Blecker, C., Gharsallaoui, A., Corsaro, M. M., Besbes, S., & Attia, H. (2021). Rheological and emulsifying properties of an exopolysaccharide produced by potential probiotic *Leuconostoc citreum*-BMS strain. *Carbohydrate Polymers*, *256*, 117523. https://doi.org/10.1016/j.carbpol.2020.117523

Ahmadi, M., Vahabzadeh, F., Bonakdarpour, B., Mofarrah, E., & Mehranian, M. (2005). Application of the central composite design and response surface methodology to the advanced treatment of olive oil processing wastewater using Fenton's peroxidation. *Journal of Hazardous Materials*, *123*(1–3), 187–195. https://doi.org/10.1016/j.jhazmat.2005.03.042

Ahmed, K. B. A., Kalla, D., Uppuluri, K. B., & Anbazhagan, V. (2014). Green synthesis of silver and gold nanoparticles employing levan, a biopolymer from *Acetobacter xylinum* NCIM 2526, as a reducing agent and capping agent. *Carbohydrate Polymers*, *112*, 539–545. https://doi.org/10.1016/j.carbpol.2014.06.033

Ahmed, Z., Wang, Y., Anjum, N., Ahmad, A., & Khan, S. T. (2013). Characterization of exopolysaccharide produced by *Lactobacillus kefiranofaciens* ZW3 isolated from Tibet kefir – Part II. *Food Hydrocolloids*, *30*(1), 343–350. https://doi.org/10.1016/j.foodhyd.2012.06.009

Akturk, O. (2020). Colloidal stability and biological activity evaluation of microbial exopolysaccharide levan-capped gold nanoparticles. *Colloids and Surfaces B: Biointerfaces*, *192*, 111061. https://doi.org/10.1016/j.colsurfb.2020.111061

Al- Nahas. (2011). Characterization of an exopolysaccharide-producing marine bacterium, isolate *Pseudoalteromonas* sp. AM. *African Journal of Microbiology Research*, *5*(22). https://doi.org/10.5897/AJMR11.757

Alle, M., G, B. reddy, Kim, T. H., Park, S. H., Lee, S.-H., & Kim, J.-C. (2020). Doxorubicin-carboxymethyl xanthan gum capped gold nanoparticles: Microwave synthesis, characterization, and anti-cancer activity. *Carbohydrate Polymers*, *229*, 115511. https://doi.org/10.1016/j.carbpol.2019.115511

Alves, V. D., Costa, N., & Coelhoso, I. M. (2010). Barrier properties of biodegradable composite films based on kappa-carrageenan/pectin blends and mica flakes. *Carbohydrate Polymers*, *79*(2), 269–276. https://doi.org/10.1016/j.carbpol.2009.08.002

Alves, V. D., Ferreira, A. R., Costa, N., Freitas, F., Reis, M. A. M., & Coelhoso, I. M. (2011). Characterization of biodegradable films from the extracellular polysaccharide produced by *Pseudomonas oleovorans* grown on glycerol byproduct. *Carbohydrate Polymers*, *83*(4), 1582–1590. https://doi.org/10.1016/j.carbpol.2010.10.010

Alves, V. D., Freitas, F., Costa, N., Carvalheira, M., Oliveira, R., Gonçalves, M. P., & Reis, M. A. M. (2010). Effect of temperature on the dynamic and steady-shear rheology of a new microbial extracellular polysaccharide produced from glycerol byproduct. *Carbohydrate Polymers*, *79*(4), 981–988. https://doi.org/10.1016/j.carbpol.2009.10.026

Alves, V. D., Freitas, F., Torres, C. A. V., Cruz, M., Marques, R., Grandfils, C., Gonçalves, M. P., Oliveira, R., & Reis, M. A. M. (2010). Rheological and morphological characterization of the culture broth during exopolysaccharide production by *Enterobacter* sp. *Carbohydrate Polymers*, *81*(4), 758–764. https://doi.org/10.1016/j.carbpol.2010.03.048

Ambebila, E. N., Santamaría, E., Maestro, A., Gutiérrez, J. M., & González, C. (2019). Gellan Hydrogels: Preparation, Rheological Characterization and Application in Encapsulation of Curcumin. *Food Biophysics*, *14*(2), 154–163. https://doi.org/10.1007/s11483-019-09568-0

Anastase-Ravion, S., Carreno, M.-P., Blondin, C., Ravion, O., Champion, J., Chaubet, F., Haeffner-Cavaillon, N., & Letourneur, D. (2002). Heparin-like polymers modulate proinflammatory cytokine production by lipopolysaccharide-stimulated human monocytes. *Journal of Biomedical Materials Research*, *60*(3), 375–383. https://doi.org/10.1002/jbm.10112

Anjugam, M., Vaseeharan, B., Iswarya, A., Divya, M., Prabhu, N. M., & Sankaranarayanan, K. (2018). Biological synthesis of silver nanoparticles using β-1, 3 glucan binding protein and their antibacterial, antibiofilm and cytotoxic potential. *Microbial Pathogenesis*, *115*, 31–40. https://doi.org/10.1016/j.micpath.2017.12.003

Antunes, S., Freitas, F., Sevrin, C., Grandfils, C., & Reis, M. A. M. (2017). Production of FucoPol by *Enterobacter* A47 using waste tomato paste by-product as sole carbon source. *Bioresource Technology*, *227*, 66–73. https://doi.org/10.1016/j.biortech.2016.12.018

Arad, S. (Malis), Rapoport, L., Moshkovich, A., van Moppes, D., Karpasas, M., Golan, R., & Golan, Y. (2006). Superior Biolubricant from a Species of Red Microalga. *Langmuir*, *22*(17), 7313–7317. https://doi.org/10.1021/la060600x

Ariede, M. B., Candido, T. M., Jacome, A. L. M., Velasco, M. V. R., de Carvalho, J. C. M., & Baby, A. R. (2017). Cosmetic attributes of algae—A review. *Algal Research*, *25*, 483–487. https://doi.org/10.1016/j.algal.2017.05.019

Assunção, J., Guedes, A., & Malcata, F. (2017). Biotechnological and Pharmacological Applications of Biotoxins and Other Bioactive Molecules from Dinoflagellates. *Marine Drugs*, *15*(12), 393. https://doi.org/10.3390/md15120393

Ayyash, M., Abu-Jdayil, B., Itsaranuwat, P., Galiwango, E., Tamiello-Rosa, C., Abdullah, H., Esposito, G., Hunashal, Y., Obaid, R. S., & Hamed, F. (2020). Characterization, bioactivities, and rheological properties of exopolysaccharide produced by novel probiotic *Lactobacillus plantarum* C70 isolated from camel milk. *International Journal of Biological Macromolecules*, *144*, 938–946. https://doi.org/10.1016/j.ijbiomac.2019.09.171

Azarifar, M., Ghanbarzadeh, B., Sowti Khiabani, M., Akhondzadeh Basti, A., Abdulkhani, A., Noshirvani, N., & Hosseini, M. (2019). The optimization of gelatin-CMC based active films containing chitin nanofiber and *Trachyspermum ammi* essential oil by response surface methodology. *Carbohydrate Polymers*, *208*, 457–468. https://doi.org/10.1016/j.carbpol.2019.01.005

Bae, I. Y., Oh, I.-K., Lee, S., Yoo, S.-H., & Lee, H. G. (2008). Rheological characterization of levan polysaccharides from *Microbacterium laevaniformans*. *International Journal of Biological Macromolecules*, *42*(1), 10–13. https://doi.org/10.1016/j.ijbiomac.2007.08.006

Bae, S.-Y., Yim, J. H., Lee, H. K., & Pyo, S. (2006). Activation of murine peritoneal macrophages by sulfated exopolysaccharide from marine microalga *Gyrodinium impudicum* (strain KG03): Involvement of the NF-κB and JNK pathway. *International Immunopharmacology*, *6*(3), 473–484.

Baptista, S., Pereira, J. R., Gil, C. V., Torres, C. A. V., Reis, M. A. M., & Freitas, F. (2022). Development of Olive Oil and α-Tocopherol Containing Emulsions Stabilized by FucoPol: Rheological and Textural Analyses. *Polymers*, *14*(12), 2349. https://doi.org/10.3390/polym14122349

Bastarrachea, L., Dhawan, S., & Sablani, S. S. (2011). Engineering Properties of Polymeric-Based Antimicrobial Films for Food Packaging: A Review. *Food Engineering Reviews*, *3*(2), 79–93. https://doi.org/10.1007/s12393-011-9034-8

Bejar, V., Calvo, C., Moliz, J., Diaz-Martinez, F., & Quesada, E. (1996). Effect of growth conditions on the rheological properties and chemical composition of *Volcaniella eurihalina* exopolysaccharide. *Applied Biochemistry and Biotechnology*, *59*(1), 77–86. https://doi.org/10.1007/BF02787859

Blakeney, A. B., Harris, P. J., Henry, R. J., & Stone, B. A. (1983). A simple and rapid preparation of alditol acetates for monosaccharide analysis. *Carbohydrate Research*, *113*(2), 291–299.

Blumenkrantz, N., & Asboe-Hansen, G. (1973). New method for quantitative determination of uronic acid. *Analytical Biochemistry*, *54*, 484–489.

Bolla, P. K., Rodriguez, V. A., Kalhapure, R. S., Kolli, C. S., Andrews, S., & Renukuntla, J. (2018). A review on pH and temperature responsive gels and other less explored drug delivery systems. *Journal of Drug Delivery Science and Technology*, *46*, 416–435. https://doi.org/10.1016/j.jddst.2018.05.037

Bramhachari, P. V., & Dubey, S. K. (2006). Isolation and characterization of exopolysaccharide produced by *Vibrio harveyi* strain VB23. *Letters in Applied Microbiology*, *43*(5), 571–577. https://doi.org/10.1111/j.1472-765X.2006.01967.x

Bramhachari, P. V., Kishor, P. B. K., Ramadevi, R., Kumar, R., Rao, B. R., & Dubey, S. K. (2007). Isolation and characterization of mucous exopolysaccharide (EPS) produced by *Vibrio furnissii* strain VB0S3. *Journal of Microbiology and Biotechnology*, *17*(1), 44–51.

Cai, W., Hu, T., Bakry, A. M., Zheng, Z., Xiao, Y., & Huang, Q. (2018). Effect of ultrasound on size, morphology, stability and antioxidant activity of selenium nanoparticles dispersed by a hyperbranched polysaccharide from *Lignosus rhinocerotis*. *Ultrasonics Sonochemistry*, *42*, 823–831.
https://doi.org/10.1016/j.ultsonch.2017.12.022

Cai, W., Hu, T., & Huang, Q. (2021). A polysaccharide from *Lignosus rhinocerotis* sclerotia: Self-healing properties and the effect of temperature on its rheological behavior. *Carbohydrate Polymers*, *267*, 118223.
https://doi.org/10.1016/j.carbpol.2021.118223

Cambon-Bonavita, M.-A., Raguénès, G., Jean, J., Vincent, P., & Guezennec, J. (2002). A novel polymer produced by a bacterium isolated from a deep-sea hydrothermal vent polychaete annelid. *Journal of Applied Microbiology*, *93*(2), 310–315. https://doi.org/10.1046/j.1365-2672.2002.01689.x

Cao, B., Zhang, Q., Guo, J., Guo, R., Fan, X., & Bi, Y. (2021). Synthesis and evaluation of Grateloupia Livida polysaccharides-functionalized selenium nanoparticles. *International Journal of Biological Macromolecules*, *191*, 832–839. https://doi.org/10.1016/j.ijbiomac.2021.09.087

Carreau, P. J. (1972). Rheological Equations from Molecular Network Theories. *Journal of Rheology*, *16*(1), 99–127.

Carrión, O., Delgado, L., & Mercade, E. (2015). New emulsifying and cryoprotective exopolysaccharide from Antarctic *Pseudomonas* sp. ID1. *Carbohydrate Polymers*, *117*, 1028–1034. https://doi.org/10.1016/j.carbpol.2014.08.060

Casillo, A., Lanzetta, R., Parrilli, M., & Corsaro, M. (2018). Exopolysaccharides from Marine and Marine Extremophilic Bacteria: Structures, Properties, Ecological Roles and Applications. *Marine Drugs*, *16*(2), 69. https://doi.org/10.3390/md16020069

Casillo, A., Parrilli, E., Sannino, F., Mitchell, D. E., Gibson, M. I., Marino, G., Lanzetta, R., Parrilli, M., Cosconati, S., Novellino, E., Randazzo, A., Tutino, M. L., & Corsaro, M. M. (2017). Structure-activity relationship of the exopolysaccharide from a psychrophilic bacterium: A strategy for cryoprotection. *Carbohydrate Polymers*, *156*, 364–371. https://doi.org/10.1016/j.carbpol.2016.09.037

Chalkiadakis, E., Dufourcq, R., Schmitt, S., Brandily, C., Kervarec, N., Coatanea, D., Amir, H., Loubersac, L., Chanteau, S., Guezennec, J., Dupont-Rouzeyrol, M., & Simon-Colin, C. (2013). Partial characterization of an exopolysaccharide secreted by a marine bacterium, *Vibrio neocaledonicus* sp. Nov., from New Caledonia. *Journal of Applied Microbiology*, *114*(6), 1702–1712. https://doi.org/10.1111/jam.12184

Chen, C.-Y., Zhao, X.-Q., Yen, H.-W., Ho, S.-H., Cheng, C.-L., Lee, D.-J., Bai, F.-W., & Chang, J.-S. (2013). Microalgae-based carbohydrates for biofuel production. *Biochemical Engineering Journal*, *78*, 1–10. https://doi.org/10.1016/j.bej.2013.03.006

Chen, X., Song, L., Wang, H., Liu, S., Yu, H., Wang, X., Li, R., Liu, T., & Li, P. (2019). Partial Characterization, the Immune Modulation and Anticancer Activities of Sulfated Polysaccharides from Filamentous Microalgae *Tribonema* sp. *Molecules*, *24*(2), 322. https://doi.org/10.3390/molecules24020322

Chen, X., Yan, J.-K., & Wu, J.-Y. (2016). Characterization and antibacterial activity of silver nanoparticles prepared with a fungal exopolysaccharide in water. *Food Hydrocolloids*, *53*, 69–74. https://doi.org/10.1016/j.foodhyd.2014.12.032

Chen, X., Zhao, X., Gao, Y., Yin, J., Bai, M., & Wang, F. (2018). Green Synthesis of Gold Nanoparticles Using Carrageenan Oligosaccharide and Their *In Vitro* Antitumor Activity. *Marine Drugs*, *16*(8), 277. https://doi.org/10.3390/md16080277

Cheng, Y., Xiao, X., Li, X., Song, D., Lu, Z., Wang, F., & Wang, Y. (2017). Characterization, antioxidant property and cytoprotection of exopolysaccharide-capped elemental selenium particles synthesized by *Bacillus paralicheniformis* SR14. *Carbohydrate Polymers*, *178*, 18–26. https://doi.org/10.1016/j.carbpol.2017.08.124

Choo, W.-T., Teoh, M.-L., Phang, S.-M., Convey, P., Yap, W.-H., Goh, B.-H., & Beardall, J. (2020). Microalgae as Potential Anti-Inflammatory Natural Product Against Human Inflammatory Skin Diseases. *Frontiers in Pharmacology*, *11*, 1086. https://doi.org/10.3389/fphar.2020.01086

Concórdio-Reis, P., Alves, V. D., Moppert, X., Guézennec, J., Freitas, F., & Reis, M. A. M. (2021). Characterization and Biotechnological Potential of Extracellular Polysaccharides Synthesized by *Alteromonas* Strains Isolated from French Polynesia Marine Environments. *Marine Drugs*, *19*(9), 522. https://doi.org/10.3390/md19090522

Concórdio-Reis, P., Pereira, C. V., Batista, M. P., Sevrin, C., Grandfils, C., Marques, A. C., Fortunato, E., Gaspar, F. B., Matias, A. A., Freitas, F., & Reis, M. A. M. (2020). Silver nanocomposites based on the bacterial fucose-rich polysaccharide secreted by *Enterobacter* A47 for wound dressing applications: Synthesis, characterization and *in vitro* bioactivity. *International Journal of Biological Macromolecules*. https://doi.org/10.1016/j.ijbiomac.2020.07.072

Concórdio-Reis, P., Pereira, J. R., Torres, C. A. V., Sevrin, C., Grandfils, C., & Freitas, F. (2018). Effect of mono- and dipotassium phosphate concentration on extracellular polysaccharide production by the bacterium *Enterobacter* A47. *Process Biochemistry*. https://doi.org/10.1016/j.procbio.2018.09.001

Concórdio-Reis, P., Reis, M. A. M., & Freitas, F. (2020). Biosorption of Heavy Metals by the Bacterial Exopolysaccharide FucoPol. *Applied Sciences*, *10*(19), 6708. https://doi.org/10.3390/app10196708

Costa, J. A. V., Lucas, B. F., Alvarenga, A. G. P., Moreira, J. B., & de Morais, M. G. (2021). Microalgae Polysaccharides: An Overview of Production, Characterization, and Potential Applications. *Polysaccharides*, *2*(4), 759–772. https://doi.org/10.3390/polysaccharides2040046

Cruz, M., Freitas, F., Torres, C. A. V., Reis, M. A. M., & Alves, V. D. (2011). Influence of temperature on the rheological behavior of a new fucose-containing bacterial exopolysaccharide. *International Journal of Biological Macromolecules*, *48*(4), 695–699. https://doi.org/10.1016/j.ijbiomac.2011.02.012

Dave, S. R., Upadhyay, K. H., Vaishnav, A. M., & Tipre, D. R. (2020). Exopolysaccharides from marine bacteria: Production, recovery and applications. *Environmental Sustainability*, *3*(2), 139–154. https://doi.org/10.1007/s42398-020-00101-5

De Philippis, R., Margheri, M. C., Materassi, R., & Vincenzini, M. (1998). Potential of Unicellular Cyanobacteria from Saline Environments as Exopolysaccharide Producers. *Applied and Environmental Microbiology*, *64*(3), 1130–1132. https://doi.org/10.1128/AEM.64.3.1130-1132.1998

De Ruiter, G. A., Schols, H. A., Voragen, A. G. J., & Rombouts, F. M. (1992). Carbohydrate analysis of water-soluble uronic acid-containing polysaccharides with high-performance anion-exchange chromatography using methanolysis combined with

TFA hydrolysis is superior to four other methods. *Analytical Biochemistry*, *207*(1), 176–185. https://doi.org/10.1016/0003-2697(92)90520-H

Dehghan-Baniani, D., Chen, Y., Wang, D., Bagheri, R., Solouk, A., & Wu, H. (2020). Injectable in situ forming kartogenin-loaded chitosan hydrogel with tunable rheological properties for cartilage tissue engineering. *Colloids and Surfaces B: Biointerfaces*, *192*, 111059. https://doi.org/10.1016/j.colsurfb.2020.111059

Delattre, C., Pierre, G., Laroche, C., & Michaud, P. (2016). Production, extraction and characterization of microalgal and cyanobacterial exopolysaccharides. *Biotechnology Advances*, *34*(7), 1159–1179.
https://doi.org/10.1016/j.biotechadv.2016.08.001

Delbarre-Ladrat, C., Salas, M. L., Sinquin, C., Zykwinska, A., & Colliec-Jouault, S. (2017). Bioprospecting for Exopolysaccharides from Deep-Sea Hydrothermal Vent Bacteria: Relationship between Bacterial Diversity and Chemical Diversity. *Microorganisms*, *5*(3), 63. https://doi.org/10.3390/microorganisms5030063

Delbarre-Ladrat, C., Sinquin, C., Lebellenger, L., Zykwinska, A., & Colliec-Jouault, S. (2014). Exopolysaccharides produced by marine bacteria and their applications as glycosaminoglycan-like molecules. *Frontiers in Chemistry*, *2*. https://doi.org/10.3389/fchem.2014.00085

Devi, L., Gupta, R., Jain, S. K., Singh, S., & Kesharwani, P. (2020). Synthesis, characterization and *in vitro* assessment of colloidal gold nanoparticles of Gemcitabine with natural polysaccharides for treatment of breast cancer. *Journal of Drug Delivery Science and Technology*, *56*, 101565. https://doi.org/10.1016/j.jddst.2020.101565

Dhar, S., Reddy, E. M., Shiras, A., Pokharkar, V., & Prasad, B. L. V. (2008). Natural Gum Reduced/Stabilized Gold Nanoparticles for Drug Delivery Formulations. *Chemistry - A European Journal*, *14*(33), 10244–10250.
https://doi.org/10.1002/chem.200801093

Di Pippo, F., Ellwood, N. T. W., Gismondi, A., Bruno, L., Rossi, F., Magni, P., & De Philippis, R. (2013). Characterization of exopolysaccharides produced by seven biofilm-forming cyanobacterial strains for biotechnological applications. *Journal of Applied Phycology*, *25*(6), 1697–1708. https://doi.org/10.1007/s10811-013-0028-1

Dimopoulou, M., Alba, K., Sims, I. M., & Kontogiorgos, V. (2021). Structure and rheology of pectic polysaccharides from baobab fruit and leaves. *Carbohydrate Polymers*, *273*, 118540. https://doi.org/10.1016/j.carbpol.2021.118540

Dodgson, K. S., & Price, R. G. (1962). A note on the determination of the ester sulphate content of sulphated polysaccharides. *Biochemical Journal*, *84*(1), 106.

Donot, F., Fontana, A., Baccou, J. C., & Schorr-Galindo, S. (2012). Microbial exopolysaccharides: Main examples of synthesis, excretion, genetics and extraction. *Carbohydrate Polymers*, *87*(2), 951–962. https://doi.org/10.1016/j.carbpol.2011.08.083

Dourado, F., Madureira, P., Carvalho, V., Coelho, R., Coimbra, M. A., Vilanova, M., Mota, M., & Gama, F. M. (2004). Purification, structure and immunobiological activity of an arabinan-rich pectic polysaccharide from the cell walls of Prunus dulcis seeds. *Carbohydrate Research*, *339*(15), 2555–2566.

Dranca, F., Vargas, M., & Oroian, M. (2020). Physicochemical properties of pectin from *Malus domestica* 'Fălticeni' apple pomace as affected by non-conventional extraction techniques. *Food Hydrocolloids*, *100*, 105383. https://doi.org/10.1016/j.foodhyd.2019.105383

Dufourcq, R., Chalkiadakis, E., Fauchon, M., Deslandes, E., Kerjean, V., Chanteau, S., Petit, E., Guezennec, J., & Dupont-Rouzeyrol, M. (2014). Isolation and partial characterization of bacteria (*Pseudoalteromonas* sp.) with potential antibacterial activity from a marine costal environment from New Caledonia. *Letters in Applied Microbiology*, *58*(2), 102–108. https://doi.org/10.1111/lam.12162

Dutta, S., & Bhadury, P. (2020). Effect of arsenic on exopolysaccharide production in a diazotrophic cyanobacterium. *Journal of Applied Phycology*, *32*(5), 2915–2926. https://doi.org/10.1007/s10811-020-02206-0

Dvir, I., Stark, A. H., Chayoth, R., Madar, Z., & Arad, S. M. (2009). Hypocholesterolemic Effects of Nutraceuticals Produced from the Red Microalga *Porphyridium* sp. In Rats. *Nutrients*, *1*(2), 156–167. https://doi.org/10.3390/nu1020156

Engler, A. J., Sen, S., Sweeney, H. L., & Discher, D. E. (2006). Matrix Elasticity Directs Stem Cell Lineage Specification. *Cell*, *126*(4), 677–689. https://doi.org/10.1016/j.cell.2006.06.044

Escárcega-González, C. E., Garza-Cervantes, J. A., Vázquez-Rodríguez, A., & Morones-Ramírez, J. R. (2018). Bacterial Exopolysaccharides as Reducing and/or Stabilizing Agents during Synthesis of Metal Nanoparticles with Biomedical Applications. *International Journal of Polymer Science*, *2018*, 1–15. https://doi.org/10.1155/2018/7045852

Fagioli, L., Pavoni, L., Logrippo, S., Pelucchini, C., Rampoldi, L., Cespi, M., Bonacucina, G., & Casettari, L. (2018). Linear Viscoelastic Properties of Selected Polysaccharide Gums as Function of Concentration, pH, and Temperature. *Journal of Food Science*, 1750-3841.14407. https://doi.org/10.1111/1750-3841.14407

Fan, Y., Yang, J., Duan, A., & Li, X. (2021). Pectin/sodium alginate/xanthan gum edible composite films as the fresh-cut package. *International Journal of Biological Macromolecules*, *181*, 1003–1009. https://doi.org/10.1016/j.ijbiomac.2021.04.111

Farinha, I., Duarte, P., Pimentel, A., Plotnikova, E., Chagas, B., Mafra, L., Grandfils, C., Freitas, F., Fortunato, E., & Reis, M. A. M. (2015). Chitin–glucan complex production by *Komagataella pastoris*: Downstream optimization and product characterization. *Carbohydrate Polymers*, *130*, 455–464. https://doi.org/10.1016/j.carbpol.2015.05.034

Ferreira, A. R. V., Torres, C. A. V., Freitas, F., Reis, M. A. M., Alves, V. D., & Coelhoso, I. M. (2014). Biodegradable films produced from the bacterial polysaccharide FucoPol. *International Journal of Biological Macromolecules*, *71*, 111–116. https://doi.org/10.1016/j.ijbiomac.2014.04.022

Ferreira, A. R. V., Torres, C. A. V., Freitas, F., Sevrin, C., Grandfils, C., Reis, M. A. M., Alves, V. D., & Coelhoso, I. M. (2016). Development and characterization of bilayer films of FucoPol and chitosan. *Carbohydrate Polymers*, *147*, 8–15. https://doi.org/10.1016/j.carbpol.2016.03.089

Ferreira, A. S., Mendonça, I., Póvoa, I., Carvalho, H., Correia, A., Vilanova, M., Silva, T. H., Coimbra, M. A., & Nunes, C. (2021). Impact of growth medium salinity on galactoxylan exopolysaccharides of *Porphyridium purpureum*. *Algal Research*, *59*, 102439. https://doi.org/10.1016/j.algal.2021.102439

Ferreira, J. A., Domingues, M. R. M., Reis, A., Figueiredo, C., Monteiro, M. A., & Coimbra, M. A. (2011). Aldobiouronic acid domains in *Helicobacter pylori*. *Carbohydrate Research*, *346*(5), 638–643. https://doi.org/10.1016/j.carres.2011.01.009

Ferreira, S. S., Passos, C. P., Madureira, P., Vilanova, M., & Coimbra, M. A. (2015). Structure–function relationships of immunostimulatory polysaccharides: A review. *Carbohydrate Polymers*, *132*, 378–396. https://doi.org/10.1016/j.carbpol.2015.05.079

Fialho, L., Araújo, D., Alves, V. D., Roma-Rodrigues, C., Baptista, P. V., Fernandes, A. R., Freitas, F., & Reis, M. A. M. (2019). Cation-mediated gelation of the fucose-rich polysaccharide FucoPol: Preparation and characterization of hydrogel beads and their cytotoxicity assessment. *International Journal of Polymeric Materials and Polymeric Biomaterials*, 1–10. https://doi.org/10.1080/00914037.2019.1695205

Finore, I., Di Donato, P., Mastascusa, V., Nicolaus, B., & Poli, A. (2014). Fermentation Technologies for the Optimization of Marine Microbial Exopolysaccharide Production. *Marine Drugs*, *12*(5), 3005–3024. https://doi.org/10.3390/md12053005

Fondi, M., Maida, I., Perrin, E., Mellera, A., Mocali, S., Parrilli, E., Tutino, M. L., Liò, P., & Fani, R. (2015). Genome-scale metabolic reconstruction and constraint-based modelling of the Antarctic bacterium *Pseudoalteromonas haloplanktis* TAC125: Modelling of *P. haloplanktis* TAC125 metabolism. *Environmental Microbiology*, *17*(3), 751–766. https://doi.org/10.1111/1462-2920.12513

Freitas, F., Alves, V. D., Carvalheira, M., Costa, N., Oliveira, R., & Reis, M. A. M. (2009). Emulsifying behaviour and rheological properties of the extracellular polysaccharide produced by *Pseudomonas oleovorans* grown on glycerol byproduct. *Carbohydrate Polymers*, *78*(3), 549–556. https://doi.org/10.1016/j.carbpol.2009.05.016

Freitas, F., Alves, V. D., Gouveia, A. R., Pinheiro, C., Torres, C. A. V., Grandfils, C., & Reis, M. A. M. (2014). Controlled Production of Exopolysaccharides from Enterobacter A47 as a Function of Carbon Source with Demonstration of Their Film and Emulsifying Abilities. *Applied Biochemistry and Biotechnology*, *172*(2), 641–657. https://doi.org/10.1007/s12010-013-0560-0

Freitas, F., Alves, V. D., Pais, J., Costa, N., Oliveira, C., Mafra, L., Hilliou, L., Oliveira, R., & Reis, M. A. M. (2009). Characterization of an extracellular polysaccharide produced by a *Pseudomonas* strain grown on glycerol. *Bioresource Technology*, *100*(2), 859–865. https://doi.org/10.1016/j.biortech.2008.07.002

Freitas, F., Alves, V. D., Reis, M. A., Crespo, J. G., & Coelhoso, I. M. (2014). Microbial polysaccharide-based membranes: Current and future applications. *Journal of Applied Polymer Science*, *131*(6), n/a-n/a. https://doi.org/10.1002/app.40047

Freitas, F., Alves, V. D., Torres, C. A. V., Cruz, M., Sousa, I., Melo, M. J., Ramos, A. M., & Reis, M. A. M. (2011). Fucose-containing exopolysaccharide produced by the newly isolated *Enterobacter* strain A47 DSM 23139. *Carbohydrate Polymers*, *83*(1), 159–165. https://doi.org/10.1016/j.carbpol.2010.07.034

Freitas, F., Torres, C. A. V., Araújo, D., Farinha, I., Pereira, J. R., Concórdio-Reis, P., & Reis, M. A. M. (2021). Advanced Microbial Polysaccharides. In B. Rehm & M. F. Moradali (Eds.), *Biopolymers for Biomedical and Biotechnological Applications* (1st ed., pp. 19–62). Wiley. https://doi.org/10.1002/9783527818310.ch2

Freitas, F., Torres, C. A. V., & Reis, M. A. M. (2017). Engineering aspects of microbial exopolysaccharide production. *Bioresource Technology*. https://doi.org/10.1016/j.biortech.2017.05.092

Gaignard, C., Laroche, C., Pierre, G., Dubessay, P., Delattre, C., Gardarin, C., Gourvil, P., Probert, I., Dubuffet, A., & Michaud, P. (2019). Screening of marine microalgae: Investigation of new exopolysaccharide producers. *Algal Research*, *44*, 101711. https://doi.org/10.1016/j.algal.2019.101711

Gao, F., Woolschot, S., Cabanelas, I. T. D., Wijffels, R. H., & Barbosa, M. J. (2021). Light spectra as triggers for sorting improved strains of *Tisochrysis lutea*. *Bioresource Technology*, *321*, 124434. https://doi.org/10.1016/j.biortech.2020.124434

Gao, Z., Yang, J., Wu, J., Li, H., Wu, C., Yin, Z., Xu, J., Zhu, L., Gao, M., & Zhan, X. (2022). Structural characterization and *in vitro* evaluation of the prebiotic potential of

an exopolysaccharide produced by *Bacillus thuringiensis* during fermentation. *LWT*, *163*, 113532. https://doi.org/10.1016/j.lwt.2022.113532

Gauthier, M. J. (1977). *Alteromonas citrea*, a New Gram-Negative, Yellow-Pigmented Species from Seawater. *International Journal of Systematic Bacteriology*, *27*(4), 349–354. https://doi.org/10.1099/00207713-27-4-349

Gauthier, M. J., & Breittmayer, V. A. (1979). A New Antibiotic-Producing Bacterium from Seawater: *Alteromonas aurantia* sp. nov. *International Journal of Systematic Bacteriology*, *29*(4), 366–372. https://doi.org/10.1099/00207713-29-4-366

Gedikli, S., Güngör, G., Toptaş, Y., Sezgin, D. E., Demirbilek, M., Yazıhan, N., Aytar Çelik, P., Denkbaş, E. B., Bütün, V., & Çabuk, A. (2018). Optimization of hyaluronic acid production and its cytotoxicity and degradability characteristics. *Preparative Biochemistry and Biotechnology*, 1–9. https://doi.org/10.1080/10826068.2018.1476885

Ghelich, R., Jahannama, M. R., Abdizadeh, H., Torknik, F. S., & Vaezi, M. R. (2019). Central composite design (CCD)-Response surface methodology (RSM) of effective electrospinning parameters on PVP-B-Hf hybrid nanofibrous composites for synthesis of HfB2-based composite nanofibers. *Composites Part B: Engineering*, *166*, 527–541. https://doi.org/10.1016/j.compositesb.2019.01.094

González-Garcinuño, Á., Masa, R., Hernández, M., Domínguez, Á., Tabernero, A., & del Valle, E. (2019). Levan-Capped Silver Nanoparticles for Bactericidal Formulations: Release and Activity Modelling. *International Journal of Molecular Sciences*, *20*(6), 1502. https://doi.org/10.3390/ijms20061502

Grinev, V. S., Tregubova, K. V., Anis'kov, A. A., Sigida, E. N., Shirokov, A. A., Fedonenko, Y. P., & Yegorenkova, I. V. (2020). Isolation, structure, and potential biotechnological applications of the exopolysaccharide from *Paenibacillus polymyxa* 92. *Carbohydrate Polymers*, *232*, 115780. https://doi.org/10.1016/j.carbpol.2019.115780

Gruppuso, M., Turco, G., Marsich, E., & Porrelli, D. (2021). Polymeric wound dressings, an insight into polysaccharide-based electrospun membranes. *Applied Materials Today*, *24*, 101148. https://doi.org/10.1016/j.apmt.2021.101148

Gu, J., Zhang, H., Zhang, J., Wen, C., Zhou, J., Yao, H., He, Y., Ma, H., & Duan, Y. (2020). Optimization, characterization, rheological study and immune activities of polysaccharide from *Sagittaria sagittifolia* L. *Carbohydrate Polymers*, *246*, 116595. https://doi.org/10.1016/j.carbpol.2020.116595

Guerreiro, B. M., Freitas, F., Lima, J. C., Silva, J. C., Dionísio, M., & Reis, M. A. M. (2020). Demonstration of the cryoprotective properties of the fucose-containing polysaccharide FucoPol. *Carbohydrate Polymers*, *245*, 116500.

https://doi.org/10.1016/j.carbpol.2020.116500

Guerrini, F., Cangini, M., Boni, L., Trost, P., & Pistocchi, R. (2000). Metabolic responses of the diatom *Achnanthes brevipes* (Bacillariophyceae) to nutrient limitation. *Journal of Phycology*, *36*(5), 882–890. https://doi.org/10.1046/j.1529-8817.2000.99070.x

Guezennec, J. (2002). Deep-sea hydrothermal vents: A new source of innovative bacterial exopolysaccharides of biotechnological interest? *Journal of Industrial Microbiology and Biotechnology*, *29*(4), 204–208. https://doi.org/10.1038/sj.jim.7000298

Guezennec, J., Herry, J. M., Kouzayha, A., Bachere, E., Mittelman, M. W., & Bellon Fontaine, M. N. (2012). Exopolysaccharides from unusual marine environments inhibit early stages of biofouling. *International Biodeterioration & Biodegradation*, *66*(1), 1–7. https://doi.org/10.1016/j.ibiod.2011.10.004

Guézennec, J., Moppert, X., Raguénès, G., Richert, L., Costa, B., & Simon-Colin, C. (2011). Microbial mats in French Polynesia and their biotechnological applications. *Process Biochemistry*, *46*(1), 16–22. https://doi.org/10.1016/j.procbio.2010.09.001

Guillard, R. R. L., & Ryther, J. H. (1962). Studies of marine planktonic diatoms. I. *Cyclotella nana* Hustedt, and *Detonula confervacea* (cleve) Gran. *Canadian Journal of Microbiology*, *8*(2), 229–239. https://doi.org/10.1139/m62-029

Guzmán, S., Gato, A., Lamela, M., Freire-Garabal, M., & Calleja, J. M. (2003). Anti-inflammatory and immunomodulatory activities of polysaccharide from *Chlorella stigmatophora* and *Phaeodactylum tricornutum*: Anti-inflammatory and immunomodulatory activities. *Phytotherapy Research*, *17*(6), 665–670. https://doi.org/10.1002/ptr.1227

Hamed, M., Coelho, E., Bastos, R., Evtuguin, D. V., Ferreira, S. S., Lima, T., Vilanova, M., Sila, A., Coimbra, M. A., & Bougatef, A. (2022). Isolation and identification of an arabinogalactan extracted from pistachio external hull: Assessment of immunostimulatory activity. *Food Chemistry*, *373*, 131416. https://doi.org/10.1016/j.foodchem.2021.131416

Hamidi, M., Kozani, P. S., Kozani, P. S., Pierre, G., Michaud, P., & Delattre, C. (2019). Marine Bacteria versus Microalgae: Who Is the Best for Biotechnological Production of Bioactive Compounds with Antioxidant Properties and Other Biological Applications? *Marine Drugs*, *18*(1), 28. https://doi.org/10.3390/md18010028

Han, M., Du, C., Xu, Z.-Y., Qian, H., & Zhang, W.-G. (2016). Rheological properties of phosphorylated exopolysaccharide produced by *Sporidiobolus pararoseus* JD-2. *International Journal of Biological Macromolecules*, *88*, 603–613. https://doi.org/10.1016/j.ijbiomac.2016.04.035

Hasui, M., Matsuda, M., Okutani, K., & Shigeta, S. (1995). *In vitro* antiviral activities of sulfated polysaccharides from a marine microalga (*Cochlodinium polykrikoides*) against human immunodeficiency virus and other enveloped viruses. *International Journal of Biological Macromolecules*, *17*(5), 293–297. https://doi.org/10.1016/0141-8130(95)98157-T

Hasui, M., Matsuda, M., Yoshimatsu, S., & Okutani, K. (1995). Production of a Lactate-Associated Galactan Sulfate by a Dinoflagellate *Gymnodinium* A_3. *Fisheries Science*, *61*(2), 321–326. https://doi.org/10.2331/fishsci.61.321

Hilliou, L., Freitas, F., Oliveira, R., Reis, M. A. M., Lespineux, D., Grandfils, C., & Alves, V. D. (2009). Solution properties of an exopolysaccharide from a *Pseudomonas* strain obtained using glycerol as sole carbon source. *Carbohydrate Polymers*, *78*(3), 526–532. https://doi.org/10.1016/j.carbpol.2009.05.011

Hoppe, A., Güldal, N. S., & Boccaccini, A. R. (2011). A review of the biological response to ionic dissolution products from bioactive glasses and glass-ceramics. *Biomaterials*, *32*(11), 2757–2774. https://doi.org/10.1016/j.biomaterials.2011.01.004

Hu, H., & Xu, F.-J. (2020). Rational design and latest advances of polysaccharide-based hydrogels for wound healing. *Biomater. Sci.*, *8*(8), 2084–2101. https://doi.org/10.1039/D0BM00055H

Hu, Y., Jeong, D., Kim, Y., Kim, S., & Jung, S. (2020). Preparation of Succinoglycan Hydrogel Coordinated With Fe^{3+} Ions for Controlled Drug Delivery. *Polymers*, *12*(4), 977. https://doi.org/10.3390/polym12040977

Huang, H., & Yang, X. (2004). Synthesis of polysaccharide-stabilized gold and silver nanoparticles: A green method. *Carbohydrate Research*, *339*(15), 2627–2631. https://doi.org/10.1016/j.carres.2004.08.005

Hui, E., Gimeno, K. I., Guan, G., & Caliari, S. R. (2019). Spatiotemporal Control of Viscoelasticity in Phototunable Hyaluronic Acid Hydrogels. *Biomacromolecules*, *20*(11), 4126–4134. https://doi.org/10.1021/acs.biomac.9b00965

Insulkar, P., Kerkar, S., & Lele, S. S. (2018). Purification and structural-functional characterization of an exopolysaccharide from *Bacillus licheniformis* PASS26 with in-vitro antitumor and wound healing activities. *International Journal of Biological Macromolecules*, *120*, 1441–1450. https://doi.org/10.1016/j.ijbiomac.2018.09.147

Ivanova, E. P., Kiprianova, E. A., Mikhailov, V. V., Levanova, G. F., Garagulya, A. D., Gorshkova, N. M., Yumoto, N., & Yoshikawa, S. (1996). Characterization and Identification of Marine *Alteromonas nigrifaciens* Strains and Emendation of the Description. *International Journal of Systematic Bacteriology*, *46*(1), 223–228. https://doi.org/10.1099/00207713-46-1-223

Jajesniak, P., Omar Ali, H. E. M., & Wong, T. S. (2014). Carbon Dioxide Capture and Utilization using Biological Systems: Opportunities and Challenges. *Journal of Bioprocessing & Biotechniques*, *04*(03). https://doi.org/10.4172/2155-9821.1000155

Jayawardena, T. U., Sanjeewa, K. K. A., Nagahawatta, D. P., Lee, H.-G., Lu, Y.-A., Vaas, A. P. J. P., Abeytunga, D. T. U., Nanayakkara, C. M., Lee, D.-S., & Jeon, Y.-J. (2020). Anti-Inflammatory Effects of Sulfated Polysaccharide from *Sargassum swartzii* in Macrophages via Blocking TLR/NF-Kb Signal Transduction. *Marine Drugs*, *18*(12), 601. https://doi.org/10.3390/md18120601

Jesus Raposo, M. F., Morais, A. M. M. B., & Morais, R. M. S. C. (2014). Bioactivity and Applications of Polysaccharides from Marine Microalgae. In K. G. Ramawat & J.-M. Mérillon (Eds.), *Polysaccharides* (pp. 1–38). Springer International Publishing. https://doi.org/10.1007/978-3-319-03751-6_47-1

Jesus Raposo, M., Morais, A., & Morais, R. (2015). Marine Polysaccharides from Algae with Potential Biomedical Applications. *Marine Drugs*, *13*(5), 2967–3028. https://doi.org/10.3390/md13052967

Ji, S., Li, H., Wang, G., Lu, T., Ma, W., Wang, J., Zhu, H., & Xu, H. (2020). Rheological behaviors of a novel exopolysaccharide produced by *Sphingomonas* WG and the potential application in enhanced oil recovery. *International Journal of Biological Macromolecules*, *162*, 1816–1824.
https://doi.org/10.1016/j.ijbiomac.2020.08.114

Jia, X., Liu, Q., Zou, S., Xu, X., & Zhang, L. (2015). Construction of selenium nanoparticles/β-glucan composites for enhancement of the antitumor activity. *Carbohydrate Polymers*, *117*, 434–442. https://doi.org/10.1016/j.carbpol.2014.09.088

Jiang, H., Wang, R., Zhou, F., Wu, Y., Li, S., Huo, G., Ye, J., Hua, C., & Wang, Z. (2022). Preparation, physicochemical characterization, and cytotoxicity of selenium nanoparticles stabilized by *Oudemansiella raphanipies* polysaccharide. *International Journal of Biological Macromolecules*, *211*, 35–46.
https://doi.org/10.1016/j.ijbiomac.2022.05.011

Joulak, I., Concórdio-Reis, P., Torres, C. A. V., Sevrin, C., Grandfils, C., Attia, H., Freitas, F., Reis, M. A. M., & Azabou, S. (2022). Sustainable use of agro-industrial wastes as potential feedstocks for exopolysaccharide production by selected *Halomonas* strains. *Environmental Science and Pollution Research*, *29*(15), 22043–22055. https://doi.org/10.1007/s11356-021-17207-w

Joulak, I., Finore, I., Nicolaus, B., Leone, L., Moriello, A. S., Attia, H., Poli, A., & Azabou, S. (2019). Evaluation of the production of exopolysaccharides by newly isolated *Halomonas* strains from Tunisian hypersaline environments. *International Journal of Biological Macromolecules*, *138*, 658–666.

https://doi.org/10.1016/j.ijbiomac.2019.07.128

Kaewprachu, P., Jaisan, C., Klunklin, W., Phongthai, S., Rawdkuen, S., & Tongdeesoontorn, W. (2022). Mechanical and Physicochemical Properties of Composite Biopolymer Films Based on Carboxymethyl Cellulose from Young Palmyra Palm Fruit Husk and Rice Flour. *Polymers*, *14*(9), 1872. https://doi.org/10.3390/polym14091872

Kamerling, J. P., Gerwig, G. J., Vliegenhart, J. F. G., & Clamp, J. R. (1975). Characterization by gas chromatography-mass spectrometry of pertrimethylsilyl glycosides obtained in the methanolysis of glycoproteins and glycolipids. *Biochemical Journal*, *151*, 491–495.

Kanamarlapudi, S. L. R. K., & Muddada, S. (2017). Characterization of Exopolysaccharide Produced by *Streptococcus thermophilus* CC30. *BioMed Research International*, *2017*, 1–11. https://doi.org/10.1155/2017/4201809

Kang, M., Oderinde, O., Liu, S., Huang, Q., Ma, W., Yao, F., & Fu, G. (2019). Characterization of Xanthan gum-based hydrogel with Fe^{3+} ions coordination and its reversible sol-gel conversion. *Carbohydrate Polymers*, *203*, 139–147. https://doi.org/10.1016/j.carbpol.2018.09.044

Kang, M.-C., Lee, H., Choi, H.-D., & Jeon, Y.-J. (2019). Antioxidant properties of a sulfated polysaccharide isolated from an enzymatic digest of *Sargassum thunbergii*. *International Journal of Biological Macromolecules*, *132*, 142–149. https://doi.org/10.1016/j.ijbiomac.2019.03.178

Kanmani, P., & Lim, S. T. (2013). Synthesis and structural characterization of silver nanoparticles using bacterial exopolysaccharide and its antimicrobial activity against food and multidrug resistant pathogens. *Process Biochemistry*, *48*(7), 1099–1106. https://doi.org/10.1016/j.procbio.2013.05.011

Khurana, A., Tekula, S., Saifi, M. A., Venkatesh, P., & Godugu, C. (2019). Therapeutic applications of selenium nanoparticles. *Biomedicine & Pharmacotherapy*, *111*, 802–812. https://doi.org/10.1016/j.biopha.2018.12.146

Kim, S., Cho, D.-H., Kweon, D.-K., Jang, E.-H., Hong, J.-Y., & Lim, S.-T. (2020). Improvement of mechanical properties of orodispersible hyaluronic acid film by carboxymethyl cellulose addition. *Food Science and Biotechnology*, *29*(9), 1233–1239. https://doi.org/10.1007/s10068-020-00771-1

Kim, S. J., Kim, B.-G., Park, H. J., & Yim, J. H. (2016). Cryoprotective properties and preliminary characterization of exopolysaccharide (P-Arcpo 15) produced by the Arctic bacterium *Pseudoalteromonas elyakovii* Arcpo 15. *Preparative Biochemistry and Biotechnology*, *46*(3), 261–266. https://doi.org/10.1080/10826068.2015.1015568

Kim, S. J., & Yim, J. H. (2007). Cryoprotective properties of exopolysaccharide (P-21653) produced by the Antarctic bacterium, *Pseudoalteromonas arctica* KOPRI 21653. *Journal of Microbiology (Seoul, Korea)*, *45*(6), 510–514.

Klosterhoff, R. R., Bark, J. M., Glänzel, N. M., Iacomini, M., Martinez, G. R., Winnischofer, S. M. B., & Cordeiro, L. M. C. (2018). Structure and intracellular antioxidant activity of pectic polysaccharide from acerola (*Malpighia emarginata*). *International Journal of Biological Macromolecules*, *106*, 473–480. https://doi.org/10.1016/j.ijbiomac.2017.08.032

Kong, H., Yang, J., Zhang, Y., Fang, Y., Nishinari, K., & Phillips, G. O. (2014). Synthesis and antioxidant properties of gum arabic-stabilized selenium nanoparticles. *International Journal of Biological Macromolecules*, *65*, 155–162. https://doi.org/10.1016/j.ijbiomac.2014.01.011

Kontogiorgos, V., Margelou, I., Georgiadis, N., & Ritzoulis, C. (2012). Rheological characterization of okra pectins. *Food Hydrocolloids*, *29*(2), 356–362. https://doi.org/10.1016/j.foodhyd.2012.04.003

Kumar, A. S., Mody, K., & Jha, B. (2007). Bacterial exopolysaccharides – a perception. *Journal of Basic Microbiology*, *47*(2), 103–117. https://doi.org/10.1002/jobm.200610203

Kumar, S. S. D., Rajendran, N. K., Houreld, N. N., & Abrahamse, H. (2018). Recent advances on silver nanoparticle and biopolymer-based biomaterials for wound healing applications. *International Journal of Biological Macromolecules*, *115*, 165–175. https://doi.org/10.1016/j.ijbiomac.2018.04.003

Kumari, Y., Singh, S. K., Kumar, R., Kumar, B., Kaur, G., Gulati, M., Tewari, D., Gowthamarajan, K., Karri, V. V. S. N. R., Ayinkamiye, C., Khursheed, R., Awasthi, A., Pandey, N. K., Mohanta, S., Gupta, S., Corrie, L., Patni, P., Kumar, R., & Kumar, R. (2020). Modified apple polysaccharide capped gold nanoparticles for oral delivery of insulin. *International Journal of Biological Macromolecules*, *149*, 976–988. https://doi.org/10.1016/j.ijbiomac.2020.01.302

Lagaron, J. M., Catalá, R., & Gavara, R. (2004). Structural characteristics defining high barrier properties in polymeric materials. *Materials Science and Technology*, *20*(1), 1–7. https://doi.org/10.1179/026708304225010442

Laroche, C. (2022). Exopolysaccharides from Microalgae and Cyanobacteria: Diversity of Strains, Production Strategies, and Applications. *Marine Drugs*, *20*(5), 336. https://doi.org/10.3390/md20050336

Laubach, J., Joseph, M., Brenza, T., Gadhamshetty, V., & Sani, R. K. (2021). Exopolysaccharide and biopolymer-derived films as tools for transdermal drug delivery. *Journal of Controlled Release*, *329*, 971–987.

https://doi.org/10.1016/j.jconrel.2020.10.027

Le Costaouëc, T., Cérantola, S., Ropartz, D., Ratiskol, J., Sinquin, C., Colliec-Jouault, S., & Boisset, C. (2012). Structural data on a bacterial exopolysaccharide produced by a deep-sea *Alteromonas macleodii* strain. *Carbohydrate Polymers*, *90*(1), 49–59. https://doi.org/10.1016/j.carbpol.2012.04.059

Lee, J.-B., Hayashi, K., Hirata, M., Kuroda, E., Suzuki, E., Kubo, Y., & Hayashi, T. (2006). Antiviral Sulfated Polysaccharide from *Navicula directa*, a Diatom Collected from Deep-Sea Water in Toyama Bay. *Biological & Pharmaceutical Bulletin*, *29*(10), 2135–2139. https://doi.org/10.1248/bpb.29.2135

Levy-Ontman, O., Huleihel, M., Hamias, R., Wolak, T., & Paran, E. (2017). An anti-inflammatory effect of red microalga polysaccharides in coronary artery endothelial cells. *Atherosclerosis*, *264*, 11–18.
https://doi.org/10.1016/j.atherosclerosis.2017.07.017

Li, H., & Hou, W. (2011). Influences of pH and electrolyte on the rheological properties of aqueous solution of exopolysaccharide secreted by a deep-sea mesophilic bacterium. *Food Hydrocolloids*, *25*(6), 1547–1553.
https://doi.org/10.1016/j.foodhyd.2011.01.014

Li, J., Shen, B., Nie, S., Duan, Z., & Chen, K. (2019). A combination of selenium and polysaccharides: Promising therapeutic potential. *Carbohydrate Polymers*, *206*, 163–173. https://doi.org/10.1016/j.carbpol.2018.10.088

Li, J., Xu, H., Chen, X., Xu, L., Cheng, R., Zhang, J., & Wang, S. (2017). Characterization of an exopolysaccharide with distinct rheological properties from *Paenibacillus edaphicus* NUST16. *International Journal of Biological Macromolecules*, *105*, 1–8. https://doi.org/10.1016/j.ijbiomac.2017.06.030

Li, S., Ma, Y., Ji, T., Sameen, D. E., Ahmed, S., Qin, W., Dai, J., Li, S., & Liu, Y. (2020). Cassava starch/carboxymethylcellulose edible films embedded with lactic acid bacteria to extend the shelf life of banana. *Carbohydrate Polymers*, *248*, 116805. https://doi.org/10.1016/j.carbpol.2020.116805

Liu, G., Yang, X., Zhang, J., Liang, L., Miao, F., Ji, T., Ye, Z., Chu, M., Ren, J., & Xu, X. (2021). Synthesis, stability and anti-fatigue activity of selenium nanoparticles stabilized by *Lycium barbarum* polysaccharides. *International Journal of Biological Macromolecules*, *179*, 418–428. https://doi.org/10.1016/j.ijbiomac.2021.03.018

Liu, L., Pohnert, G., & Wei, D. (2016). Extracellular Metabolites from Industrial Microalgae and Their Biotechnological Potential. *Marine Drugs*, *14*(10), 191. https://doi.org/10.3390/md14100191

Liu, S.-B., Chen, X.-L., He, H.-L., Zhang, X.-Y., Xie, B.-B., Yu, Y., Chen, B., Zhou, B.-C., & Zhang, Y.-Z. (2013). Structure and Ecological Roles of a Novel

Exopolysaccharide from the Arctic Sea Ice Bacterium *Pseudoalteromonas* sp. Strain SM20310. *Applied and Environmental Microbiology*, *79*(1), 224–230. https://doi.org/10.1128/AEM.01801-12

Liu, X., Zhang, M., Liu, H., Zhou, A., Cao, Y., & Liu, X. (2018). Preliminary characterization of the structure and immunostimulatory and anti-aging properties of the polysaccharide fraction of *Haematococcus pluvialis*. *RSC Advances*, *8*(17), 9243–9252. https://doi.org/10.1039/C7RA11153C

Liu, Y., Zeng, S., Liu, Y., Wu, W., Shen, Y., Zhang, L., Li, C., Chen, H., Liu, A., Shen, L., Hu, B., & Wang, C. (2018). Synthesis and antidiabetic activity of selenium nanoparticles in the presence of polysaccharides from *Catathelasma ventricosum*. *International Journal of Biological Macromolecules*, *114*, 632–639. https://doi.org/10.1016/j.ijbiomac.2018.03.161

Llamas, I., Mata, J. A., Tallon, R., Bressollier, P., Urdaci, M. C., Quesada, E., & Béjar, V. (2010). Characterization of the Exopolysaccharide Produced by Salipiger mucosus A3T, a Halophilic Species Belonging to the Alphaproteobacteria, Isolated on the Spanish Mediterranean Seaboard. *Marine Drugs*, *8*(8), 2240–2251. https://doi.org/10.3390/md8082240

Lo, Y. M., Robbins, K. L., Argin-Soysal, S., & Sadar, L. N. (2003). Viscoelastic Effects on the Diffusion Properties of Curdlan Gels. *Journal of Food Science*, *68*(6), 2057–2065. https://doi.org/10.1111/j.1365-2621.2003.tb07018.x

Loaëc, M., Olier, R., & Guezennec, J. (1998). Chelating properties of bacterial exopolysaccharides from deep-sea hydrothermal vents. *Carbohydrate Polymers*, *35*(1–2), 65–70. https://doi.org/10.1016/S0144-8617(97)00109-4

López, O. V., & García, M. A. (2012). Starch films from a novel (Pachyrhizus ahipa) and conventional sources: Development and characterization. *Materials Science and Engineering: C*, *32*(7), 1931–1940. https://doi.org/10.1016/j.msec.2012.05.035

Lu, S., Xia, D., Huang, G., Jing, H., Wang, Y., & Gu, H. (2010). Concentration effect of gold nanoparticles on proliferation of keratinocytes. *Colloids and Surfaces B: Biointerfaces*, *81*(2), 406–411. https://doi.org/10.1016/j.colsurfb.2010.06.019

Maalej, H., Hmidet, N., Boisset, C., Bayma, E., Heyraud, A., & Nasri, M. (2016). Rheological and emulsifying properties of a gel-like exopolysaccharide produced by *Pseudomonas stutzeri* AS22. *Food Hydrocolloids*, *52*, 634–647. https://doi.org/10.1016/j.foodhyd.2015.07.010

Maalej, H., Moalla, D., Boisset, C., Bardaa, S., Ayed, H. B., Sahnoun, Z., Rebai, T., Nasri, M., & Hmidet, N. (2014). Rhelogical, dermal wound healing and *in vitro* antioxidant properties of exopolysaccharide hydrogel from *Pseudomonas stutzeri* AS22. *Colloids and Surfaces B: Biointerfaces*, *123*, 814–824.

https://doi.org/10.1016/j.colsurfb.2014.10.017

Magaletti, E., Urbani, R., Sist, P., Ferrari, C. R., & Cicero, A. M. (2004). Abundance and chemical characterization of extracellular carbohydrates released by the marine diatom *Cylindrotheca fusiformis* under N- and P-limitation. *European Journal of Phycology*, *39*(2), 133–142. https://doi.org/10.1080/0967026042000202118

Mandal, S. K., Singh, R. P., & Patel, V. (2011). Isolation and Characterization of Exopolysaccharide Secreted by a Toxic Dinoflagellate, *Amphidinium carterae* Hulburt 1957 and Its Probable Role in Harmful Algal Blooms (HABs). *Microbial Ecology*, *62*(3), 518–527. https://doi.org/10.1007/s00248-011-9852-5

Manivasagan, P., Kang, K.-H., Kim, D. G., & Kim, S.-K. (2015). Production of polysaccharide-based bioflocculant for the synthesis of silver nanoparticles by *Streptomyces* sp. *International Journal of Biological Macromolecules*, *77*, 159–167. https://doi.org/10.1016/j.ijbiomac.2015.03.022

Markou, G., & Nerantzis, E. (2013). Microalgae for high-value compounds and biofuels production: A review with focus on cultivation under stress conditions. *Biotechnology Advances*, *31*(8), 1532–1542.
https://doi.org/10.1016/j.biotechadv.2013.07.011

Marques, M. S., Zepon, K. M., Heckler, J. M., Morisso, F. D. P., da Silva Paula, M. M., & Kanis, L. A. (2019). One-pot synthesis of gold nanoparticles embedded in polysaccharide-based hydrogel: Physical-chemical characterization and feasibility for large-scale production. *International Journal of Biological Macromolecules*, *124*, 838–845. https://doi.org/10.1016/j.ijbiomac.2018.11.231

Martínez-Checa, F., Béjar, V., Llamas, I., del Moral, A., & Quesada, E. (2005). Alteromonas hispanica sp. Nov., a polyunsaturated-fatty-acid-producing, halophilic bacterium isolated from Fuente de Piedra, southern Spain. *International Journal of Systematic and Evolutionary Microbiology*, *55*(6), 2385–2390.
https://doi.org/10.1099/ijs.0.63809-0

Martínez-Checa, F., Toledo, F. L., El Mabrouki, K., Quesada, E., & Calvo, C. (2007). Characteristics of bioemulsifier V2-7 synthesized in culture media added of hydrocarbons: Chemical composition, emulsifying activity and rheological properties. *Bioresource Technology*, *98*(16), 3130–3135.
https://doi.org/10.1016/j.biortech.2006.10.026

Martínez-Gómez, K., Flores, N., Castañeda, H. M., Martínez-Batallar, G., Hernández-Chávez, G., Ramírez, O. T., Gosset, G., Encarnación, S., & Bolivar, F. (2012). New insights into *Escherichia coli* metabolism: Carbon scavenging, acetate metabolism and carbon recycling responses during growth on glycerol. *Microbial Cell Factories*, *11*(1), 46. https://doi.org/10.1186/1475-2859-11-46

Martínez-Ruvalcaba, A., Chornet, E., & Rodrigue, D. (2007). Viscoelastic properties of dispersed chitosan/xanthan hydrogels. *Carbohydrate Polymers*, *67*(4), 586–595. https://doi.org/10.1016/j.carbpol.2006.06.033

Martin-Pastor, M., Ferreira, A. S., Moppert, X., Nunes, C., Coimbra, M. A., Reis, R. L., Guezennec, J., & Novoa-Carballal, R. (2019). Structure, rheology, and copper-complexation of a hyaluronan-like exopolysaccharide from *Vibrio*. *Carbohydrate Polymers*, *222*, 114999. https://doi.org/10.1016/j.carbpol.2019.114999

Massana Roquero, D., Othman, A., Melman, A., & Katz, E. (2022). Iron(III)-cross-linked alginate hydrogels: A critical review. *Materials Advances*, *3*(4), 1849–1873. https://doi.org/10.1039/D1MA00959A

Mata, J. A., Bjar, V., Bressollier, P., Tallon, R., Urdaci, M. C., Quesada, E., & Llamas, I. (2008). Characterization of exopolysaccharides produced by three moderately halophilic bacteria belonging to the family Alteromonadaceae. *Journal of Applied Microbiology*, *105*(2), 521–528. https://doi.org/10.1111/j.1365-2672.2008.03789.x

Matos, M. S., Romero-Díez, R., Álvarez, A., Bronze, M. R., Rodríguez-Rojo, S., Mato, R. B., Cocero, M. J., & Matias, A. A. (2019). Polyphenol-Rich Extracts Obtained from Winemaking Waste Streams as Natural Ingredients with Cosmeceutical Potential. *Antioxidants*, *8*(9), 355. https://doi.org/10.3390/antiox8090355

Matsuda, M., Yamori, T., Naitoh, M., & Okutani, K. (2003). Structural Revision of Sulfated Polysaccharide B-1 Isolated from a Marine *Pseudomonas* Species and Its Cytotoxic Activity Against Human Cancer Cell Lines. *Marine Biotechnology*, *5*(1), 13–19. https://doi.org/10.1007/s10126-002-0046-5

Matsui, M. S., Muizzuddin, N., Arad, S., & Marenus, K. (2003). Sulfated Polysaccharides from Red Microalgae Have Antiinflammatory Properties *In Vitro* and *In Vivo*. *Applied Biochemistry and Biotechnology*, *104*(1), 13–22. https://doi.org/10.1385/ABAB:104:1:13

Matsuyama, H., Minami, H., Sakaki, T., Kasahara, H., Baba, S., Ishimaru, S., Hirota, K., & Yumoto, I. (2015). *Alteromonas gracilis* sp. Nov., a marine polysaccharide-producing bacterium. *International Journal of Systematic and Evolutionary Microbiology*, *65*(Pt_5), 1498–1503. https://doi.org/10.1099/ijs.0.000127

Medhat, D., Hussein, J., El-Naggar, M. E., Attia, M. F., Anwar, M., Latif, Y. A., Booles, H. F., Morsy, S., Farrag, A. R., Khalil, W. K. B., & El-Khayat, Z. (2017). Effect of Au-dextran NPs as anti-tumor agent against EAC and solid tumor in mice by biochemical evaluations and histopathological investigations. *Biomedicine & Pharmacotherapy*, *91*, 1006–1016. https://doi.org/10.1016/j.biopha.2017.05.043

Medina-Cabrera, E. V., Gansbiller, M., Rühmann, B., Schmid, J., & Sieber, V. (2021). Rheological characterization of *Porphyridium sordidum* and *Porphyridium purpureum* exopolysaccharides. *Carbohydrate Polymers*, *253*, 117237. https://doi.org/10.1016/j.carbpol.2020.117237

Medina-Cabrera, E. V., Rühmann, B., Schmid, J., & Sieber, V. (2020). Characterization and comparison of *Porphyridium sordidum* and *Porphyridium purpureum* concerning growth characteristics and polysaccharide production. *Algal Research*, *49*, 101931. https://doi.org/10.1016/j.algal.2020.101931

Miao, M., Huang, C., Jia, X., Cui, S. W., Jiang, B., & Zhang, T. (2015). Physicochemical characteristics of a high molecular weight bioengineered α-D-glucan from *Leuconostoc citreum* SK24.002. *Food Hydrocolloids*, *50*, 37–43. https://doi.org/10.1016/j.foodhyd.2015.04.009

Mishra, A., & Jha, B. (2009). Isolation and characterization of extracellular polymeric substances from micro-algae *Dunaliella salina* under salt stress. *Bioresource Technology*, *100*(13), 3382–3386. https://doi.org/10.1016/j.biortech.2009.02.006

Montreuil, J., Bouquelet, S., Debray, H., Fournet, B., Spik, G., & Strecker, G. (1986). Glycoproteins. In *Carbohydrate Analysis: A Practical Approach* (Chaplin, M.F. and Kennedy, J.K., pp. 143–204). IRL Press.

More, T. T., Yadav, J. S. S., Yan, S., Tyagi, R. D., & Surampalli, R. Y. (2014). Extracellular polymeric substances of bacteria and their potential environmental applications. *Journal of Environmental Management*, *144*, 1–25. https://doi.org/10.1016/j.jenvman.2014.05.010

Morris, V. J., & Chilvers, G. R. (1983). Rheological studies of specific cation forms of kappa carrageenan gels. *Carbohydrate Polymers*, *3*(2), 129–141. https://doi.org/10.1016/0144-8617(83)90003-6

Moscovici, M. (2015). Present and future medical applications of microbial exopolysaccharides. *Frontiers in Microbiology*, *6*. https://doi.org/10.3389/fmicb.2015.01012

Mota, R., Guimarães, R., Büttel, Z., Rossi, F., Colica, G., Silva, C. J., Santos, C., Gales, L., Zille, A., De Philippis, R., Pereira, S. B., & Tamagnini, P. (2013). Production and characterization of extracellular carbohydrate polymer from *Cyanothece* sp. CCY 0110. *Carbohydrate Polymers*, *92*(2), 1408–1415. https://doi.org/10.1016/j.carbpol.2012.10.070

Naraginti, S., Kumari, P. L., Das, R. K., Sivakumar, A., Patil, S. H., & Andhalkar, V. V. (2016). Amelioration of excision wounds by topical application of green synthesized, formulated silver and gold nanoparticles in albino Wistar rats. *Materials Science and Engineering: C*, *62*, 293–300. https://doi.org/10.1016/j.msec.2016.01.069

Navarro Gallón, S. M., Alpaslan, E., Wang, M., Larese-Casanova, P., Londoño, M. E., Atehortúa, L., Pavón, J. J., & Webster, T. J. (2019). Characterization and study of the antibacterial mechanisms of silver nanoparticles prepared with microalgal exopolysaccharides. *Materials Science and Engineering: C*. https://doi.org/10.1016/j.msec.2019.01.134

Netsopa, S., Niamsanit, S., Sakloetsakun, D., & Milintawisamai, N. (2018). Characterization and Rheological Behavior of Dextran from *Weissella confusa* R003. *International Journal of Polymer Science*, *2018*, 1–10. https://doi.org/10.1155/2018/5790526

Nichols, C. A. M., Guezennec, J., & Bowman, J. P. (2005). Bacterial Exopolysaccharides from Extreme Marine Environments with Special Consideration of the Southern Ocean, Sea Ice, and Deep-Sea Hydrothermal Vents: A Review. *Marine Biotechnology*, *7*(4), 253–271. https://doi.org/10.1007/s10126-004-5118-2

Nichols, C. M., Lardière, S. G., Bowman, J. P., Nichols, P. D., A.E. Gibson, J., & Guézennec, J. (2005). Chemical Characterization of Exopolysaccharides from Antarctic Marine Bacteria. *Microbial Ecology*, *49*(4), 578–589. https://doi.org/10.1007/s00248-004-0093-8

Nicoletti, M. (2016). Microalgae Nutraceuticals. *Foods*, *5*(3), 54. https://doi.org/10.3390/foods5030054

Niculescu, A.-G., & Grumezescu, A. M. (2022). An Up-to-Date Review of Biomaterials Application in Wound Management. *Polymers*, *14*(3), 421. https://doi.org/10.3390/polym14030421

Norton, C. F., & Jones, G. E. (1969). A marine isolate of *Pseudomonas nigrifaciens*: II. Characterization of its blue pigment. *Archiv Für Mikrobiologie*, *64*(4), 369–376. https://doi.org/10.1007/BF00417018

Núñez-Pons, L., Avila, C., Romano, G., Verde, C., & Giordano, D. (2018). UV-Protective Compounds in Marine Organisms from the Southern Ocean. *Marine Drugs*, *16*(9), 336. https://doi.org/10.3390/md16090336

Nwodo, U., Green, E., & Okoh, A. (2012). Bacterial Exopolysaccharides: Functionality and Prospects. *International Journal of Molecular Sciences*, *13*(12), 14002–14015. https://doi.org/10.3390/ijms131114002

Olafsdottir, A., Thorlacius, G. E., Omarsdottir, S., Olafsdottir, E. S., Vikingsson, A., Freysdottir, J., & Hardardottir, I. (2014). A heteroglycan from the cyanobacterium *Nostoc commune* modulates LPS-induced inflammatory cytokine secretion by THP-1 monocytes through phosphorylation of ERK1/2 and Akt. *Phytomedicine*, *21*(11), 1451–1457. https://doi.org/10.1016/j.phymed.2014.04.023

Olivas, G. I., & Barbosa-Cánovas, G. V. (2008). Alginate–calcium films: Water vapor permeability and mechanical properties as affected by plasticizer and relative humidity. *LWT - Food Science and Technology*, *41*(2), 359–366. https://doi.org/10.1016/j.lwt.2007.02.015

Oppenheimer, C. H., & Zobell, C. E. (1952). The growth and viability of sixty-three species of marine bacteria as influenced by hydrostatic pressure. *J. Mar. Res.*, *11*, 10–18.

Overmann, J., & Lepleux, C. (2016). Marine Bacteria and Archaea: Diversity, Adaptations, and Culturability. In L. J. Stal & M. S. Cretoiu (Eds.), *The Marine Microbiome* (pp. 21–55). Springer International Publishing. https://doi.org/10.1007/978-3-319-33000-6_2

Pagano, C., Puglia, D., Luzi, F., Michele, A. D., Scuota, S., Primavilla, S., Ceccarini, M. R., Beccari, T., Iborra, C. A. V., Ramella, D., Ricci, M., & Perioli, L. (2021). Development and Characterization of Xanthan Gum and Alginate Based Bioadhesive Film for Pycnogenol Topical Use in Wound Treatment. *Pharmaceutics*, *13*(3), 324. https://doi.org/10.3390/pharmaceutics13030324

Pandeirada, C. O., Maricato, É., Ferreira, S. S., Correia, V. G., Pinheiro, B. A., Evtuguin, D. V., Palma, A. S., Correia, A., Vilanova, M., Coimbra, M. A., & Nunes, C. (2019). Structural analysis and potential immunostimulatory activity of *Nannochloropsis oculata* polysaccharides. *Carbohydrate Polymers*, *222*, 114962. https://doi.org/10.1016/j.carbpol.2019.06.001

Parani, M., Lokhande, G., Singh, A., & Gaharwar, A. K. (2016). Engineered Nanomaterials for Infection Control and Healing Acute and Chronic Wounds. *ACS Applied Materials & Interfaces*, *8*(16), 10049–10069. https://doi.org/10.1021/acsami.6b00291

Parikh, A., & Madamwar, D. (2006). Partial characterization of extracellular polysaccharides from cyanobacteria. *Bioresource Technology*, *97*(15), 1822–1827. https://doi.org/10.1016/j.biortech.2005.09.008

Passos, C. P., & Coimbra, M. A. (2013). Microwave superheated water extraction of polysaccharides from spent coffee grounds. *Carbohydrate Polymers*, *94*(1), 626–633.

Paz-Samaniego, R., Carvajal-Millan, E., Brown-Bojorquez, F., Rascón-Chu, A., López-Franco, Y. L., Sotelo-Cruz, N., & Lizardi-Mendoza, J. (2015). Gelation of Arabinoxylans from Maize Wastewater—Effect of Alkaline Hydrolysis Conditions on the Gel Rheology and Microstructure. In M. Samer (Ed.), *Wastewater Treatment Engineering*. InTech. https://doi.org/10.5772/61022

Pereira, J. R., Araújo, D., Freitas, P., Marques, A. C., Alves, V. D., Sevrin, C., Grandfils, C., Fortunato, E., Reis, M. A. M., & Freitas, F. (2021). Production of medium-chain-length polyhydroxyalkanoates by *Pseudomonas chlororaphis* subsp. aurantiaca: Cultivation on fruit pulp waste and polymer characterization. *International Journal of Biological Macromolecules*, *167*, 85–92. https://doi.org/10.1016/j.ijbiomac.2020.11.162

Pettolino, F. A., Walsh, C., Fincher, G. B., & A. Bacic. (2012). Determining the polysaccharide composition of plant cell walls. *Nature Protocols*, *7*(9), 1590–1607.

Phélippé, M., Gonçalves, O., Thouand, G., Cogne, G., & Laroche, C. (2019). Characterization of the polysaccharides chemical diversity of the cyanobacteria *Arthrospira platensis*. *Algal Research*, *38*, 101426.
https://doi.org/10.1016/j.algal.2019.101426

Piermaria, J. A., Pinotti, A., Garcia, M. A., & Abraham, A. G. (2009). Films based on kefiran, an exopolysaccharide obtained from kefir grain: Development and characterization. *Food Hydrocolloids*, *23*(3), 684–690.
https://doi.org/10.1016/j.foodhyd.2008.05.003

Poli, A., Anzelmo, G., & Nicolaus, B. (2010). Bacterial Exopolysaccharides from Extreme Marine Habitats: Production, Characterization and Biological Activities. *Marine Drugs*, *8*(6), 1779–1802. https://doi.org/10.3390/md8061779

Pooja, D., Panyaram, S., Kulhari, H., Rachamalla, S. S., & Sistla, R. (2014). Xanthan gum stabilized gold nanoparticles: Characterization, biocompatibility, stability and cytotoxicity. *Carbohydrate Polymers*, *110*, 1–9.
https://doi.org/10.1016/j.carbpol.2014.03.041

Pradeepa, Vidya, S. M., Mutalik, S., Udaya Bhat, K., Huilgol, P., & Avadhani, K. (2016). Preparation of gold nanoparticles by novel bacterial exopolysaccharide for antibiotic delivery. *Life Sciences*, *153*, 171–179.
https://doi.org/10.1016/j.lfs.2016.04.022

Qin, G., Zhu, L., Chen, X., Wang, P. G., & Zhang, Y. (2007). Structural characterization and ecological roles of a novel exopolysaccharide from the deep-sea psychrotolerant bacterium *Pseudoalteromonas* sp. SM9913. *Microbiology*, *153*(5), 1566–1572. https://doi.org/10.1099/mic.0.2006/003327-0

Qiu, W.-Y., Wang, Y.-Y., Wang, M., & Yan, J.-K. (2018). Construction, stability, and enhanced antioxidant activity of pectin-decorated selenium nanoparticles. *Colloids and Surfaces B: Biointerfaces*, *170*, 692–700.
https://doi.org/10.1016/j.colsurfb.2018.07.003

Raguénès, G., Cambon-Bonavita, M. A., Lohier, J. F., Boisset, C., & Guezennec, J. (2003). A Novel, Highly Viscous Polysaccharide Excreted by an *Alteromonas*

Isolated from a Deep-Sea Hydrothermal Vent Shrimp. *Current Microbiology*, *46*(6), 448–452. https://doi.org/10.1007/s00284-002-3922-3

Raguénès, G., Christen, R., Guezennec, J., Pignet, P., & Barbier, G. (1997). *Vibrio diabolicus* sp. Nov., a New Polysaccharide-Secreting Organism Isolated from a Deep-Sea Hydrothermal Vent Polychaete Annelid, Alvinella pompejana. *International Journal of Systematic Bacteriology*, *47*(4), 989–995. https://doi.org/10.1099/00207713-47-4-989

Raguénès, G. H. C., Peres, A., Ruimy, R., Pignet, P., Christen, R., Loaec, M., Rougeaux, H., Barbier, G., & Guezennec, J. G. (1997). *Alteromonas infernus* sp. Nov., a new polysaccharide-producing bacterium isolated from a deep-sea hydrothermal vent. *Journal of Applied Microbiology*, *82*(4), 422–430. https://doi.org/10.1046/j.1365-2672.1997.00125.x

Raguénès, G., Pignet, P., Gauthier, G., Peres, A., Christen, R., Rougeaux, H., Barbier, G., & Guezennec, J. (1996). Description of a new polymer-secreting bacterium from a deep-sea hydrothermal vent, *Alteromonas macleodii* subsp. Fijiensis, and preliminary characterization of the polymer. *Applied and Environmental Microbiology*, *62*(1), 67–73. https://doi.org/10.1128/aem.62.1.67-73.1996

Ramos, K. D. D. (2021). *Development of wound healing biomaterials based on bacterial exopolysaccharides* [Nova School of Science and Technology]. http://hdl.handle.net/10362/129170

Rana, S., & Upadhyay, L. S. B. (2020). Microbial exopolysaccharides: Synthesis pathways, types and their commercial applications. *International Journal of Biological Macromolecules*, *157*, 577–583. https://doi.org/10.1016/j.ijbiomac.2020.04.084

Raposo, M. F. de J., Morais, A. M. M. B., & Morais, R. M. S. C. (2014). Influence of sulphate on the composition and antibacterial and antiviral properties of the exopolysaccharide from *Porphyridium cruentum*. *Life Sciences*, *101*(1–2), 56–63. https://doi.org/10.1016/j.lfs.2014.02.013

Raposo, M., Morais, R., & Bernardo de Morais, A. (2013). Bioactivity and Applications of Sulphated Polysaccharides from Marine Microalgae. *Marine Drugs*, *11*(1), 233–252. https://doi.org/10.3390/md11010233

Rasulov, B., Rustamova, N., Yili, A., Zhao, H.-Q., & Aisa, H. A. (2015). Synthesis of silver nanoparticles on the basis of low and high molar mass exopolysaccharides of *Bradyrhizobium japonicum* 36 and its antimicrobial activity against some pathogens. *Folia Microbiologica*. https://doi.org/10.1007/s12223-015-0436-5

Raveendran, P., Fu, J., & Wallen, S. L. (2003). Completely “Green” Synthesis and Stabilization of Metal Nanoparticles. *Journal of the American Chemical Society*, *125*(46), 13940–13941. https://doi.org/10.1021/ja029267j

Rebocho, A. T., Freitas, F., Pereira, J. R., Neves, L. A., Alves, V. D., Sevrin, C., Grandfils, C., & Reis, M. A. (2019). Production of medium-chain length polyhydroxyalkanoates by *Pseudomonas citronellolis* grown in apple pulp waste. *Applied Food Biotechnology*, *6*(1). https://doi.org/10.22037/afb.v6i1.21793

Remya, N. S., Syama, S., Sabareeswaran, A., & Mohanan, P. V. (2016). Toxicity, toxicokinetics and biodistribution of dextran stabilized Iron oxide Nanoparticles for biomedical applications. *International Journal of Pharmaceutics*, *511*(1), 586–598. https://doi.org/10.1016/j.ijpharm.2016.06.119

Richardson, R. K., & Ross-Murphy, S. B. (1987). Non-linear viscoelasticity of polysaccharide solutions. 2: Xanthan polysaccharide solutions. *International Journal of Biological Macromolecules*, *9*(5), 257–264. https://doi.org/10.1016/0141-8130(87)90063-8

Rimington, C. (1931). The carbohydrate complex of serum protein II: Improved method for isolation and determination of structure. Isolation of glucosaminodimannose from protein of blood. *Biochemical Journal*, *25*, 1062–1071.

Roca, C., Alves, V. D., Freitas, F., & Reis, M. A. M. (2015). Exopolysaccharides enriched in rare sugars: Bacterial sources, production, and applications. *Frontiers in Microbiology*, *6*. https://doi.org/10.3389/fmicb.2015.00288

Roca, C., Lehmann, M., Torres, C. A. V., Baptista, S., Gaudêncio, S. P., Freitas, F., & Reis, M. A. M. (2016). Exopolysaccharide production by a marine *Pseudoalteromonas* sp. Strain isolated from Madeira Archipelago ocean sediments. *New Biotechnology*, *33*(4), 460–466. https://doi.org/10.1016/j.nbt.2016.02.005

Rodrigues, T. A. (2021). *Preparation and characterization of hydrogels based on biopolymers: FucoPol and Chitin-glucan complex (CGC)* [Nova School of Science and Technology]. http://hdl.handle.net/10362/115104

Rodríguez, S., Gatto, F., Pesce, L., Canale, C., Pompa, P. P., Bardi, G., Lopez, D., & Torres, F. G. (2018). Monitoring cell substrate interactions in exopolysaccharide-based films reinforced with chitin whiskers and starch nanoparticles used as cell substrates. *International Journal of Polymeric Materials and Polymeric Biomaterials*, *67*(6), 333–339. https://doi.org/10.1080/00914037.2017.1297942

Rodriguez, S., Torres, F. G., & López, D. (2017). Preparation and Characterization of Polysaccharide Films from the Cyanobacteria *Nostoc commune*. *Polymers from Renewable Resources*, *8*(4), 133–150. https://doi.org/10.1177/204124791700800401

Rougeaux, H., Talaga, P., Carlson, R. W., & Guezennec, J. (1998). Structural studies of an exopolysaccharide produced by *Alteromonas macleodii* subsp. Fijiensis

originating from a deep-sea hydrothermal vent. *Carbohydrate Research*, *312*(1–2), 53–59. https://doi.org/10.1016/S0008-6215(97)10061-1

Roux, P., Siano, R., Collin, K., Bilien, G., Sinquin, C., Marchand, L., Zykwinska, A., Delbarre-Ladrat, C., & Schapira, M. (2021). Bacteria enhance the production of extracellular polymeric substances by the green dinoflagellate *Lepidodinium chlorophorum*. *Scientific Reports*, *11*(1), 4795. https://doi.org/10.1038/s41598-021-84253-2

Roy Chowdhury, S., Sengupta, S., Biswas, S., Sinha, T. K., Sen, R., Basak, R. K., Adhikari, B., & Bhattacharyya, A. (2014). Bacterial Fucose-Rich Polysaccharide Stabilizes MAPK-Mediated Nrf2/Keap1 Signaling by Directly Scavenging Reactive Oxygen Species during Hydrogen Peroxide-Induced Apoptosis of Human Lung Fibroblast Cells. *PLoS ONE*, *9*(11), e113663. https://doi.org/10.1371/journal.pone.0113663

Roy, S. S., & Pal, R. (2015). Microalgae in Aquaculture: A Review with Special References to Nutritional Value and Fish Dietetics. *Proceedings of the Zoological Society*, *68*(1), 1–8. https://doi.org/10.1007/s12595-013-0089-9

Rütering, M., Schmid, J., Gansbiller, M., Braun, A., Kleinen, J., Schilling, M., & Sieber, V. (2018). Rheological characterization of the exopolysaccharide Paenan in surfactant systems. *Carbohydrate Polymers*, *181*, 719–726. https://doi.org/10.1016/j.carbpol.2017.11.086

Safarzadeh Kozani, P., Safarzadeh Kozani, P., Hamidi, M., Valentine Okoro, O., Eskandani, M., & Jaymand, M. (2021). Polysaccharide-based hydrogels: Properties, advantages, challenges, and optimization methods for applications in regenerative medicine. *International Journal of Polymeric Materials and Polymeric Biomaterials*, 1–15. https://doi.org/10.1080/00914037.2021.1962876

Sahana, T. G., & Rekha, P. D. (2019). A bioactive exopolysaccharide from marine bacteria Alteromonas sp. PRIM-28 and its role in cell proliferation and wound healing *in vitro*. *International Journal of Biological Macromolecules*, *131*, 10–18. https://doi.org/10.1016/j.ijbiomac.2019.03.048

Sahana, T. G., & Rekha, P. D. (2020). A novel exopolysaccharide from marine bacterium *Pantoea* sp. YU16-S3 accelerates cutaneous wound healing through Wnt/β-catenin pathway. *Carbohydrate Polymers*, *238*, 116191. https://doi.org/10.1016/j.carbpol.2020.116191

Salvada, J., Alke, B., Brazinha, C., Alves, V. D., & Coelhoso, I. M. (2022). Development and Characterisation of Arabinoxylan-Based Composite Films. *Coatings*, *12*(6), 813. https://doi.org/10.3390/coatings12060813

Samain, E., Miles, M., Bozzi, L., Dubreucq, G., & Rinaudo, M. (1997). Simultaneous production of two different gel-forming exopolysaccharides by an *Alteromonas* strain originating from deep sea hydrothermal vents. *Carbohydrate Polymers*, *34*(4), 235–241. https://doi.org/10.1016/S0144-8617(97)00129-X

Saravanan, C., Rajesh, R., Kaviarasan, T., Muthukumar, K., Kavitake, D., & Shetty, P. H. (2017). Synthesis of silver nanoparticles using bacterial exopolysaccharide and its application for degradation of azo-dyes. *Biotechnology Reports*, *15*, 33–40. https://doi.org/10.1016/j.btre.2017.02.006

Saravanan, P., & Jayachandran, S. (2007). Preliminary characterization of exopolysaccharides produced by a marine biofilm-forming bacterium *Pseudoalteromonas ruthenica* (SBT 033): EPS produced by P. ruthenica. *Letters in Applied Microbiology*, *46*(1), 1–6. https://doi.org/10.1111/j.1472-765X.2007.02215.x

Sathiyanarayanan, G., Dineshkumar, K., & Yang, Y.-H. (2017). Microbial exopolysaccharide-mediated synthesis and stabilization of metal nanoparticles. *Critical Reviews in Microbiology*, *43*(6), 731–752. https://doi.org/10.1080/1040841X.2017.1306689

Sathiyanarayanan, G., Vignesh, V., Saibaba, G., Vinothkanna, A., Dineshkumar, K., Viswanathan, M. B., & Selvin, J. (2014). Synthesis of carbohydrate polymer encrusted gold nanoparticles using bacterial exopolysaccharide: A novel and greener approach. *RSC Adv.*, *4*(43), 22817–22827. https://doi.org/10.1039/C4RA01428F

Scala, A., Piperno, A., Hada, A., Astilean, S., Vulpoi, A., Ginestra, G., Marino, A., Nostro, A., Zammuto, V., & Gugliandolo, C. (2019). Marine Bacterial Exopolymers-Mediated Green Synthesis of Noble Metal Nanoparticles with Antimicrobial Properties. *Polymers*, *11*(7), 1157. https://doi.org/10.3390/polym11071157

Schmid, J., Sieber, V., & Rehm, B. (2015). Bacterial exopolysaccharides: Biosynthesis pathways and engineering strategies. *Frontiers in Microbiology*, *6*. https://doi.org/10.3389/fmicb.2015.00496

Segeren, A. J. M., Boskamp, J. V., & van den Tempel, M. (1974). Rheological and swelling properties of alginate gels. *Faraday Discussions of the Chemical Society*, *57*, 255. https://doi.org/10.1039/dc9745700255

Selvakumar, R., Aravindh, S., Ashok, A. M., & Balachandran, Y. L. (2014). A facile synthesis of silver nanoparticle with SERS and antimicrobial activity using *Bacillus subtilis* exopolysaccharides. *Journal of Experimental Nanoscience*, *9*(10), 1075–1087. https://doi.org/10.1080/17458080.2013.778425

Selvendran, R. R., March, J. F., & Ring, S. G. (1979). Determination of aldoses and uronic acid content of vegetable fiber,. *Analytical Biochemistry*, *96*(2), 282–292.

Senni, K., Gueniche, F., Changotade, S., Septier, D., Sinquin, C., Ratiskol, J., Lutomski, D., Godeau, G., Guezennec, J., & Colliec-Jouault, S. (2013). Unusual Glycosaminoglycans from a Deep Sea Hydrothermal Bacterium Improve Fibrillar Collagen Structuring and Fibroblast Activities in Engineered Connective Tissues. *Marine Drugs*, *11*(4), 1351–1369. https://doi.org/10.3390/md11041351

Serra, A. T., Matias, A. A., Frade, R. F. M., Duarte, R. O., Feliciano, R. P., Bronze, M. R., Figueira, M. E., de Carvalho, A., & Duarte, C. M. M. (2010). Characterization of traditional and exotic apple varieties from Portugal. Part 2 – Antioxidant and antiproliferative activities. *Journal of Functional Foods*, *2*(1), 46–53. https://doi.org/10.1016/j.jff.2009.12.005

Setyaningsih, I., Prasetyo, H., Agungpriyono, D. R., & Tarman, K. (2020). Antihyperglycemic activity of *Porphyridium cruentum* biomass and extracellular polysaccharide in streptozotocin-induced diabetic rats. *International Journal of Biological Macromolecules*, *156*, 1381–1386. https://doi.org/10.1016/j.ijbiomac.2019.11.178

Shao, L., Wu, Z., Zhang, H., Chen, W., Ai, L., & Guo, B. (2014). Partial characterization and immunostimulatory activity of exopolysaccharides from *Lactobacillus rhamnosus* KF5. *Carbohydrate Polymers*, *107*, 51–56. https://doi.org/10.1016/j.carbpol.2014.02.037

Sharifi, H., Zabihzadeh, S. M., & Ghorbani, M. (2018). The application of response surface methodology on the synthesis of conductive polyaniline/cellulosic fiber nanocomposites. *Carbohydrate Polymers*, *194*, 384–394. https://doi.org/10.1016/j.carbpol.2018.04.083

Shen, S., Chen, X., Shen, Z., & Chen, H. (2021). Marine Polysaccharides for Wound Dressings Application: An Overview. *Pharmaceutics*, *13*(10), 1666. https://doi.org/10.3390/pharmaceutics13101666

Shi, X.-L., Wu, Y.-H., Jin, X.-B., Wang, C.-S., & Xu, X.-W. (2017). *Alteromonas lipolytica* sp. Nov., a poly-beta-hydroxybutyrate-producing bacterium isolated from surface seawater. *International Journal of Systematic and Evolutionary Microbiology*, *67*(2), 237–242. https://doi.org/10.1099/ijsem.0.001604

Shimada, A., Nakata, H., & Nakamura, I. (1997). Acidic exopolysaccharide produced by *Enterobacter* sp. *Journal of Fermentation and Bioengineering*, *84*(2), 113–118. https://doi.org/10.1016/S0922-338X(97)82538-X

Silva, F. M., & Silva, C. L. M. (1999). Colour changes in thermally processed cupuaçu (*Theobroma grandiflorum*) puree: Critical times and kinetics modelling. *International Journal of Food Science & Technology*, *34*(1), 87–94. https://doi.org/10.1046/j.1365-2621.1999.00246.x

Silva, J. B., Pereira, J. R., Marreiros, B. C., Reis, M. A. M., & Freitas, F. (2021). Microbial production of medium-chain length polyhydroxyalkanoates. *Process Biochemistry*, *102*, 393–407. https://doi.org/10.1016/j.procbio.2021.01.020

Singh, J., & Saxena, R. C. (2015). Chapter 2—An Introduction to Microalgae: Diversity and Significance. In S.-K. Kim (Ed.), *Handbook of Marine Microalgae* (pp. 11–24). Academic Press. https://doi.org/10.1016/B978-0-12-800776-1.00002-9

Singh, S., Kant, C., Yadav, R. K., Reddy, Y. P., & Abraham, G. (2019). Cyanobacterial Exopolysaccharides: Composition, Biosynthesis, and Biotechnological Applications. In *Cyanobacteria* (pp. 347–358). Elsevier. https://doi.org/10.1016/B978-0-12-814667-5.00017-9

Singh, S., Sran, K. S., Pinnaka, A. K., & Roy Choudhury, A. (2019). Purification, characterization and functional properties of exopolysaccharide from a novel halophilic *Natronotalea sambharensis* sp. Nov. *International Journal of Biological Macromolecules*, *136*, 547–558. https://doi.org/10.1016/j.ijbiomac.2019.06.080

Sittikijyothin, W., Torres, D., & Gonçalves, M. P. (2005). Modelling the rheological behaviour of galactomannan aqueous solutions. *Carbohydrate Polymers*, *59*(3), 339–350. https://doi.org/10.1016/j.carbpol.2004.10.005

Sivasankar, P., Seedevi, P., Poongodi, S., Sivakumar, M., Murugan, T., Sivakumar, L., Sivakumar, K., & Balasubramanian, T. (2018). Characterization, antimicrobial and antioxidant property of exopolysaccharide mediated silver nanoparticles synthesized by *Streptomyces violaceus* MM72. *Carbohydrate Polymers*, *181*, 752–759. https://doi.org/10.1016/j.carbpol.2017.11.082

Soanen, N., Da Silva, E., Gardarin, C., Michaud, P., & Laroche, C. (2016). Improvement of exopolysaccharide production by *Porphyridium marinum*. *Bioresource Technology*, *213*, 231–238. https://doi.org/10.1016/j.biortech.2016.02.075

Spolaore, P., Joannis-Cassan, C., Duran, E., & Isambert, A. (2006). Commercial applications of microalgae. *Journal of Bioscience and Bioengineering*, *101*(2), 87–96. https://doi.org/10.1263/jbb.101.87

St.Cyr, J. (2009). Dermal benefits of topical D-ribose. *Clinical, Cosmetic and Investigational Dermatology*, 151. https://doi.org/10.2147/CCID.S7487

Stolz, P. and Obermayer, P. (2005). Manufacturing microalgae for skin care. *Cosmetics Toiletries*, *120*(3), 99–106.

Storz, H., Zimmermann, U., Zimmermann, H., & Kulicke, W.-M. (2010). Viscoelastic properties of ultra-high viscosity alginates. *Rheologica Acta*, *49*(2), 155–167. https://doi.org/10.1007/s00397-009-0400-x

Su, Z.-J., Wei, Y.-Y., Yin, D., Shuai, X.-H., Zeng, Y., & Hu, T.-J. (2013). Effect of *Sophora subprosrate* polysaccharide on oxidative stress induced by PCV2 infection in RAW264.7 cells. *International Journal of Biological Macromolecules*, *62*, 457–464. https://doi.org/10.1016/j.ijbiomac.2013.09.026

Sun, L., Wang, C., Shi, Q., & Ma, C. (2009). Preparation of different molecular weight polysaccharides from *Porphyridium cruentum* and their antioxidant activities. *International Journal of Biological Macromolecules*, *45*(1), 42–47. https://doi.org/10.1016/j.ijbiomac.2009.03.013

Sun, M.-L., Zhao, F., Shi, M., Zhang, X.-Y., Zhou, B.-C., Zhang, Y.-Z., & Chen, X.-L. (2016). Characterization and Biotechnological Potential Analysis of a New Exopolysaccharide from the Arctic Marine Bacterium *Polaribacter* sp. SM1127. *Scientific Reports*, *5*(1), 18435. https://doi.org/10.1038/srep18435

Tabernero, A., & Cardea, S. (2020). Microbial Exopolysaccharides as Drug Carriers. *Polymers*, *12*(9), 2142. https://doi.org/10.3390/polym12092142

Tang, L., Luo, X., Wang, M., Wang, Z., Guo, J., Kong, F., & Bi, Y. (2021). Synthesis, characterization, *in vitro* antioxidant and hypoglycemic activities of selenium nanoparticles decorated with polysaccharides of *Gracilaria lemaneiformis*. *International Journal of Biological Macromolecules*, *193*, 923–932. https://doi.org/10.1016/j.ijbiomac.2021.10.189

Tang, S., Wang, T., Jiang, M., Huang, C., Lai, C., Fan, Y., & Yong, Q. (2019). Construction of arabinogalactans/selenium nanoparticles composites for enhancement of the antitumor activity. *International Journal of Biological Macromolecules*, *128*, 444–451. https://doi.org/10.1016/j.ijbiomac.2019.01.152

Tilmans, J., & Philippi, J. (1929). Uber den gehalt der wichtigsten protein der nahrangsmittel an kohlehydrat andu¨ber ein kolorimetriches verfharen zur quantitativen beshimmung von stucksoffreiem zucker in elweiss. *Biochimie Zeitung*, *215*(36–60).

Tomé, L. C., Gonçalves, C. M. B., Boaventura, M., Brandão, L., Mendes, A. M., Silvestre, A. J. D., Neto, C. P., Gandini, A., Freire, C. S. R., & Marrucho, I. M. (2011). Preparation and evaluation of the barrier properties of cellophane membranes modified with fatty acids. *Carbohydrate Polymers*, *83*(2), 836–842. https://doi.org/10.1016/j.carbpol.2010.08.060

Tomé, L. C., Silva, N. H. C. S., Soares, H. R., Coroadinha, A. S., Sadocco, P., Marrucho, I. M., & Freire, C. S. R. (2015). Bioactive transparent films based on polysaccharides and cholinium carboxylate ionic liquids. *Green Chemistry*, *17*(8), 4291–4299. https://doi.org/10.1039/C5GC00416K

Torres, C. A. V., Antunes, S., Ricardo, A. R., Grandfils, C., Alves, V. D., Freitas, F., & Reis, M. A. M. (2012). Study of the interactive effect of temperature and pH on

exopolysaccharide production by *Enterobacter* A47 using multivariate statistical analysis. *Bioresource Technology*, *119*, 148–156. https://doi.org/10.1016/j.biortech.2012.05.106

Torres, C. A. V., Ferreira, A. R. V., Freitas, F., Reis, M. A. M., Coelhoso, I., Sousa, I., & Alves, V. D. (2015). Rheological studies of the fucose-rich exopolysaccharide FucoPol. *International Journal of Biological Macromolecules*, *79*, 611–617. https://doi.org/10.1016/j.ijbiomac.2015.05.029

Torres, M., Hong, K.-W., Chong, T.-M., Reina, J. C., Chan, K.-G., Dessaux, Y., & Llamas, I. (2019). Genomic analyses of two *Alteromonas stellipolaris* strains reveal traits with potential biotechnological applications. *Scientific Reports*, *9*(1). https://doi.org/10.1038/s41598-018-37720-2

Trabelsi, L., Chaieb, O., Mnari, A., Abid-Essafi, S., & Aleya, L. (2016). Partial characterization and antioxidant and antiproliferative activities of the aqueous extracellular polysaccharides from the thermophilic microalgae *Graesiella* sp. *BMC Complementary and Alternative Medicine*, *16*(210). https://doi.org/10.1186/s12906-016-1198-6

Uhliariková, I., Matulová, M., & Capek, P. (2021). Optimizing acid hydrolysis for monosaccharide compositional analysis of *Nostoc* cf. Linckia acidic exopolysaccharide. *Carbohydrate Research*, *508*, 108400. https://doi.org/10.1016/j.carres.2021.108400

Umemura, K., Yanase, K., Suzuki, M., Okutani, K., Yamori, T., & Andoh, T. (2003). Inhibition of DNA topoisomerases I and II, and growth inhibition of human cancer cell lines by a marine microalgal polysaccharide. *Biochemical Pharmacology*, *66*(3), 481–487. https://doi.org/10.1016/S0006-2952(03)00281-8

Urbani, R., Magaletti, E., Sist, P., & Cicero, A. M. (2005). Extracellular carbohydrates released by the marine diatoms Cylindrotheca closterium, T*halassiosira pseudonana* and *Skeletonema costatum*: Effect of P-depletion and growth status. *Science of The Total Environment*, *353*(1–3), 300–306. https://doi.org/10.1016/j.scitotenv.2005.09.026

Venil, C. K., Dufossé, L., & Renuka Devi, P. (2020). Bacterial Pigments: Sustainable Compounds With Market Potential for Pharma and Food Industry. *Frontiers in Sustainable Food Systems*, *4*, 100. https://doi.org/10.3389/fsufs.2020.00100

Vieira, H., Leal, M. C., & Calado, R. (2020). Fifty Shades of Blue: How Blue Biotechnology is Shaping the Bioeconomy. *Trends in Biotechnology*, *38*(9), 940–943. https://doi.org/10.1016/j.tibtech.2020.03.011

Vieira, T. M., Alves, V. D., & Moldão Martins, M. (2022). Application of an Eco-Friendly Antifungal Active Package to Extend the Shelf Life of Fresh Red Raspberry (*Rubus idaeus* L. cv. 'Kweli'). *Foods*, *11*(12), 1805. https://doi.org/10.3390/foods11121805

Vieira, T. M., Moldão-Martins, M., & Alves, V. D. (2021). Design of Chitosan and Alginate Emulsion-Based Formulations for the Production of Monolayer Crosslinked Edible Films and Coatings. *Foods*, *10*(7), 1654. https://doi.org/10.3390/foods10071654

Vincent, P., Pignet, P., Talmont, F., Bozzi, L., Fournet, B., Guezennec, J., Jeanthon, C., & Prieur, D. (1994). Production and Characterization of an Exopolysaccharide Excreted by a Deep-Sea Hydrothermal Vent Bacterium Isolated from the Polychaete Annelid *Alvinella pompejana*. *Applied and Environmental Microbiology*, *60*(11), 4134–4141. https://doi.org/10.1128/aem.60.11.4134-4141.1994

Vining, G. (2010). Technical Advice: Residual Plots to Check Assumptions. *Quality Engineering*, *23*(1), 105–110. https://doi.org/10.1080/08982112.2011.535696

Vishnu Priya, M., Sivshanmugam, A., Boccaccini, A. R., Goudouri, O. M., Sun, W., Hwang, N., Deepthi, S., Nair, S. V., & Jayakumar, R. (2016). Injectable osteogenic and angiogenic nanocomposite hydrogels for irregular bone defects. *Biomedical Materials*, *11*(3), 035017. https://doi.org/10.1088/1748-6041/11/3/035017

Vivek, N., Gopalan, N., Das, S., Sasikumar, K., Sindhu, R., Nampoothiri, K. M., Pandey, A., & Binod, P. (2021). Synthesis and Characterization of Transparent Biodegradable Chitosan: Exopolysaccharide Composite Films Plasticized by Bio-Derived 1,3-Propanediol. *Sustainable Chemistry*, *2*(1), 49–62. https://doi.org/10.3390/suschem2010004

Wang, C., Gao, X., Chen, Z., Chen, Y., & Chen, H. (2017). Preparation, Characterization and Application of Polysaccharide-Based Metallic Nanoparticles: A Review. *Polymers*, *9*(12), 689. https://doi.org/10.3390/polym9120689

Wang, H.-M. D., Li, X.-C., Lee, D.-J., & Chang, J.-S. (2017). Potential biomedical applications of marine algae. *Bioresource Technology*, *244*, 1407–1415. https://doi.org/10.1016/j.biortech.2017.05.198

Wang, J., Salem, D. R., & Sani, R. K. (2019). Extremophilic exopolysaccharides: A review and new perspectives on engineering strategies and applications. *Carbohydrate Polymers*, *205*, 8–26. https://doi.org/10.1016/j.carbpol.2018.10.011

Wijesekara, I., Pangestuti, R., & Kim, S.-K. (2011). Biological activities and potential health benefits of sulfated polysaccharides derived from marine algae. *Carbohydrate Polymers*, *84*(1), 14–21. https://doi.org/10.1016/j.carbpol.2010.10.062

Wu, J., Gao, H., Zhao, L., Liao, X., Chen, F., Wang, Z., & Hu, X. (2007). Chemical compositional characterization of some apple cultivars. *Food Chemistry*, *103*(1), 88–93. https://doi.org/10.1016/j.foodchem.2006.07.030

Wu, J., Gu, X., Yang, D., Xu, S., Wang, S., Chen, X., & Wang, Z. (2021). Bioactive substances and potentiality of marine microalgae. *Food Science & Nutrition*, *9*(9), 5279–5292. https://doi.org/10.1002/fsn3.2471

Wu, M., Chen, J., Huang, W., Yan, B., Peng, Q., Liu, J., Chen, L., & Zeng, H. (2020). Injectable and Self-Healing Nanocomposite Hydrogels with Ultrasensitive pH-Responsiveness and Tunable Mechanical Properties: Implications for Controlled Drug Delivery. *Biomacromolecules*, *21*(6), 2409–2420. https://doi.org/10.1021/acs.biomac.0c00347

Wu, S., Liu, G., Jin, W., Xiu, P., & Sun, C. (2016). Antibiofilm and Anti-Infection of a Marine Bacterial Exopolysaccharide Against *Pseudomonas aeruginosa*. *Frontiers in Microbiology*, *7*. https://doi.org/10.3389/fmicb.2016.00102

Xiao, R., & Zheng, Y. (2016). Overview of microalgal extracellular polymeric substances (EPS) and their applications. *Biotechnology Advances*, *34*(7), 1225–1244. https://doi.org/10.1016/j.biotechadv.2016.08.004

Xiao, Y., Huang, Q., Zheng, Z., Guan, H., & Liu, S. (2017). Construction of a *Cordyceps sinensis* exopolysaccharide-conjugated selenium nanoparticles and enhancement of their antioxidant activities. *International Journal of Biological Macromolecules*, *99*, 483–491. https://doi.org/10.1016/j.ijbiomac.2017.03.016

Xiao, Y., Zhang, X., & Huang, Q. (2022). Protective effects of *Cordyceps sinensis* exopolysaccharide-selenium nanoparticles on H_2O_2-induced oxidative stress in HepG2 cells. *International Journal of Biological Macromolecules*, *213*, 339–351. https://doi.org/10.1016/j.ijbiomac.2022.05.173

Xie, L., Shen, M., Wen, P., Hong, Y., Liu, X., & Xie, J. (2020). Preparation, characterization, antioxidant activity and protective effect against cellular oxidative stress of phosphorylated polysaccharide from *Cyclocarya paliurus*. *Food and Chemical Toxicology*, *145*, 111754. https://doi.org/10.1016/j.fct.2020.111754

Xu, X., Liu, W., & Zhang, L. (2006). Rheological behavior of *Aeromonas* gum in aqueous solutions. *Food Hydrocolloids*, *20*(5), 723–729. https://doi.org/10.1016/j.foodhyd.2005.06.012

Xu, Z., Guo, Q., Zhang, H., Wu, Y., Hang, X., & Ai, L. (2018). Exopolysaccharide produced by *Streptococcus thermophiles* S-3: Molecular, partial structural and rheological properties. *Carbohydrate Polymers*, *194*, 132–138. https://doi.org/10.1016/j.carbpol.2018.04.014

Yan, J.-K., Qiu, W.-Y., Wang, Y.-Y., Wang, W.-H., Yang, Y., & Zhang, H.-N. (2018). Fabrication and stabilization of biocompatible selenium nanoparticles by carboxylic curdlans with various molecular properties. *Carbohydrate Polymers*, *179*, 19–27. https://doi.org/10.1016/j.carbpol.2017.09.063

Yang, J., Ma, C., Tao, J., Li, J., Du, K., Wei, Z., Chen, C., Wang, Z., Zhao, C., & Ma, M. (2020). Optimization of polyvinylamine-modified nanocellulose for chlorpyrifos adsorption by central composite design. *Carbohydrate Polymers*, *245*, 116542. https://doi.org/10.1016/j.carbpol.2020.116542

Yang, L., Paulson, A. T., & Nickerson, M. T. (2010). Mechanical and physical properties of calcium-treated gellan films. *Food Research International*, *43*(5), 1439–1443. https://doi.org/10.1016/j.foodres.2010.04.010

Yim, J. H., Kim, S. J., Aan, S. H., & Lee, H. K. (2004). Physicochemical and rheological properties of a novel emulsifier, EPS-R, produced by the marine bacterium *Hahella chejuensis*. *Biotechnology and Bioprocess Engineering*, *9*(5), 405–413. https://doi.org/10.1007/BF02933066

Yim, J. H., Kim, S. J., Ahn, S. H., Lee, C. K., Rhie, K. T., & Lee, H. K. (2004). Antiviral Effects of Sulfated Exopolysaccharide from the Marine Microalga *Gyrodinium impudicum* Strain KG03. *Marine Biotechnology*, *6*(1), 17–25. https://doi.org/10.1007/s10126-003-0002-z

Yim, J. H., Kim, S. J., Ahn, S. H., & Lee, H. K. (2003). Optimal conditions for the production of sulfated polysaccharide by marine microalga *Gyrodinium impudicum* strain KG03. *Biomolecular Engineering*, *20*(4–6), 273–280. https://doi.org/10.1016/S1389-0344(03)00070-4

Yim, J. H., Kim, S. J., Ahn, S. H., & Lee, H. K. (2007). Characterization of a novel bioflocculant, p-KG03, from a marine dinoflagellate, *Gyrodinium impudicum* KG03. *Bioresource Technology*, *98*(2), 361–367. https://doi.org/10.1016/j.biortech.2005.12.021

Yin, S., & Ma, Z. (2019). “Smart” sensing interface for the improvement of electrochemical immunosensor based on enzyme-Fenton reaction triggered destruction of Fe^{3+} cross-linked alginate hydrogel. *Sensors and Actuators B: Chemical*, *281*, 857–863. https://doi.org/10.1016/j.snb.2018.11.030

Yu, P., Li, Y., Sun, H., Ke, X., Xing, J., Zhao, Y., Xu, X., Qin, M., Xie, J., & Li, J. (2022). Cartilage-Inspired Hydrogel with Mechanical Adaptability, Controllable Lubrication, and Inflammation Regulation Abilities. *ACS Applied Materials & Interfaces*, *14*(23), 27360–27370. https://doi.org/10.1021/acsami.2c04609

Yumei, L., Yamei, L., Qiang, L., & Jie, B. (2017). Rapid Biosynthesis of Silver Nanoparticles Based on Flocculation and Reduction of an Exopolysaccharide from

Arthrobacter sp. B4: Its Antimicrobial Activity and Phytotoxicity. *Journal of Nanomaterials*, *2017*, 1–8. https://doi.org/10.1155/2017/9703614

Zanchetta, P., Lagarde, N., & Guezennec, J. (2003). A New Bone-Healing Material: A Hyaluronic Acid-Like Bacterial Exopolysaccharide. *Calcified Tissue International*, *72*(1), 74–79. https://doi.org/10.1007/s00223-001-2091-x

Zarandona, I., Estupiñán, M., Pérez, C., Alonso-Sáez, L., Guerrero, P., & de la Caba, K. (2020). Chitosan Films Incorporated with Exopolysaccharides from Deep Seawater *Alteromonas* sp. *Marine Drugs*, *18*(9), 447. https://doi.org/10.3390/md18090447

Zeng, S., Ke, Y., Liu, Y., Shen, Y., Zhang, L., Li, C., Liu, A., Shen, L., Hu, X., Wu, H., Wu, W., & Liu, Y. (2018). Synthesis and antidiabetic properties of chitosan-stabilized selenium nanoparticles. *Colloids and Surfaces B: Biointerfaces*, *170*, 115–121. https://doi.org/10.1016/j.colsurfb.2018.06.003

Zhang, J., Yue, X., Zeng, Y., Hua, E., Wang, M., & Sun, Y. (2018). *Bacillus amyloliquefaciens* levan and its silver nanoparticles with antimicrobial properties. *Biotechnology & Biotechnological Equipment*, *32*(6), 1583–1589. https://doi.org/10.1080/13102818.2018.1523690

Zhang, Z., Cai, R., Zhang, W., Fu, Y., & Jiao, N. (2017). A Novel Exopolysaccharide with Metal Adsorption Capacity Produced by a Marine Bacterium *Alteromonas* sp. JL2810. *Marine Drugs*, *15*(6), 175. https://doi.org/10.3390/md15060175

Zhao, Y., Li, B., Li, C., Xu, Y., Luo, Y., Liang, D., & Huang, C. (2021). Comprehensive Review of Polysaccharide-Based Materials in Edible Packaging: A Sustainable Approach. *Foods*, *10*(8), 1845. https://doi.org/10.3390/foods10081845

Zhou, F., Wu, Z., Chen, C., Han, J., Ai, L., & Guo, B. (2014). Exopolysaccharides produced by *Rhizobium radiobacter* S10 in whey and their rheological properties. *Food Hydrocolloids*, *36*, 362–368. https://doi.org/10.1016/j.foodhyd.2013.08.016

Zobell, C. E. (1941). Studies on marine bacteria. I. The cultural requirements of heterotrophic aerobes. *J Mar Res*, *4*, 42–75.

Zuidema, J. M., Rivet, C. J., Gilbert, R. J., & Morrison, F. A. (2014). A protocol for rheological characterization of hydrogels for tissue engineering strategies: A Protocol for Rheological Characterization of Hydrogels. *Journal of Biomedical Materials Research Part B: Applied Biomaterials*, *102*(5), 1063–1073. https://doi.org/10.1002/jbm.b.33088

Zykwinska, A., Berre, L. T.-L., Sinquin, C., Ropartz, D., Rogniaux, H., Colliec-Jouault, S., & Delbarre-Ladrat, C. (2018). Enzymatic depolymerization of the GY785 exopolysaccharide produced by the deep-sea hydrothermal bacterium *Alteromonas*

infernus: Structural study and enzyme activity assessment. *Carbohydrate Polymers*, *188*, 101–107. https://doi.org/10.1016/j.carbpol.2018.01.086

Zykwinska, A., Marquis, M., Sinquin, C., Cuenot, S., & Colliec-Jouault, S. (2016). Assembly of HE800 exopolysaccharide produced by a deep-sea hydrothermal bacterium into microgels for protein delivery applications. *Carbohydrate Polymers*, *142*, 213–221. https://doi.org/10.1016/j.carbpol.2016.01.056

Appendixes | A

Appendix A.1

Examples of the two distinctive HPSEC results, one and two chromatographic peaks, obtained from molecular mass distribution determination (Fig. A.1).

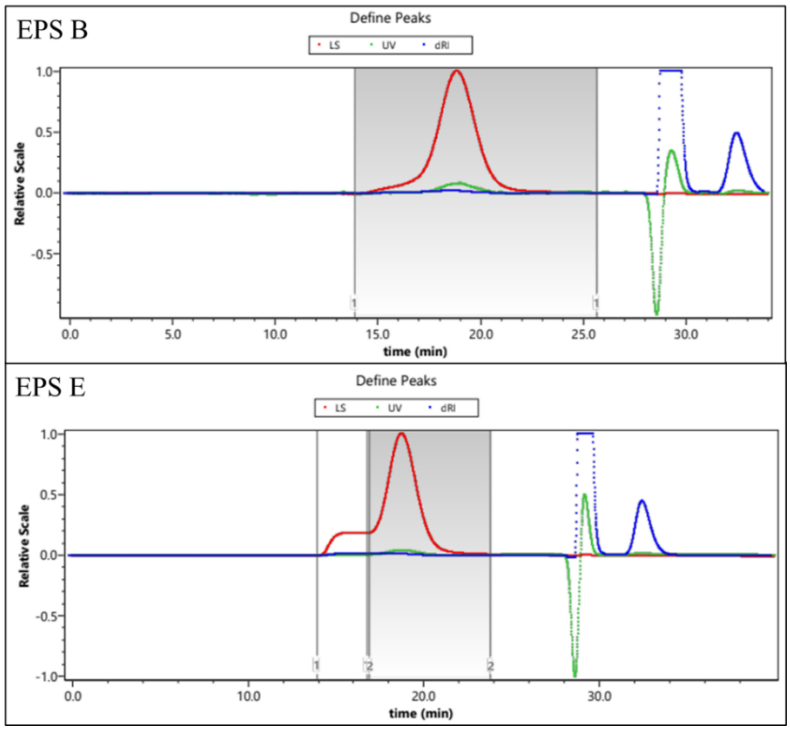

Figure A.1. Molecular weight determination of EPS B and EPS E.

Appendix A.2

Thermal degradation steps of the EPS (Table A.1).

Table A.1. Thermal degradation steps of the EPS produced by Alteromonas strains isolated from French Polynesia.

EPS	Temperature (°C)	Weight loss (%)
A	40.20 – 192.81 193.18 – 405.15	14.6 42.5
B	40.59 – 186.14 186.33 – 418.89	13.8 36.4
C	37.97 – 189.07 189.47 – 428.81	14.2 30.2
D	38.6 – 183.88 184.46 – 385.68	12.7 45.1
E	36.61 – 188.77 189.49 – 390.41	17.5 44.8
F	45.14 – 173.09 212.40 – 385.88	12.1 41.5

Appendix A.3

Images of gels homogeneous gels that did not sustain their structure in the inversion test (-), and small non-homogeneous gels (--) (Fig. A.2).

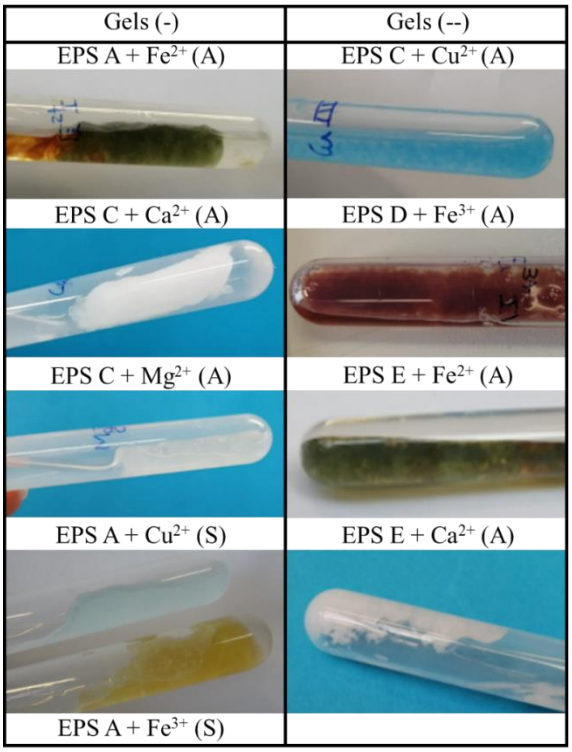

Figure A.2. Results from gel formations type (-) and (--) with different cations under standard and alkaline conditions.

Appendix A.4

Analysis of variance (ANOVA) of the full quadratic model developed for describing the impact of Fe^{3+} and EPS concentration on the EPA A hydrogels' strength.

Table A.2. Analysis of variance (ANOVA) for the full quadratic model describing EPS A hydrogels strength as function of Fe^{3+} and EPS concentration.

Source of variation	Sum of squares	Degrees of freedom	Mean square	*f*-value	*p*-value
Model	2.616×10^9	5	5.233×10^8	30.35	0.0010
X_1 – Fe^{3+}	1.676×10^8	1	1.676×10^8	9.72	0.0263
X_2 – EPS	1.704×10^9	1	1.704×10^9	98.84	0.0002
$X_1 X_2$	1.407×10^8	1	1.407×10^8	8.16	0.0356
X_1^2	5.941×10^8	1	5.941×10^8	34.46	0.0020
X_2^2	1.724×10^7	1	1.724×10^7	0.9997	0.3633*
Lack of Fit	5.336×10^7	3	1.779×10^7	1.08	0.5130*
Pure Error	3.285×10^7	2	1.642×10^7		

* Not significant (*p*-value>0.05).

2022

PATRÍCIA CONCÓRDIO DOS REIS

DEVELOPMENT OF NEW BIOACTIVE MATERIALS BASED ON MICROBIAL EXPOLYSACCHARIDES OF MARINE ORIGIN